Sequence stratigraphic evolution of the Albian to Recent section of the Dampier Sub-basin, North West Shelf, Australia

Jonathan N.F. Hull

B.Sc. (Hons) Geology and Applied Geology – University of Glasgow

M.Sc. (Dist) Petroleum Geology – University of Aberdeen

National Centre for Petroleum Geology and Geophysics

Thesis submitted to the University of Adelaide in fulfillment of the requirement of the degree Doctor of Philosophy

August 1999

TABLE OF CONTENTS

TABLE OF FIGURES

ABSTRACT

An integrated biostratigraphic, wireline, seismic, lithological and 3D-Chronostrat sequence stratigraphic study has been conducted to investigate the evolution of the Albian to Recent section of the Dampier Sub-basin on Australia's North West Shelf. The study used 4100 km of regional seismic data and 38 wells with a variable suite of wireline logs, biostratigraphic reports and lithology data.

During the study, a model for the sequence stratigraphic interpretation of the carbonate wireline log motifs was developed from biostratigraphic constraints, wireline log patterns and theoretical considerations. This model has enabled the subdivision of the section into 29 genetically-related sequences which have been further subdivided into 98 time-bounded units of strata termed 'chronosomes'. While the timing of these units has been estimated, the boundaries of the 29 sequences has been tightly constrained by reference to published foraminiferal zonations. A combination of sequence and chronosome architecture with biostratigraphic, lithostratigraphic and wireline log data have been used to generate a suite of depth, isochron, and paleogeographic maps.

The Oligocene to Recent section of the Dampier Sub-basin is characterised by a series of prograding, carbonate-dominated clinoforms within which periods of predominant progradation and aggradation have been identified. Quantitative analysis of sedimentation rates, clinoform angles and clinoform heights of this section has been conducted using stacking velocities and chronosome volumes output from 3D-Chronstrat. Calculated sedimentation rates for the aggradational sequences have shown them to be 1.5 times the sedimentation rate of the progradational sequences. The morphology of the clinoforms is a function of these progradational and aggradational periods. Progradational sequences have increasing clinoform slope angles with only a minor associated increase in clinoform height whilst aggradational sequences are characterised by decreasing clinoform angles and a marked increase in clinoform height. The aggradational sequences correspond to periods when the high-frequency (1-3 Ma) and low-frequency (10 Ma) eustatic curves of Haq *et al.* (1987) are coincident and progradational periods correspond to periods when the curves are separated. When both the high and low frequency eustatic curves combine to produce a relative sea level high significant shelf-top accommodation space is created and the margin responded by aggrading. When the rate of accommodation space creation on the shelf top is low, the sequences deposited are predominantly progradational in nature and characterised by lower sedimentation rates, progressively increasing clinoform slope angles and relatively constant clinoform height.

DECLARATION OF AUTHENTICITY

This thesis contains no material which has been accepted for the award of any other degree or diploma in any university or other tertiary institution and, to the best of my knowledge and belief, contains no material previously published or written by any other person, except where due reference is made in the text.

I give consent to this copy of my thesis, when deposited in the University Library, being available for loan and photocopying.

Jonathan Hull

31st August 1999

ACKNOWLEDGEMENTS

I wish to thank the trustees of the Northcote Trust for awarding me the Northcote Graduate Scholarship which has provided the financial support that has allowed me to undertake this course of study in Australia. The industry sponsor, Mobil Exploration & Production Australia Pty Ltd, generously donated time, resources and data and maintained an active interest throughout the duration of the project. Their involvement is greatly appreciated.

There are many people at the NCPGG who have been central to the project and I would like to thank them for the support and guidance they have given whilst I have been here. In particular I would like to thank the late Dr William Stuart without whom I would not have had the opportunity to study in Australia. My supervisors Prof. Cedric Griffiths and Dr Nick Lemon not only provided me with invaluable technical and academic support but also allowed me the freedom to develop the project in my own direction. Sincere thanks go to Dr John Kaldi for providing practical support and guidance during the latter stages of the project and also to Andy Mitchell, Nick Mann, Maureen Sutton and Barbara Wallis for their support and assistance over the past three years.

My time at the NCPGG has been enriched by the wide cross-section of students whom I have had the opportunity to study and socialise with. These people have provided a stimulating work environment and have complemented the academic side of life at the NCPGG. I would particularly like to thank Stuart Smith and Hamish Young, my fellow sequence stratigraphers and co-authors for making me think and making me laugh. I would also like to acknowledge the support and friendship of the close group of friends I have had the privilege to meet whilst I have been in Australia. In particular I would like to thank Bridget Little for her support and encouragement during the write-up phase of the thesis and for reviewing many draft copies of this manuscript. I would also like to thank Chris Cubitt and Sharon Tiainen for their efforts to engross me fully in the culture and continent that is Australia. I think I have achieved it.

I would also like to take this opportunity to thank the support and encouragement I have received from my family over the years. Without their support I would have never pursued my academic career to this extent.

CHAPTER 1 INTRODUCTION

1.1 General

The Dampier Sub-basin is one of four northeast-trending sub-basins that together comprise the Northern Carnarvon Basin located on the North West Shelf of Australia, (Figure 1.1). Since oil was first discovered onshore at Rough Range in the 1950s, there has been considerable industry activity exploring for hydrocarbons in the Northern Carnarvon Basin, the offshore continuation of the Rough Range trend. The North West Shelf is now the premier hydrocarbon province in Australia, and the Northern Carnarvon Basin accounted for more than 50% of Australia's total hydrocarbon production in 1998. This production comes primarily from Triassic to Lower Cretaceous siliciclastic reservoirs, which were deposited as a result of the progressive breakup of Gondwana. To date, much has been published on this phase of the evolution of the North West Shelf. The subsequent mid-Cretaceous to Tertiary carbonate-dominated section of the North West Shelf was deposited along a continental margin open to oceanic circulation as the Australian continent migrated northwards. This phase of the evolution of the North West Shelf is poorly understood with only a handful of papers focussing on the evolution of this section (Apthorpe, 1988; Rasidi, 1995; Romine *et al.*, 1997; Westphal and Aigner, 1997).

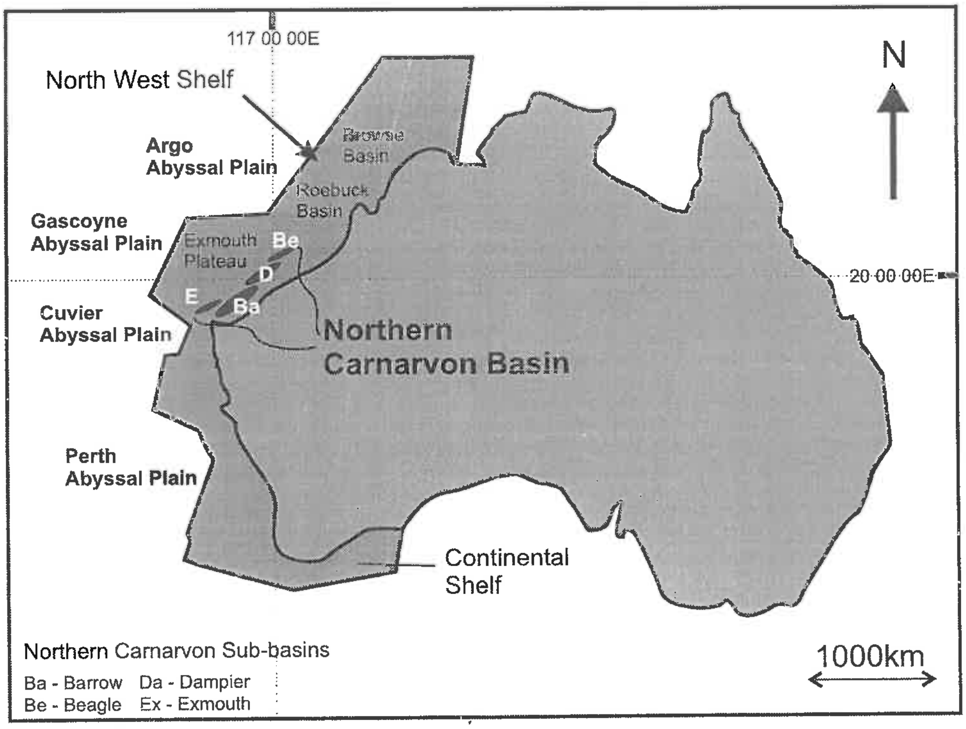

Figure 1.1 Location Map of the Dampier Sub-basin in the Northern Carnarvon Basin of Australia's North West Shelf.

1.2 Objectives

The objective of this study was to gain a high-resolution quantitative understanding of the structural and stratigraphic evolution of the Albian to Recent section of the Dampier Sub-basin. In particular, the study has focussed on the changing nature of the stratal architecture in response to tectonic events and changes in relative sea level. The study was based on the underlying hypothesis that a detailed record of Albian to Recent structural and stratigraphic evolution of the Dampier Sub-basin is contained within the preserved stratal architecture of the sequences deposited during that time. The study also aimed to further the understanding of the three-dimensional architecture of prograding carbonate systems in general and their response to changes in relative sea level.

The study has used a sequence stratigraphic approach to integrate biostratigraphic, wireline and seismic data. In doing so, the section has been subdivided into a series of genetically related packages, which provide the basis for the high-resolution quantitative analysis of sedimentation rates and styles.

1.3 Geological evolution of the Dampier Sub-Basin

The structural and sequence stratigraphic evolution of the Triassic to Lower Cretaceous siliciclastic-dominated section has been discussed extensively in the literature. Early studies adopted a tectonostratigraphic approach to their analysis of the basin (Hocking, 1988; Kopsen and McGann, 1985; Woodside Offshore Petroleum, 1988). More recent publications have adopted a sequence stratigraphic approach in an attempt to develop a predictive understanding of the sedimentary architecture (Barber, 1994; Labutis, 1994; Miller and Smith, 1996). Jablonski (1997) provides a good summary of the Triassic to early Cretaceous section using a sequence stratigraphic approach in which the section is initially subdivided into tectonically-related megasequences. Significant advances have also been made in the understanding of the structural evolution of the Dampier Sub-basin (AGSO North West Shelf Study Group, 1994; Baillie *et al.*, 1994; Driscoll and Karner, 1998; Mihut and Muller, 1998; Muller *et al.*, 1998; Newman, 1994; Stagg and Colwell, 1994; Veevers *et al.*, 1991; Yeates *et al.*, 1987).

In contrast to the wealth of papers on the Triassic to Lower Cretaceous sediments, the Albian to Recent is considerably less understood with only three papers dealing with the regional evolution of this section (Apthorpe, 1988; Romine *et al.*, 1997; Westphal and Aigner, 1997). Apthorpe (1988) used a biostratigraphic approach to subdivide the Cainozoic section into four major units or cycles whilst Romine *et al.* (1997) used a sequence stratigraphic approach and focussed on post-Valanginian break-up to mid-Miocene section. They also subdivided the section into four major units or 'supersequences', which correspond in part to Apthorpe's cycles. Westphal and Aigner (1997) used established lithostratigraphy and seismic geometries to define sequence boundaries in the section and applied a systems tract interpretation to the formations.

The Albian to Recent section of the Dampier Sub-basin is an integral part of the late stage evolution of the basin; it records sediment deposition during the time of hydrocarbon generation, migration and trapping. A quantitative understanding of sediment depositional patterns during this period will reveal the nature of the late stage evolution and will also give important information on the timing of oil generation and nature of migration pathways.

1.3.1 Structural Configuration

The Dampier Sub-basin is composed of a series of northeast-southwest-trending structural lineaments. The Rankin Trend, which constitutes the elevated inner edge of the Exmouth Plateau, forms the western shoulder of the Dampier Sub-basin. The Rankin Trend is divided into a series of discrete fault blocks by north-south trending faults. The eastern margin of the Dampier Sub-basin is formed by the Enderby Platform and Lambert Shelf, which are separated from the main depocentre by the northeast-trending Rosemary Fault system. To the north and south of the Dampier Sub-basin are the Beagle and Barrow Sub-basins respectively. Between the Rankin Trend and Rosemary Fault system are a number of northeast-trending structural lineaments, the Lewis and Kendrew Troughs and the Madeleine and Legendre Trends (Figure 1.2).

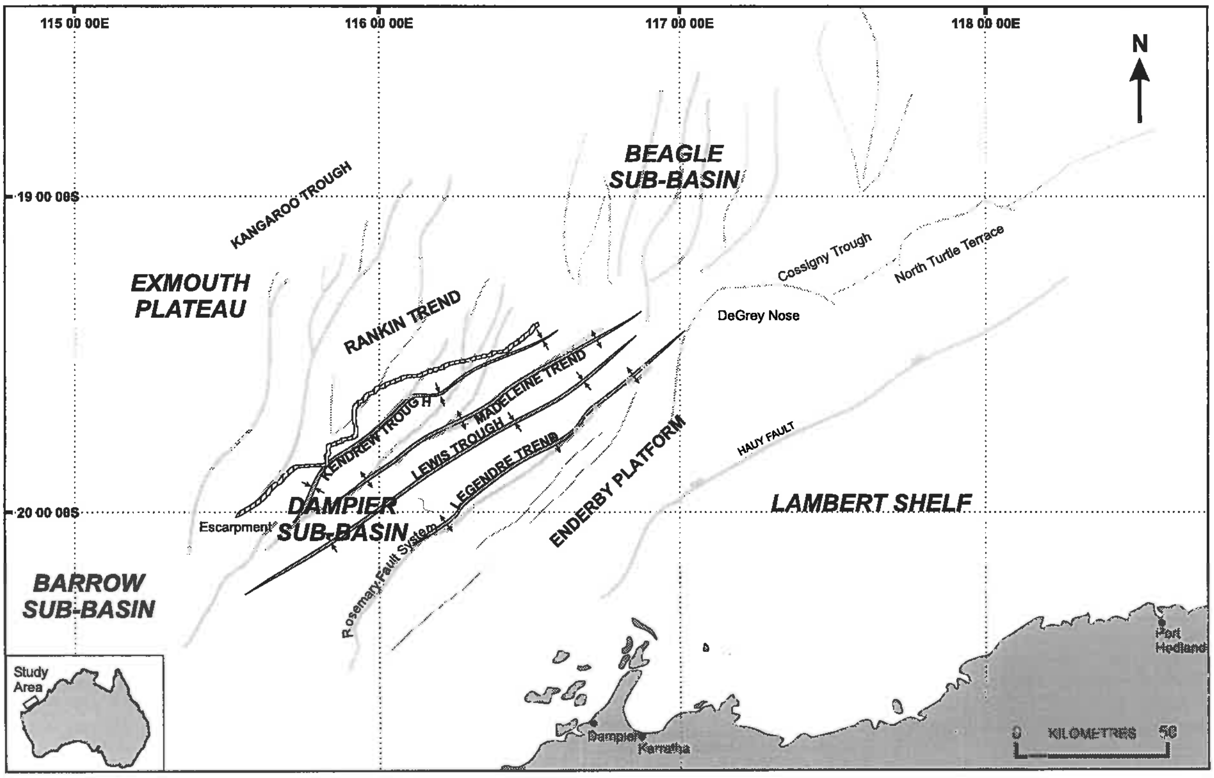

Figure 1.2 Structural elements of the Dampier Sub-basin.

1.3.2 Tectonic Evolution

Before the progressive breakup of Gondwana, Australia was joined at its southern margin to Antarctica, India was situated on the western margin and Argo Land and Burma were joined to the north of the present day Exmouth Plateau (Muller *et al.*, 1998; Veevers *et al.*, 1991). The timing and nature of the separation along Australia's margins has strongly influenced the stratigraphic development of the Dampier Sub Basin from its inception to its present day configuration.

North West Shelf

The progressive breakup of the Gondwanan continent occurred as a southward propagating rift, which began in the Oxfordian at 156 Ma, and propagated southwards until the Valanginian at 136 Ma. This progressive rifting led to the sequential formation of the Argo, Gascoyne, Cuvier and Perth Abyssal Plains (Mihut and Muller, 1998; Muller *et al.*, 1998). The creation of these abyssal plains represented the final separation of Greater India from Western Australia. Greater India continued to rotate northwestward from Australia until the Cenomanian, at which time spreading switched to an east-west axis in the Indian Ocean and Greater India commenced its drift north at a rate of 19.5 cm yr^{-1} (Klootwijk *et al.*, 1992).

Australian-Antarctic

Continental extension between Australia and Antarctica began in the late Jurassic. Prior to break-up and onset of sea-floor spreading in the Cenomanian, 360 km of continental extension had occurred (Baillie *et al.*, 1994; Powell *et al.*, 1988). From the Cenomanian to Eocene, the majority of north-south spreading in the region occurred in the Indian Ocean. As a result Australia remained at high latitudes and by the Eocene the Southern Ocean was still only 400 km across (Baillie *et al.*, 1994). After the initial late Paleocene collision between Greater India and the Eurasian Plate at 55 Ma (Klootwijk *et al.*, 1992; Powell *et al.*, 1988) the primary north-south spreading axis was relocated to the Southern Ocean, causing Australia to migrate north at a rate of 4 cm yr^{-1} (Baillie *et al.*, 1994). To the east, relative movement between Antarctica and Tasmania was transform, and as a result there was no deep ocean opening towards the Pacific until the Oligocene when the final separation of the Antarctic and Australian plates occurred (Baillie *et al.*, 1994). With the establishment of a deep ocean between Australia and Antarctica, the circum-polar current, which previously flowed around Antarctica, up the west coast and down the east coast of Australia, was able to circulate Antarctica which was now isolated at the south pole. Romine *et al.* (1997) suggest that the circum-Antarctic current caused a build-up of continental ice sheets on the Antarctic landmass which caused a global fall in sea level.

Australian - South East Asia

The Australian Plate continued migrating northwards and by the early Miocene, the northern edge of the Australian continent collided with a series of island arcs on the Eurasian Plate and then came in contact with the westward-moving Pacific plate (Baillie *et al.*, 1994). The interaction of the northward-moving Australian plate and the westward-moving Pacific plate produced two tectonic effects. Firstly, buckling occurred in the Australian lithosphere in the mid-Miocene as the continent passed over the oceanic subduction zone. Secondly, the collision induced an anti-clockwise rotational torque on the Australian continent causing dextral transcurrent movements along pre-existing fractures near the continent-ocean boundary (Veevers and Powell, 1984) (Figure 1.3). The effect of the Miocene collision can be seen along the length of the North West Shelf but its expression varies depending on the convergence angle at any point on the shelf relative to the orientation of the reactivated basement structures (Keep *et al.*, 1998). Figure 1.3 shows the rates and direction of present-day plate motions. The Australian plate can be seen to move northwards and collide with the westward-moving Pacific Plate and the Eurasian Plate. This configuration gives rise to the dextral strike slip movement in the Northern Carnarvon Basin as shown in Figure 1.3.

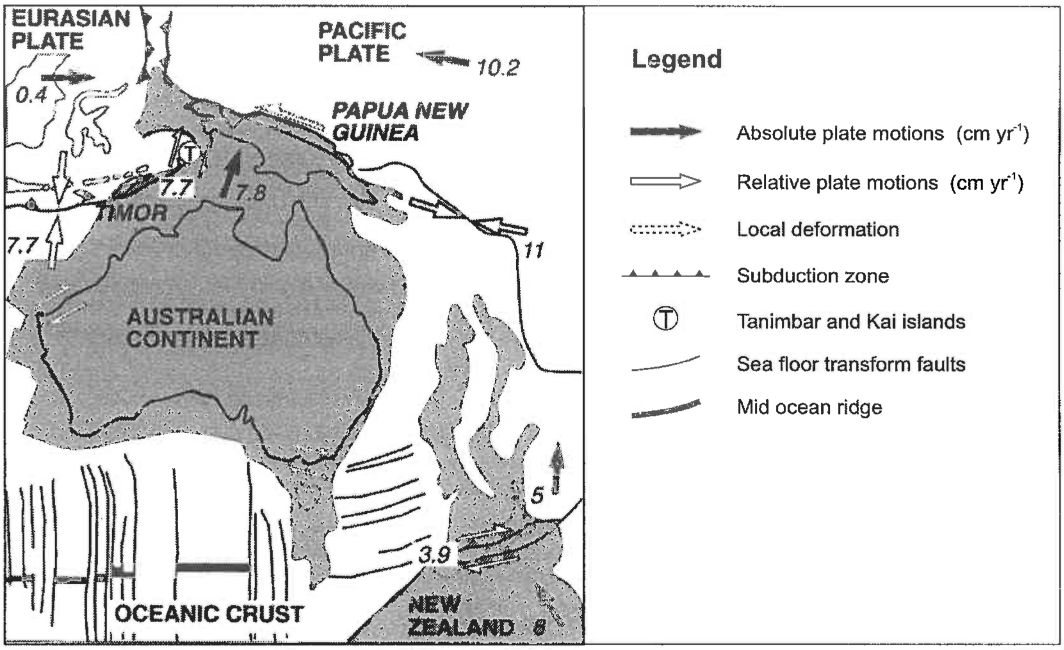

Figure 1.3 Present day plate configurations of the Australian Plate (Keep et al., 1998).

1.3.3 Stratigraphic Evolution - Permian to mid-Cretaceous

Permian - Triassic

Intra-cratonic movement on the Gondwanan continent began during the Carboniferous and culminated with basin subsidence during the Permian, causing the formation of the Westralian Superbasin (Falvey and Mutter, 1981; Yeates *et al.*, 1987). Sedimentation in the Westralian Superbasin consisted of base Triassic thin transgressive sands and carbonates which graded into widespread marine claystones, silts and carbonates of the early Triassic. As thermal subsidence associated with the Permian rifting waned, deposition of regressive fluvio-deltaic and shallow marine sedimentation occurred from the middle of the Triassic to the earliest Jurassic (Jablonski, 1997). These sands now form the hydrocarbon-bearing reservoirs of the Rankin Trend.

Early - Middle Jurassic

A further phase of rifting began in the Pliensbachian (Baillie *et al.*, 1994) and culminated in the Callovian, with break-up of Argo Land and Australia occurring in the Oxfordian at 156 Ma (Muller *et al.*, 1998). This break-up initiated sea-floor spreading in the Argo Abyssal Plain and also produced accelerated subsidence in the Dampier Sub-basin creating sediment-filled grabens. The major tectonic features of the Dampier Sub-basin, such as the Rankin Trend, Rosemary Fault System and the Lewis Trough were created at this time (Jablonski, 1997). Sediments associated with the rifting took the form of shallow marine clastics, basin floor fans and transgressive sands that progressively became finer grained as thermal subsidence waned.

Late Jurassic - Lower Cretaceous

During the Tithonian, a third phase of rifting with minor associated brittle deformation and erosional truncation occurred (Driscoll and Karner, 1998). This rifting event created the accommodation space for the deposition of the Neocomian Barrow Group Delta. The delta was supplied with sediment from a landmass to the south (Australia and Greater India), and prograded northwards towards the ocean formed by spreading in the Argo Abyssal Plain (Ross and Vail, 1994). These Barrow Group sediments thin rapidly eastwards across the Northern Barrow Sub-basin and Exmouth Plateau to become no more than a few hundred metres thick in the Dampier Sub-basin. Rifting persisted until uplift extension and finally break-up of Greater India and Australia occurred during the Valanginian. The break-up event occurred when sea-floor spreading ceased in the Argo Abyssal Plain and west-northwest rifting initiated between India and Australia which led to the formation of the Gascoyne and Cuvier Abyssal Plains (Stagg and Colwell, 1994). This is represented by the intra-Valanginian unconformity throughout the Northern Carnarvon Basin. This major tectonic rearrangement also coincided with a major eustatic fall causing incision of major river systems and a resultant influx of siliciclastics entering the Barrow Sub-basin through the Barrow-Dampier accommodation zone (Romine *et al.*, 1997), (Figure 1.4). These sands were deposited as fan and lowstand delta sandstones beyond the shelf edge of the exposed Barrow delta. The Dampier Sub-basin was largely bypassed as a repository for lowstand siliciclastics because most of the fluvial drainage from the antecedent Robe, Fortescue and Yule rivers was directed into the Barrow Sub-basin by relay ramps associated with rifting (Romine *et al.*, 1997).

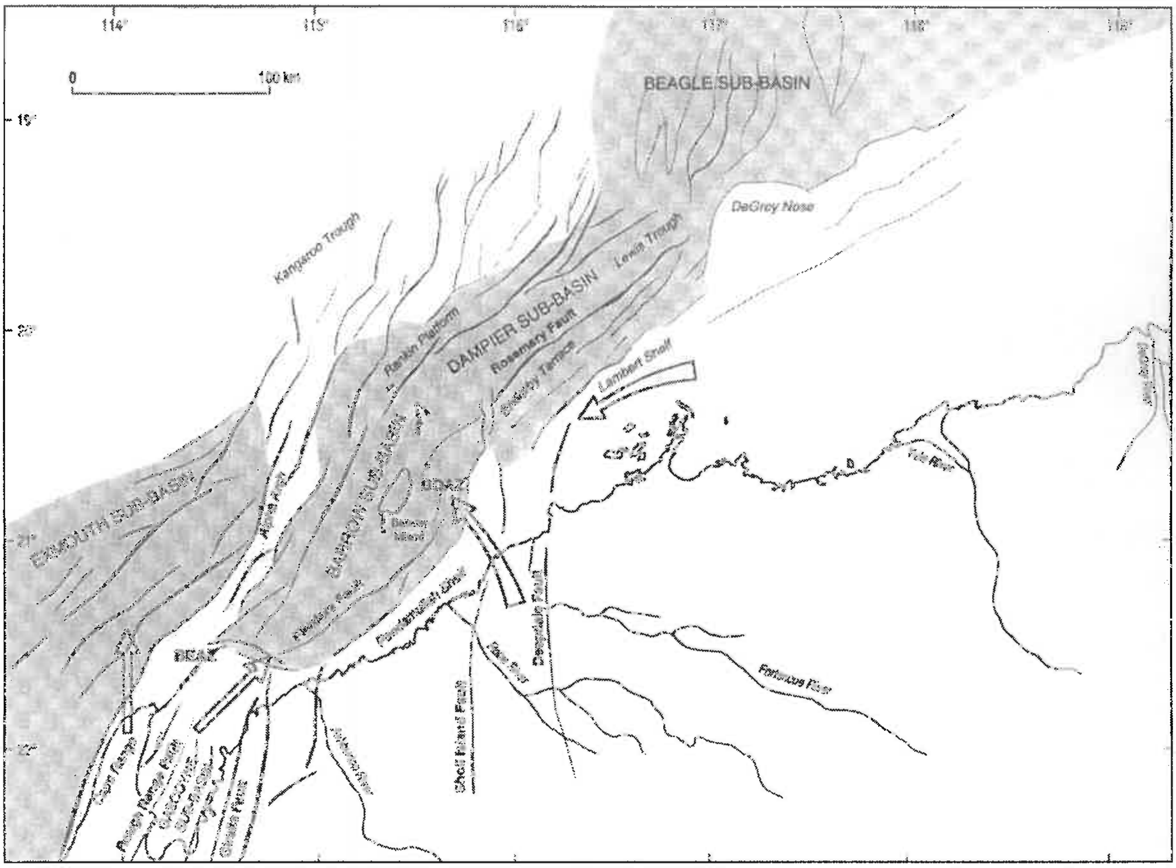

Figure 1.4 Sediment input directions to the Barrow-Dampier Sub-basins during the early Cretaceous (Romine et al., 1997).

1.3.4 Stratigraphic Evolution - mid-Cretaceous to Recent

The three papers which have been published on the mid-Cretaceous to Recent section of the Dampier Sub-basin concentrate on the basin's evolution though time (Apthorpe, 1988; Romine *et al.*, 1997; Westphal and Aigner, 1997). These studies have attempted to subdivide the section into geologically-related units and identify regional events using three differing approaches. Figure 1.5 shows the subdivisions and events defined in these three studies.

Apthorpe (1988) subdivided the Cenozoic section of the Dampier Sub-basin into four 'cycles' on the basis of biostratigraphic and lithostratigraphic data. Two of these 'cycles' have been further subdivided; 'Cycle 3' on the basis of a widespread seismically mappable erosion event and 'Cycle 1' rather arbitrarily, on the basis on lithological differences and not geological events (Figure 1.5). Within these 'cycles' the presence of other events have been noted on the basis of biostratigraphic and lithostratigraphic data.

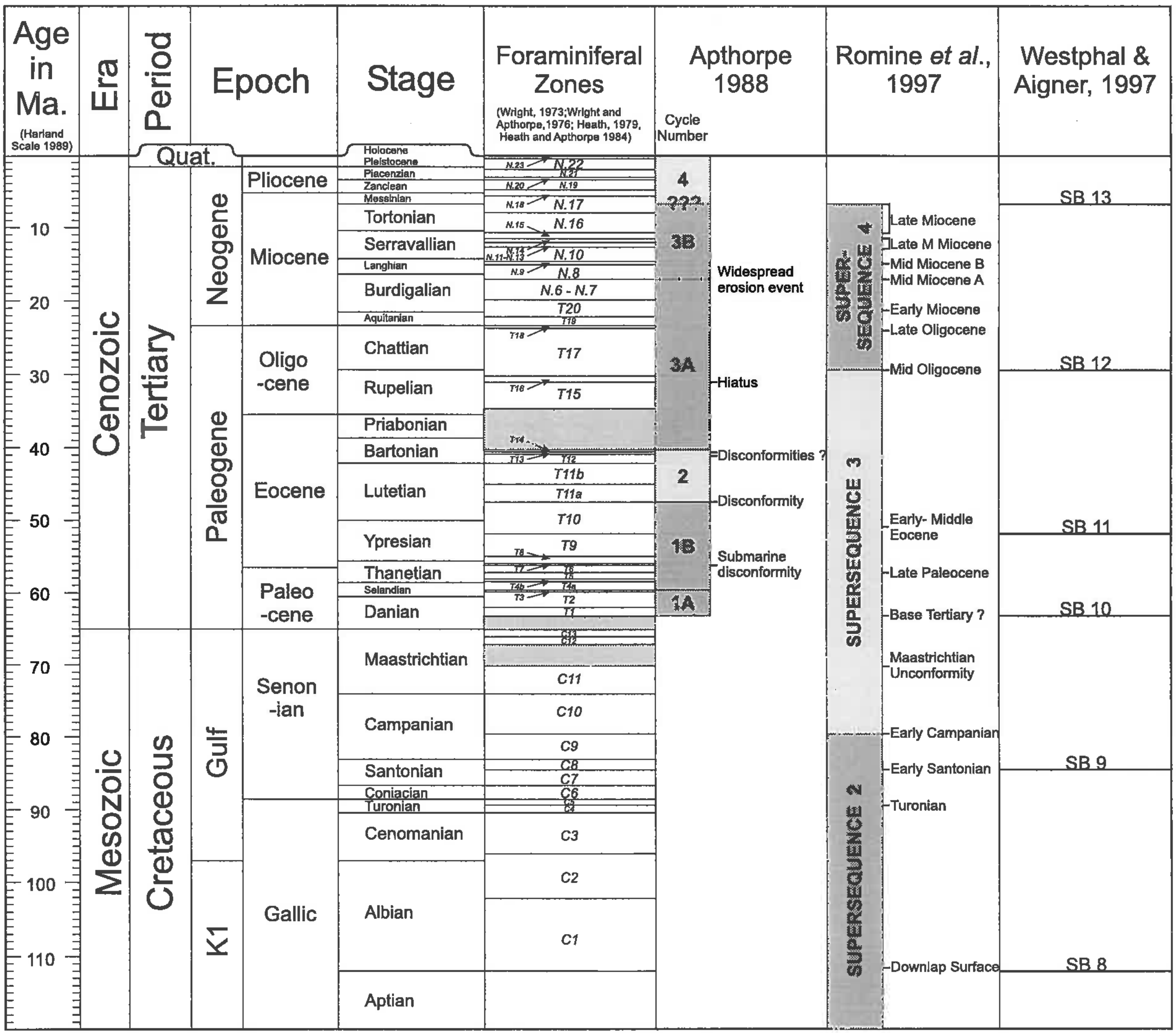

Figure 1.5 Sequence boundaries in the Albian to Recent section of the Dampier Sub-basin (Apthorpe, 1988; Romine et al., 1997; Westphal and Aigner, 1997).

Romine *et al.* (1997) used a sequence stratigraphic approach to identify two orders of tectonically-related transgressive – regressive sequences that were deposited during the phase of thermal subsidence which followed the Valanginian break-up and continued until the late Miocene collision of Australia and Southeast Asia. This Valanginian to late Miocene sequence has been called the 'Cretaceous-Tertiary Megasequence'. The boundaries of this 'megasequence' are related to major plate tectonic interactions associated with break-up and collision (Romine *et al.*, 1997). The transgressive phase of the 'Cretaceous-Tertiary Megasequence' persists from the intra-Valanginian to the early Campanian after which the 'megasequence' becomes regressive until its end in the late Miocene. Within the 'Cretaceous-Tertiary Megasequence' Romine *et al.* (1997) have identified four higher order packages of transgressive-regressive sediments which they have termed 'supersequences'. Two of these 'supersequences' are on the transgressive limb of the 'Cretaceous-Tertiary Megasequence' and two are on the regressive limb. The boundaries of these 'supersequences' have been related to eustatic variations caused by far-field plate tectonic events (Romine *et al.*, 1997). These four transgressive – regressive 'supersequences' are intra-Valanginian – mid-Aptian; mid-Aptian – early Campanian; early Campanian – mid-Oligocene and mid-Oligocene to late Miocene in age. Within these supersequences, Romine *et al.* (1997) have also identified a series of further sequence boundaries. Figure 1.5 shows the Aptian to late Miocene section of the 'Cretaceous-Tertiary Megasequence' of Romine *et al.* (1997), the constituent 'supersequences' and the identified internal sequence boundaries.

Westphal and Aigner (1997) initially used seismic termination patterns to define stratal boundaries for Triassic to Recent section of the Barrow-Dampier Sub-basins and related these to lithostratigraphic formations defined in selected wells. These were then defined as sequence boundaries and a systems tract interpretation was then attempted on the intervening formations in the wells. In taking this approach, they have found it problematic to define various systems tracts for many of the sequences as they made the critical mistake of assuming that formations are time equivalent, which is not the case. They have also found it difficult to define an age for their sequence boundaries, as the boundary between formations is commonly diachronous. The age of the 13 sequence boundaries that have been defined for the Triassic to the Recent section all correspond to formation boundaries as can be clearly seen in Figure 1.6. Of the six events that were defined for the Albian to Recent section, all have been identified by Romine *et al.* (1997) (Figure 1.5).

Intra Valanginian – mid-Aptian

Romine *et al.* (1997) defined 'Supersequence 1' as a transgressive-regressive package bounded by an intra-Valanginian sequence boundary at its base and a mid-Aptian sequence boundary at its top. As previously mentioned, the intra-Valanginian sequence boundary has been related to the break-up of India and Australia; the mid-Aptian sequence boundary has been related to a ridge jump in the developing Indian Ocean (Romine *et al.*, 1997). 'Supersequence 1' begins with a period of lowstand fan and delta deposition in front of the Barrow Delta shelf margin with associated incision of the Barrow Delta. Thermal subsidence and rising relative sea level combined to end the period of lowstand deposition and resulted in the deposition of mid-Cretaceous transgressive, back-stepping marine claystones (represented in places by the Muderong Shale), which are punctuated by regressive, shallow marine glauconitic sandstones (represented in places by the Mardie and "M. australis sands") (Jablonski, 1997). The maximum transgression of this 'supersequence' occurred during the deposition of the uppermost M. australis or A. cinctum biozones, associated with the highest rates of tectonic subsidence (Romine *et al.*, 1997). Fine-grained deposition continued until the mid-Aptian sea level fall which marked the end of 'Supersequence 1'.

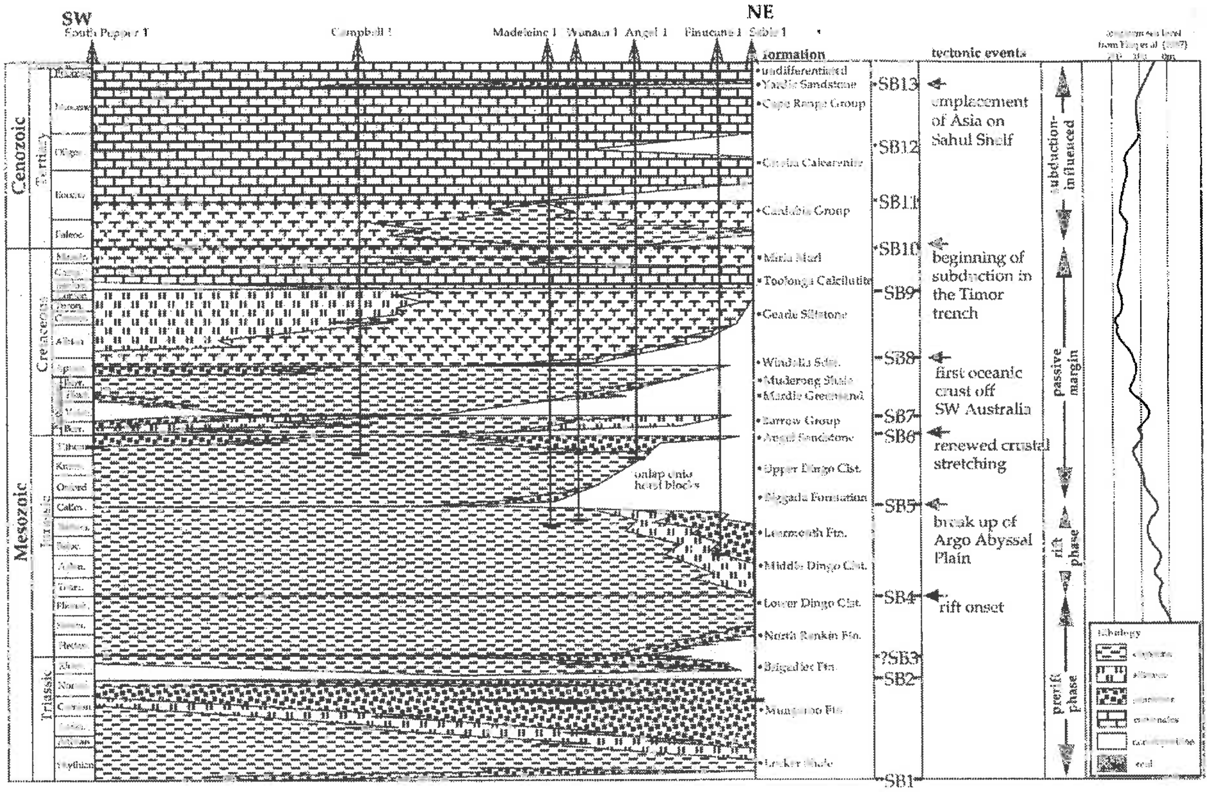

Figure 1.6 Generalised stratigraphy and sequence boundaries for the Triassic – Recent section of the Barrow-Dampier Sub-basin (Westphal and Aigner, 1997).

Mid Aptian to early Campanian

Associated with the mid-Aptian sequence boundary, which marks the base of Romine *et al.*'s 'Supersequence 2', was a basinward shift in facies that resulted in the proximal deposition of the Windalia Sandstone. Relative sea level continued to rise and by Albian times the underlying Jurassic rift topography had been infilled and free oceanic circulation had begun in the basin (Jablonski, 1997). Romine *et al.* (1997) have defined a base Albian event, which is a regional seismic downlap event, where Albian and younger sequences downlap the basal Albian sequences. This places their event slightly above the Albian-Aptian boundary, not directly on it. Westphal and Aigner have placed their basal Albian event on the Albian-Aptian boundary, which they defined as 'the seismic onlap of the Albian Gearle Siltstone on to the Barremian–Aptian Muderong Shale'. The seismic database they had access to was not sufficient to resolve the distribution of the Aptian Windalia Sandstone nor the presence of the basal Albian Windalia Radiolarite, so some uncertainty must exist with the age of their event. Relative sea level continued to rise during the Albian to Turonian and upwelling, nutrient enrichment from the free oceanic circulation and a decreased influx of terrigenous material combined to produce siliceous and calcareous biogeneic sediments (represented in places by the Windalia Radiolarite, Gearle Siltstone and Haycock Marl). Romine *et al.* (1997) have identified a Turonian (C4/C5) relative sea level fall, which they have interpreted to be related to a major shift in spreading centre as India began to drift to the northwest and break-up was initiated between Antarctica and Australia. This Turonian sea level fall had considerable associated submarine erosion before fine-grained calcareous and then carbonate deposition resumed in the basin (represented in places by the Haycock Marl and Toolonga Calcilutite). This Turonian sea level fall is not identified in the study by Westphal and Aigner (1997) (Figure 1.5).

An early Santonian (C8) sequence boundary was identified in the study by Westphal and Aigner (1997). Romine *et al.* (1997) also note the presence of an early Santonian (base C8) sequence boundary on one of their figures but it is not discussed in the text and as such the perceived importance of this event is unclear. An early Campanian unconformity and sequence boundary (C9) at the top of the fine grained carbonate sedimentation marks the end of 'Supersequence 2' and the transgressive phase of the 'Cretaceous-Tertiary Megasequence' of Romine *et al.* (1997). This early Campanian sequence boundary has not been identified by Westphal and Aigner (1997) as illustrated in Figure 1.5.

Early Campanian to mid-Oligocene

The early Campanian sequence boundary forms the base to 'Supersequence 3' of Romine *et al.* (1997) which is the first of the two regressive supersequences of the 'Cretaceous-Tertiary Megasequence'. Following the maximum transgression in the late Cretaceous, only hemipelagic and pelagic deposition occurred in the Northern Carnarvon Basin, as shoreline sedimentation was located on the craton to the east. The shorelines of sequences deposited in 'Supersequence 3' subsequently prograded basinward from their maximum landward position and the sequences are characterised largely by prograding siliciclastic wedges, punctuated by transgressive, fine-grained calcilutites and calcareous shales (Romine *et al.*, 1997). Each sequence boundary is interpreted to develop during a maximum regression associated with a fall in eustasy. Romine *et al.* (1997) have identified sequence boundaries of Maastrichtian, base Tertiary, late Paleocene and early middle Eocene age within 'Supersequence 3'.

The Maastrichtian event has not been identified by Westphal and Aigner (1997) and is below the study interval of Apthorpe (1988). A base Tertiary sequence boundary has been identified in all three studies (Apthorpe, 1988; Romine *et al.*, 1997; Westphal and Aigner, 1997) but the age of the event is somewhat uncertain as the basal Tertiary Danian section has no defined foraminiferal zones for this section of the North West Shelf (Figure 1.5). Apthorpe (1988) has subdivided the Paleocene and Eocene section of the Northern Carnarvon Basin into 'Cycle 1' and 'Cycle 2'. 'Cycle 1' has been subdivided into an early Paleocene (T1-T3) section termed 'Cycle 1A' and an end early Paleocene (T3/T4) to Middle Eocene (T10) section, termed 'Cycle 1B'. The reason for this subdivision is rather unclear and it appears to be an arbitrary subdivision based on lithology and the spatial distribution of sediments rather than on a geological event. The early Paleocene 'Cycle 1A' is characterised by sands and claystones, which are restricted to a region inshore of the Rankin Trend with only thin calcareous claystones are found in further offshore areas on the Rankin Platform. Within Apthorpe's 'Cycle 1B' a submarine disconformity of T7 age separates the late Paleocene (T5-T6) sediments from the early Eocene (T7 - T8) sediments. Romine *et al.* (1997) also identify a late Paleocene event but in their study it has been dated at base of biozone T6. Once again this event is only indicated on a figure and is not discussed in the text. Late Paleocene sediments are represented by calcareous claystones, which are interpreted to represent the maximum extent of a marine transgression whilst early Eocene sediments are typified by warm water sub-tropical facies (Apthorpe, 1988). During the early Eocene (T9), a rapid cooling in oceanic temperatures has been interpreted from faunal assemblages. This was accompanied by an increase in continental runoff resulting in sediments of T9-T10 age being more silt-rich (Apthorpe, 1988).

An early–middle Eocene event has been identified in all three studies and this forms the top to Apthorpe's 'Cycle 1'. Apthorpe (1988) has defined this event to be of T10-T11 age; Romine *et al.* (1997) have defined it to be of low T10 age and Westphal and Aigner (1997) have defined it to be 'at the boundary of the Giralia Calcarenite and underlying Cardabia Group'. Figure 1.5 shows the significant duration on the boundary of these two formations and demonstrates problems associated with dating the boundary SB11 that has been defined using formation names. The subsequent middle Eocene (T10/T11) siltstones and calcisiltites to late Eocene (T14) cherty calcilutites have been classified as 'Cycle 2' by Apthorpe. 'Cycle 2' marks the transition from an essentially clastic to carbonate-dominated regime in the Northern Carnarvon Basin (Apthorpe, 1988). Apthorpe also makes suggestions of further disconformities of T12/T13 and late Eocene (T14) age but neither of these have been identified by the other two sets of workers. The end of Apthorpe's 'Cycle 2' and Romine *et al.*'s 'Supersequence 3' is represented by the base Oligocene unconformity and sequence boundary. As discussed in section 1.3.2, the base Oligocene event is interpreted as being associated with the final break-up of the Australian and Antarctic continents south of Tasmanian. The establishment of the circum-polar current and isolation of the Antarctica at the south pole restricted ice sheets to the Antarctic landmass and caused an associated global fall in sea level (Romine *et al.*, 1997). Australia now moved rapidly northwards to lower latitudes, which were ideal for the development of carbonate margins.

Base Oligocene – late Miocene

A regional hiatus is recorded across the basin at the end of the Eocene to early Oligocene and this has been identified in all three studies. Both Apthorpe (1988) and Romine *et al.* (1997) recognise this event as a significant event which forms the boundary between Apthorpe's 'Cycle 2' and 'Cycle3' and Romine *et al.*'s 'Supersequence 3' and 'Supersequence 4'. However, Apthorpe (1988) places the base of the subsequent 'Cycle 3' at the base of the T16 biozone and Romine *et al.* (1997) place the base of the subsequent 'Supersequence 4' at the base of the T17 biozone. Westphal and Aigner (1997) also identify an SB12 event of this age 'which separates the Oligocene-Miocene Cape Range Group from the Eocene-Oligocene Giralia Calcarenite'. Due to the extremely diachronous nature of the base of the Cape Range Group, it is again problematic to assign an accurate age to an event defined using formation names.

Following the base Oligocene unconformity associated with the final break-up of Australia and Antarctica, sedimentation resumed in the late Oligocene as a large progradational carbonate wedge. Sedimentation continued until the late Miocene when Australia collided with Southeast Asia. The sediments deposited between these two unconformities constitute Apthorpe's 'Cycle 3' and Romine *et al.*'s 'Supersequence 4'. Apthorpe further subdivided these sediments into 'Cycle 3A' and 'Cycle 3B' on the basis of a large, widespread, seismically mappable, erosion event of Burdigalian (N7) age. 'Cycle 3A' encompasses sediment of Aquitanian to Burdigalian age (N1-N7), and foraminiferal evidence from the base of the sequence indicates there was a water depth of several hundred metres during the building of this carbonate wedge (Apthorpe, 1988). Deposition of 'Cycle 3B' began with widespread marly limestones of Burdigalian to Langhian age (N8-N9) which are interpreted to have formed in relatively deep water corresponding to an eustatic sea level high. Above these marly limestones, the section grades into calcarenites with entirely benthic faunas deposited in response to the shelf building vertically and filling accommodation space created by the relative sea level high (Apthorpe, 1988).

Within 'Supersequence 4' Romine *et al.* (1997) have identified other sequence boundaries of late Oligocene, early Miocene, mid-Miocene A, mid-Miocene B, and late mid-Miocene age (Figure 1.5). They have also identified a mid-Miocene barrier reef system which prograded basinward between the mid-Miocene B and the late mid-Miocene sequence boundaries. Well data also indicate the presence of siliciclastics in the section, the origins of which are unclear but have been attributed to lowstand fans onlapping carbonate margins (Romine *et al.*, 1997).

Late Miocene to Recent

The late Miocene unconformity associated with the collision of Australia and Southeast Asia has been identified as a major boundary in all three studies. It forms the uppermost boundary of 'Supersequence 4' and the 'Cretaceous-Tertiary Megasequence' and has been dated to occur in the Messinian N17 biozone in the study by Romine *et al.* (1997). The late Miocene unconformity marks the boundary between 'Cycle 3' and 'Cycle 4' in the study by Apthorpe (1988). However, in this study the age of the boundary is poorly constrained and believed to be strongly diachronous, ranging from mid-Serravallian (N14) to Pleistocene (N22) in age (Apthorpe, 1988). Westphal and Aigner (1997) have identified the presence of the late Miocene unconformity which separates "unnamed carbonates and their basal sandstone unit from the underlying calcareous Cape Range Group". The event was dated as middle to upper Miocene in that study, as once again absence of biostratigraphic data precluded accurate dating of the event.

Apthorpe (1988) has attributed the formation of 'Cycle 4' to flexure of the North West Shelf in response to the collision of Australia and Southeast Asia. Sediments of 'Cycle 4' are characterised by poorly sorted carbonates in which bioclastic fragments are enclosed in a matrix of silt to mud-sized carbonates and form a large progradational wedge termed the 'Brigadier Wedge'. Foraminiferal evidence indicates this wedge commenced deposition in around 1400 m of water and ended with a water depth around 600 m (Apthorpe, 1988). The collision-influenced section is considerably less understood and documented, partly due to a lack of samples from the section.

1.3.5 Present day sedimentation on the North West Shelf

By Oligocene times, the North West Shelf had subsided considerably and deep-water pelagic carbonates were deposited on the outer margin of the north west shelf. However, nearer to land, the productivity of calcareous organisms was considerably higher and prograding wedges of shelf carbonate built outward into deeper water (Exon and Colwell, 1994). In the deep water, the combined thickness of the Oligocene to Recent sediments is no more than 600 m thick whilst on the shelf the prograding Oligocene to Recent carbonates are usually in the order of 1000-2000 m thick (Exon and Colwell, 1994). This pronounced thickness variation caused by the differing origins of the carbonate sediment has controlled the morphology of the shelf since the initiation of the strongly prograding carbonates at the base of the Oligocene as demonstrated in Figure 1.7. The Ocean Drilling Program (ODP) sites on the Exmouth and Wombat Plateaus (Figure 1.8) are basinward of the strongly prograding carbonate section of the North West Shelf and record 580 m and 180 m of Cainozoic section respectively (Exon and von Rad, 1994). Composite logs for these ODP sites show the Cainozoic sediments to be characterised by fine-grained pelagic carbonates with variable foraminiferal content (Figure 1.9).

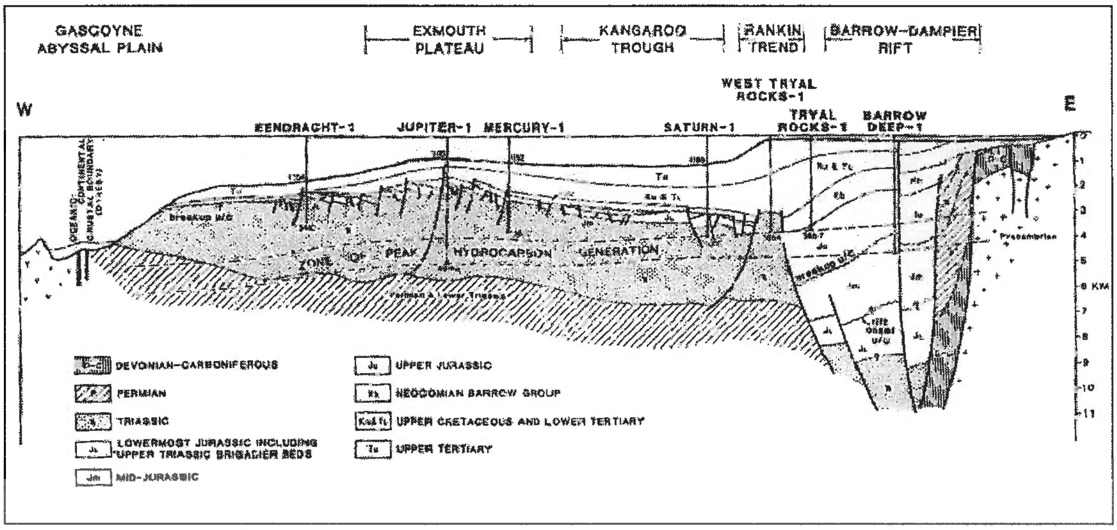

Figure 1.7 West-east cross section from Gascoyne Abyssal Plain to Barrow-Dampier rift (modified after Barber, 1988).

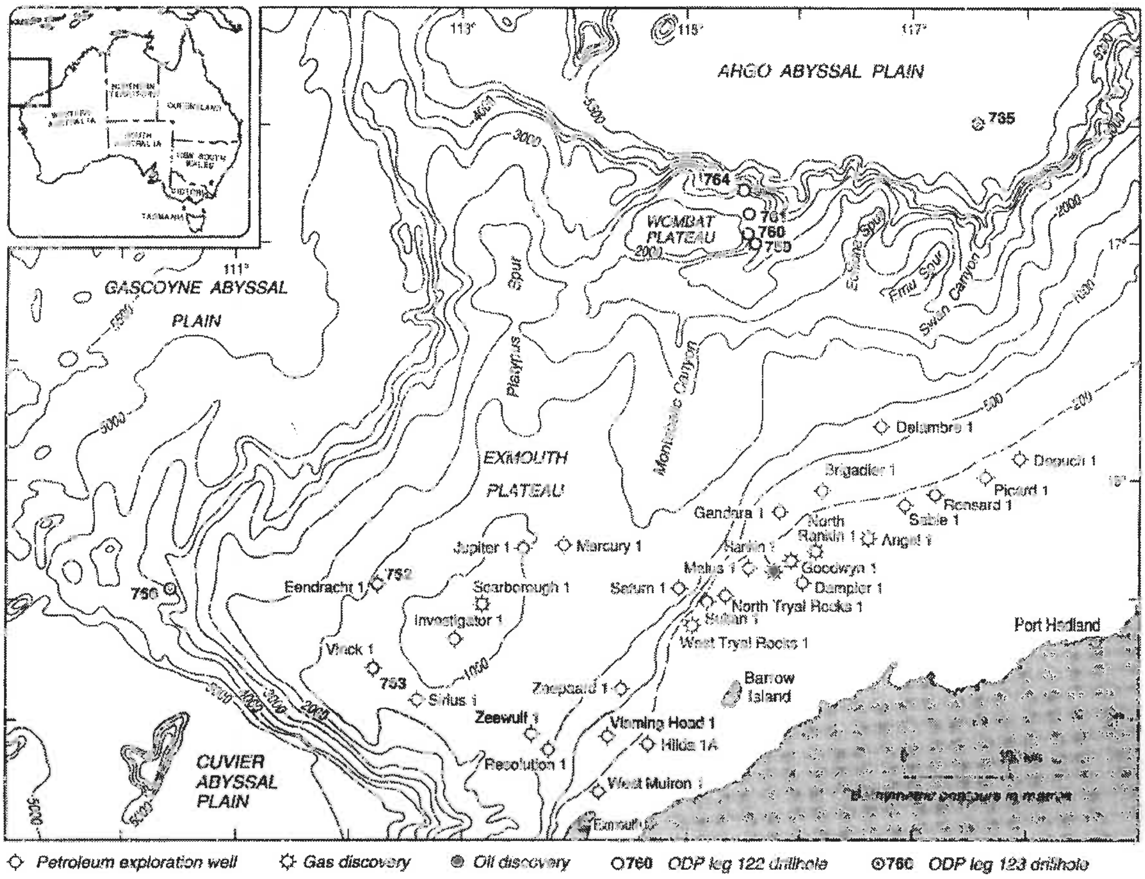

Figure 1.8 Bathymetric map of the Exmouth Plateau showing ODP sites and selected petroleum exploration wells (Exon and von Rad, 1994).

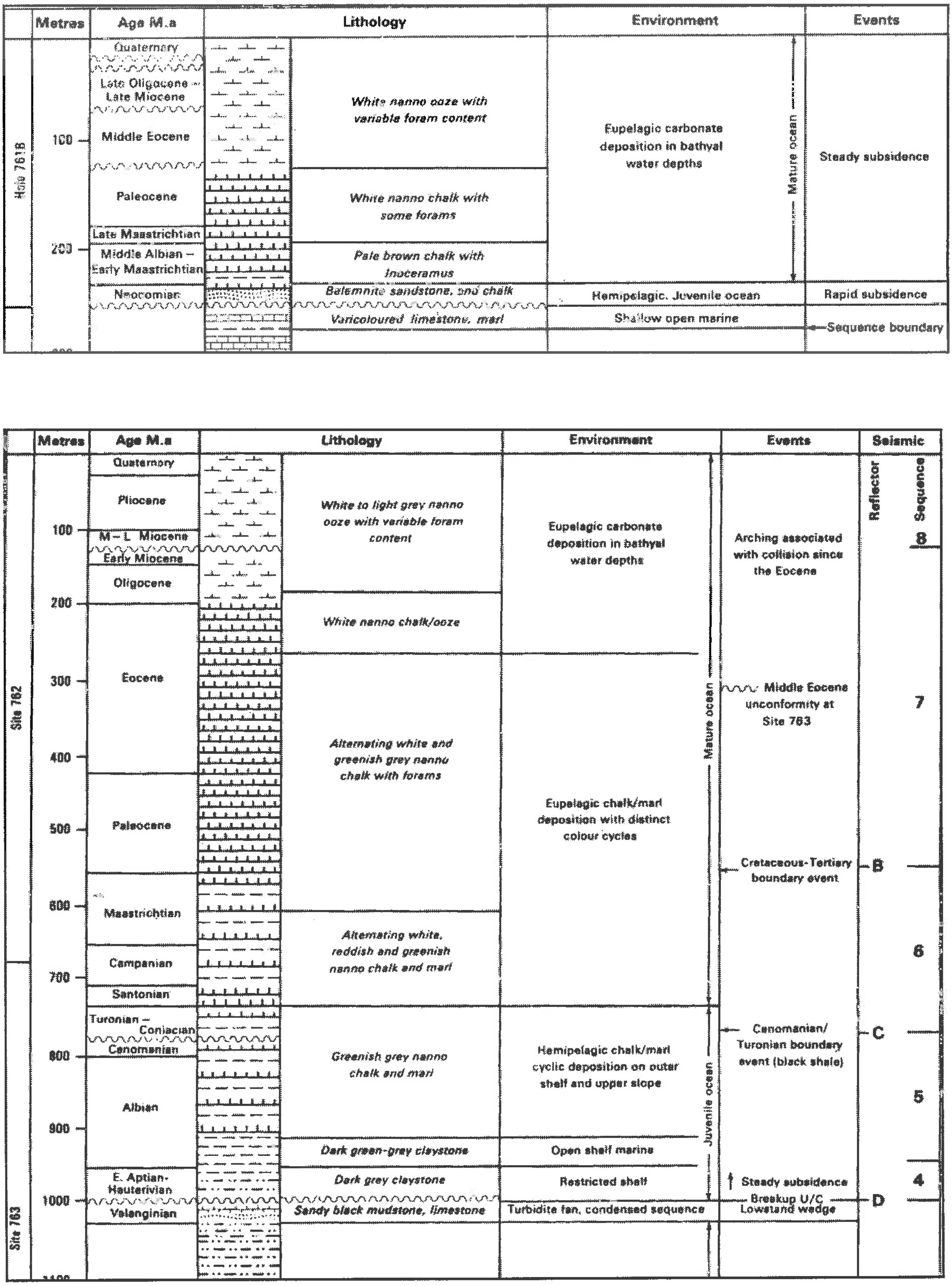

Figure 1.9 Composite lithological log of Exmouth Plateau ODP sites 762 & 763 and Wombat Plateau ODP site 761 (Exon and von Rad, 1994).

The present day North West Shelf is a high energy, tide-dominated non-rimmed carbonate margin (Dix, 1989). The margin is formed by a 20 km wide shallow inner shelf situated shoreward of the regional 10 m isobath on which a series of islands, coral and algal reefs and inter-tidal to shallow-subtidal rock platforms can be identified. Along the shelf margin (200 m), or seaward of the continental shelf, few such features can be identified as demonstrated in Figure 1.10. The daily wind pattern for the Onslow area of the North West Shelf (Figure 1.10) is bimodal (Commonwealth Bureau of Meteorology, 1972). Wind roses for 0900 hrs and 1500 hrs (Figure 1.11) demonstrate morning winds to be typically easterly and south easterly in direction whilst afternoon winds are stronger and predominantly westerly and northwesterly in direction (Dix, 1989). The North West Shelf has a tidal range which ranges from microtidal (<2 m) at the Exmouth Gulf to macrotidal (+10 m) north of Broome. In the area of the Dampier Sub-basin tides are commonly 3-4 m in height (Holloway, 1983).

In an environmental study of the dispersal patterns of hydrocarbons discharged during the drilling operations at the North Rankin A platform, Chegwidden *et al.* (1993) sampled hydrocarbon concentrations in seabed sediments surrounding the platform. Samples were recorded along two axes, one which was parallel to the predominant current direction and the other which was perpendicular to it. The predominant current direction was derived from a combination of 1363 days of current speed and direction data measured prior to 1988 and from current speed and direction information for the 12 months preceding the 29th February 1992. This analysis suggested that prevailing current direction was perpendicular to the coast in a northwest - southeast direction as shown by the rose diagram in Figure 1.12. The study showed that the transition between contaminated and non-contaminated sediments was between one and several kilometres in the current direction and over two hundred metres perpendicular to the current direction. The results of this study imply that sediment transport on the North West Shelf is predominantly perpendicular to the coast and relatively minor parallel to the coast.

Along the inner shelf, coarse-grained sands and gravels are deposited on the subtidal and intertidal rock platforms. Fleshy algae are abundant on these sand-covered platforms and on relict coral reef frameworks. Supratidal to subtidal sediments are composed of skeletal (molluscs, foraminifera, bryozoans, corals, calcareous red algae) and rock fragments (derived from rock platforms) (Dix, 1989). Calcareous chlorophytes (*Penicillus* and *Halimeda*) are not important sediment contributors (Dix, 1989). The mud content of the inner shelf facies is generally low <3 weight %. Dix (1989) has interpreted the high-energy nearshore setting of the Onslow area to be a result of the absence of shelf margin combined with large tidal ranges of 2-4m. This combination allows the relatively unimpeded transport of large volumes of water to and from the inner shelf region twice daily. The environment thus exists for significant carbonate production on the inner shelf caused by the continuous recharge of seawater and the subsequent off-bank transport of this sediment by a combination of tidal currents and winds. The studies by Dix (1989) and Chegwidden *et al.* (1993) have both shown the predominant current and wind direction to be perpendicular to the coastline.

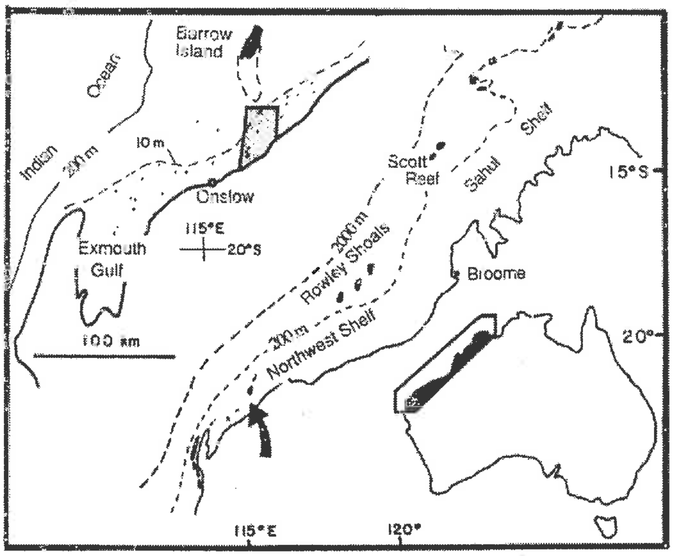

Figure 1.10 Map of the North West Shelf of Australia showing numerous islands, reefs and rock platforms on the inner shelf with only a few on the shelf margin or seaward of the continental shelf (Dix, 1989).

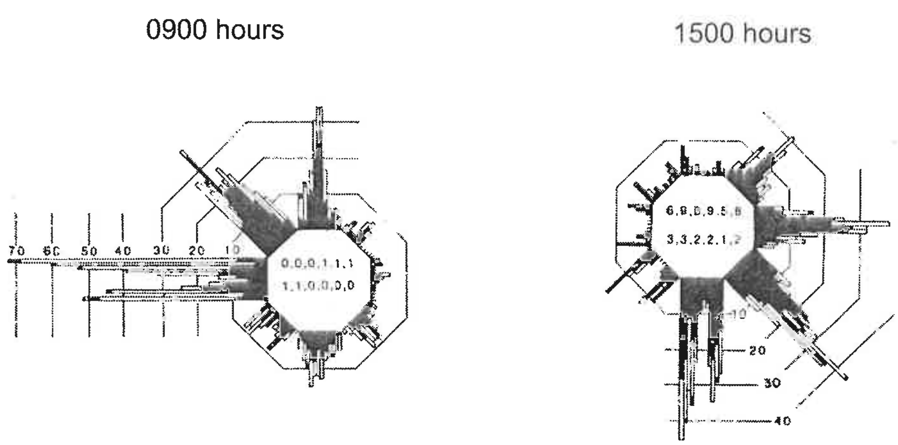

Wind roses for 0900 and 1500 hours for the Onslow area of the North West Shelf compiled from the Commonwealth Bureau of Meteorology (1972) as presented in Dix, (1989). The monthly wind directions (octagon faces) are represented by columns (January to December clockwise): inner black £ 18 km/h; white 18-36 km/h; outer black >36 km/h. Expanded octagon outlines indicate wind frequency (%) and numbers within the octagons refer to the number of calm days per month.

Figure 1.11 Rose diagram showing monthly wind directions the Onslow area of the North West Shelf (Dix, 1989)

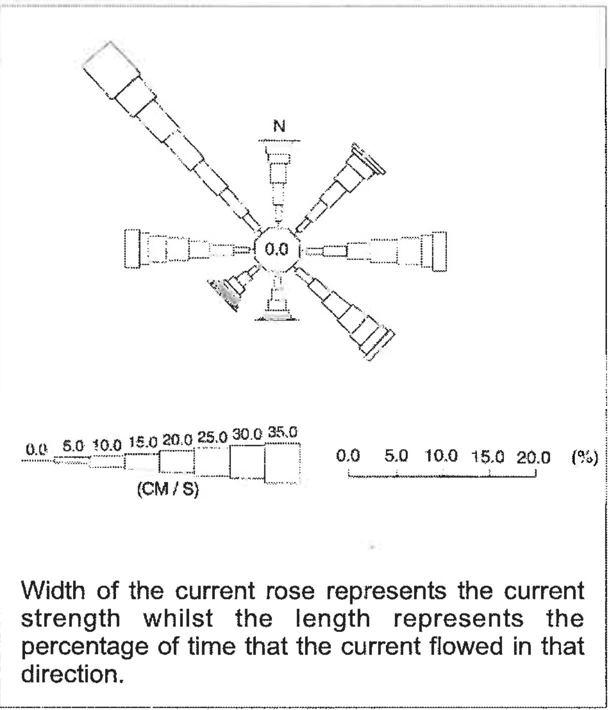

Figure 1.12 Rose diagram showing the prevailing current direction at the North Rankin 'A' platform (width represents current strength while length represents the percentage of time that the current flowed in that direction).

It can be concluded that there are two present day mechanisms for carbonate deposition on the North West Shelf which combine to produce the observed seismic geometries (Figure 1.7). Carbonate production occurs in shallow nearshore high-energy environments producing coarse grained sediments, which are deposited in the nearshore environment, and fine grained sediment, which is transported offshore by a combination of tidal currents and wind. This off-bank transport of carbonate lithologies produces the characteristic progradational geometries as observed on seismic. Carbonate sedimentation on the North West Shelf also exists as a foraminiferal pelagic rain. In areas basinward of the slope break of the progradational clinoforms, only the pelagic carbonates are deposited and they form a blanket of carbonate sediment of constant thickness. From the observed seismic geometries, it is clear that the shallow marine nearshore carbonates are volumetrically more significant and therefore produced at much greater rates than the deepwater pelagic carbonates.

CHAPTER 2 CARBONATE SEQUENCE STRATIGRAPHY - CONCEPTS AND PRINCIPLES

2.1 Sequence stratigraphy

In the late 1960's, Peter Vail and several co-workers at Exxon Production Research Company began to recognise unconformity-bound sequences on panels of seismic. By tying the seismic reflections to wells across a basin, Vail found that a single reflection, which is formed as a result of the contrast in acoustic impedance between two units, could be associated with differing lithologies at the basin margin and basin centre. He conjectured that seismic reflectors may represent time equivalent or chronostratigraphic surfaces. Prior to this, seismic reflections were considered to be lithology or lithostratigraphic boundaries. Detailed analysis of well data showed this to be incorrect. Exxon further developed these ideas through detailed outcrop studies complemented by well and seismic data. The ideas were first published in 1977 as AAPG Memoir No 26, entitled Seismic Stratigraphy - Applications to Hydrocarbon Exploration (Payton, 1977). Exxon and a small number of universities further developed these ideas in the late 1970's to mid 1980's. This phase of work was published in 1988 as SEPM Special Publication No. 42, entitled 'Sea-level Changes - An Integrated Approach' (Wilgus *et al.*, 1988). Texts by Van Wagoner *et al.* (1990) and Emery and Myers (1996) provide a good synthesis of the techniques and models as they now stand.

2.1.1 Sequence stratigraphic principles

Sequence stratigraphy is a predictive tool which describes the stratal architecture of sediments deposited in response to changes in relative sea level. Differentiating the individual contributing factors that cause changes in relative sea level is not a trivial problem, as many of the causative mechanisms will give similar resulting sediment geometries. The tectonic regime in which the sediments are being deposited also has a significant bearing on the nature of sediment deposition. For example, sediments deposited in a rift setting will have a much stronger 'tectonic signature' than sediments deposited on a passive margin. As a result, some workers have proposed a different terminology for sequences developed in rift settings as compared to those developed on passive margins (Prosser, 1993). Many workers have related stratal architecture of sediments to the interplay of three main variables interact to control sequence development: eustatic sea level changes; subsidence rate and sediment supply (Curray, 1964; Hardenbol *et al.*, 1981; Krumbein and Sloss, 1963). These factors have been summarised by Galloway (1989) and presented in Figure 2.1. Within the eustatic component of the control on sequence deposition three separate types of eustasy have been defined as glacial, tectonic and geoidal. Glacial eustasy results from the changing volumes of continental ice caps whilst tectonic eustasy results from changes in ocean volume by large scale lithospheric plate interactions. Galloway (1989) describes the geoid as the equipotential surface of the combined rotational and gravitational potential fields which corresponds to mean geodetic sea level. This surface has been shown to vary from an ideal mathematical surface by several tens of metres.

Changes in relative sea level, be they 'local' tectonic or eustatic in origin, control the space available for sediment deposition. This is termed 'accommodation space' (Jervey, 1988). The interplay between relative sea level changes and sediment supply therefore controls the geometry of the sequences deposited within the accommodation space (Galloway, 1989). Where sediment supply is greater than the rise in relative sea level, accommodation space is progressively filled from the landward direction and the section progrades. Where the sediment supply rate increases at the same rate as accommodation space the sediments build vertically and aggrade and when sediment supply rate is less than the rise of relative sea level the sediments move landward and retrograde. Figure 2.2 shows progradational, aggradational and retrogradational stratigraphic architectures and the variables that control their formation. Change in any three of the variables can potentially develop the same stratigraphic architecture (Galloway, 1989).

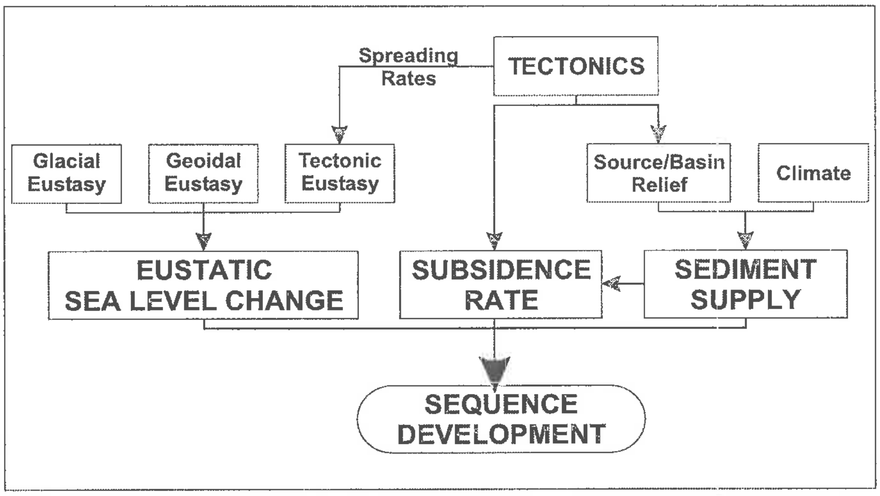

Figure 2.1 Variables that influence depositional history and sequence stratigraphy of prograding basin margins (Galloway, 1989).

2.1.2 The Exxon sequence stratigraphic model

Mitchum (1977a) published a model of basin development which sought to link stratigraphic architecture with rates of change in relative sea level. The sedimentary package was subdivided on the basis of depositional units that were deposited under similar rates of change and direction (rising or falling) of relative sea level conditions. The strength of this model is that it provided a predictive framework in which to interpret basin architecture. This model has since been referred to in the literature as the Exxon sequence stratigraphic model. Sediments deposited under similar direction and rate of change of relative sea level are known as a systems tract. A systems tract has been defined as a linkage of contemporaneous depositional systems, where a depositional system is a three dimensional assemblage of lithofacies, genetically linked by active or inferred processes and environments (Brown and Fisher, 1977). The Exxon model subdivides the sediments into three systems tracts (lowstand, transgressive and highstand) based on location with respect to the relative sea level curve. The Exxon model identifies Type I and Type II sequences based on the magnitude of the relative sea level fall and associated shelf top erosion and is summarised below (Figure 2.2).

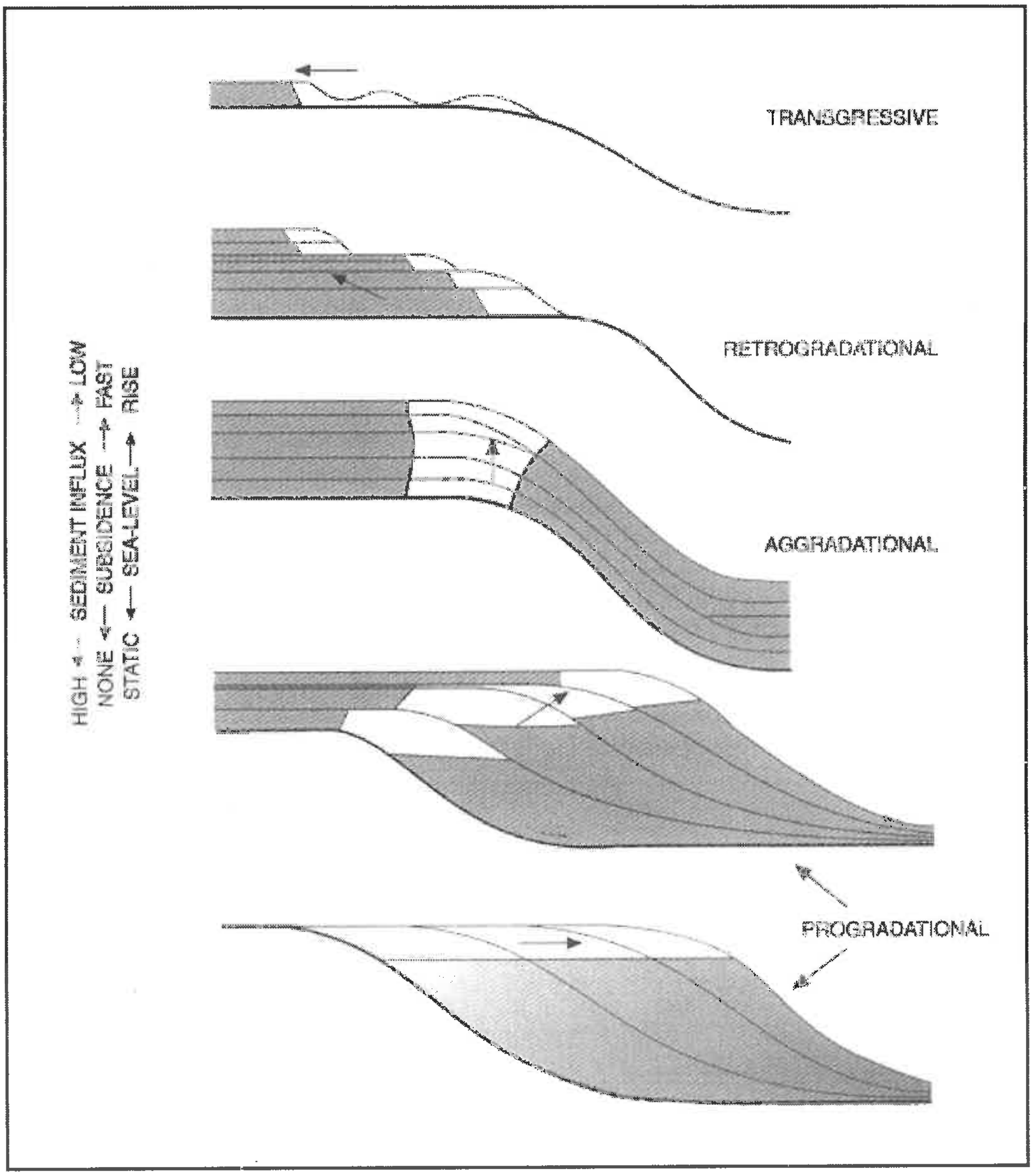

Figure 2.2 Progradational, aggradational and retrogradational stacking patterns (Galloway, 1989).

In a Type I sequence, when relative sea level falls beyond the previous shelf break and exposes the previous shelf top, accommodation space moves basinward causing the locus of sediment deposition to also shift basinwards. Simultaneously, rivers which feed the basin, incise the shelf top and erode the underlying sediments and form what are called 'incised valleys' (Figure 2.3a). Sediments deposited at this stage are termed the 'lowstand systems tract'. In the early stages of the lowstand systems tract when relative sea level is falling, accommodation space migrates basinwards, and the sedimentation style is characterised by large-scale slope failures resulting in slope bypass and deposition of submarine fans. As the rate of relative sea level fall decreases towards zero at the lowest point of the relative sea level curve, accommodation space begins to be created again and a lowstand progradational package forms. This package is characterised by upward-thickening beds and bed sets, which result from an increasing rate of accommodation space creation due to an increasing rate of relative sea level rise. As the rate of relative sea level rise increases further, the exposed shelf is transgressed causing the incised valleys to be backfilled and the shelf to flood. More accommodation space is available proximally and sediments deposited are restricted to the proximal edge of the basin. Sediments deposited at this stage form the 'transgressive systems tract' and are commonly seen to have similar topset thicknesses. At the point of maximum rate of sea level rise (the inflection point on the rising limb of the sea level curve) and maximum landward transgression a surface called the maximum flooding surface is formed. At this time basinal localities are starved of sediment and a 'condensed section' of pelagic anoxic sediments may be formed, (Figure 2.3b) (Loutit *et al.*, 1988). Following the maximum flooding surface, relative sea level continues to rise but at a rate which decreases towards zero at the top of the relative sea level curve. Sediments deposited are commonly seen to be initially aggradational and later progradational in nature due to the migrating locus of accommodation space from shelf top to slope in response to the slowing of relative sea level rise. Sediments deposited on this limb of the relative sea level curve are termed 'highstand systems tract' and have characteristically upward-thinning beds and bed sets (Figure 2.3c). A subsequent sea level fall exposes the shelf, which becomes subject to sub-aerial erosion and incision by fluvial systems. This exposure surface and its basinward expression are termed the 'sequence boundary'.

The Type II sequence differs from a Type I sequence in that, when relative sea level falls, it only falls over the proximal area of the highstand topsets without falling beyond the previous offlap break as it does in Type I sequence. The result is the formation of a sequence boundary that may cut into the previous topsets but has no associated slope incision or submarine fan deposition. The systems tract that follows a Type II relative sea level fall is termed the shelf margin systems tract. It is initially progradational in nature and evolves to a more aggradational nature as a result of an increase in the rate of accommodation space being created on the rising limb of the sea level curve. The shelf margin systems tract, like the Type I prograding lowstand systems tract, will have upward-thickening beds and bed sets in response to the increasing rate of accommodation space creation. The shelf margin systems tract passes into the retrogradational transgressive systems tract and subsequent highstand systems tract; these are the same for both Type I and Type II sequences (Figure 2.4).

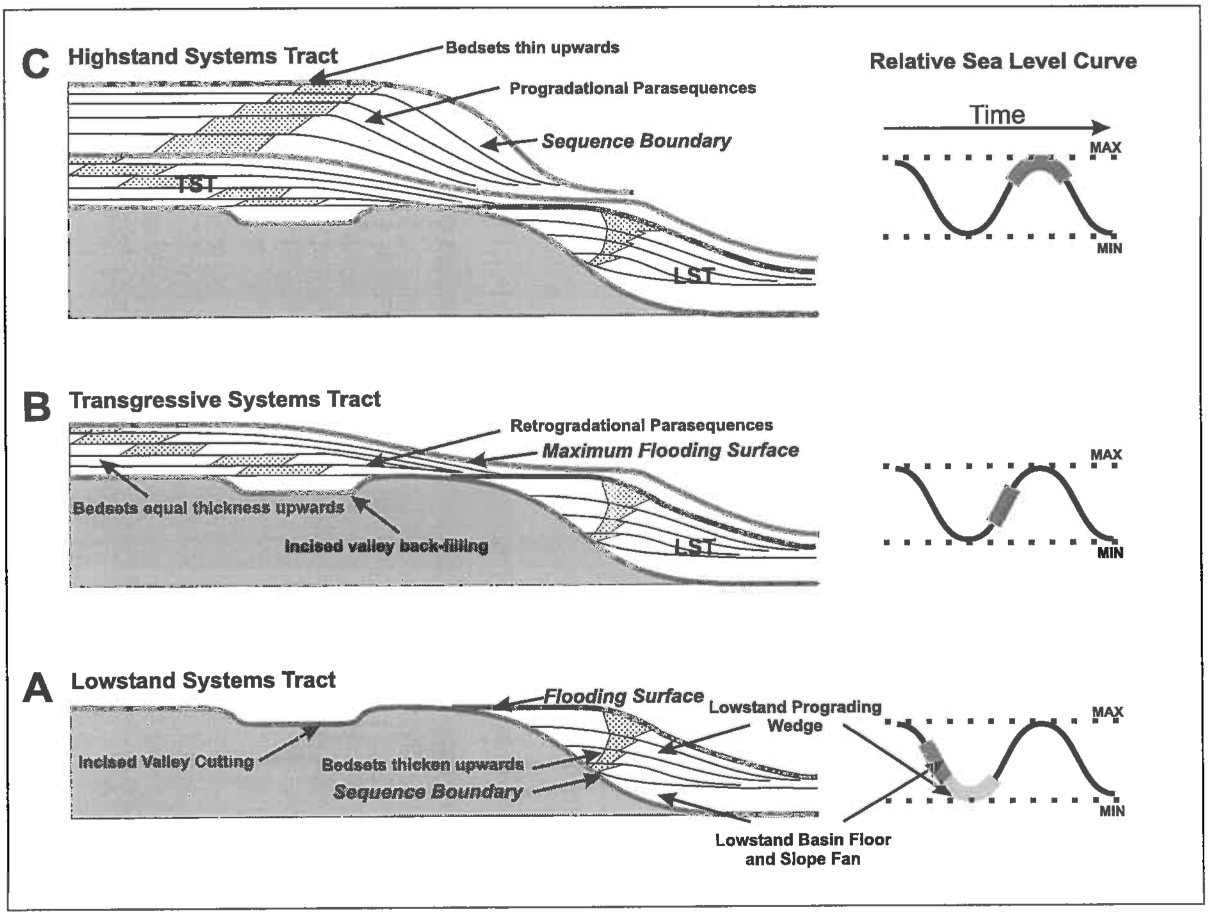

Figure 2.3 Stratigraphic architecture resulting from one complete cycle of relative sea level rise and fall.

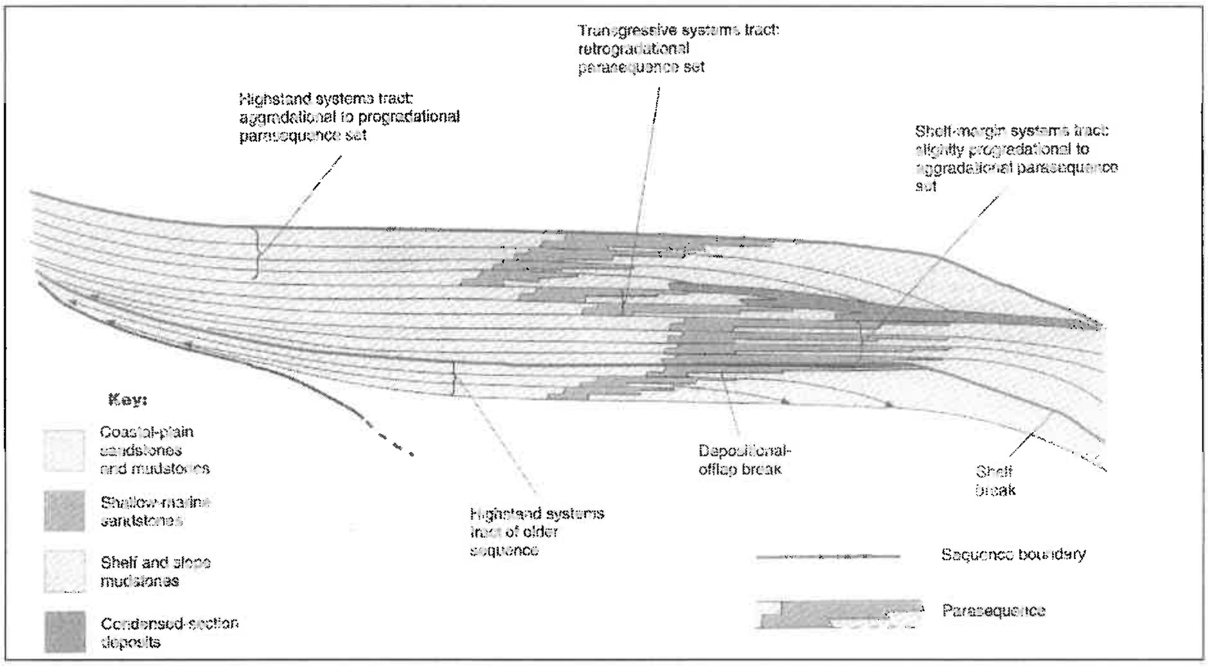

Figure 2.4 Stratal architecture for a Type 2 sequence (Myers and Milton, (1996) after Van Wagoner et al.,(1988)).

2.2 Carbonate sequence stratigraphic models

The principles of sequence stratigraphy that were initially published as AAPG Memoir No 26, entitled Seismic Stratigraphy - Applications to Hydrocarbon Exploration (Payton, 1977) were developed within the siliciclastic regime. During the mid 1970s to late 1980s a considerable amount of literature was published on the controls on carbonate platform morphology and the close interaction with changes in relative sea level (Ahr, 1973; Buxton and Pedley, 1989; Droxler and Schlager, 1985; Harwood and Towers, 1988; Hine and Neumann, 1977; Kendall and Schlager, 1981; McIlreath and James, 1984; Neumann and MacIntyre, 1985; Read, 1982, 1985; Schlager, 1981; Schlager and Camber, 1986; Tucker, 1985; Wilber *et al.*, 1988; Wilson, 1975). However, it was not until the second seminal publication on sequence stratigraphy - SEPM Special Publication No. 42, entitled 'Sea-level Changes - An Integrated Approach' (Wilgus *et al.*, 1988) that these ideas were combined to form a sequence stratigraphic model for carbonate systems (Sarg, 1988). Within carbonate sequences, Sarg (1988) identified all the major sequence stratigraphic units, such as systems tracts, flooding surfaces and sequence boundaries that are recognised in the siliciclastic regime. Following this publication, the application of sequence stratigraphic principles to the carbonate regime has become more common-place (Burchette and Wright, 1992; Driscoll *et al.*, 1991; Glenn *et al.*, 1993; Grammer and Ginsburg, 1992; Jacquin *et al.*, 1991; Wilber *et al.*, 1990) and in 1993, AAPG Memoir 57 entitled 'Carbonate Sequence Stratigraphy – Recent Developments and Applications' (Loucks and Sarg, 1993) was published. This publication contains papers on carbonate sedimentation, carbonate sequence stratigraphic models and a series of outcrop and seismic-based sequence stratigraphic case studies.

In contrast to siliciclastic sequence stratigraphic literature, where numerous models have been proposed for differing geological settings (Galloway, 1989; Mitchum *et al.*, 1977a; Prosser, 1993; Van Wagoner *et al.*, 1988) carbonate sequence stratigraphic literature has adopted a process based approach in which the response of the various carbonate platform types to changes in relative sea level are discussed. As a result of this approach, the literature is not obscured by nomenclature and consequently models presented for the response of a carbonate platforms to changes in relative sea level have evolved consistently through the literature. For example, Sarg (1988) identified and characterised four possible types of systems tracts in the carbonate regime – lowstand, shelf margin (above a Type II boundary), transgressive and highstand and discussed the effects of rises and falls in relative sea level on facies belts within these systems tracts (Figure 2.5). Handford and Loucks (1993) further developed these ideas and produced a series of models which also combined the established static facies models of Ahr (1973), Wilson (1975) and (Read, 1982, 1985). These models investigated the response of facies belts on various types of carbonate platform to changes in relative sea level. Other authors have investigated the nature and controls of sedimentation throughout the various systems tracts. A summary of the current understanding of carbonate systems response to changes in relative sea level is outlined below.

2.2.1 Transgressive systems tracts

During the early stages of the transgressive systems tract, relative sea level begins to rise back up the slope and the shelf margin break migrates landward over the previous shelf break. As relative sea level continues to rise, the platform top becomes flooded, incised valley systems become backfilled and carbonate production is re-established. Handford and Loucks (1993) have proposed that transgressive systems tracts usually develop in three distinct phases. Firstly, the start-up phase is when carbonate production is re-established over the shelf top after being restricted to the slope during lowstand. During the start-up phase, carbonate accumulation lags behind the rise in relative sea level. The second phase is the catch-up phase, when sediment accumulation outpaces relative sea level rise and the margin builds to sea level. When established, carbonate margins can grow vertically at rates of up to 15 mka^{-1} (Wilber *et al.*, 1990). The third, keep-up phase of the transgressive systems tract is when sediment accumulation closely matches the rate of relative sea level rise and consequently the platform remains at or very close to sea level (Kendall and Schlager, 1981). This pattern of growth in response to relative sea level rise and creation of accommodation space is called the law of sigmoidal growth, (Neumann and MacIntyre, 1985) (Figure 2.6). The interplay between growth rates and relative sea level rise gives the characteristic retrogradational (start up) to aggradational (catch-up to keep-up) stacking geometry characteristic of transgressive systems tracts (Calvet *et al.*, 1990; Purdy and

Bertram, 1993). Transgressive systems tracts of this type have been identified in the Lincolnshire Limestone Formation of England (Emery and Dickson, 1991).

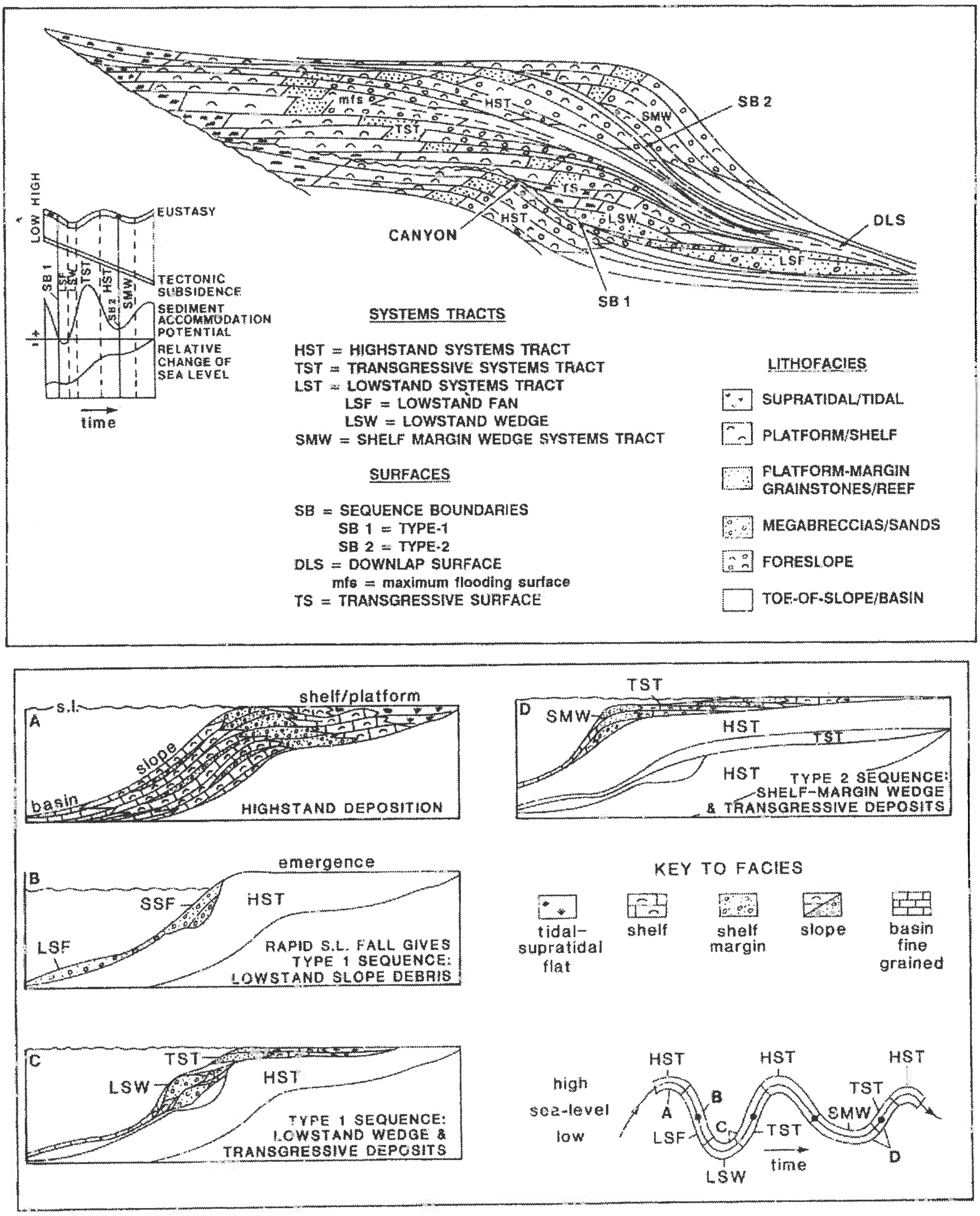

Figure 2.5 Sequence stratigraphic model for carbonate systems (Sarg, 1988).

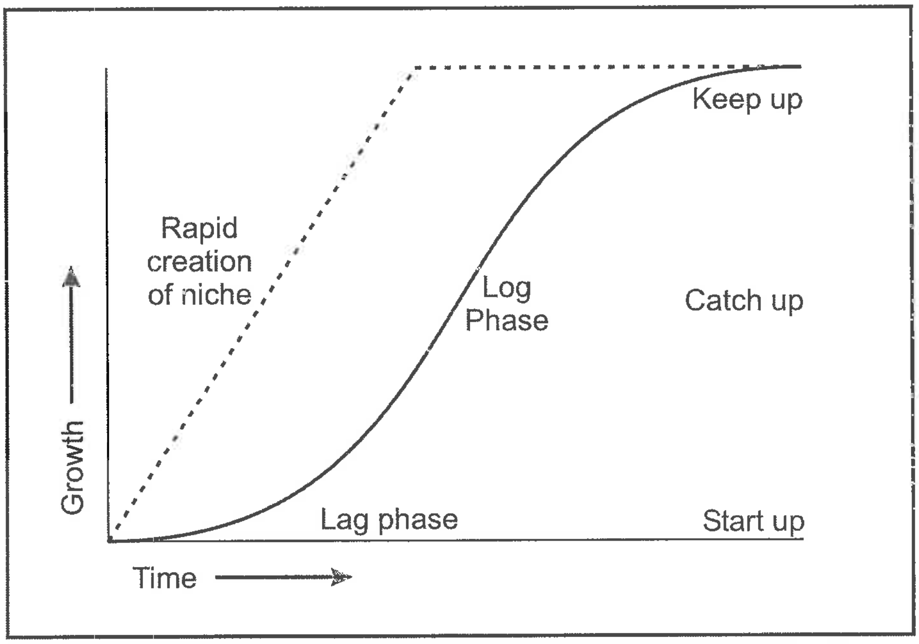

Figure 2.6 The law of sigmoidal growth (Neumann and MacIntrye, 1985).

At the top of the transgressive systems tract is the maximum flooding surface, which forms when the rate of relative sea level rise is at a maximum. At this position of the depositional cycle any siliciclastic sediment in the system will be restricted to the landward edge of the margin and consequently deposition of the cleanest carbonate of the system will occur on the margin. Figure 2.7a and Figure 2.8a show the proposed models for carbonate transgressive systems tracts in both rimmed shelf and ramp settings (Emery, 1996).

2.2.2 Highstand systems tracts

Highstand systems tracts in a carbonate regime are characterised by an increase in carbonate production as the shelf top becomes flooded and the area of carbonate production increases to a maximum (Droxler and Schlager, 1985). At this stage, the carbonate production factory is an order of magnitude larger than the belt of shallow water production which occurs during lowstands (Handford and Loucks, 1993; Schlager, 1992). During the early stages of the highstand systems tract, when the rate of sea level rise is still high and accommodation space is still being developed on the platform top, topsets may continue to aggrade as lagoonal, inter and supra-tidal facies (Emery and Myers, 1996). As the rate of sea level rise decreases, the focus of accommodation space creation moves from the shelf top to the slope (Jervey, 1988). This results in a change in depositional geometry from predominantly aggradational to progradational (Sarg, 1988). The subsequent fall in sea level shuts off sediment production on the bank top and reduces carbonate growth to fringing reefs. Figure 2.7b and

Figure 2.8b show the proposed models for the sequence stratigraphic development of highstand systems tracts for rimmed shelf and ramp environments (Emery, 1996).

Under highstand conditions, platform-top carbonate muds are exported over the bank edge and deposited on the lower slope by a process which is known as 'highstand shedding' (Glaser and Droxler, 1991; Reijmer *et al.*, 1991; Schlager *et al.*, 1994; Wilber *et al.*, 1990). This process has been documented for many modern day carbonate platforms including the Great Bahama Bank (Eberli and Ginsburg, 1989; Wilber *et al.*, 1990) and the Great Barrier Reef (Davies *et al.*, 1989). The Great Bahama Bank is composed of a series of progradational and aggradational sequences, which have prograded 25 km and aggraded 1500m since the late Cretaceous (Figure 2.9). Eberli and Ginsburg (1989) have proposed that these sequences have formed under transgressive and highstand conditions, whilst the boundaries between the sequences represent lowstand conditions with little or no progradation. By correlation to biostratigraphic data in a single well some distance from the study area, they have also tentatively proposed that the timing of the progradational and aggradational events is linked to million year cycles of Haq *et al.* (1987).

The prograding geometries of the Oligocene to Recent section of the North West Shelf are envisaged to have formed under similar depositional processes in which sediments are produced in the shallow water and transported over the margin edge, as was discussed in Section 1.3.5. The extensive biostratigraphic, wireline log and seismic database which exists for the Dampier Sub-basin has enabled high-resolution genetic subdivision of the prograding section of the North West Shelf to be made and test the theory that the stratal architecture is related to the eustatic curves of Haq *et al.* (1987). The study has shown that not only the progradational and aggradational units but also the sedimentation rate, clinoform height and clinoform angle all appear to be related to the eustatic curves of Haq *et al.* (1987).

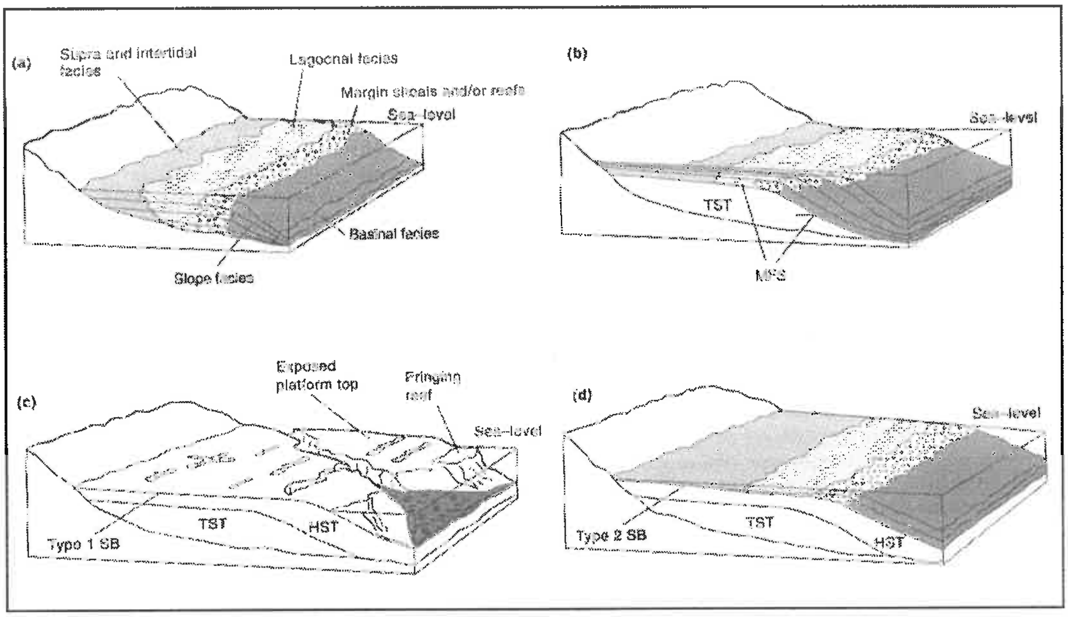

Figure 2.7 Sequence stratigraphic models for rimmed shelf systems (Emery 1996).

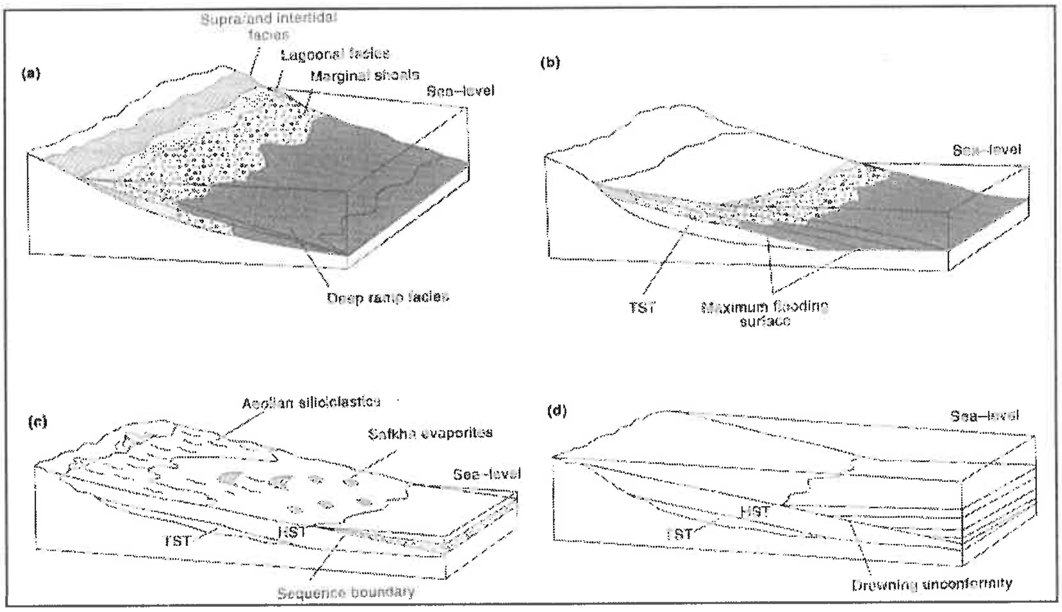

Figure 2.8 Sequence stratigraphic models for ramp systems (Emery 1996).

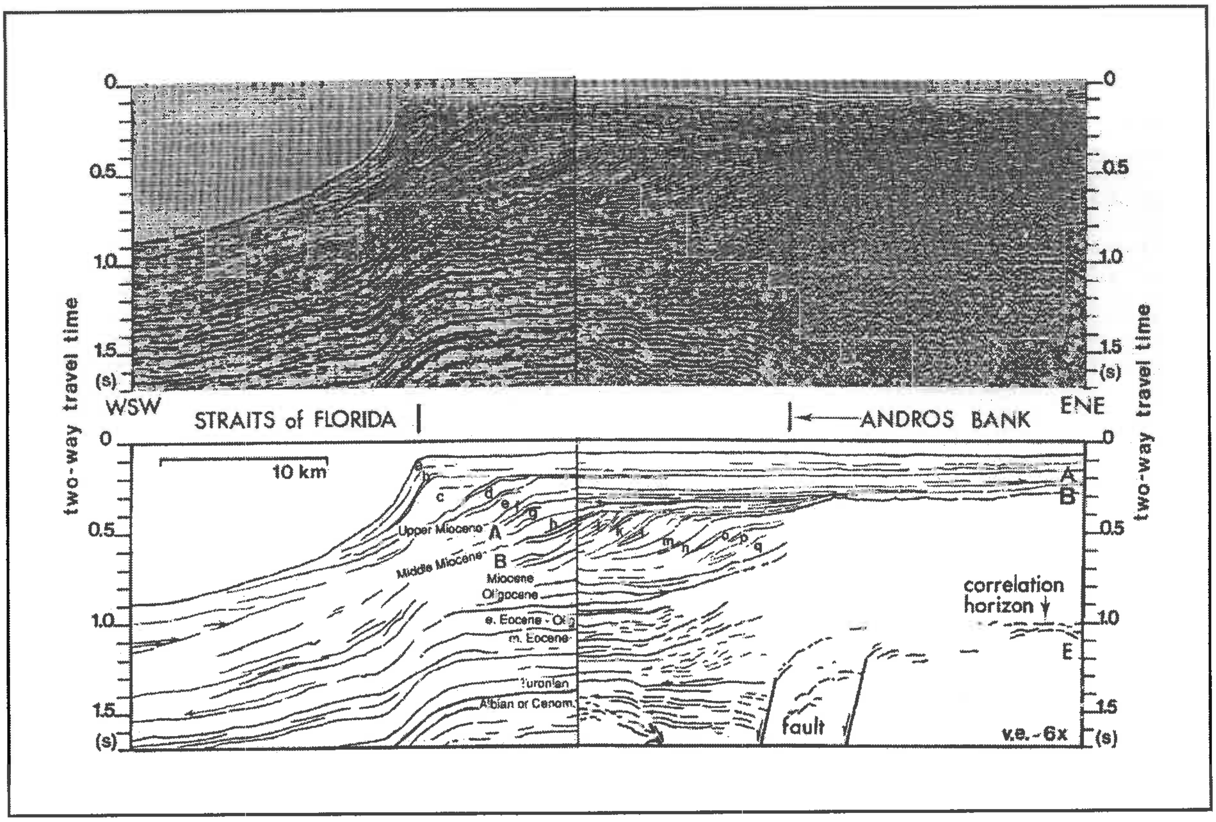

Figure 2.9 Progradational nature of the Great Bahama Bank. (Eberli and Ginsburg, 1989).

2.2.3 Lowstand systems tracts

Under lowstand conditions, the carbonate production factory is significantly reduced in size, from a wide area covering the platform top, to a narrow belt located on the platform slope. The exposed preceding highstand sediments lithify rapidly due to the basinward movement of meteoric fluids (Schlager *et al.*, 1994) making highstand deposits more resilient to erosion at times of lowstand. Combining this with the high preservation potential of highstand sediments, it can be concluded that the majority of preserved section in a rimmed margin will be highstand in origin. In a ramp setting, the decrease in carbonate production rates during lowstands does not occur because no reduction in the carbonate production factory is seen; it merely migrates basinwards on the constantly dipping slope. The lowstand systems tracts that are deposited are characterised by offlapping carbonate deposits, low carbonate production, siliciclastic input, erosion of the preceding highstand, formation of incised valley systems and the presence of evaporite minerals. The magnitude of relative sea level fall, amount of terrigenous supply and climate control the nature of the lowstand deposition.

Where the associated clastic input into the system is low, the platform may offlap and downstepping fringing carbonates will develop. Erosion of the now emergent shelf also occurs at this time. Where the associated siliciclastic sediment supply to the system is significant, it may overwhelm carbonate production and a lowstand siliciclastic system will be established. This phenomenon has been documented for several basins including the Permian of New Mexico (Saller *et al.*, 1989), the Canning Basin of Western Australia (Southgate *et al.*, 1993) and the Catalan Basin of Spain (Calvet *et al.*, 1990). On the now exposed platform top, karstification, porosity development, or cementation may occur depending on the interplay between climate and the cycle amplitude of the relative sea level curve; low frequency 2^{nd} – 3^{rd} order sea level changes in arid times tend to show the greatest porosity development (Read and Hodbury, 1993).

In arid environments, extensive sabkha evaporite development on the exposed shelf and encroachment by aeolian siliciclastics may occur (Calvet *et al.*, 1990). Humid environments are characterised by incision by fluvial channels, karstification and paleosols (Emery, 1996). Figure 2.7c and Figure 2.8c show the proposed sequence stratigraphic model for Type I lowstand development of rimmed shelf and ramp systems respectively (Emery, 1996). Figure 2.7c and Figure 2.8d show the proposed sequence stratigraphic model associated with Type II sequence boundaries. In the ramp setting, it is not possible to differentiate between Type I and Type II sequence boundaries as it is not possible to define a shelf break and therefore determine the extent of the relative sea level fall.

2.2.4 Platform drowning

In the siliciclastic regime, a lowering of relative sea level and exposure of the platform commonly produce unconformities, which if separating units of genetically different strata, are termed sequence boundaries. It has been proposed that a type of unconformity may exist that is specific to the carbonate regime, termed a 'drowning unconformity' (Schlager, 1989). A drowning unconformity is created by the drowning of a platform and the subsequent onlap of siliciclastics or other non-platform sediments (Schlager, 1989). By definition, these unconformities can only develop under transgressive or highstand conditions, as opposed to sequence boundaries, which develop under lowstand conditions. It is proposed that the rise in sea level outpaces the ability of the margin to grow vertically and so the margin falls beneath the photic zone and consequently dies. The carbonate platform subsequently becomes onlapped and buried by pelagic sediments resulting in a geometry which is remarkably similar to that which results from lowstand conditions. Figure 2.10 shows an interpreted drowning unconformity on the Wilmington Platform of New Jersey (Schlager, 1992). In this case, a succession of Cretaceous to Tertiary siliciclastics onlap and bury a late Jurassic to early Cretaceous carbonate platform.

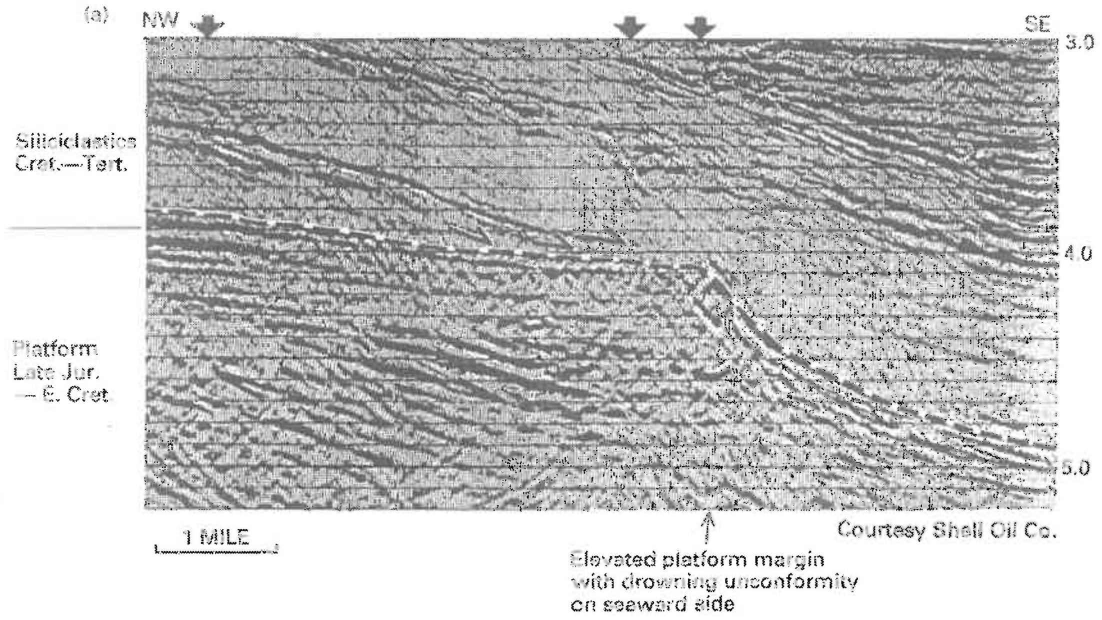

Figure 2.10 Drowning unconformity on Wilmington Platform (Schlager, 1992).

Purdy and Bertram (1993) believe the growth potential of carbonates is too great to be outpaced by a rapid rise in relative sea level. They claim the demise of a platform can only be brought about by an initial lowstand followed by a rapid transgression. During lowstand conditions, the margin top is exposed, killing carbonate growth at that site and carbonate production is relocated to a small productive band on the slope. During the subsequent transgression, the carbonate producing organisms have to re-colonise the margin first before they can attempt to grow upward and keep pace with sea level. This decreases the margin's chance of survival during a subsequent transgression. Carbonate ramps, which do not have a pronounced shelf break, will have a larger carbonate production area at lowstand and so are less likely to be a casualty of this mechanism of extinction.

This current study has shown no evidence of a drowning unconformity in the Oligocene to Recent section of the North West Shelf. The study has shown that during periods of rapid relative sea level rise, the sedimentation rate increases accordingly and the margin aggrades vertically and keeps pace with sea level. It has therefore been concluded that during the Oligocene to Recent, no relative sea level rise has been greater than the margins ability to aggrade.

2.2.5 Two-dimensional versus three-dimensional studies

To date, most of the studies of carbonate sequence stratigraphic geometries have been based on either two-dimensional outcrop or seismic data. Seismic-based studies of the Maldives and Bahamas (Eberli and Ginsburg, 1989; Purdy and Bertram, 1993) have been based on mainly dip data with only a handful of strike lines. A large number of the papers which have dealt with carbonate processes have also taken a two dimensional bias to their sampling program (Schlager, 1989; Schlager *et al.*, 1994; Wilber *et al.*, 1990). This is not surprising, as it is along the dip axis that the major variations in the carbonate models are seen. Outcrop sequence stratigraphic studies can also have a two-dimensional bias, due to the nature of the outcrop (Jacquin *et al.*, 1991). Carbonates are a living three dimensional system and so must be addressed from a three dimensional perspective.

Martinsen and Helland-Hansen (1995) addressed the strike variability of clastic depositional systems and demonstrated how contrasting prograding and retrograding stacking patterns could form during highstand conditions. Estuarine and deltaic systems showed variations on a small scale through lobe switching whilst shoreline systems tended to exhibit larger scale variations due to the nature of the depositional system. Martinsen and Helland-Hansen (1995) concluded that the predictive potential of sequence stratigraphy based on stacking patterns and systems tracts was overemphasized and when approached through the use of two dimensional data, is prone to misinterpretation. As a consequence of this, they believed that prediction in sequence stratigraphy should be limited to identification of key surfaces. These potential pit falls in interpretation identified by Martinsen and Helland-Hansen (1995) can be avoided by using a three dimensional dataset, establishing the sequence stratigraphic framework and defining the key stratigraphic surfaces. Within this framework, and using a three-dimensional dataset, it is then possible to analyse the internal stacking architecture of the defined sequences. By ignoring the information contained within stacking patterns, Martinsen and Helland-Hansen (1995) ignore a complete line of evidence on basin evolution.

Wireline data are not commonly presented in carbonate sequence stratigraphic analysis. In fact, within AAPG Memoir 57 on carbonate sequence stratigraphy (Loucks and Sarg, 1993), only two of the twenty published papers (Erlich *et al.*, 1993; Southgate *et al.*, 1993) present wireline data. The chapter on carbonate sequence stratigraphy by Emery and Myers (1996) has one diagram showing wireline data and little discussion of the wireline response is made in the text. The value of integrating wireline log data with core and seismic data in the siliciclastic regime has been demonstrated (Van Wagoner *et al.*, 1990) and is now common practice. The integration of wireline data with seismic and core data in carbonate studies will facilitate a higher-resolution genetic subdivision of the section and therefore provide a better understanding of the evolutionary nature of carbonate systems.

During this study, a method was developed to allow the sequence stratigraphic interpretation of carbonate wireline log motifs. This model has been combined with biostratigraphic data to subdivide the section into a series of genetically-related units. These units have been identified and mapped on seismic data and their distribution has been used to describe the evolution of the Albian to Recent section of the Dampier Sub-basin.

CHAPTER 3 METHODOLOGY

3.1 Project Rationale

The aim of this study was gain a quantitative understanding of the three-dimensional evolution of the Albian to Recent section of the Dampier Sub-basin. In order to do this, it was necessary to subdivide the section into a series of genetically-related packages of known age and map their spatial distribution. The Albian to Recent section was initially subdivided into major units using biostratigraphic data and then further subdivided by integrating biostratigraphic and wireline log data on the basis of log character and sequence stratigraphic principles. This allowed a chronostratigraphic framework to be constructed which defined the age of the basin-forming events. These events were transferred to seismic data and their spatial distribution was mapped throughout the basin. Using this approach, the Albian to Recent section was divided into a succession of genetically-related units which were separated by time-correlative surfaces. The internal reflection geometries of these units were further mapped to give a high-resolution image of stratal architecture and accommodation space development.

3.2 Database

This study utilised data from 38 wells distributed throughout the Dampier Sub-basin (Figure 3.1). Biostratigraphic reports contained within the well completion reports are based on foraminifera samples collected from sidewall core and ditch cuttings and are of variable quality. For each of these wells there is a suite of wireline logs, from which the gamma, sonic, neutron and density logs were selected where possible. Table 3-1 lists the wells that have been incorporated in this study. Seismic data were supplied by Mobil Exploration & Producing Australia and consist of approximately 4100 km of 2D digital data. The data were mostly from AGSO Survey CTT94-136 and have been complemented by additional regional and prospect scale lines (Figure 3.1). Table 3-2 lists the seismic lines that were used in the main seismic interpretation phase of the study and which of those have been used in the high-resolution analysis of stratal architecture using 3D-Chronostrat.

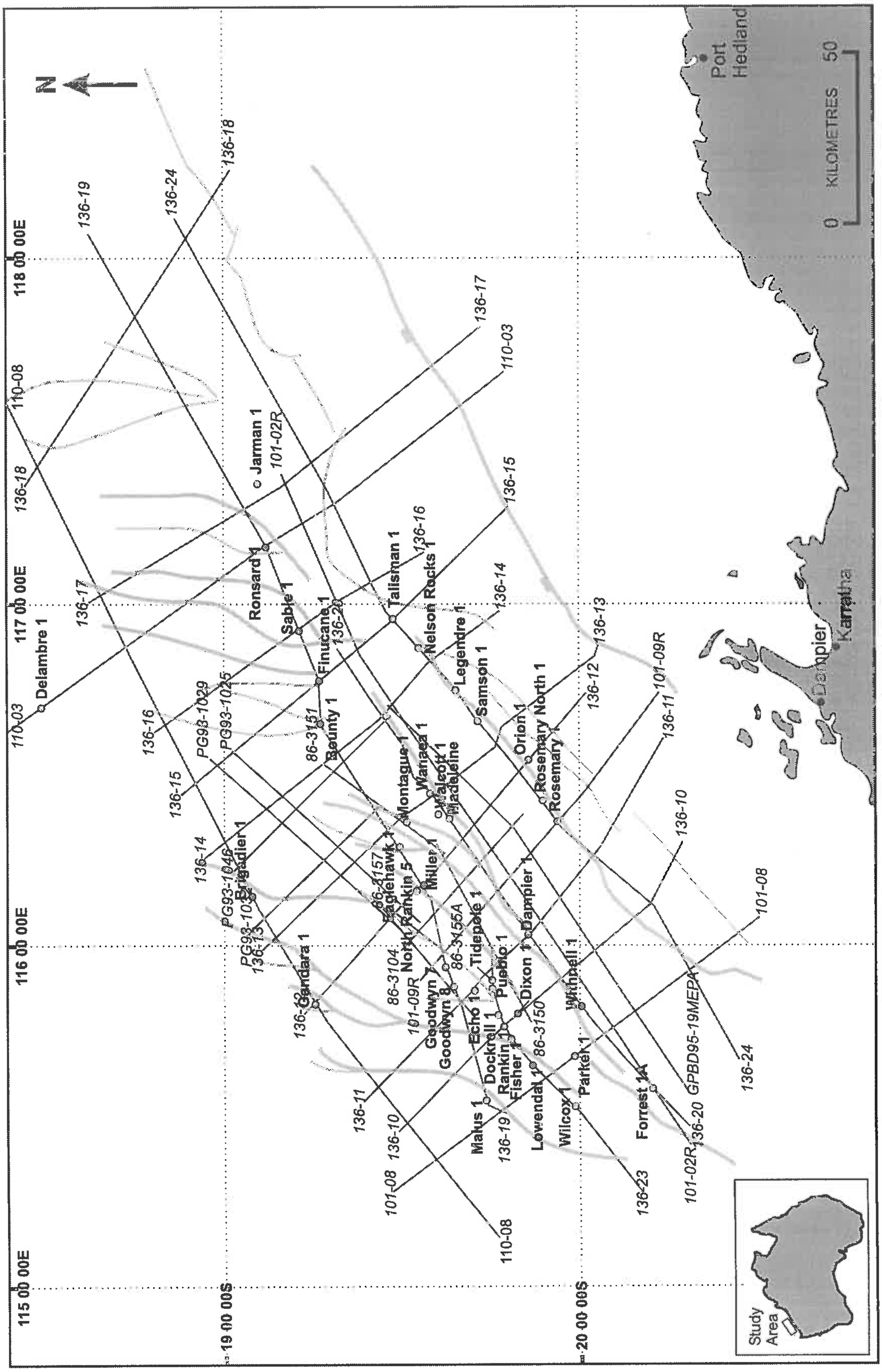

Figure 3.1 Dampier Sub-basin showing wells and seismic lines used in the study

Wells	Year Drilled	Biostrat Quality	Check Shot	Wireline logs on SeisX
Bounty 1	1983	Good	Yes	GR, DTM, RHOB, NPHI, SP
Brigadier 1	1978	Good	Yes	GR, DT, RHOB, NPHI
Dampier 1	1968	Poor	No	GR, DT, RHOB, NPHI
Delambre 1	1980	Good	Yes	GR, DT, RHOB, NPHI
Dixon 1	1984	Good	Yes	GR, DT, RHOB, NPHI
Dockrell 1	1973	Good	Yes	GR, DTM, RHOB, NPHI
Eaglehawk 1	1972	Average	Yes	GR, DTM, RHOB, NPHI
Echo 1	1988	Good	Yes	GR, DT, RHOB, NPHI
Finucane 1	1978	Good	Yes	GR, DT, RHOB, NPHI
Fisher 1	1981	Good	Yes	GR, DTM, RHOB, NPHI
Forest 1A	1992	Average	Yes	GR, DT
Gandara 1	1979	Good	Yes	GR, DT, RHOB, NPHI, SP
Goodwyn 7		Good	Yes	GR, DTM, RHOB, NPHI, SP
Goodwyn 8		Good	Yes	GR, DTM, RHOB, NPHI, SP
Jarman 1	1978	Good	Yes	GR, DTM, RHOB, NPHI
Legendre 1	1968	Poor	Yes	GR, DT, RHOB, SNP, SP
Lowendal 1	1974	Good	Yes	GR, DT, RHOB, NPHI, SP
Madeleine 1	1969	F poor	Yes	GR, DT, RHOB, NPHI
Malus 1	1972	Poor	Yes	GR, DT, RHOB, NPHI
Miller 1	1978	Good	Yes	GR, DTM, RHOB, NPHI
Montague 1	1984	Good	Yes	GR, DT, RHOB, NPHI
Nelson Rocks 1	1973	Good	Yes	GR, DT, RHOB
North Rankin 5	1976	Good	No	GR, DT, DTM RHOB, NPHI, SP
Orion 1	1990	Poor	No	GR, DT, RHOB, NPHI
Parker 1	1979	Good	Yes	GR, DTM, RHOB, NPHI
Pueblo 1	1979	Good	Yes	GR, DTM, MSFL, NPHI
Rankin 1	1971	Poor	Yes	GR, DTM, RHOB, SNP, SP
Ronsard 1	1973	Good	Yes	GR, DTM, RHOB, NPHI, SP
Rosemary North 1	1982	Good	Yes	GR, DT, RHOB, NPHI
Sable 1	1972	Average	Yes	GR, DT
Samson 1	1984	Good	No	GR, DTM, RHOB, NPHI, SP
Talisman 1	1984	Good	Yes	GR, DT, RHOB, NPHI
Tidepole 1	1975	Good	Yes	GR, DT, RHOB, NPHI
Walcott 1	1979	Good	No	GR, DT, RHOB, NPHI
Wanaea 1	1989	Good	Yes	GR, DTM
Wilcox 1	1983	Good	Yes	GR, DT, RHOB, NPHI
Withnell 1	1976	Good	Yes	GR, DTM, RHOB, NPHI

Table 3-1 Well data used in the study

Line Name	Vintage	Line Length (km)	Chronostrat
101-02R	1992	278.8	No
101-08	1992	110.1	Yes
101-09R	1992	123.3	Yes
110-03	1992	197.9	Yes
110-08	1992	383.2	Yes
136-09	1994	137.231	No
136-10	1994	126.356	Yes
136-11	1994	145.275	Yes
136-12	1994	131.513	Yes
136-13	1994	141.694	Yes
136-14	1994	118.856	Yes
136-15	1994	136.069	Yes
136-16	1994	99.675	Yes
136-17	1994	146.4	Yes
136-18	1994	115.369	Yes
136-20	1994	207.8	Yes
136-23	1994	92.438	Yes
136-24	1994	315.244	Yes
139-19	1994	322.8	Yes
85DB-13	1985	82.9	No
86-3104	1986	60.2	Yes
86-3150	1986	67.1	Yes
86-3151	1986	45.7	No
86-3155A	1986	34.1	No
86-3157	1986	62.5	Yes
GPBD95-19MEPA	1995	152.3	No
PG93-1025	1993	78.9	Yes
PG93-1029	1993	84.2	Yes
PG93-1032	1993	35.8	Yes
PG93-1042	1993	71.4	Yes
	Total line km =	4105.12	

Table 3-2 Seismic data used in the study

3.3 Biostratigraphic and wireline log interpretation

The Albian to Recent section of the Dampier Sub-basin is poorly sampled in terms of core data and has limited biostratigraphic data collected from sidewall cores and cuttings data. Wireline logs provide the most complete dataset with which to define a series of 1D sequence stratigraphic subdivisions of the succession. Wireline logs are routinely used as an integral part of siliciclastic sequence stratigraphic studies (Van Wagoner *et al.*, 1990) but the literature review (Chapter 2) has highlighted a paucity of papers that discuss the wireline response to carbonate environments. For the purposes of this study, a model has been developed for the sequence stratigraphic interpretation of carbonate wireline log motifs (Hull *et al.*, 1998). This model has facilitated the high-resolution subdivision of the section by integrating the biostratigraphic and wireline log data in a sequence stratigraphic context.

3.3.1 Biostratigraphic data

Well completion reports for 50 wells in the Dampier Sub-basin were examined to determine the quality and nature of biostratigraphic data. Wells were then selected on the basis of data quality and location. The biostratigraphic data for wells in the Dampier Sub-basin consist of palynological data for the Neocomian and older section and foraminiferal data for the Albian to Recent section. This study has solely used foraminiferal data in its analysis of the section. The biostratigraphic reports describe the foraminiferal assemblages present in the sidewall cores and cuttings and assign samples to biozones defined by Apthorpe (1979), Heath (1979), Heath and Apthorpe (1984), Wright (1973) and Wright and Apthorpe (1976) (Figure 3.2). The biostratigraphic reports also identify missing biozones in the record and some reports also give an interpretation of depositional environment.

The quality of the biostratigraphic data varies between wells depending on the age of the wells and on the company which drilled the well. In the wells drilled in the early 1970s the biostratigraphic subdivision of the section was poor and at best stage names have been defined in the Cretaceous section whilst the Tertiary section is commonly described as 'undifferentiated Tertiary'. In the mid-1970s to mid-1980s, Woodside Offshore Petroleum collected cuttings and sidewall core data for the Albian to Recent section of the wells drilled at this time and conducted routine paleontological analysis on the samples recovered. The paleontological reports are included in the well completion reports for these wells and identify the depth intervals of the defined foraminiferal zones for the Northwest Shelf (Apthorpe, 1979; Heath, 1979; Heath and Apthorpe, 1984; Wright, 1973; Wright and Apthrope, 1976). However, none of the paleontological reports present relative abundance data for species within each of the samples. Within these wells, the Albian to early Miocene section is commonly well defined from the faunal assemblages but in the mid-Miocene to Recent section the recovery of age diagnostic faunas is not as good as the section below and dating of the assemblages is more problematic. In many wells no samples were collected until the marine riser was installed, which is commonly after approximately 500 meters of drilling. In the mid-Miocene to Recent section of these wells, the sediments are commonly defined as a range of biozones or as 'undifferentiated'. Wells that have been drilled by companies other than Woodside Offshore Petroleum have not routinely recovered samples from the late Cretaceous and Tertiary sections. Wells that have been drilled from the late 1980s to the present day tend to drill through the Upper Cretaceous and Tertiary sections as quickly as possible with no samples recovered from this section. In many of the modern wells, riserless drilling continues throughout the whole of the Tertiary section and consequently no samples are recorded.

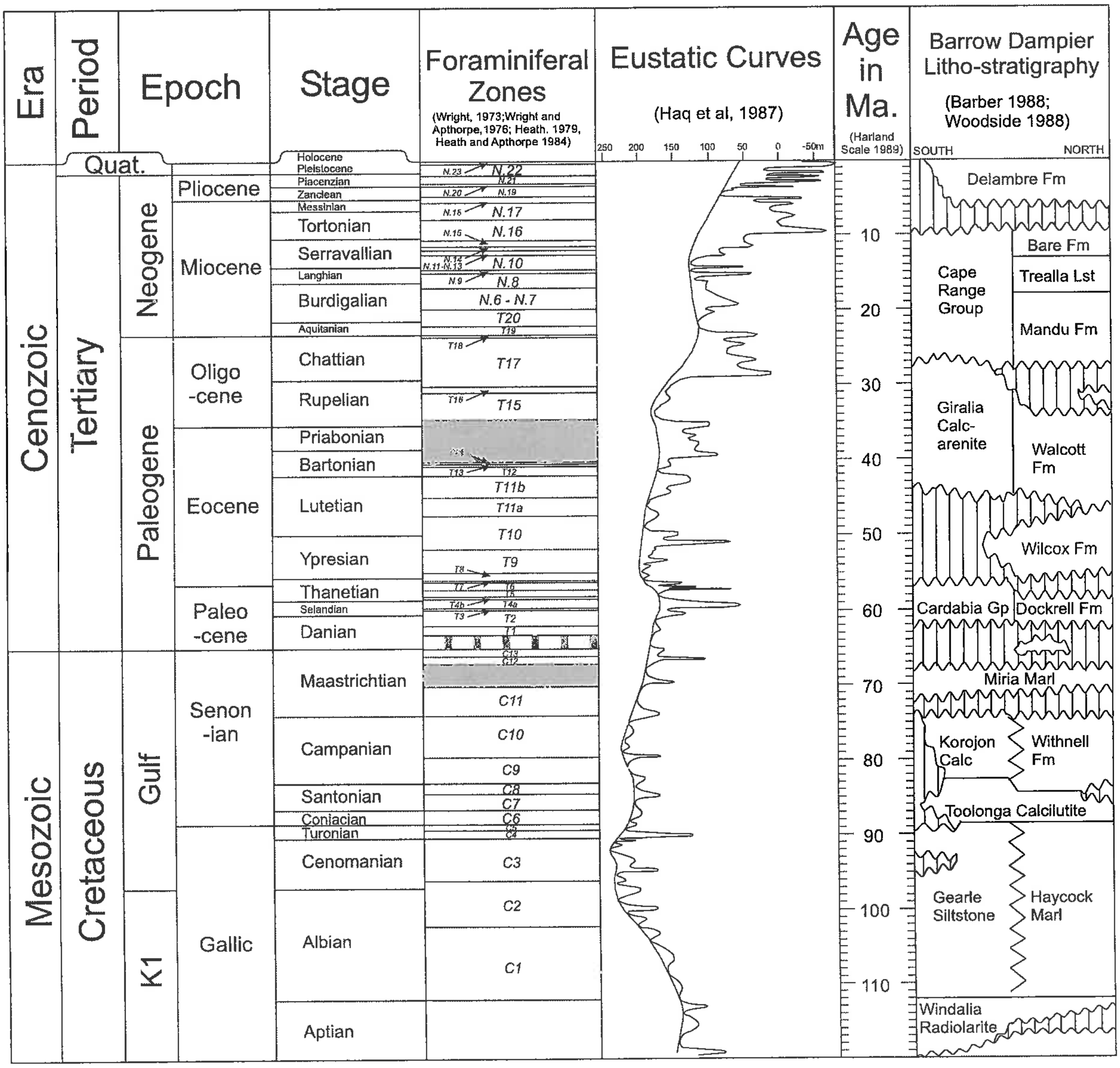

Figure 3.2 Foraminiferal zones for the Albian to Recent section of the North West Shelf (Young and Laurie, 1996)

Reliability of biostratigraphic age dating

The absolute ages of the foraminiferal zones defined for the North West Shelf and the correlation of these zones to international biozones has been made by the Australian Geological Survey Organisation (Young and Laurie, 1996). In the late Cretaceous section, Young and Laurie (1996) have used the absolute ages of the Aptian to Maastrichtian geomagnetic reversals of Harland *et al.* (1982) to date the stage boundaries, as these are generally agreed upon in the literature. Within text by Harland *et al.* (1989), a table of errors to one standard deviation are presented along with a discussion of the reliability and origin of the stage names and dates. In the Tertiary section of the North West Shelf, the age of the subdivisions are known from a combination of $^{40}Ar/^{39}Ar$ dating and biostratigraphic interpolations linked to the magnetostratigraphic record (Young and Laurie, 1996). For further discussion on the age information and errors associated with the age dating of the Tertiary, Young and Laurie (1996) refer the reader to the discussion by Berggren *et al.* (1995).

3.3.2 Wireline log data

Tertiary sediments are not common targets for hydrocarbon exploration in the Dampier Sub-basin and as a result only a skeleton suite of logs (gamma and sonic) are run in the upper section of the well prior to casing. Due to the hydrocarbon-bearing nature of the Cretaceous section, a more extensive logging suite is commonly run which normally consists of resistivity, density, neutron, gamma and sonic logs. In some wells this tool string is run to the surface but this is not the norm. As a result of the nature of the wireline log coverage, this project has focussed primarily on the integration of the gamma and sonic logs with the biostratigraphic and seismic data.

3.3.3 Integration of biostratigraphic and wireline log data

The Albian to Recent section of the Dampier Sub-basin was initially subdivided on the basis of major unconformities, as evidenced by missing section observed on biostratigraphic and sonic logs. Biostratigraphic reports were used to determine the timing and extent of missing section across the basin. Many of the biostratigraphic hiatuses were associated with pronounced log breaks which facilitated the ease of correlation across the basin (Figure 3.3). This gross subdivision of the section provided the rigid framework from which further subdivision of the section was possible. Biostratigraphic data also revealed the presence of regional flooding events and other localised episodes of missing section. These events were also identified on wireline logs and correlated throughout the basin. Using the wireline log character, biostratigraphic constraints and the theoretical understanding of carbonate depositional systems, a model was developed for the sequence stratigraphic interpretation of carbonate wireline log motifs as discussed in the following chapter.

3.3.4 Generation of time-depth curves and synthetic seismograms

Wireline log depths have been converted to two-way times using check shot surveys, which have been recorded for the majority of the wells in the study (Table 3-1). In check shot surveys, an explosive source is repeatedly detonated at a short distance from the well whilst a receiver is lowered down the hole and at regular intervals the travel time from the source to receiver (one-way travel time) is recorded. This travel time is then corrected to the vertical to give an accurate record of travel time versus depth at the well. Log depths are converted to travel time by integrating the interval transit time of the sonic log. However, there is commonly a significant rounding error associated with such an integral and the calculated travel time values must be calibrated for the interval between checkshots. This corrected sonic log is used in the generation of synthetic seismograms. Figure 3.4 shows the difference between recorded and adjusted sonic log, which is calculated as drift. The circles represent checkshot data, which the sonic log has been adjusted to honour.

The wireline logs for all the wells were converted to two-way time using checkshot surveys where available (Table 3-1). Wells without checkshot surveys have been depth converted to two-way time using only the sonic log and consequently the time-depth curve for these wells may not be as reliable. Synthetic seismograms were created for some wells using the density and sonic logs, which have been adjusted to honour the check shot data. However, as many of the wells did not have a density tool on the logging run through the upper section, the generation of synthetic seismograms was not satisfactory. Consequently, more importance has been placed on the two-way time converted wireline logs in identifying the seismic response of the events defined on wireline log.

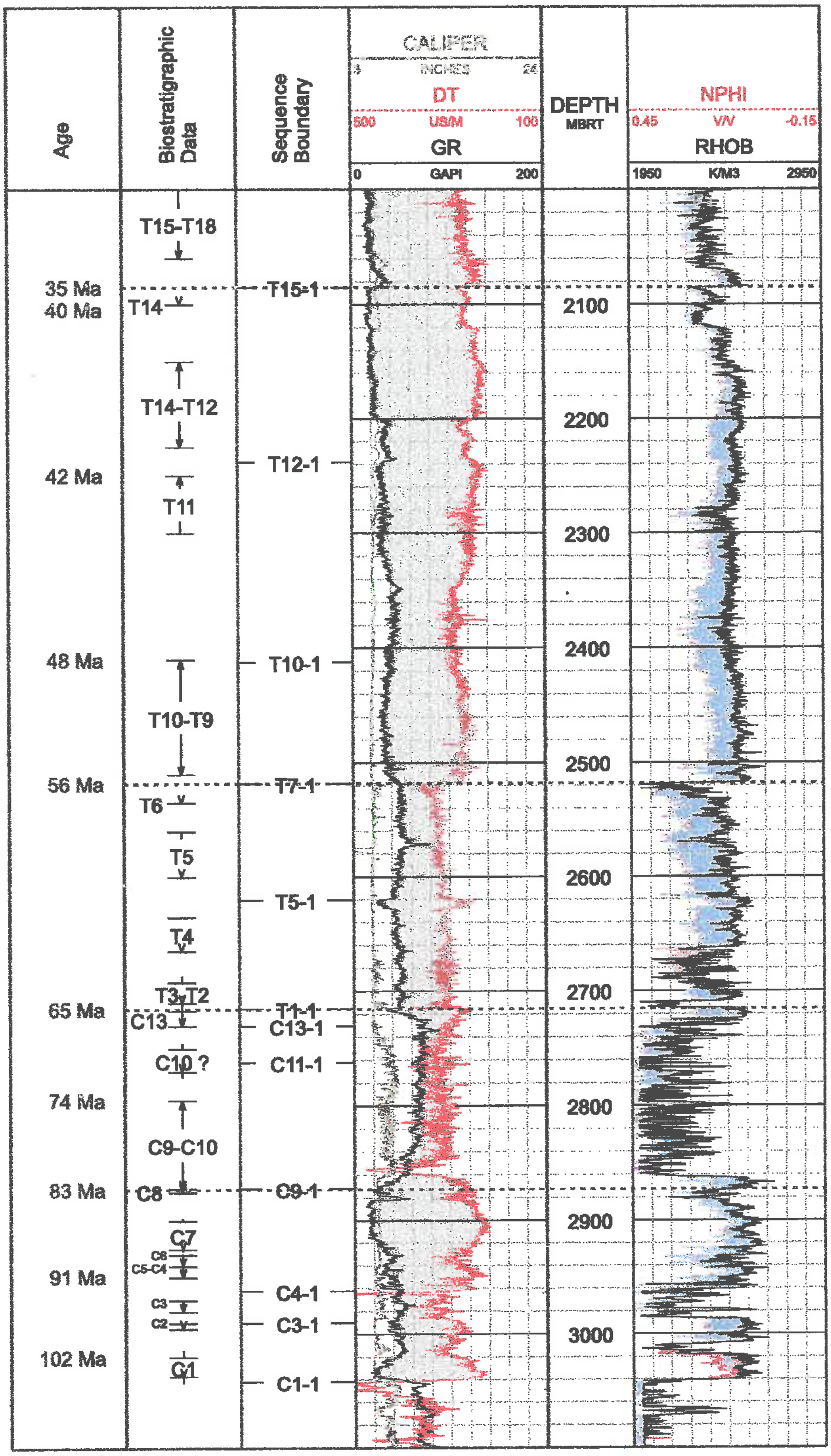

Figure 3.3 Wireline log suite for the Albian to Eocene section of Lowendal-1, showing biostratigraphic data and associated wireline log signature.

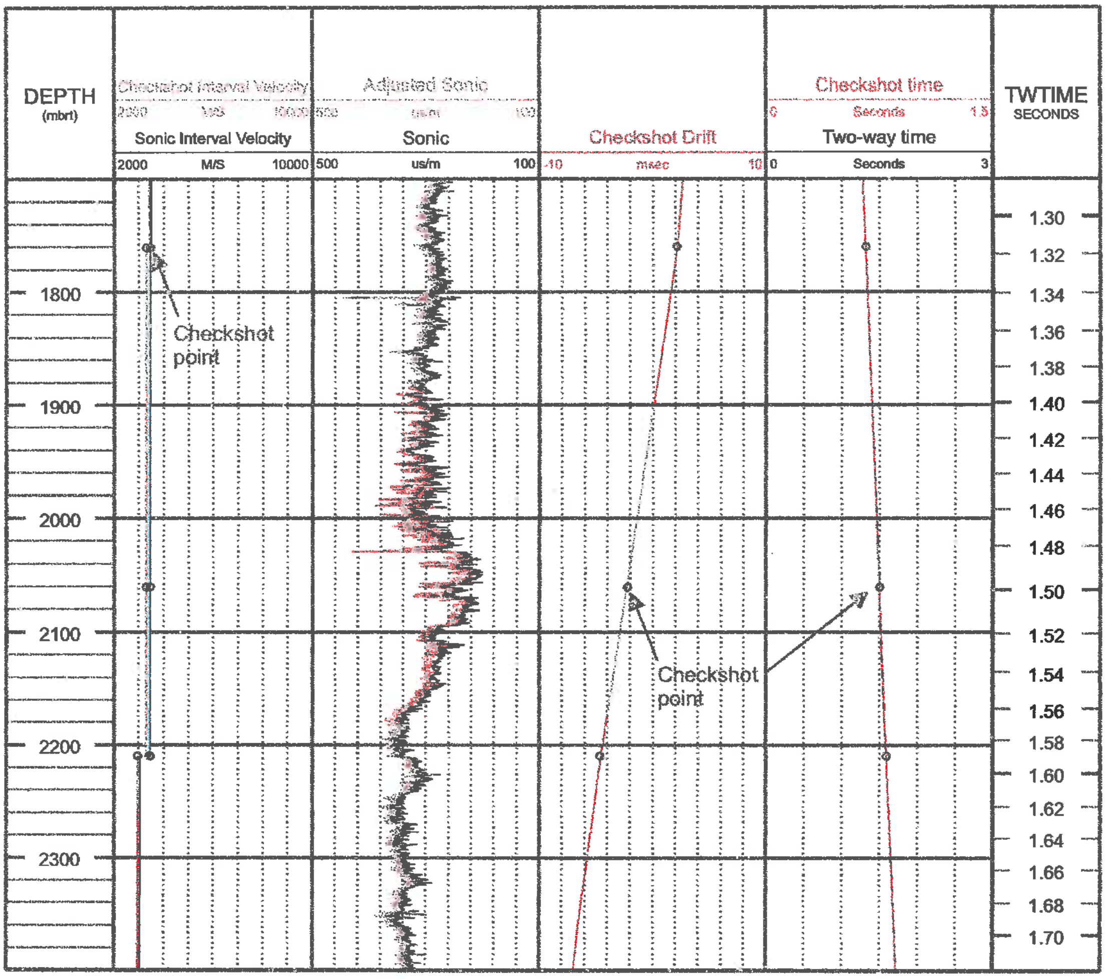

Figure 3.4 Sonic and adjusted sonic logs used to depth-convert wireline logs.

3.4 Seismic Interpretation

A regional grid of seismic data (as described in Section 3.2) was loaded onto a 2D workstation for interpretation using the seismic interpretation software SeisX (Paradigm Geophysical, 1997). Wireline log data have been converted to two-way time (as described in Section 3.3.4), and loaded into the seismic database along with the sequence stratigraphic picks defined during the wireline and biostratigraphic analysis. The spatial distribution of these events has been mapped on the seismic data to investigate their three-dimensional nature. Using a series of two-way time and isochron maps it has been possible to investigate the timing and nature of the basin-fill history of the Dampier Sub-basin.

3.4.1 Mapping methodology

Wireline logs and the associated sequence stratigraphic picks were posted on the seismic display window in order to identify the seismic response of events (Figure 3.5). A seismic pick was made at the nearest trough, peak or crossover on the seismic wavelet. This event was then mapped throughout the immediate area to ensure it corresponded with the other wells in the area. The seismic picks were adjusted and the wireline pick was re-evaluated until a consistent signature for the sequence stratigraphic event could be identified on seismic. The event was then mapped throughout the extent of seismic database using standard seismic interpretation techniques (Mitchum and Vail, 1977) and information from all available wells to constrain the interpretation. Stratal termination patterns were also used to constrain the position of the picked horizon. In the upper section, where biostratigraphic data were scarce and had not permitted further subdivision of the section, sequence boundaries were identified by stratal termination patterns using the model shown in Figure 3.6.

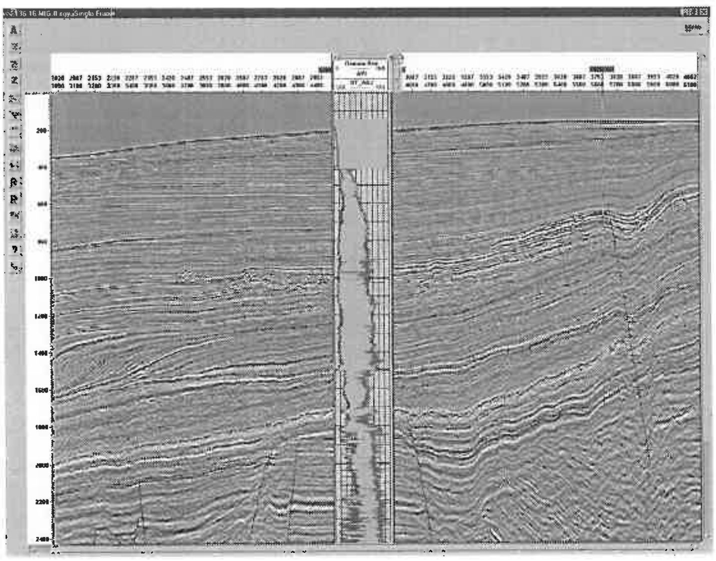

Figure 3.5 Example of wireline and sequence stratigraphic events displayed in the seismic window.

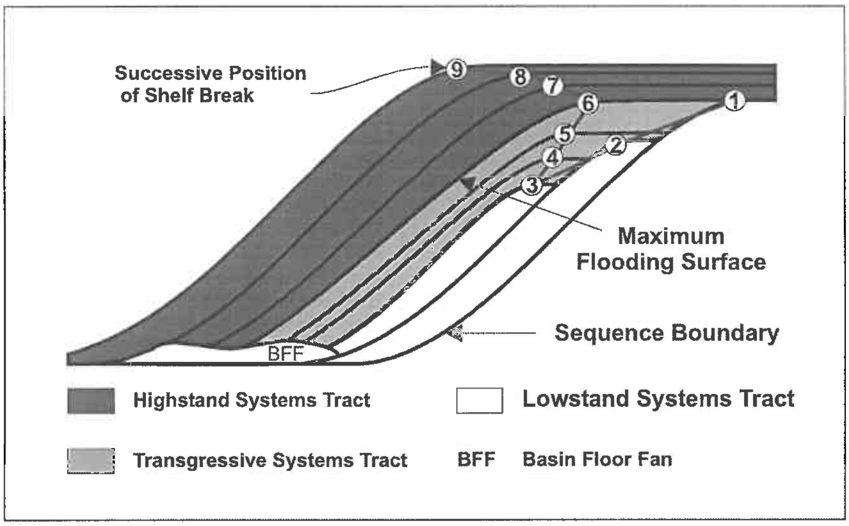

Figure 3.6 Stratal termination patterns that have been used to pick sequence boundaries in areas with poor or no biostratigraphic constraints (Hull et al., 1998).

3.4.2 Two-way time and isochron maps

A series of two-way time and isochron maps were generated to investigate the nature of sediment deposition and basin development from the Albian to Recent section of the Dampier Sub-basin. By gridding the horizons mapped on the 2D seismic lines, it was possible to generate a two-way time map for each horizon to illustrate the present day configuration of the sediments. During the study, 30 events were identified and their spatial distribution mapped throughout the seismic database. These two-way time maps were useful in defining structural trends in the basin.

Variation in sediment thickness was analysed by generating a series of time-thickness or isochron maps. Isochron maps are commonly used to interpret the structural and stratigraphic environment at the time of deposition as they clearly show the progressive evolution of sedimentary depocentres in a basin. Isochron maps were generated for each stratigraphic unit in the study by subtracting the top horizon from the bottom horizon and gridding the resultant file. During this process, the output file was carefully examined to ensure it accurately represented the data being gridded. It was noted that erroneous results were generated for two particular styles of stratal termination. In the first case, sediments were predicted beyond the zero edge of a stratigraphic unit where two coalescing horizons, which defined the edge of the stratigraphic unit, did not meet exactly (Figure 3.7). The second case occurred where the lower boundary of the stratigraphic unit was represented by different horizons at various locations within the database (Figure 3.8). At locations where the lower horizon changed, no thickness was calculated for the stratigraphic unit and the thickness was reduced to zero within the gridding distance. To correct for this problem, a dummy horizon was created for the base of the affected sequence by duplicating the lower horizon and extending it to either the edge of the data or where it terminated against the upper horizon (Figure 3.8).

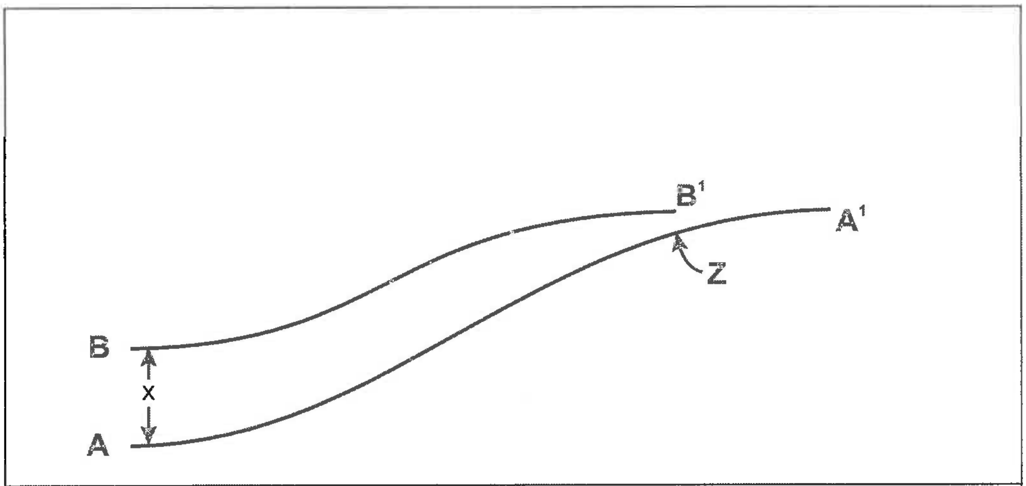

A sediment body is defined by the onlap of BB' on AA'. At the onlap position (Z) x = 0 and therefore the isochron map should have a zero edge at this point. If BB' does not coalesce with AA' the grid will predict values for x between Z and A' for which x values should be zero.

Figure 3.7 Erroneous gridding results due to non-coalescence of terminating horizons.

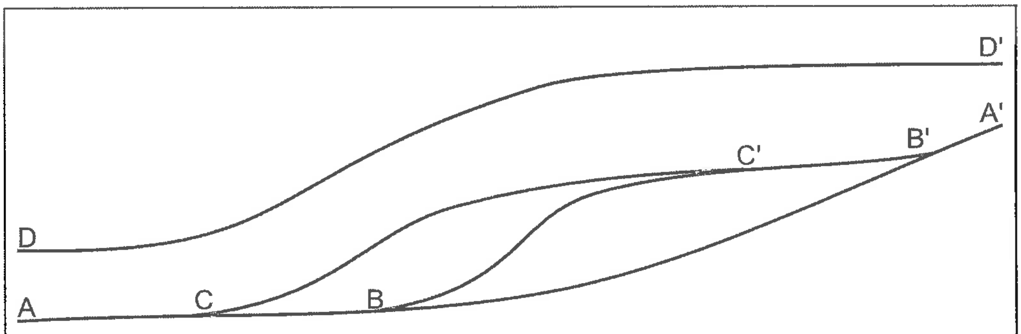

The top of the sequence CD is represented by the horizon DD'. The base of the sequence CD is represented by a composite event of AC, CC', C'B' and B'A'.

Figure 3.8 Gridding problems associated with the base of a sequence represented by differing reflectors across the basin.

In some areas of the study, the line spacing was broad, controlled by the regional nature of the seismic surveys. This large line spacing (up to 35 km in the northern region of the study) caused problems when gridding the horizons to generate the two-way time and isochron maps. The gridding process in SeisX works by defining a grid cell size and a maximum gridding distance. The gridding distance is the number of adjacent grid cells used to calculate a grid cell value. Thus a combination of the grid cell size and gridding distance must be greater than half the largest line separation in order to interpolate between lines. A smaller grid cell size will give a smoother appearance to the resultant grid. However, if the grid cell size is too small, it will require a large gridding distance to interpolate between adjacent lines and this will tend to smooth out localised features on the map. To address this problem, the maps were initially generated using a grid cell size of 650 x 650 m and a maximum gridding distance of 35 grid cells, giving a range of 22 km over which the gridding calculation took place. This gave a coarse resultant grid which was improved by re-gridding using a grid cell size of 250 x 250 m and with a maximum gridding distance equal to the ratio of the original grid size to the new grid cell size, in this case a ratio of 2.6.

3.4.3 Isopach maps and depth conversions

Isopach maps are used to illustrate the variations in absolute thickness of basin fill. In many instances there will be little difference between the thickness distribution on the isopach and isochron maps. This will be the case particularly if the sediments are homogeneous in nature and thus have a similar interval velocity. However, if there is a marked variability in the sediment type and interval velocities, a noticeable difference can be seen between the isochron and isopach maps.

Using SeisX it is possible to create isopach maps for a stratigraphic unit defined by two horizons. Within SeisX there is a well database which has a defined time-depth curve for each well. Using these curves it is possible to relate the horizon depth in time (as picked on the seismic section) to the wireline depth in metres at the well bore. SeisX then calculates an interval velocity for the stratigraphic unit between the upper and lower horizons at each well location in the database. The interval velocities are then extrapolated throughout the seismic database to create a velocity model along each seismic line. To create the isopach, this velocity model is simply multiplied by the isochron for the stratigraphic unit (created by subtracting the two-way time depth of the upper horizon from the lower horizon). The resultant isopach is divided by two to account for two-way time and then gridded throughout the basin.

Several errors may be introduced whilst producing depth sections and these must be considered when producing isopach maps. The main source of error exists in deriving accurate interval velocities, which are needed to facilitate a successful translation of the isochron into an isopach map. In this study, checkshot surveys were used to create the time-depth curves for each well using the process described in Section 3.3.4. Using these curves and knowing the time difference, δT, between the two horizons, it was possible to work out a thickness, δZ, from the time-depth curve (Figure 3.9). An interval velocity was calculated from δZ and δT and this was then interpolated throughout the study area and used to convert two-way time to thickness. In essence, the calculation of the interval velocity was directly dependent on the quality of the time-depth curve which in turn was dependent on the quality of the checkshot and sonic data. The majority of the wells in the Dampier Sub-basin have targeted lower Cretaceous to Triassic plays and as a result, data in the upper Cretaceous to Tertiary section are often sparse. Commonly, only a handful of checkshots are recorded in the upper section with a large spacing between samples. In wells with a large checkshot spacing (200-500 m), the time depth curve produced will be interpolated between the data points using either a linear or best fit polynomial function. The time-depth curve thus averages the time across the interval and may not pick up variations in interval velocity which exist at a smaller scale (<500 m), (Figure 3.10).

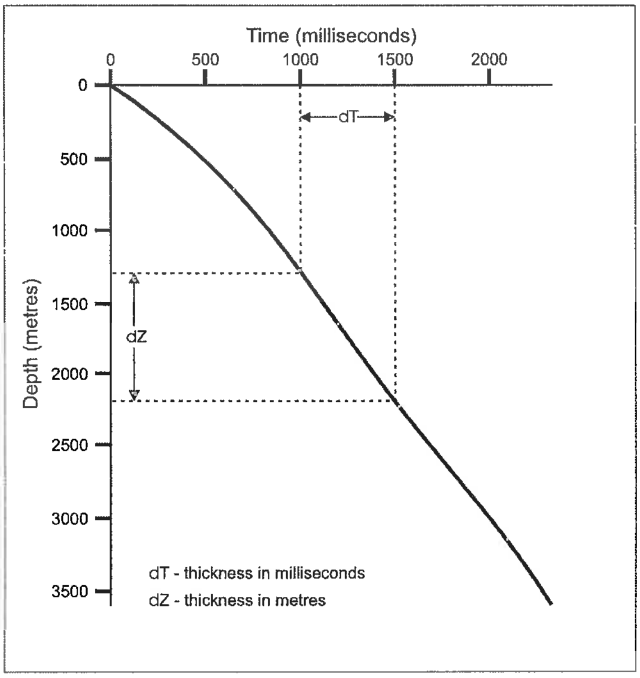

Figure 3.9 Thickness estimates from time-depth curves

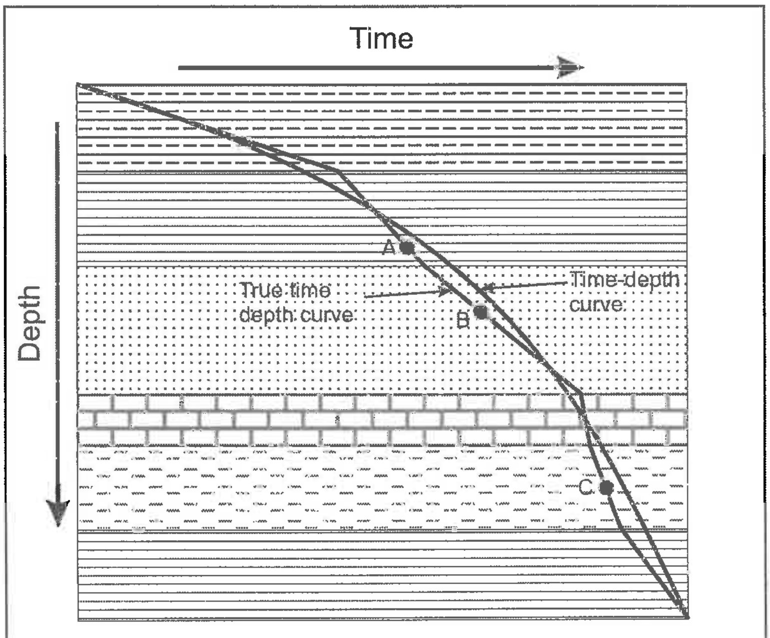

The time which a seismic wave takes to pass through a body of rock depends upon the interval velocity of the sediment. Hard cemented lithologies such as limestones will have a fast interval velocity and therefore a short interval transit time. If the checkshot spacing is too large, such as between B and C it will not pick up the lithology with the high interval velocity. Also if the first checkshot is recorded at A then no information of the interval velocity variations through the upper section will be available for constraining the time depth model.

Figure 3.10 Errors associated with large checkshot spacing

Additional errors may be introduced in the calculation of isopach thickness in areas where well control is sparse and large gridding distances have to be invoked. Stacking velocities associated with the seismic data may also be used to produce interval velocity maps. These give a much better spatial coverage than the one-dimensional well data but the stacking velocities represent the cumulative summation of velocities and therefore will never identify low velocity zones.

A further source of error arises in regions where the sediment package being investigated is thin, typically less than 100 ms. In this case, inaccuracies in the seismic pick and the tie to well log data may cause anomalously large interval velocities to be calculated. For example, a 12 ms mistie on the seismic data in an area where the isochron is only 60 ms thick, represents an error of 20%, which in a sediment with an interval velocity 3500 ms^{-1}, would give a predicted interval velocity of 3500 ms^{-1} ± 700 ms^{-1}. The thinner the isochron is, the larger the percentage error will be and consequently the larger the resultant error in isopach thickness will be. The most accurate interval velocities will be calculated in the thickest section where percentage error is the smallest.

In this project, a velocity map was constructed from the time-depth curves generated in SeisX for the T15-1–T20-1 sequence (Figure 3.11). This map exhibits some of the problems described above. The area of high interval velocity (5000 ms^{-1}) depicted by the red shading south-east of Talisman-1 was interpreted to be erroneous related to the lack of well control and the thin nature of the sediments (60 ms) in this area as depicted on the isochron map (Figure 3.12). The area of low interval velocity (2500 ms^{-1} –3000 ms^{-1}) represented by both areas of blue shading again corresponded to areas of thin sedimentation and low well density. In areas where there was high well density and thick sediment accumulation, such as on lines 136-23 and 136-19, a more homogenous interval velocity was calculated. Most of the wells had calculated interval velocities of 3300 ms^{-1} – 3800 ms^{-1} for this sequence; these were considered realistic results for the sediments. Comparing the isochron map (Figure 3.12) with the isopach map (Figure 3.13), it appears that all the main features that were apparent on the isochron map were also apparent on the isopach map. The erroneous areas in the map of interval velocity did not have a significant effect on the isopach map due to the thin nature of the sediments in these locations, the cause of the errors in the first place. In areas where sufficient well density and sediment thickness minimise gridding and calculation errors in the predicted interval velocity, the resultant map shows little variation of interval velocities. As a result, the depositional patterns as outlined on the isopach map are a good representation of the isochron map.

The study has defined a series of sequence stratigraphic events which have been used to subdivide the section. The absolute age of each event is subject to error within the biostratigraphic constraints of the data. As a result, error bars have been associated with each sequence stratigraphic event defined in the study. These will be further discussed in the following chapter.

As all the features displayed on the isopach map are evident on the isochron map, a decision was made to base the analysis of the sediment depositional patterns from the seismic data on isochron maps alone. Adoption of this approach it ensured all interpretations of sediment distribution patterns were based on raw seismic data which are not be subject to errors resulting from the process of calculating and interpolating interval velocities. However, volumes of sediment and sedimentation rates have been calculated at a later stage of the project using 3D-Chronostrat. By separating the stratal interpretation and the quantitative interpretation of sedimentation in this manner, errors which may result from the depth conversion would not affect the interpretation of stratal architecture.

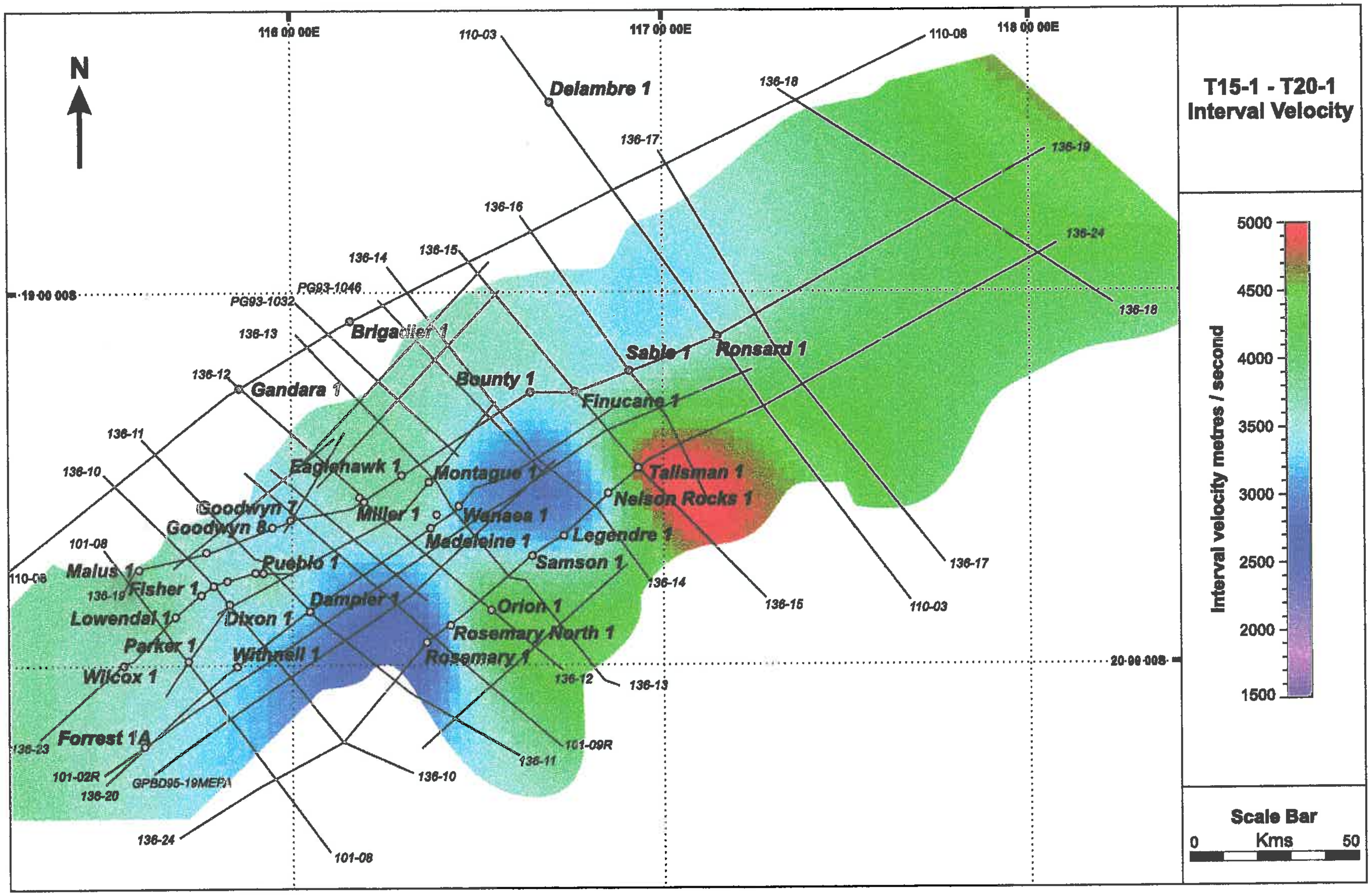

Figure 3.11 Interval velocity map calculated from time-depth curves for sequence T15-1–T20-1.

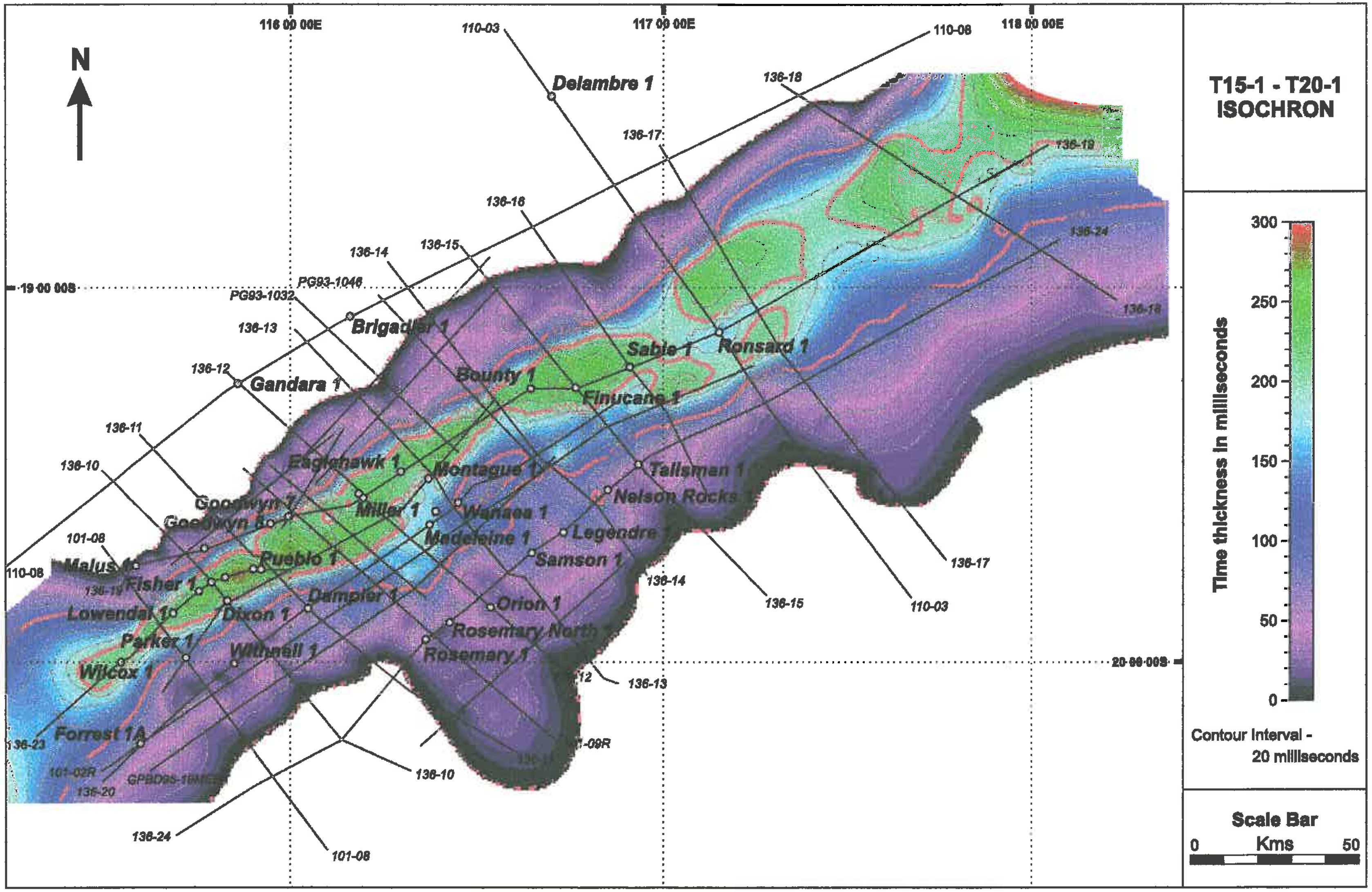

Figure 3.12 Isochron map for sequence T15-1–T20-1.

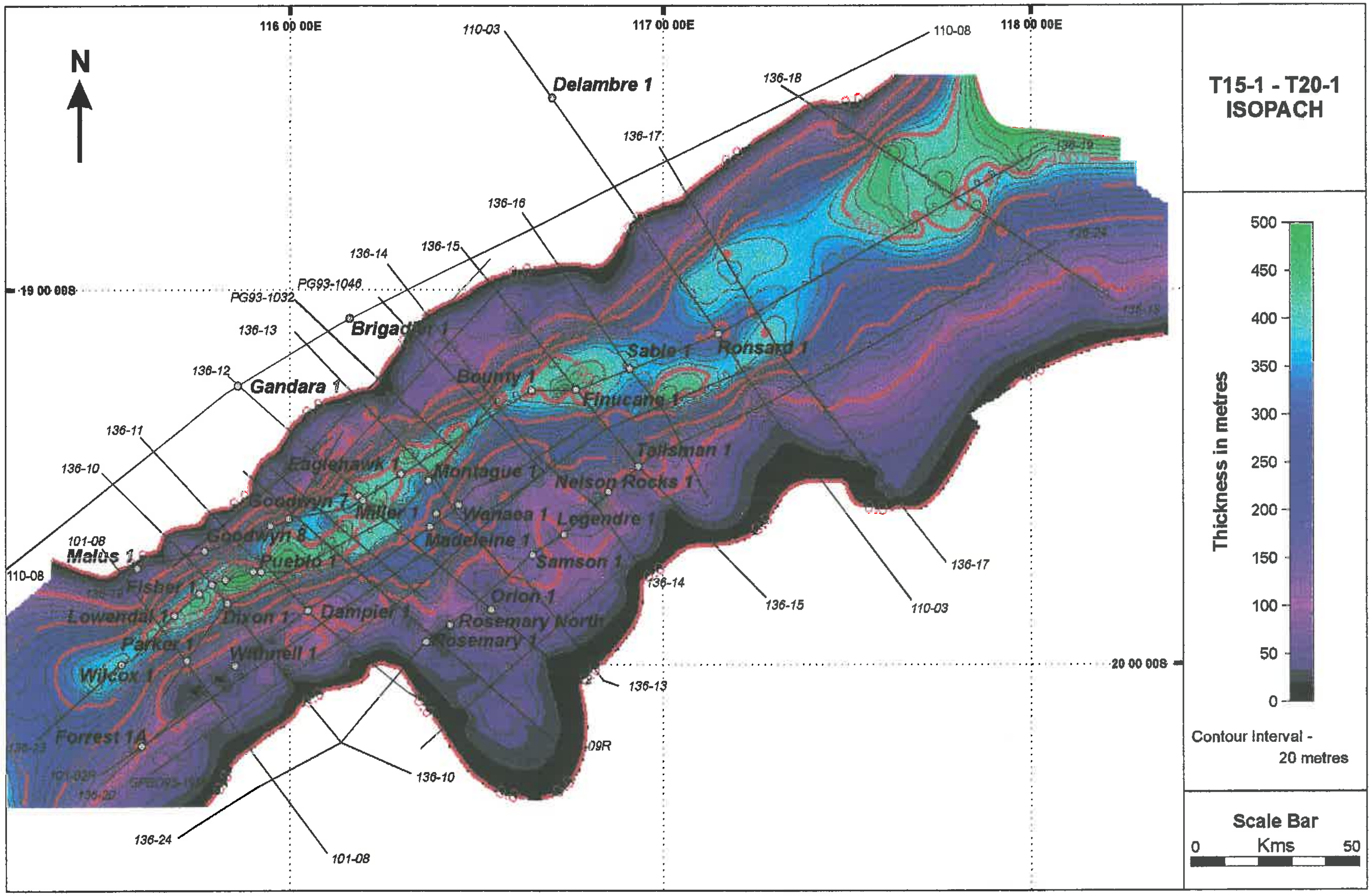

Figure 3.13 Resultant isopach calculated for the T15-1 to T20-1 sequence

3.5 3D-Chronostrat Analysis

Chronostratigraphic charts present the spatial distribution of geological units in relative geological time rather than depth and illustrate their temporal relationship to surfaces of non-deposition, condensation and erosion (Milton, 1996). They are a useful method of ensuring that interpretations are valid in geological time as well as space. Chronostratigraphic diagrams are based on the assumption that seismic reflectors represent time boundaries (Mitchum *et al.*, 1977d; Vail and Mitchum, 1977b). Sediment packages defined by these time boundaries are related genetically and have been termed chronosomes (Schultz, 1982). The basic procedures for generating chronostratigraphic charts from seismic data, also known as Wheeler diagrams, have been outlined in the literature (Milton, 1996; Mitchum *et al.*, 1977a; Mitchum *et al.*, 1977b; Vail *et al.*, 1977a; Wheeler, 1958) and are summarised in Figure 3.14.

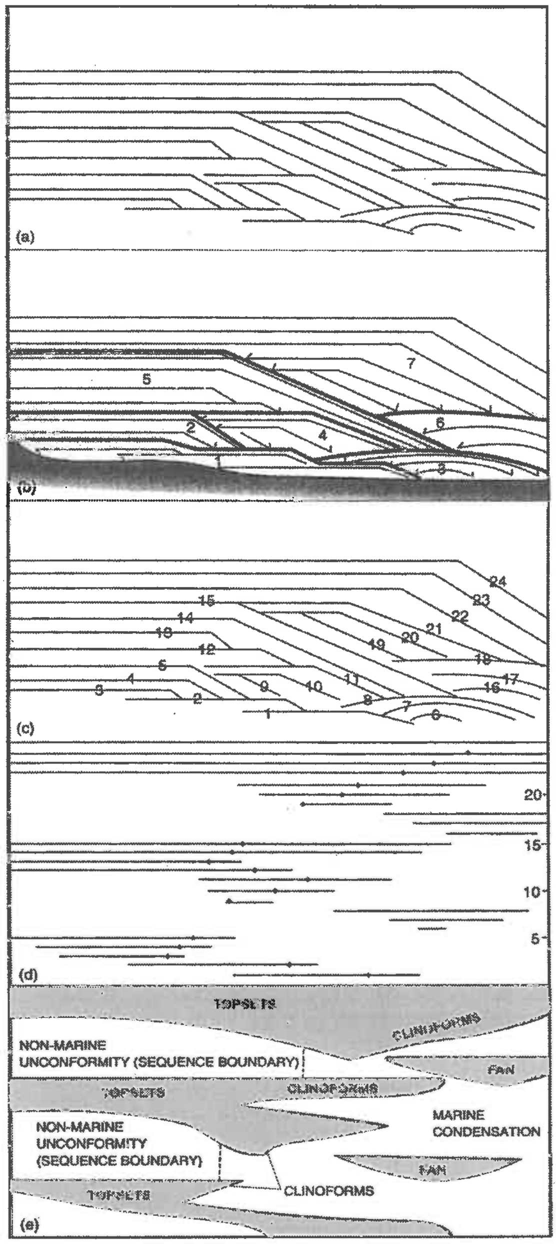

Figure 3.14 The process of constructing a chronostratigraphic chart from seismic data; (a) sketch seismic line; (b) a seismic stratigraphic breakdown of the line; (c) numbering of the reflections; (d) transfer of the reflections to the time axis in numeric order; (e) a chronostratigraphic interpretation of the seismic data (Milton, 1996)

In order to investigate the internal stratal architecture and stacking patterns of the Albian to Tertiary section of the Dampier Sub-basin, the sequences defined and mapped on the seismic database were analysed using a suite of programs called 3D-Chronostrat (Nordlund, 1992). These programs automate the construction of chronostratigraphic charts for each seismic line in the database and build a three-dimensional chronostratigraphy for the data set. These programs are extremely powerful in visualising the three-dimensional nature of basin-fill history. By mapping every seismic reflector which can be loop-tied on at least four lines, these programs generate a series of chronostratigraphic sections, Wheeler diagrams (Figure 3.15) and hiatus plots for each individual seismic line, and a series of maps of chronosome thickness, depth and distribution for the whole basin. The output from the 3D-Chronostrat suite of programs gives a high-resolution three-dimensional image of the stratal architecture and enables a quantitative analysis of the basin's evolution to be made at a significantly higher resolution than has previously been possible. The three-dimensional chronostratigraphic evolution of a basin and individual systems tracts is rarely discussed in the literature.

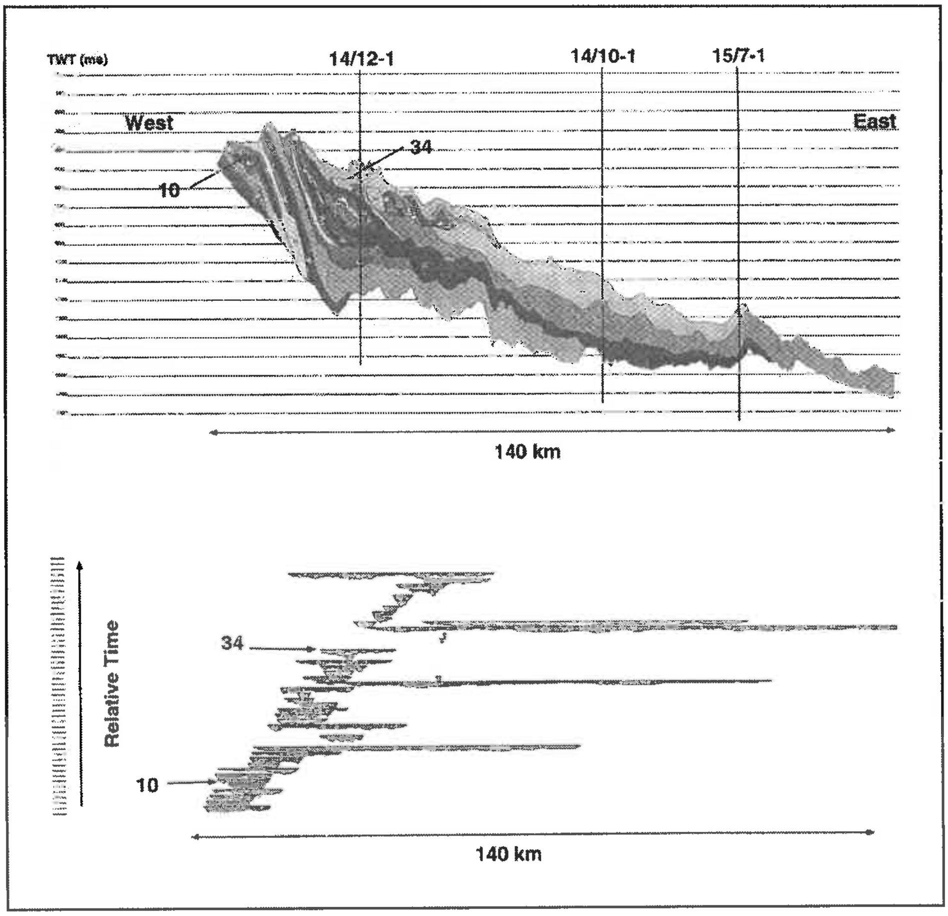

Figure 3.15 Chronostratigraphic section and associated Wheeler diagram showing the progradational nature of the Tertiary section of the Outer Moray Firth, North Sea (Griffiths and Hadler-Jacobsen, 1995).

3.5.1 3D-Chronostrat - program description

3D-Chronostrat is a suite of programs that can be used to analyse the high-resolution stacking architecture of a basin by subdividing the basin fill into a series of genetically linked, three-dimensional time-bounded packages, which have been termed chronosomes (Schultz, 1982). The procedure for the application of the 3D-Chronostrat programs to this project is summarised below and has in part been paraphrased from Griffiths and Hadler-Jacobsen (1995). For further description of the application and uses of these programs see Griffiths and Nordlund (1993; 1996) and Nordlund and Griffiths (1993a; 1993b).

The 3D-Chronostrat suite of programs is composed of three separate programs called DIGITIZE, CHRONOSTRAT and 3D GRID. DIGITIZE is a form of seismic interpretation package which is used to digitize and tie seismic reflectors throughout a data set. Images of seismic lines are loaded into DIGITIZE. The events identified and mapped during the seismic interpretation phase of the project are again identified. The spatial distribution of all further reflectors that can be loop-tied on at least four seismic lines are mapped throughout the data set. Horizons are terminated against each other either as onlap, downlap or truncation. This termination style is critical to the program and must be identical on all lines for any two horizons that coalesce to form one edge of a discrete sediment body (Figure 3.16). DIGITIZE checks there are no ambiguous terminations between two horizons and then sorts and sequentially numbers the digitized 3D horizons from the base upwards. The completed DIGITIZE output file forms the input file for the CHRONSTRAT program.

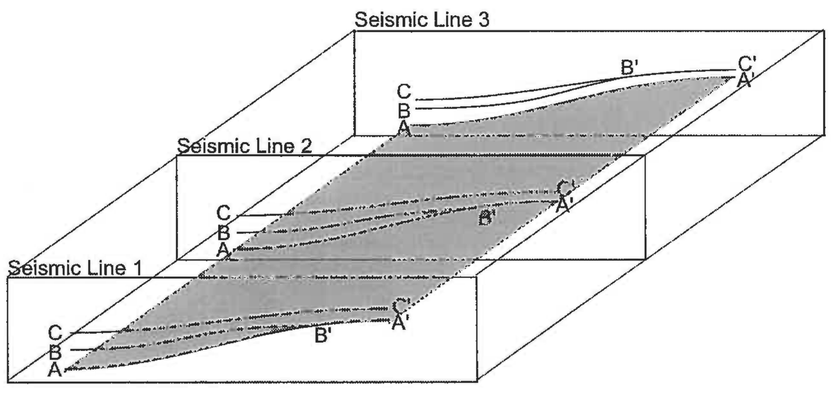

The nature of the termination of BB' on AA' must be the same on seismic lines 1, 2 and 3. In the above example BB' onlaps AA' on seismic lines 1 and 2. However, on seismic line 3 CC' truncates BB' before it onlaps AA', in these situations BB' is mapped on top of CC' until CC' onlaps AA' thus correctly defining the sediment body AA'-BB'.

Figure 3.16 3D-Chronostrat requires the termination pattern of a discrete edge of a sediment body to be identical on all adjacent seismic lines to enable the program to correctly sort and sequentially number the defined chronosomes.

CHRONOSTRAT takes the input DIGITIZE file of digitized 3D horizons and analyses the stratal terminations on each 2D section. On the basis of the stratigraphic consequences of each tie, the 3D horizons are linked to define a series of three-dimensional reflection-bounded units or chronosomes. The CHRONOSTRAT program produces a series of these chronosomes which describe the basin fill history; in essence they define a three-dimensional chronostratigraphy for the basin, (Nordlund and Griffiths, 1993b).

The third 3D-Chronostrat program, 3D-GRID, is primarily a visualisation and gridding package. It uses the three-dimensional chronostratigraphy defined from CHRONOSTRAT to display the basin development, chronosome by chronosome. 3D grid can also be used to grid horizon depths, chronosome thicknesses and obtain quantitative information such as area and volume for each chronosome. 3D GRID can also be used to display 2D sections in the form of Wheeler diagrams that have been constructed using the three-dimensional chronostratigraphy generated in the CHRONOSTRAT program.

3.5.2 Calculation of sediment volumes

Quantitative information on sediment volumes within a stratal package and the rates at which these sediments have accumulated can reveal important insights into the depositional controls on a basin. Within the 3D-Chronostrat suite of programs, an isochron map can be generated for each chronosome defined from the digitised horizons and by specifying a function that relates time and depth, the volumes of each of these chronosomes can be calculated. However, 3D-Chronostrat can only accommodate linear relationships between time and depth and consequently the accuracy of calculated volumes depends on the ability of a linear function to accurately describe the time-depth relationship. In the Outer Moray Firth, Griffiths and Hadler-Jacobsen (1995) used check shot data to convert log depths to two-way time and observed a one-to-one relationship between depth and two-way time over their interval of interest. This one-to-one relationship was then used in their calculation of sediment volumes. Over a small interval, such as that modelled by Griffiths and Hadler-Jacobsen (1995), a linear one to one relationship between two-way time and depth may be a reasonable approximation. However, over large study intervals, the time to depth relationships are commonly non-linear. In this study wireline log depths have been converted to two-way time using check shot data. The resultant time-depth curves demonstrate a non-linear relationship between two-way time and depth for the Albian to Recent section of the Dampier Sub-basin (Figure 3.17). If a linear relationship were applied it would only be accurate at the point where the linear function and the actual time-depth function coincide as illustrated in Figure 3.17.

To obtain more accurate sediment volumes, the calculated chronosome volumes were initially output from 3D-Chronostrat using a one-to-one time-depth relationship. This gave a 'two-way time volume' for each chronosome. This 'two-way time volume' was then converted into an absolute volume using an interval velocity, which was calculated from the associated seismic stacking velocities using Equation 3.1. The calculation of the interval velocity was performed at the midpoint of the thickest section of each chronosome as identified from the chronosome thickness maps to ensure the majority of the sediment in the chronosome would be accurately converted. Whilst this method still applies a linear function relating time and depth it is a considerable improvement on the 3D-Chronostrat method as it defines a new time-depth relationship for each chronosome as opposed to a single linear function for the whole section. However, in situations where the chronosome is steeply dipping and has considerable thickness away from the central point, inaccuracies may arise in the depth conversion. As the 3D-Chronostrat suite of programs contain no facility for conducting a sophisticated depth conversion, it may be advisable for future studies to use depth converted seismic lines in DIGITIZE.

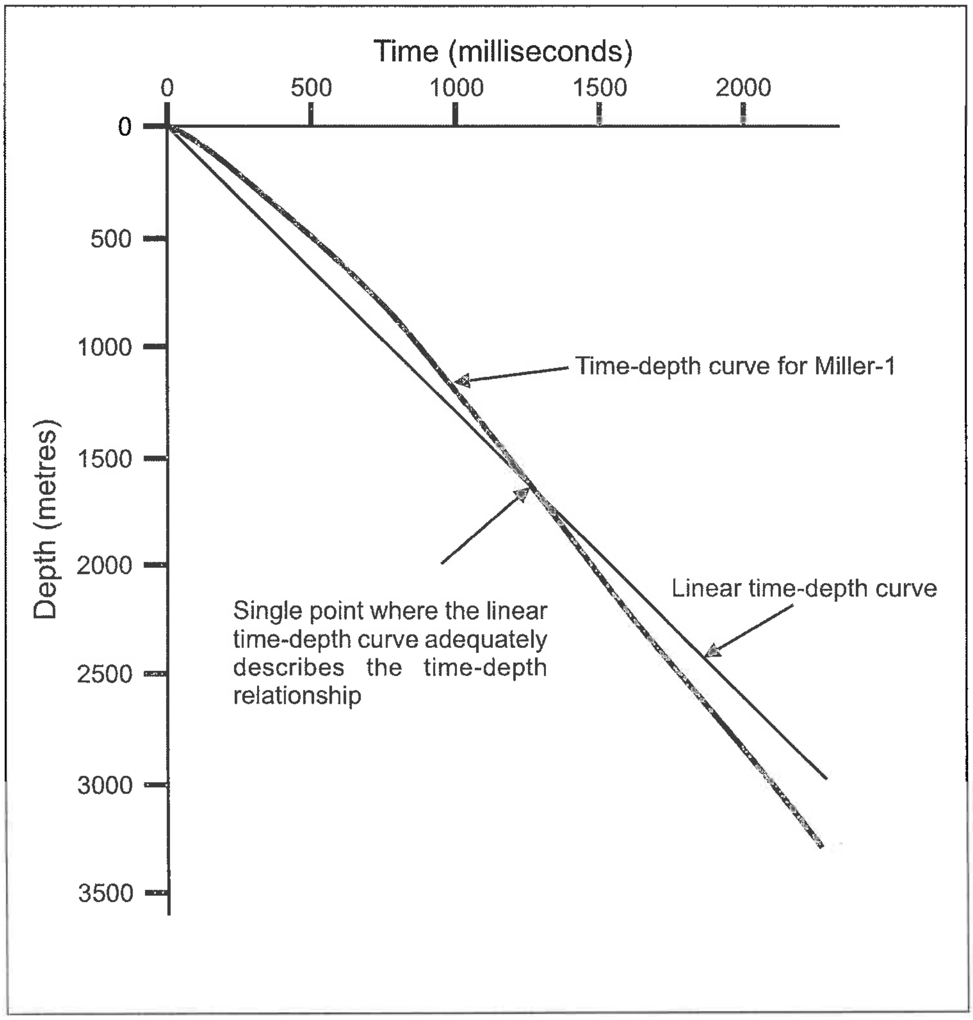

Figure 3.17 Time-depth curve for Miller-1showing the inability of a linear function to accurately describe the time-depth relationship at a well location.

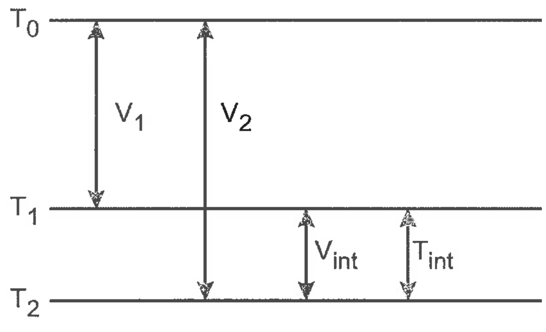

$$V_{int}.T_{int} = 0.5.V_2T_2 - 0.5.V_1T_1$$

$$T_{int} = 0.5.(T_2 - T_1)$$

$$V_{int} = (0.5.(V_2T_2 - V_1T_1))/(0.5.(T_2 - T_1))$$

$$V_{int} = (V_2T_2 - V_1T_1)/(T_2 - T_1))$$

Equation 3.1 Equation used to calculate interval velocities from RMS velocities.

3.5.3 Wheeler Diagrams

Within the 3D-Chronostrat suite of programs, 3D GRID can be used to generate a two-dimensional Wheeler diagram for each seismic line using the three-dimensional chronostratigraphy defined from CHRONOSTRAT. A Wheeler diagram that has been constructed using a three-dimensional chronostratigraphy will record periods of out-of-plane deposition as periods of non-deposition. If the same Wheeler diagram had been constructed purely from the two-dimensional chronostratigraphy, this period of non-deposition would not have been identified and the duration of subsequent chronosomes will be assumed to be the duration of the chronosome plus the period of non-deposition.

In conventional Wheeler diagrams the stratal architecture is displayed in geological time with the lowest or earliest point in the chronosome representing the location of the initial sedimentation in that chronosome. The Wheeler diagrams produced by 3D GRID differ from conventional Wheeler diagrams in two ways. Firstly, Wheeler diagrams produced by 3D GRID display chronosomes in relative time with each chronosome occupying an equal amount of time. Secondly the variation in chronosome thickness as displayed on the Wheeler diagram reflects variations in relative sediment thickness within each chronosome and not the relative timing of sedimentation within each chronosome. The difference between the two types of Wheeler diagrams is demonstrated in Figure 3.18.

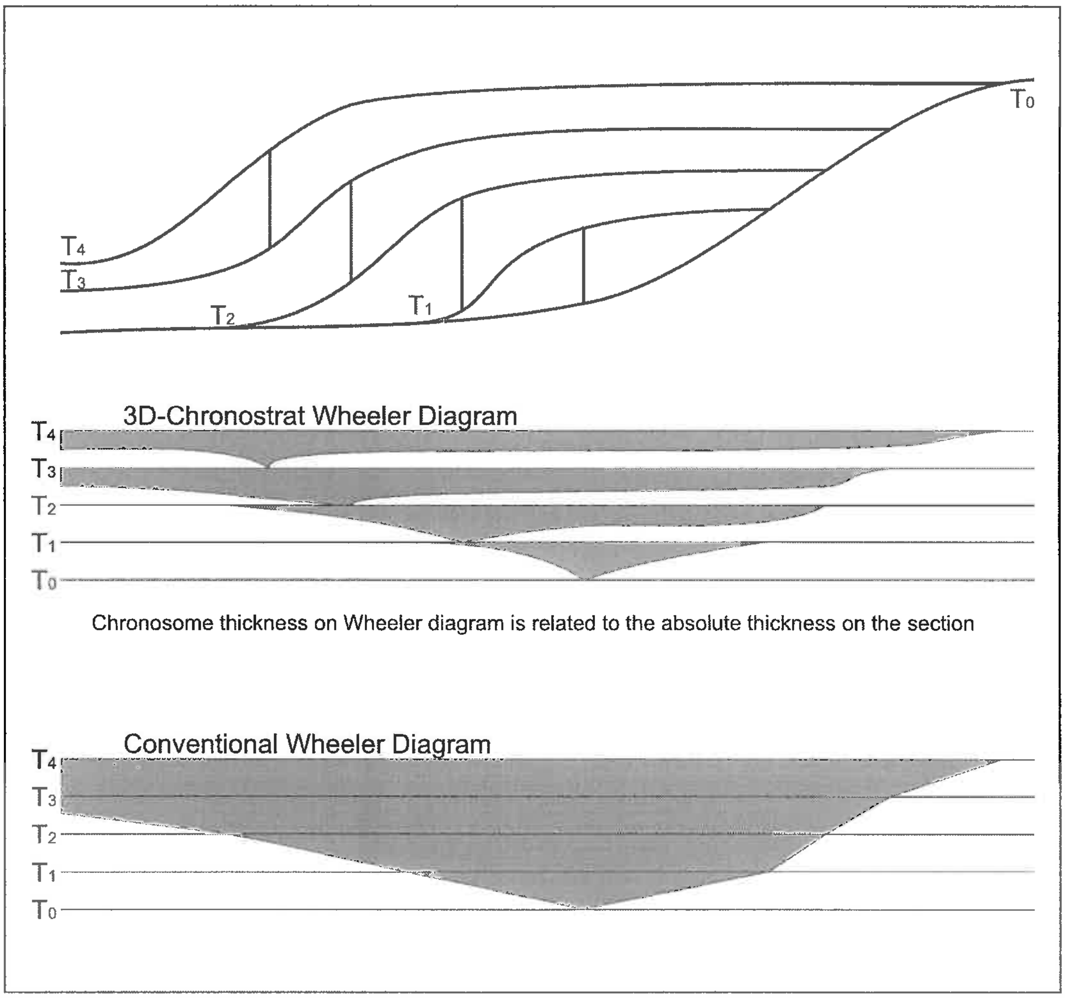

Figure 3.18 Variations in 3D Grid produced Wheeler Diagrams and conventional Wheeler diagrams.

3D-Chronostrat can only deal with straight seismic lines, where a line is more complex it has to be subdivided into individual straight segments which 3D-Chronostrat treats separately. The output can then be graphically reconstructed to form one complete line and so does not pose a problem for the 3D-Chronostrat sections. However, it is a problem for Wheeler diagrams, where the thickness of the chronosome as displayed on the Wheeler diagrams is scaled according to the thickness of the chronosome on the 3D-Chronostrat section. As each segment of a complex line is treated as a separate line the thickness of the chronosomes will be scaled according to the maximum thickness of each section and not the whole line. It is therefore not possible to evaluate thickness variations across sections of a composite line on the basis of the Wheeler diagrams. On Wheeler diagrams where a complex line has been subdivided into individual straight sections, the segment junction has been clearly indicated by a vertical line.

3.6 Paleogeographic Maps

A series of paleogeographic maps have been generated for the Albian to Pliocene sequences of the Dampier Sub-basin using a combination of the biostratigraphic, seismic, wireline log and sedimentological evidence. Sedimentological evidence has been obtained primarily from sidewall core reports with some additional cuttings evidence. Sidewall core samples for key wells within the basin have been viewed as a cross-reference for the descriptions contained within the well completion reports. However, this was not possible for many of the wells along the inner margin of the basin as a fire in the late 1980s at the Woodside core store destroyed the majority of samples.

A lack of samples in the Pliocene to Recent section has prevented paleogeographic maps for the uppermost two sequences defined within this study to be constructed. An environmental interpretation of the faunal assemblages described in the biostratigraphic reports for several key wells has been made by Louise Christian (pers com) and these interpretations are included as Appendix A. These interpretations have complemented the environmental interpretation already existing and helped constrain palaeowater depths.

CHAPTER 4 RESULTS - BIOSTRATIGRAPHIC AND WIRELINE LOG ANALYSIS

4.1 Introduction

Using the methodology and project rationale outlined in Chapter 3, the Albian to Recent section of the Dampier Sub-basin was subdivided into a series of genetically-related units separated by time-correlative surfaces. The section was initially subdivided into major stratigraphic units bound by biostratigraphic events of regional significance. These units were then further subdivided into sequences using a model that was developed for the sequence stratigraphic interpretation of carbonate wireline log motifs and all available biostratigraphic constraints.

Using this integrated biostratigraphic and wireline approach, the section was divided into genetically-related packages of sediment separated by time-correlative regional events of determinable age. These events provided the high-resolution framework within which quantitative analysis of the evolution of the basin could be made. This framework of events has been termed a chronostratigraphic framework.

4.1.1 The nature of the biostratigraphic record

The nature of the sediment preserved at any one well location is in part a result of the interplay of subsidence and relative sea level. If the well location had been subject to a constant rate of subsidence throughout its entire depositional history then all sediment deposited would be preserved. However, the interplay of subsidence and relative sea level controls the nature of accommodation space available for sediment deposition and hence the nature of the sediment preserved. When subsidence and relative sea level rise combine to generate significant amounts of accommodation space, sediment will be deposited and preferentially preserved. When subsidence and relative sea level negate each other, the amount of accommodation space is reduced, little or no sediments are deposited and those previously deposited whilst subsidence and relative sea level rise were in unison may be removed. Therefore the sediment column preserved at a single well location records sediments deposited when subsidence and relative sea level combine to create accommodation space and the intervening hiatal surfaces represent periods when accommodation space has been destroyed. This is most clearly demonstrated in Figure 4.1 which shows the combination of an individual relative sea level curve and a constant subsidence curve and demonstrates how they interact to control the nature of the sedimentary succession preserved at a single well location. It is evident from Figure 4.1 that the geological time encompassed in a hiatal surface can be significant and have similar duration to that encompassed in the preserved sedimentary succession.

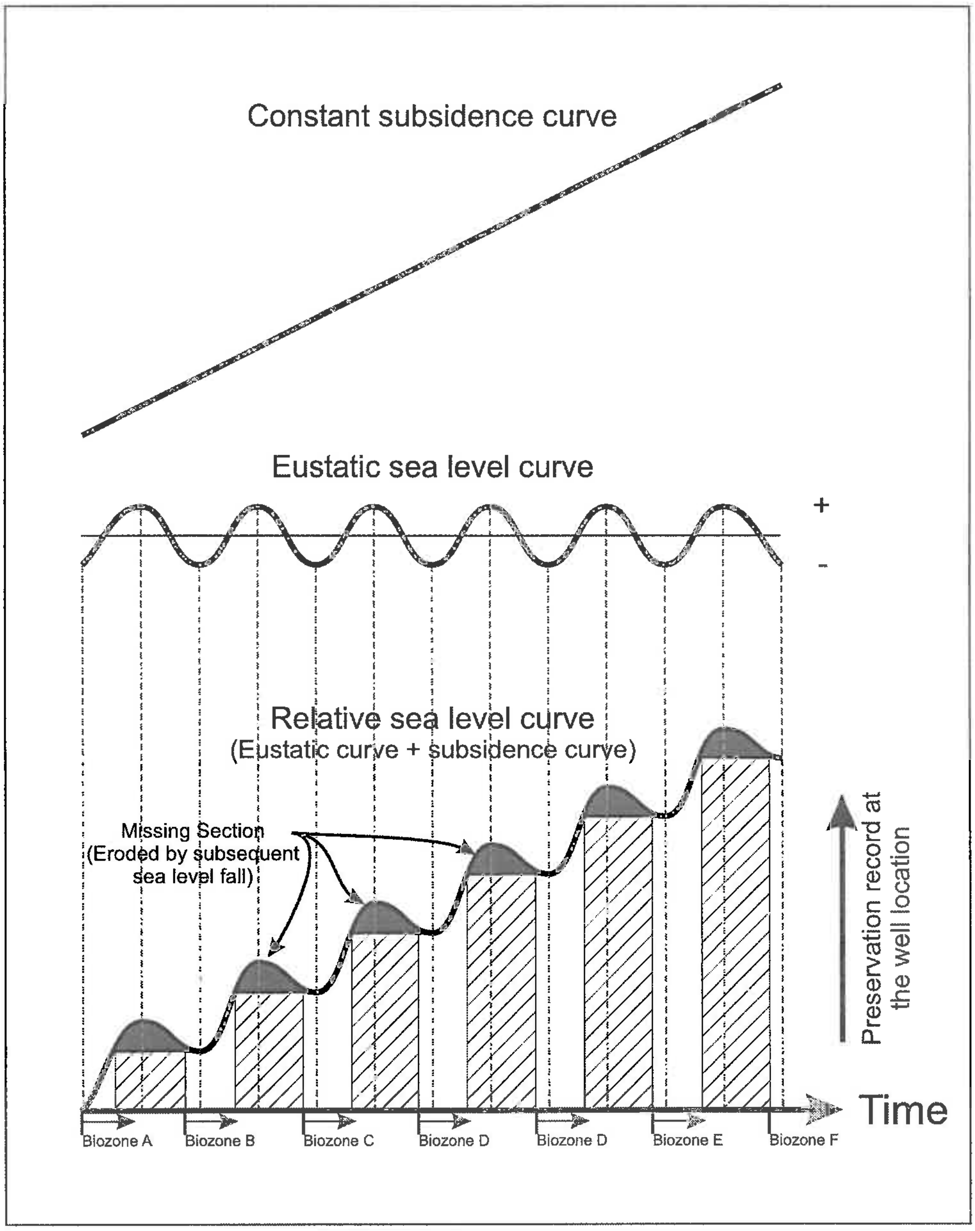

Figure 4.1 Preservation record at one well as a function of subsidence and relative sea level

The subsidence rate at any single well location may vary though time as a result of the regional tectonic regime or localised tectonic events such as fault block movement. These tectonic events will accentuate the preservation potential or erosion of sediments and will therefore control the nature of the preserved sediment at the well location. The events can be easily identified from well data with anomalously high subsidence being represented by expanded sections and localised uplift represented by the absence of biozones which are present in other areas of the basin. In practice it is hard to quantify the change in subsidence rate and to do so would require sophisticated thermal and structural modelling. It is therefore the norm to analyse changes in the sedimentary succession with respect to relative sea level.

4.1.2 Dating biostratigraphic events

From Figure 4.1, it is evident that hiatal surfaces can have a significant duration and consequently the absolute age for the missing section can vary within the range of the last preserved sediment before the missing section and the first preserved sediment after the missing section. It is not possible to accurately define the timing of the onset of the erosive event as it will erode the sediment deposited immediately prior to it. However, the timing of the end of the event can be accurately defined from the age of the first sediments deposited immediately above the event. Events in this study have therefore been named and dated according to the age of the sediments deposited immediately after each event. Error bars indicating the range of possible ages of these events have been defined from the duration of the associated missing section at each well. The age and error bars defined for each event at each well location are then combined to derive the age and error of the event across the whole basin.

4.2 Biostratigraphic analysis

The Albian to Recent section of the Dampier Sub-basin was initially subdivided into a series of megasequences separated by basin-wide episodes of missing section defined from the biostratigraphic reports. Within the reports, missing section is identified where sediments of a particular biozone have not been identified in the well. In biostratigraphic reports with good sample density, it has been possible to positively identify and accurately date the timing of the missing section and this is commonly stated as a conclusion in the biostratigraphic report. In wells with a lower sample density it is often ambiguous whether sediments of that age are missing from the section or have not been sampled. In this situation, the nature of the missing section is determined on the basis of the geological information in the surrounding wells and by wireline log character. By collating the episodes of missing section across the basin, it is evident which events are regionally significant and which are more localised in their extent.

This study has used biostratigraphic data from thirty-seven wells to subdivide the section into megasequences and later constrain the wireline log interpretation. Figure 4.2a shows the location of these wells whilst Figure 4.2b, summarises the biostratigraphic age of the sediments contained within these wells. On Figure 4.2b missing section is identified in black, present section is identified in grey and sediments of undefined age are shaded with hashes. Figure 4.2b clearly shows several episodes of missing section that persist throughout the majority of the wells in the study area.

The section was subdivided into genetically-related units which were separated by major episodes of missing section of late Santonian (C8), Maastrichtian (C12), Danian (T1-T4), Thanetian (T6-T7), late Eocene to early Oligocene (T15) and Burdigalian (N6-N8) age. Other events of Ypresian-Lutetian (T10), Bartonian (T12), and late Miocene (N16-N18) age are suggested from the biostratigraphic data but these are not as accurately defined from biostratigraphic data or considered to be as regionally extensive. These episodes of missing section have been interpreted as regional unconformities and therefore sequence boundaries. Due to localised tectonics and basin topography, the duration of some of these events is seen to vary throughout the basin. All the sequence boundaries that have been defined in this project have been named and dated according to the first preserved sediment following the period of missing section identified from the biostratigraphic data. For example, from Figure 4.2 it can be seen that the Thanetian (T6-T7) event begins in the T5 biozone in certain wells (Wilcox 1 and Delambre 1) and persists until T8 in other wells (Fisher 1 and Lowendal 1). However in Finucane-1, Miller-1, Goodwyn-7 & 8, Tidepole-1 and Gandara-1, T7 aged sediment has been recorded directly above the period of missing section and as such this event has been dated as a T7 aged event (Figure 4.2). Using this method, sequence stratigraphic events of C9, C13, T1, T7, T15 and N8 age have been determined for these episodes of missing section. Sequence stratigraphic events in this study been named after the biozone in which they occur and are numbered sequentially from the base of each biozone. In the case of the major basin-forming events, they have been termed C9-1, C13-1, T1-1, T7-1, T15-1 and N8-1 respectively.

Combined subsidence and sea level curves have been generated for Wilcox-1 and Finucane-1 to demonstrate the nature of the biostratigraphic events that have been recorded in these wells (Figure 4.3). For simplicity, the subsidence rate has been kept constant throughout the Albian to Recent section of these wells. This is represented by the same gradient on all preserved portions of the curve. The periods of missing section have been shaded black, and these define the portions of the curve when the sea level has fallen. The shape of the curve during these periods of missing section is unconstrained as the data recording its shape has been eroded. The age of the missing section has been determined from the age of the first preserved sediments immediately above the events and consequently this has been equated to the start of an instantaneous relative sea-level fall. The shape of the curve in the absent biozones has been defined from the subsidence curve, giving an asymmetric shape to the overall curve during the period of missing section in Figure 4.3. However, if the age of the event, which has resulted in the missing section, were taken at the middle of the missing biozones, a symmetrical curve would result. By combining all the information on the age of the relative sea level falls from all wells across the basin, it is possible to constrain the age of the events and thus the shape of the combined subsidence and relative sea level curves. Biostratigraphic data has constrained the age of the base Tertiary relative sea level fall to being of T1 age as T1 sediments are recorded directly above the events in certain wells in the basin (Figure 4.2). Therefore, in Wilcox-1, the event that separates T1 from C7-C8 sediments has been dated as a T1 event and the asymmetrical shape of the combined subsidence and sea level curves is a reasonable approximation for the relative sea level curve in this area. Thus from Figure 4.3, it can be concluded that in the Dampier Sub-basin, the relative sea level curve is asymmetric in nature and with relative sea level falls being short lived phenomenon which punctuate long periods of sedimentation.

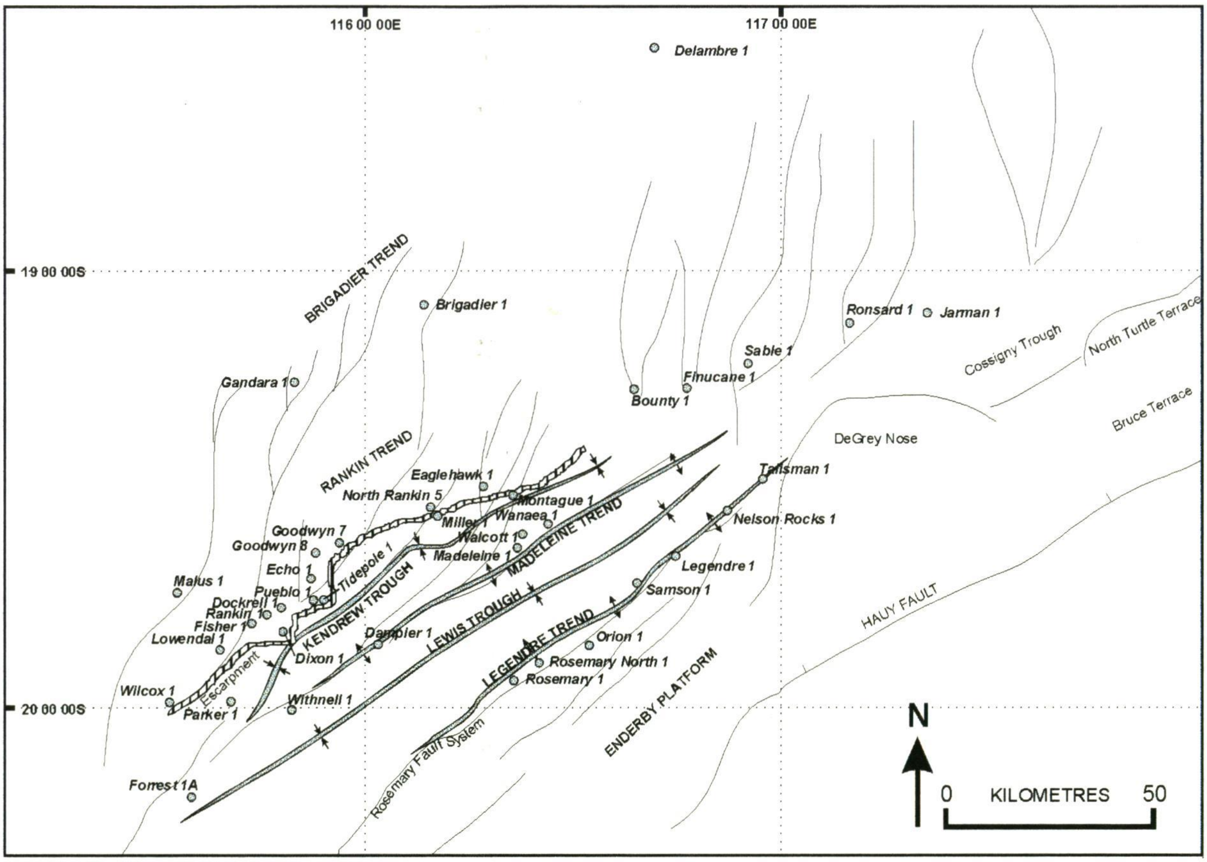

Legend

Sediments of this age have been positively identified from the presence of diagnostic foraminifera assemblages.

Missing section - the absence of any diagnostic assemblages of this age has been identified.

Undifferentiated - diagnostic age determinations have not been possible. This can either be due to poor foraminifera recovery rates in which case stage names are normally only defined or due to poor sampling resolution in which case it is not possible to determine the absence or presence of a biozone.

Biostratigraphic reports contain no mention of the presence or absence of assemblages of this age.

Figure 4.2a (above) Location map showing the distribution of the wells which have been analysed during the biostratigraphic analysis of the data. In the Albian to Recent sediments in the Dampier Sub-basin the biostratigraphic reports are based on foraminiferal data recovered from sidewall core and cuttings data.

Figure 4.2b (opposite) Summary diagram illustrating the age of sedimentary packages in the Dampier Sub-basin as determined from biostratigraphic data. Major basin-wide unconformities are clearly shown on this diagram by the presence of laterally extensive missing section (in black).

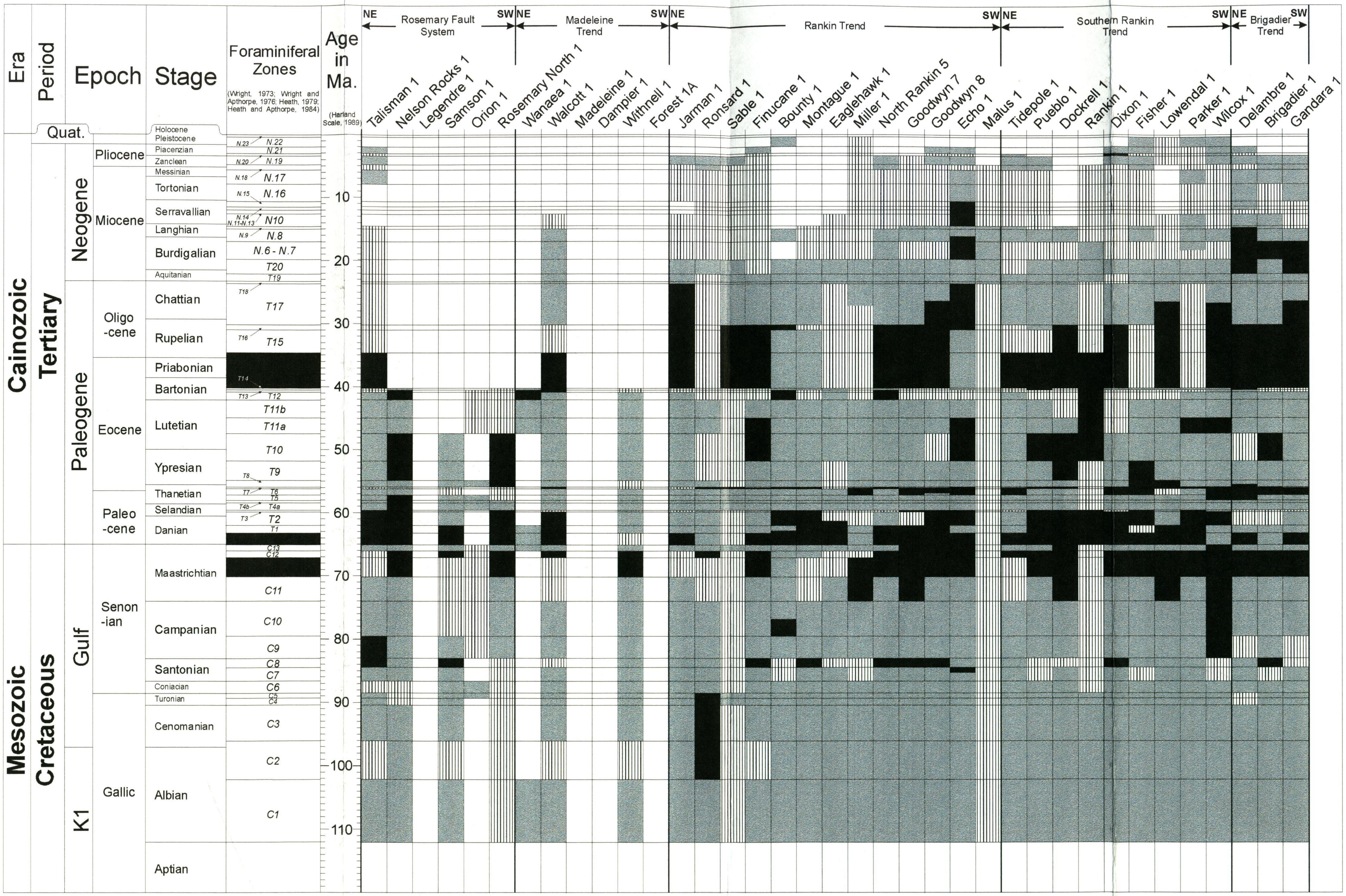
Era
Period
Epoch
Stage
Foraminiferal Zones
(Wright, 1973; Wright and Apthorpe, 1976; Heath, 1979; Heath and Apthorpe, 1984)
Age in Ma.
(Harland Scale, 1989)
Cainozoic
Mesozoic
Tertiary
Cretaceous
Quat.
Neogene
Paleogene
Gulf
K1
Pliocene
Miocene
Oligo -cene
Eocene
Paleo -cene
Senon -ian
Gallic
Holocene
Pleistocene
Piacenzian
Zanclean
Messinian
Tortonian
Serravallian
Langhian
Burdigalian
Aquitanian
Chattian
Rupelian
Priabonian
Bartonian
Lutetian
Ypresian
Thanetian
Selandian
Danian
Maastrichtian
Campanian
Santonian
Coniacian
Turonian
Cenomanian
Albian
Aptian
N.23 N.22
N.21
N.20 N.19
N.18 N.17
N.15 N.16
N.14 N.11-N.13 N10
N.9 N.8
N.6 - N.7
T20
T19
T18
T17
T16 T15
T14
T13 T12
T11b
T11a
T10
T8 T9
T7 T6 T5
T4b T4a
T3 T2
T1
C13
C12
C11
C10
C9
C8
C7
C6
C5
C4
C3
C2
C1
10
20
30
40
50
60
70
80
90
100
110
NE Rosemary Fault System SW
NE Madeleine Trend SW
NE Rankin Trend SW
NE Southern Rankin Trend SW
NE Brigadier Trend SW
Talisman 1
Nelson Rocks 1
Legendre 1
Samson 1
Orion 1
Rosemary North 1
Wanaea 1
Walcott 1
Madeleine 1
Dampier 1
Withnell 1
Forest 1A
Jarman 1
Ronsard 1
Sable 1
Finucane 1
Bounty 1
Montague 1
Eaglehawk 1
Miller 1
North Rankin 5
Goodwyn 7
Goodwyn 8
Echo 1
Malus 1
Tidepole 1
Pueblo 1
Dockrell 1
Rankin 1
Dixon 1
Fisher 1
Lowendal 1
Parker 1
Wilcox 1
Delambre 1
Brigadier 1
Gandara 1

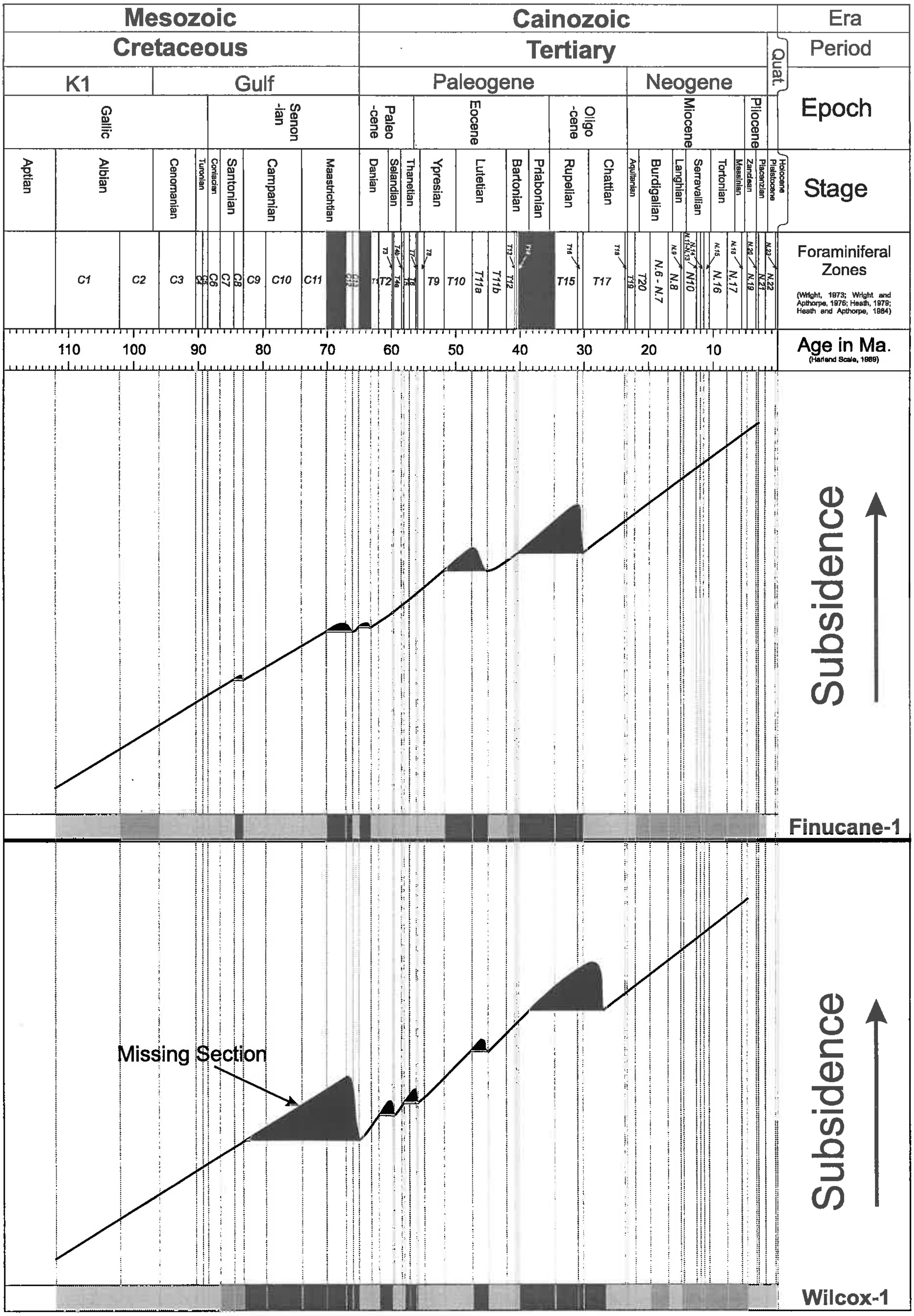

Figure 4.3 Combined subsidence and relative sea level curve for Wilcox-1 and Finucane-1

4.3 Wireline log analysis

The six major unconformities defined from the biostratigraphic analysis were identified on wireline logs and correlated throughout the basin. On wireline logs these events had a characteristic and repeatable log motif; this facilitated the ease of correlation in wells with poor biostratigraphic resolution. Figure 4.4 shows the type wireline response for the six major unconformities as identified by missing section in the biostratigraphic reports.

These six major unconformities, as defined from biostratigraphic data, are seen to correspond closely to the boundaries of long-term trends in the log data. These trends can be clearly defined on the gamma, sonic, neutron and density logs for Lowendal-1 and Montague-1 (Figure 4.5). In both Lowendal –1 and Montague-1, the log suites can be divided into packages of C1-1–C9-1, C9-1–C13-1, C13-1–T1-1, T1-1–T7-1, T7-1–T15-1 and T15-1–N8-1 age. These units can be most clearly defined on the neutron and density logs but can also be identified on the sonic and gamma logs. In Montague-1, where the density log has been recorded for the upper section of the well, the log shift across the N8-1 boundary is clearly evident and a further log shift can also be seen to occur at what has been correlated to be the N17-1 sequence boundary. These long-term trends in the log data are interpreted to represent periods where the sediments have undergone a similar burial history with the breaks at the top and base of the packages representing changes in subsidence regime. The subdivision of the section on the basis of the log response corresponds closely to and thus supports the biostratigraphic subdivision of the section and the recognition of the C9-1, C13-1, T1-1, T7-1, T15-1 and N8-1 events as major unconformities. Whilst these long-term trends can be identified in all wells across the basin, diversions from these patterns are also evident and these have been interpreted to be related to localised tectonic events.

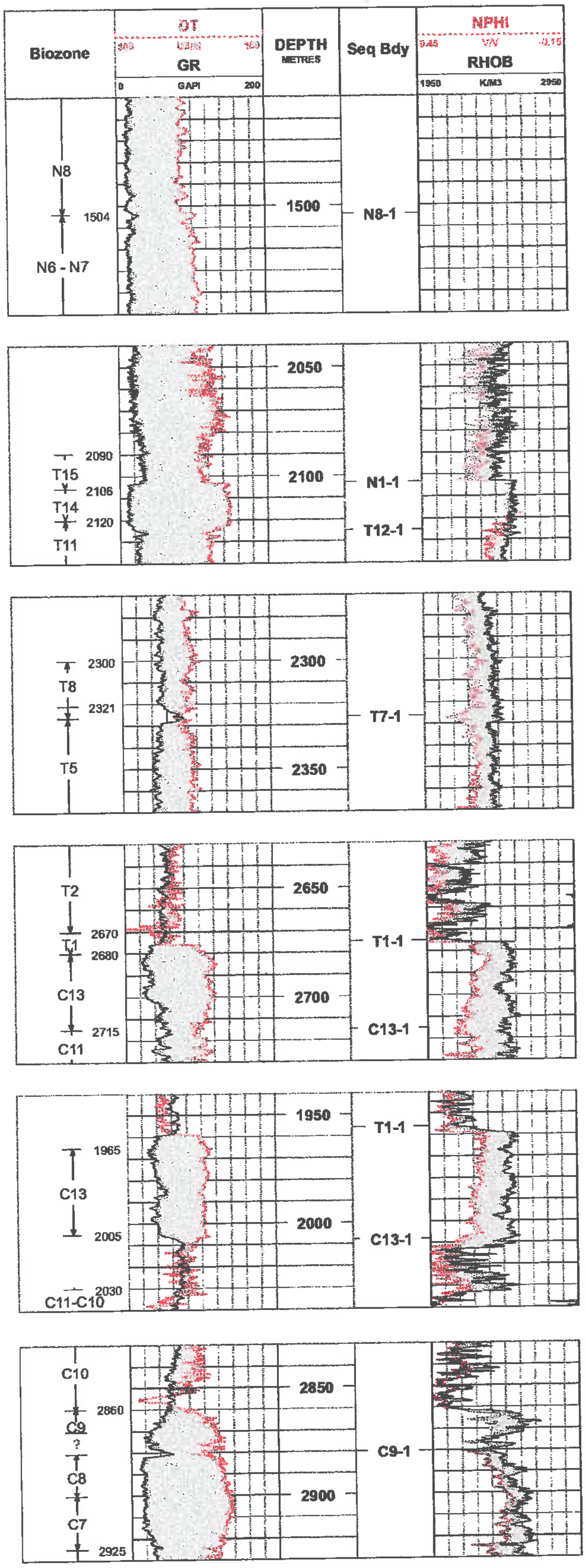

N8-1 **Type Well - Fisher 1**

Description

Normally exhibited as a small increase in the gamma API reading and the base of an upwardly increasing trend of interval transit time on the sonic log. Neutron and density logs show a minor shift to higher porosities and lower densities.

N1-1 **Type Well - Bounty 1**

Description

Commonly associated with significant missing section. Gamma log shows an abrupt increase in API with the sonic showing a corresponding increase in interval travel time. Neutron and density logs show an abrupt increase in porosity and decrease in density respectively.

T7-1 **Type Well - Miller 1**

Description

Commonly completely removes T6 and part of T5 aged sediment below. Gamma and sonic logs show an abrupt, short lived increase in reading. An increase in porosity at the boundary is noted on the neutron log which is sometimes associated with an increase in density.

T1-1 **Type Well - Gandara 1**

Description

A widespread event which removes most of the Danian section in the area. A marked increase in interval transit time and an increase in the gamma API values are common. An abrupt shift to higher porosities and lower densities is common on the density-neutron logs.

C13-1 **Type Well - Ronsard 1**

Description

A short lived widepsread event which removes the majority of C12 sediments from the basin. Gamma logs show an abrupt shift to lower values as do the interval transit times. Neutron and density logs show a sharp increase to a lower porosities and higher densties.

C9-1 **Type Well - Lowendal 1**

Description

A widespread event which has removed C8 sediments from a large area of the basin. It is represented by an abrupt kick on the gamma and sonic logs at the base of an upwardly increasing trend. Neutron and density logs show an overall shift to higher porosities and lower densities.

Figure 4.4 Type wireline log examples of major basin-forming events.

Figure 4.5 Wireline log suites for Lowendal-1 and Montague-1 with biostratigraphic data and interpreted sequence boundaries (Scale 1:5000)

4.3.1 Albian – Maastrichtian sediments

The Albian to Maastrichtian (C1-1 – T1-1) section of the study wells in the Dampier Sub-basin has a characteristic wireline log response that is common to all wells in the basin. Lowendal-1 has an expanded Albian to base Tertiary section, which is typical of the log response for this section (Figure 4.5). Within this late Cretaceous section the C9-1 boundary can be seen to subdivide the section into two packages of genetically-related sediments with similar log responses. Below the C9-1 boundary, sonic log readings of 250-400 μsm^{-1} mirror a strongly varying gamma log signature (between 10-50 API). Above the C9-1 boundary, the logs record less vertical variation and are characterised by high gamma responses (60-70 API) associated with medium interval transit times as recorded by the sonic log (350 μsm^{-1}). The neutron and density tools also clearly define the C9-1 boundary showing a shift to lower neutron porosities and bulk densities in the C10 and C11 sediments above the C9-1 boundary than below it. C13 sediments throughout the basin are characterised by low gamma and sonic values (30 API and 250-300 μsm^{-1}) with the neutron density logs showing a large separation with high densities (2.55-2.65 kgm^{-3}) and low neutron porosities (0.25–0.3 p.u.) as typified by Bounty-1 (Figure 4.6).

In two areas of the study, late Cretaceous sediments are missing and Tertiary sediments are seen to rest unconformably on middle to late Cretaceous aged sediments. Wilcox-1 has no recorded presence of Campanian or Maastrichtian sediments and has base Paleocene (T1) sediments resting directly on top of Santonian C7 and C8 aged sediments (Figure 4.2). The sharp nature of the contact as demonstrated on the gamma, sonic, neutron and density logs combined with the recorded absence of Campanian to Maastrichtian faunas suggests this is most probably an erosive event as opposed to a condensed section. This is the only well in the study in which the base Tertiary event is seen to remove all Campanian and Maastrichtian sediments. However, in other wells in the study (Echo-1, Dockrell-1, Goodwyn-7 and Goodwyn-8), the absence of C13 aged sediments has also been identified from biostratigraphic data (Figure 4.2). In these wells, Paleocene sediments are seen to rest upon Campanian – Maastrichtian age C10-C11 aged sediments. The wireline logs for these wells demonstrate this boundary to be associated with a shift to higher gamma and bulk density values (Figure 4.7). This variety in log response of the late Cretaceous sediments throughout the basin is interpreted to be related to localised tectonic events.

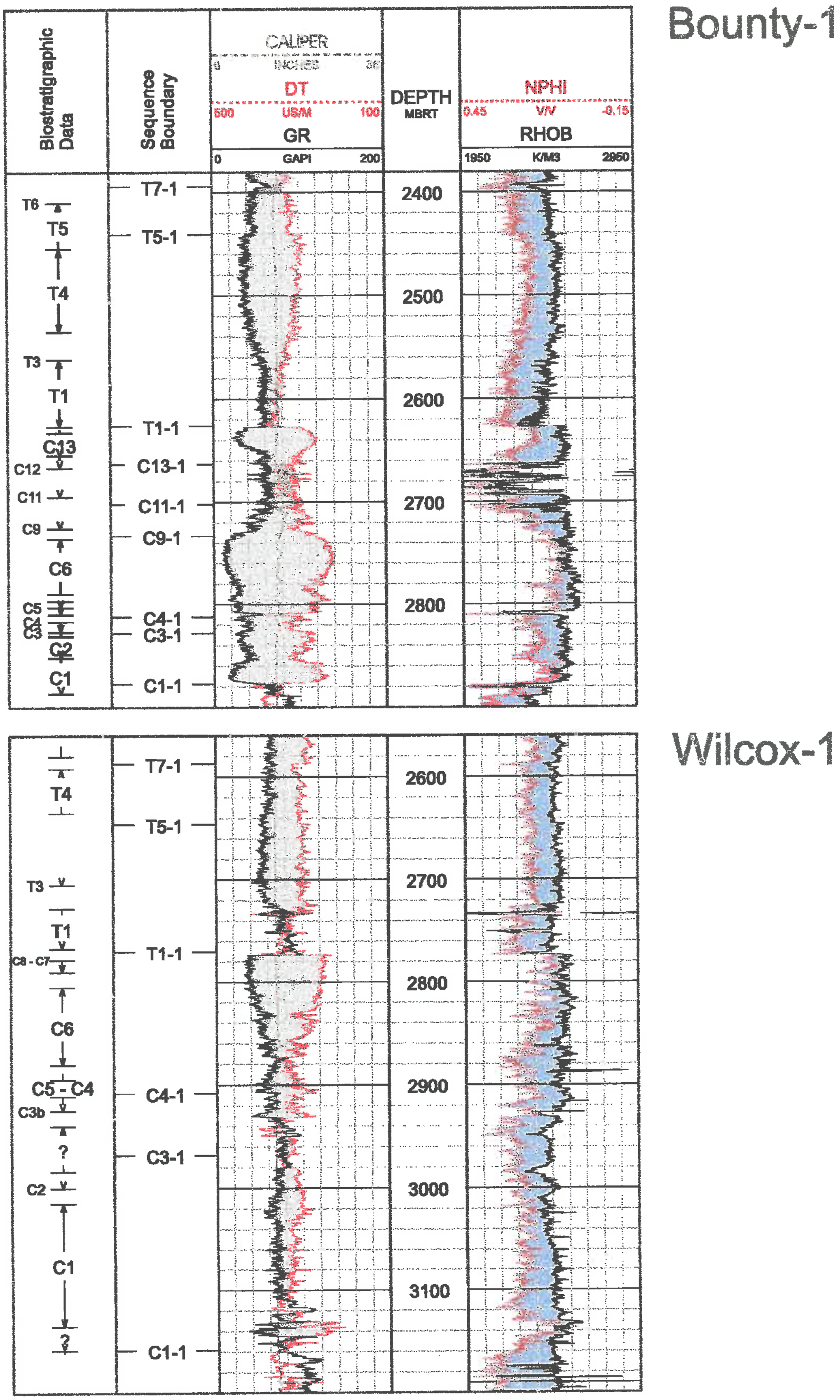

Figure 4.6 Cretaceous to early Tertiary sections of Bounty-1 and Wilcox-1

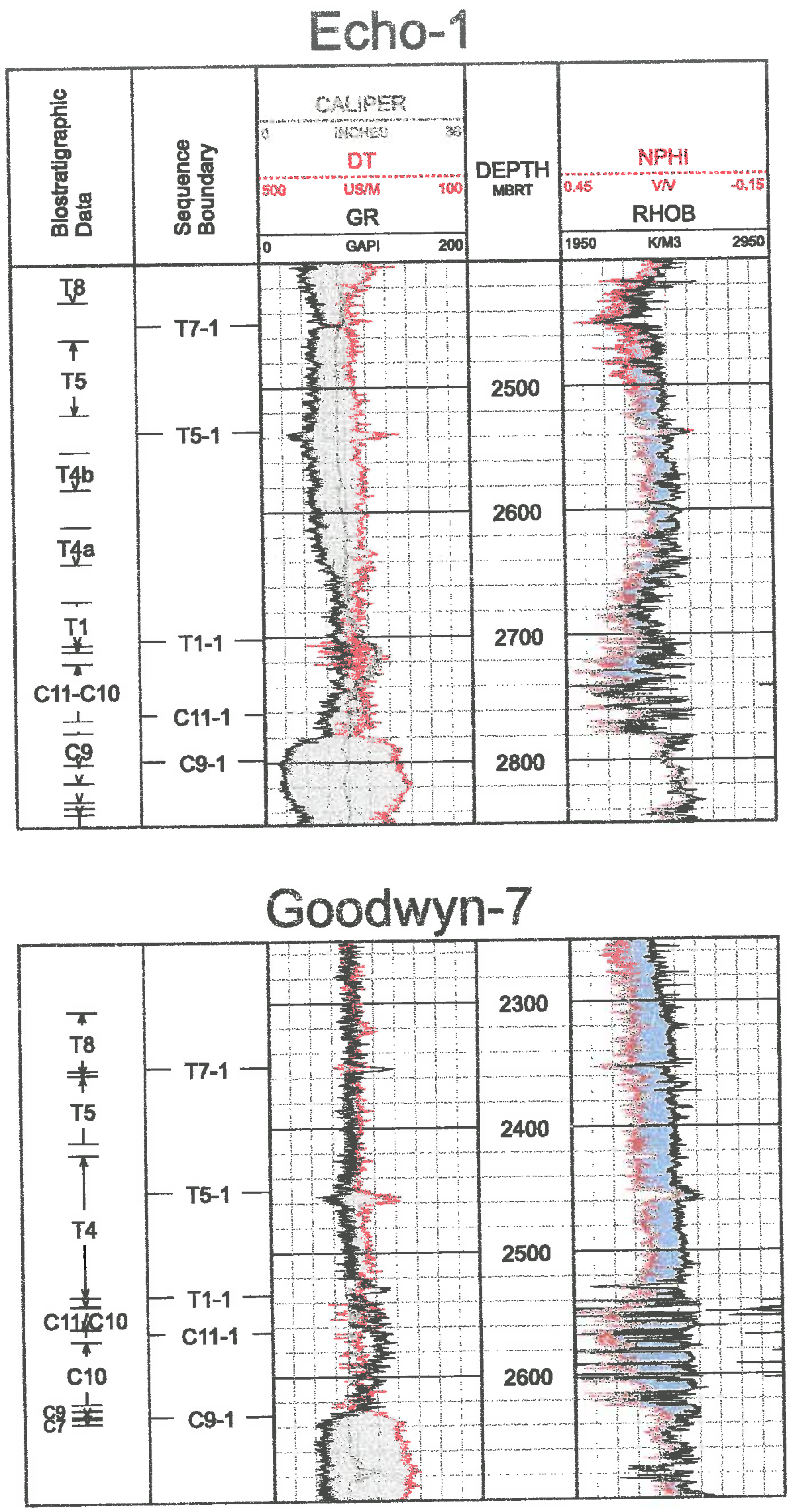

Figure 4.7 Campanian to Paleocene sediments in Echo-1 and Goodwyn-7

4.3.2 Paleocene – Eocene sediments

The base Tertiary event T1-1 is a clearly identifiable log shift which separates the Tertiary and Cretaceous sediments of the Dampier Sub-basin. The sediments deposited on top of the boundary are diachronous in age and make it difficult to determine the age of the event. The first sediment deposited above the base Tertiary event in Bounty-1, Brigadier-1, Delambre-1, Finucane-1, Fisher-1, Gandara-1, Miller-1, Ronsard-1, Tidepole-1, Withnell-1, and Wanaea-1 are Danian (T1) in age (Figure 4.2). In Lowendal-1 and North Rankin-5 the oldest Tertiary sediment is T2 aged sediment and in the remainder of the study wells T4 sediment is the first recorded above the Maastrichtian C13 sediments (Figure 4.2). In accordance with the naming procedure for stratigraphic events in this project this event has been named T1-1 after the earliest recorded sedimentation following the event. In all the above mentioned wells the wireline signature of this event is a sharp upward increase to higher gamma and slower sonic values and a corresponding increase in neutron and decrease in bulk densities, as evident in Bounty-1 (Figure 4.6).

The wireline response of the T1-1 event is seen to change with the amount of missing section associated with the boundary. In the above list of wells which record the deposition of T1 aged sediments directly on top of C13 sediments, the wireline log signature records an upward increase in gamma, sonic and neutron values and decrease in bulk density as typified by Ronsard-1 (Figure 4.8). Where T1 to T3 sediments are thin or missing, the wireline log response of the T1-1 event only shows a short lived excursion to higher gamma, sonic and neutron porosity values and lower bulk densities before returning to similar readings to the late Cretaceous sediments. This is clearly demonstrated in the log suite for Montague-1 (Figure 4.8). Following the base Tertiary T1-1 event, sedimentation resumed in some parts of the Dampier Sub-basin during the Danian but it was not until the Selandian that the first significant flood occurred over the whole basin and deposited sediments of T4 age.

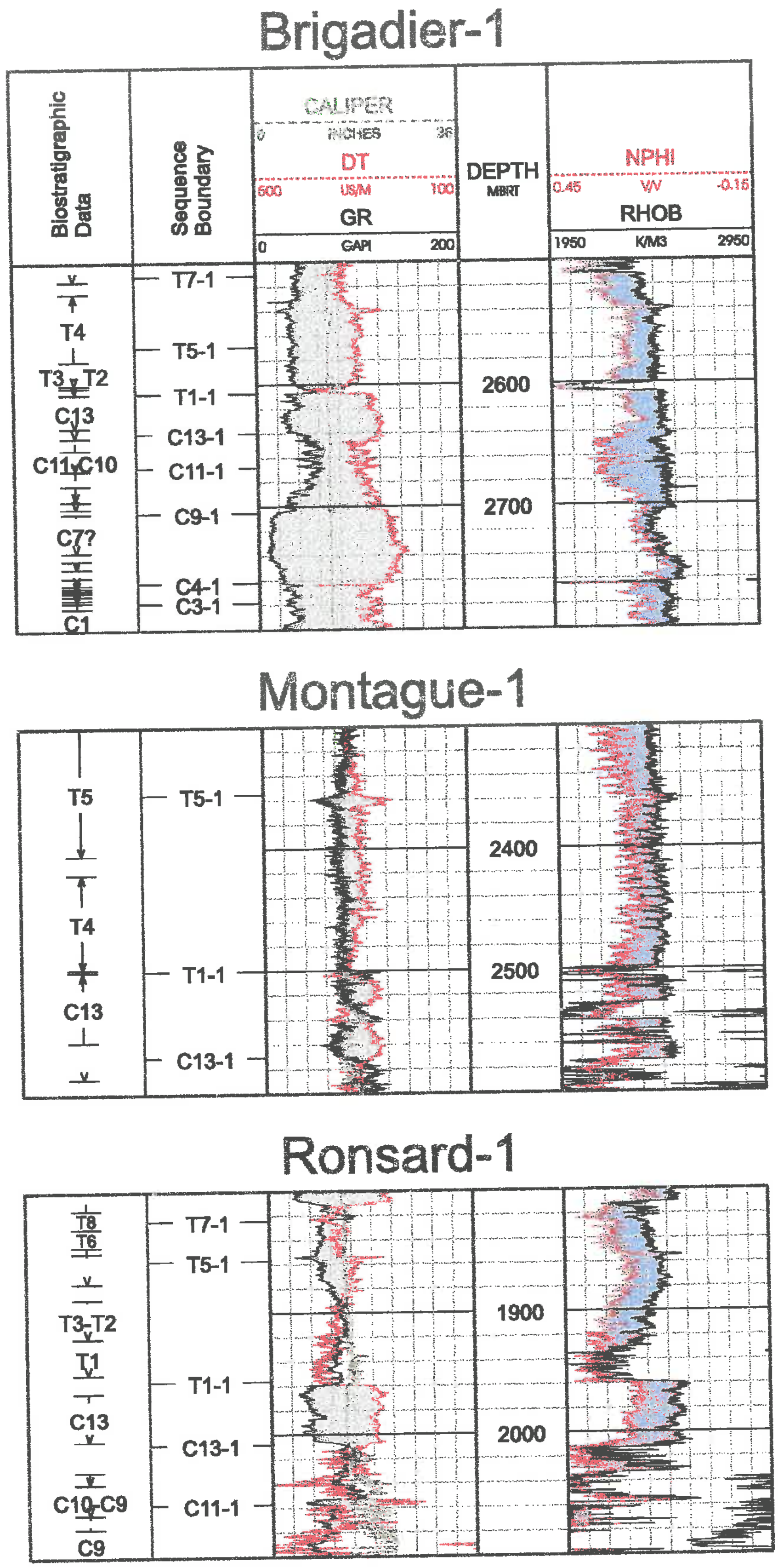

Figure 4.8 Wireline log response of the base Tertiary T1-1 event in Brigadier-1, Montague-1 and Ronsard-1.

A basal Eocene event (T7-1) with associated missing section has been identified on the Rankin and Brigadier Trends and its presence has also been suggested in some of the wells in the Madeleine Trend and Rosemary Fault System (Figure 4.2). Similar to the base Tertiary T1-1 event, the base Eocene event is a diachronous erosive surface with the age of the first Eocene sediments deposited directly on top of the event varying throughout the basin (Figure 4.2). In accordance with the procedure that has been adopted for naming stratigraphic events in this project the age of this event has been defined as the age of the first phase of Eocene sedimentation above the identified missing section. From Figure 4.2 it can be seen that T8 aged sedimentation has been identified in the majority of study wells but T7 aged sedimentation has also been identified in a number of the study wells – Finucane-1, Gandara-1, Goodwyn-7, Goodwyn-8, Miller-1, Nelson Rocks-1 and Tidepole-1 (Figure 4.2). These wells have constrained the base Eocene event to being of T7 age.

The wireline log character of the Paleocene sediments deposited between the T1-1 and T7-1 events is typified by the log response of these sediments in Bounty-1 which show an upwardly-decreasing gamma log signature and associated sonic log signature (Figure 4.6). In these sediments, the neutron and density logs exhibit upwardly-decreasing porosities and increasing density corresponding to the upwardly-decreasing gamma log. The top of this package of sediment (the T7-1 event) is marked by a sharp increase in the gamma and sonic logs throughout all the study wells in the basin. The neutron and density log response to this base Eocene event is most commonly an upward increase in neutron porosity and bulk density as is displayed in Tidepole-1 (Figure 4.9). The exceptions to this neutron and density log response are Dixon-1 and Parker -1 which both exhibit an upward decrease in neutron porosity associated with the T7-1 boundary. Lowendal-1 and Fisher-1 both record an abrupt upward increase in density and decrease in gamma, sonic and porosity values as shown at a depth of 2518 m in Lowendal-1 (Figure 4.5). In these two wells, the base Eocene T7-1 event is associated with more missing section than elsewhere in the basin with sediments of biozones T7 and T8 missing in Lowendal-1 and biozones T7-T9 missing in Fisher-1. The log response across the T7-1 boundary in these two wells is interpreted to be related to periods of localised uplift.

Elsewhere in the Dampier Sub–basin, the Paleocene and Eocene sediments record a continuous period of regional deposition which shows no pronounced shifts in log trends. In wells where the majority of the section is preserved, the wireline log response of these sediments is one of overall upward-decreasing gamma and sonic profiles which is accompanied by an upward decrease in neutron porosity and increase in bulk density as exhibited by Bounty-1 (2050–2550 m, Figure 4.6).

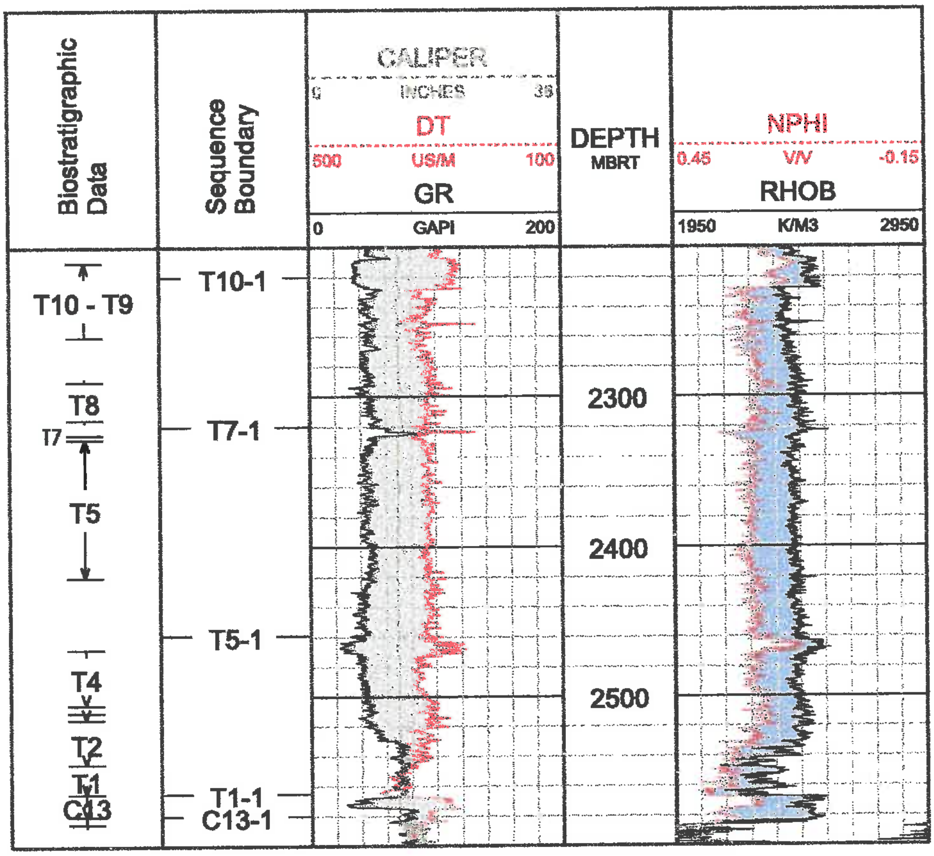

Figure 4.9 Typical log response for the T7-1 event in Tidepole-1

4.3.3 Oligocene – Recent sediments

At the top of the Paleocene to Eocene section, a major episode with missing section can be identified from the biostratigraphic data. In fact, no foraminiferal zones have been defined for part of the Bartonian and the whole Priabonian section of the North West Shelf (Figure 4.2). The wireline log suites for all wells in this study show that this episode of missing section was a significant event, defining the upper boundary of the Paleocene / Eocene long-term trend. The biostratigraphic reports for all wells studied in the basin identify a hiatus, which separates the late Eocene T14 sediments from the overlying Oligocene sediments. The age of this event is difficult to define as there is once again a strong diachroneity in the age of the sediment above the boundary, which is further confounded by the inability to accurately define the age of these immediately overlying sediments (Figure 4.2). However, in the biostratigraphic reports for Bounty-1, Montague-1 and Echo-1, sediments of T15 age have been positively identified above the boundary and the associated pronounced wireline log break (Figure 4.10). These wells constrain this boundary to being base Oligocene in age and it has therefore been termed T15-1.

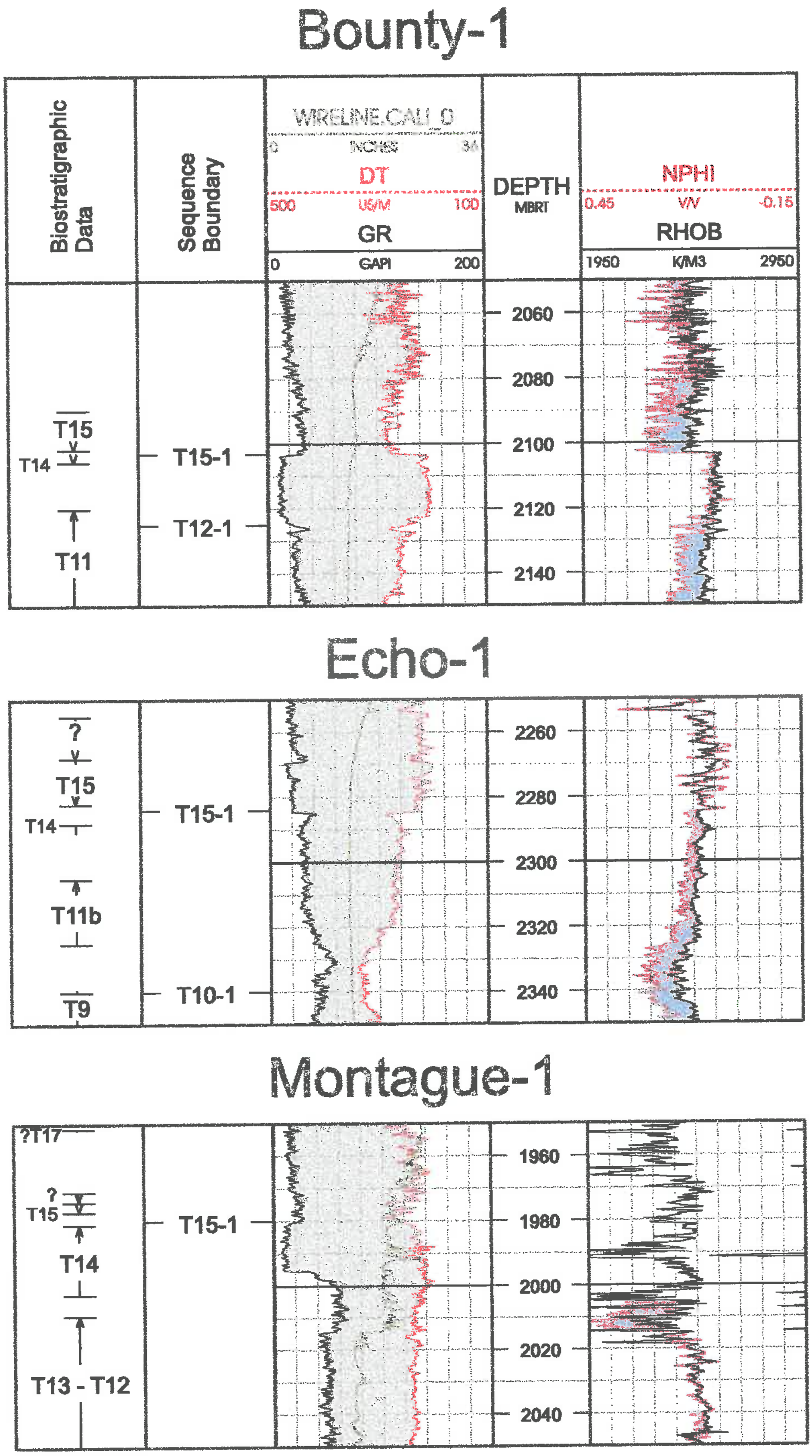

Figure 4.10 Wireline log and biostratigraphic response of the base Oligocene event (T15-1) in Bounty-1, Echo-1 and Montague-1. (Scale 1:200)

The base Oligocene T15-1 event marks a major break in the wireline log trends in the Dampier Sub-basin. The late Eocene T14 sediments of the Dampier Sub-basin are characterised by low gamma and sonic values in all of the study wells. The base Oligocene event is represented by a short-lived upward increase in gamma values above these T14 sediments before returning to the low gamma values. The sonic, neutron and density logs show a variety of responses to the base Oligocene event that appears to be dependent on the location of the well in the basin (Figure 4.11).

The Oligocene and Miocene sediments of the Dampier Sub-basin are characterised by low gamma and low sonic values which show minor up-well variations compared with the underlying Albian to Eocene section as demonstrated in Figure 4.6. Within the Oligocene to Recent section of the Dampier Sub-basin, it is often not possible to precisely determine which biozone a recovered sample represents and in these cases a range of biozones is interpreted from the faunal assemblage present. In the late Oligocene to early Miocene (T17-N8) and latest Miocene to Recent (N18–N23) sections, biozone definition has been possible but in the mid-to late Miocene section (biozones N10–N17) biozone definition has only been possible in a handful of wells (Figure 4.2). The Oligocene to Recent section of the Dampier Sub-basin has been subdivided into sequences on the basis of biostratigraphic constraints and a model that has been developed for the sequence stratigraphic interpretation of carbonate wireline log motifs. This model is discussed in Section 4.4.

Biostratigraphic data identify the absence of Burdigalian N6–N7 aged sediment with subsequent sedimentation beginning during the N8 biozone (Figure 4.2). This event has been termed N8-1. On wireline log data, the N8-1 event has been shown to be significant and is seen to subdivide long-term trends in the sonic, neutron and density data as demonstrated by both Lowendal-1 and Montague-1 in Figure 4.5. The gamma and sonic response of the N8-1 event is a short-lived upward increase in gamma values which then returns to the low gamma values characteristic of the Oligocene to Recent section. The sonic logs record a bulk shift to higher or slower sonic values at the top of a long-term upwardly-decreasing trend in the sonic values. In the few wells which have neutron and density logs over this interval, the logs record a shift to higher neutron porosities and lower bulk densities. Variations from these characteristic log responses occur in Brigadier-1, Haycock-1, Walcott-1 and Wilcox-1 and in the wells along the Rosemary Fault system. The Brigadier, Haycock, Walcott and Wilcox wells record an upward decrease in neutron porosity and increase in bulk density across the N8-1 event whilst the wells along the Rosemary Fault System exhibit an upward decrease in sonic interval velocity across the N8-1 event (Figure 4.12).

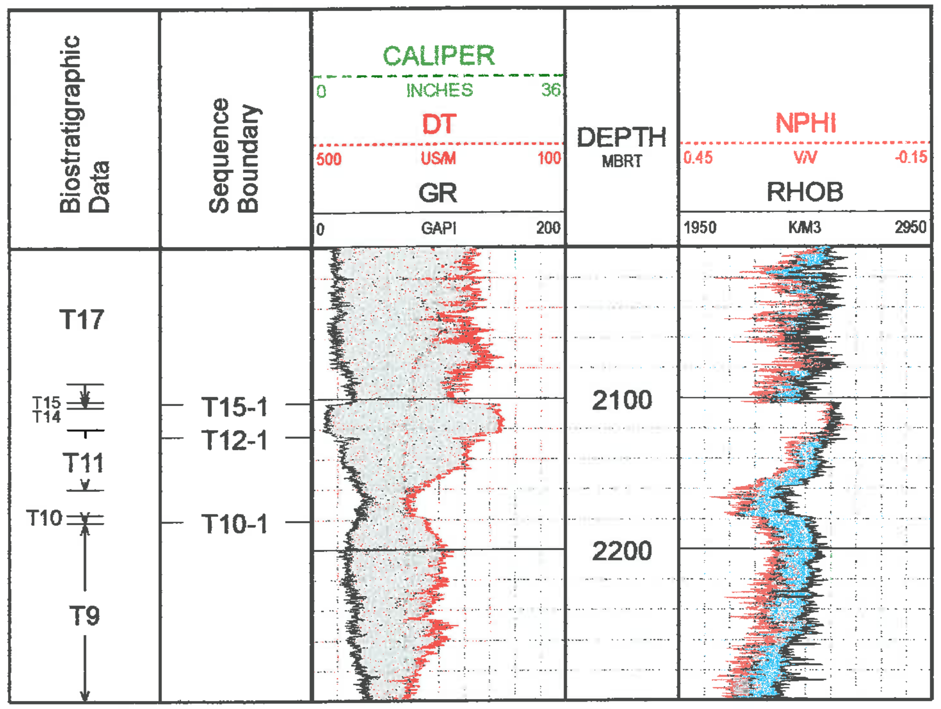

Type 1
Example - Bounty-1

Wells - Bounty-1, Brigadier-1, Delambre-1, Echo-1, Eaglehawk-1, Gandara-1, Miller-1, Montague-1, Parker-1

Type 4
Example - Walcott-1

Wells - Legendre-1, Madeleine-1, Nelson Rocks-1, Samson-1, Talisman-1, Walcott-1 and Wanaea-1

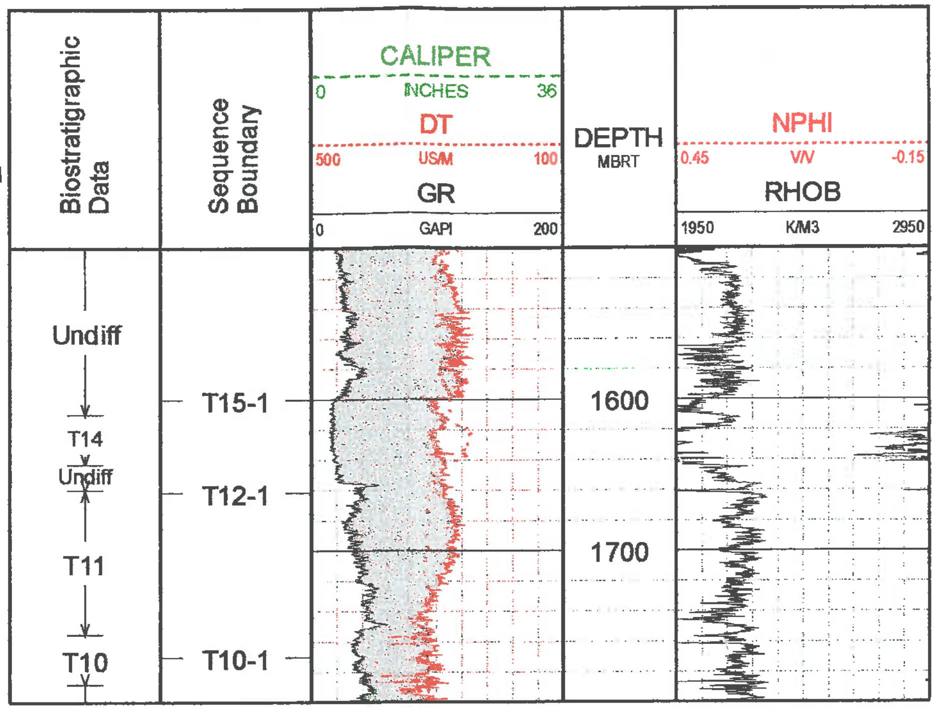

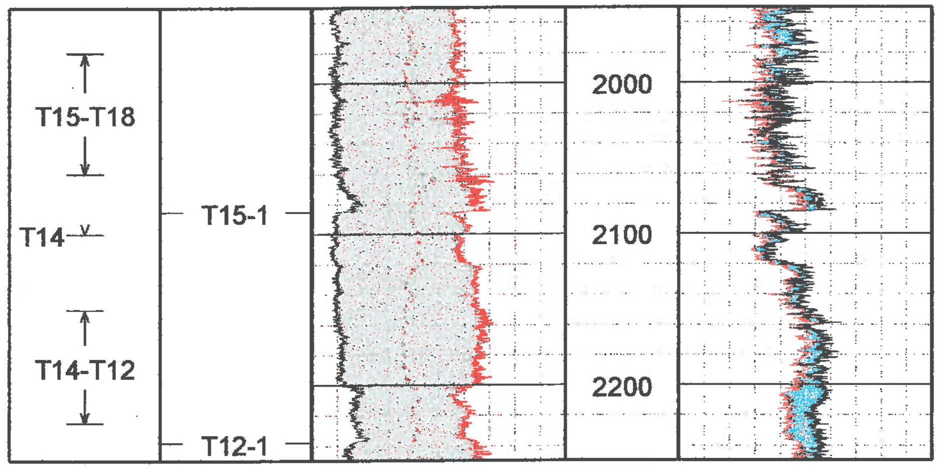

Type 2
Example - Lowendal-1

Wells - Dampier-1, Dockrell-1, Dixon-1, Fisher-1, Haycock-1, Lowendal-1, Orion-1, Rankin-1, Rosemary-1, Rosemary North-1, Tidepole-1, Wilcox-1 and Withnell-1

Map showing the spatial distribution of the various wireline log responses of the base Oligocene T15-1 event

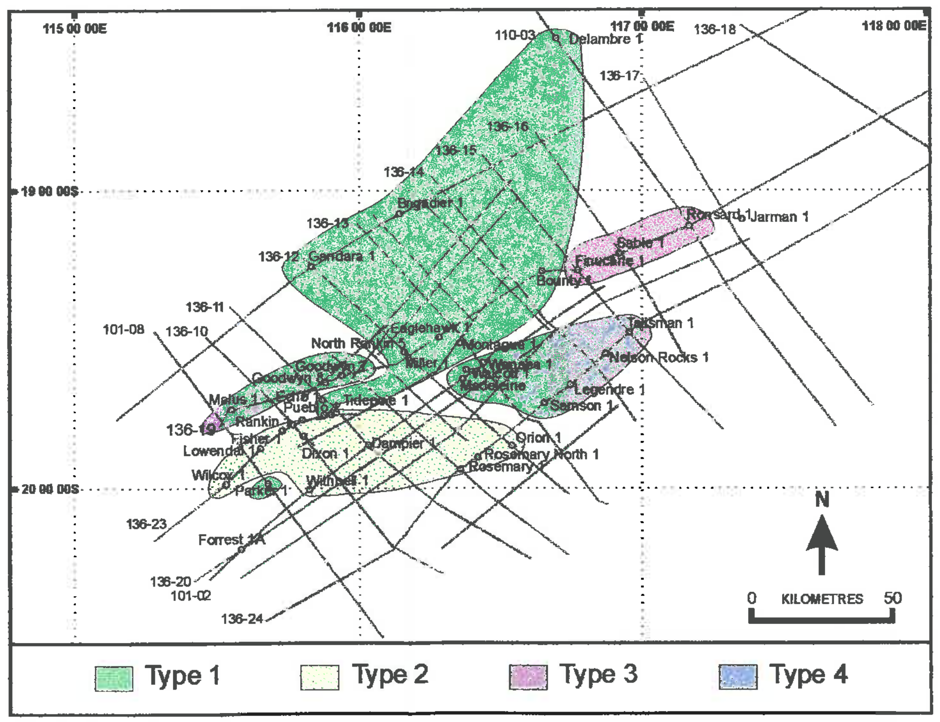

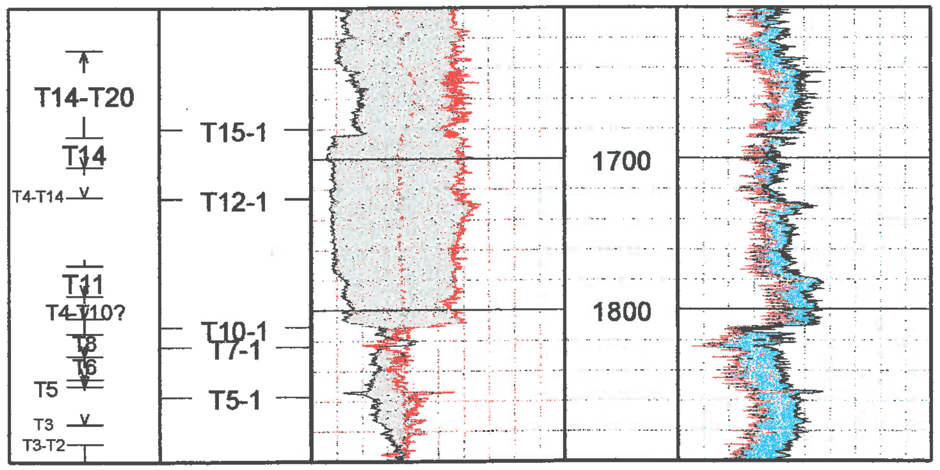

Type 3
Example - Ronsard-1

Wells - Finucane-1, Goodwyn-7, Goodwyn-8, Malus-1, Ronsard-1 and Sable-1

Figure 4.11 Various wireline log responses of the base Oligocene T15-1 event in the Dampier Sub-basin and their spatial distribution. (Wireline log scale 1:5000)

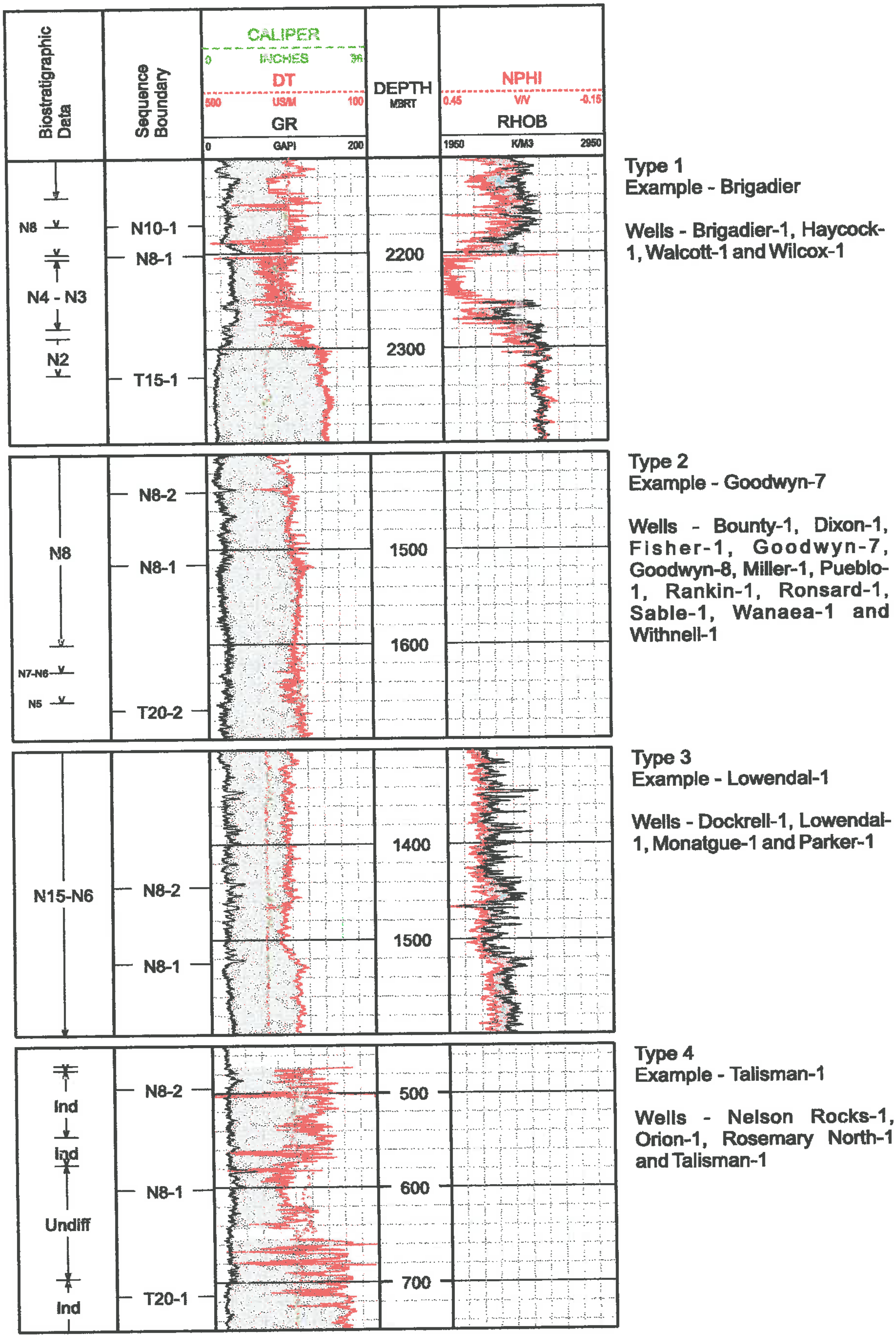

Figure 4.12 Wireline log response of the N8-1 event throughout the basin

The biostratigraphic data for the mid-Miocene to Recent section of the Dampier Sub-basin do not conclusively indicate any further regional episodes of missing section (Figure 4.2). The mid-Miocene to Recent section is also characterised by uniformly low gamma values, which show some minor short-lived upward increases in gamma values. However, the sonic logs through this section show further variation and suggest the succession can be further subdivided into genetically-related units. The sonic log profiles through the mid-Miocene to Recent section of many wells show high frequency variations in interval transit times values (±100 μsm^{-1}) over small vertical distances as demonstrated in Lowendal-1 (1000-1300 m) and Montague-1 (450-1520 m) in Figure 4.5. The corresponding gamma profiles record consistently low values interrupted by upward increases of short duration similar to that observed at the N8-1 event. The biostratigraphic age of the sediments that exhibit these significant variations in sonic values is not well constrained and many of the samples are described as mid-Miocene. However, from the biostratigraphic dating that does exist, it can be concluded that this log pattern is confined to sediments younger than N8 and older than N18 in age. Through this succession, an increase and later decrease in log separation between the gamma and sonic logs is observed with the interval transit time of the sediments decreasing and then increasing upwards through the sequence. A sharp increase in interval transit time and recorded gamma values at the top of the log trend signifies the end of this sediment package. Haycock-1 and Wilcox-1 clearly demonstrate the wireline log response of these sediments and the sharp contact that marks the top of the sonic trend, which began after the mid-Miocene N8-1 event. This event is defined to be of N18 age following the identification of N18 aged sediment on top of the pronounced break in log character in the majority of the study wells. The N18-1 event clearly separates the sonic, gamma, neutron and density log trends of the N8-1–N18-1 sediments from the overlying N18-1–Recent as demonstrated in Lowendal-1 and Monatgue-1 (Figure 4.5) and Fisher-1 and Wilcox-1 (Figure 4.13).

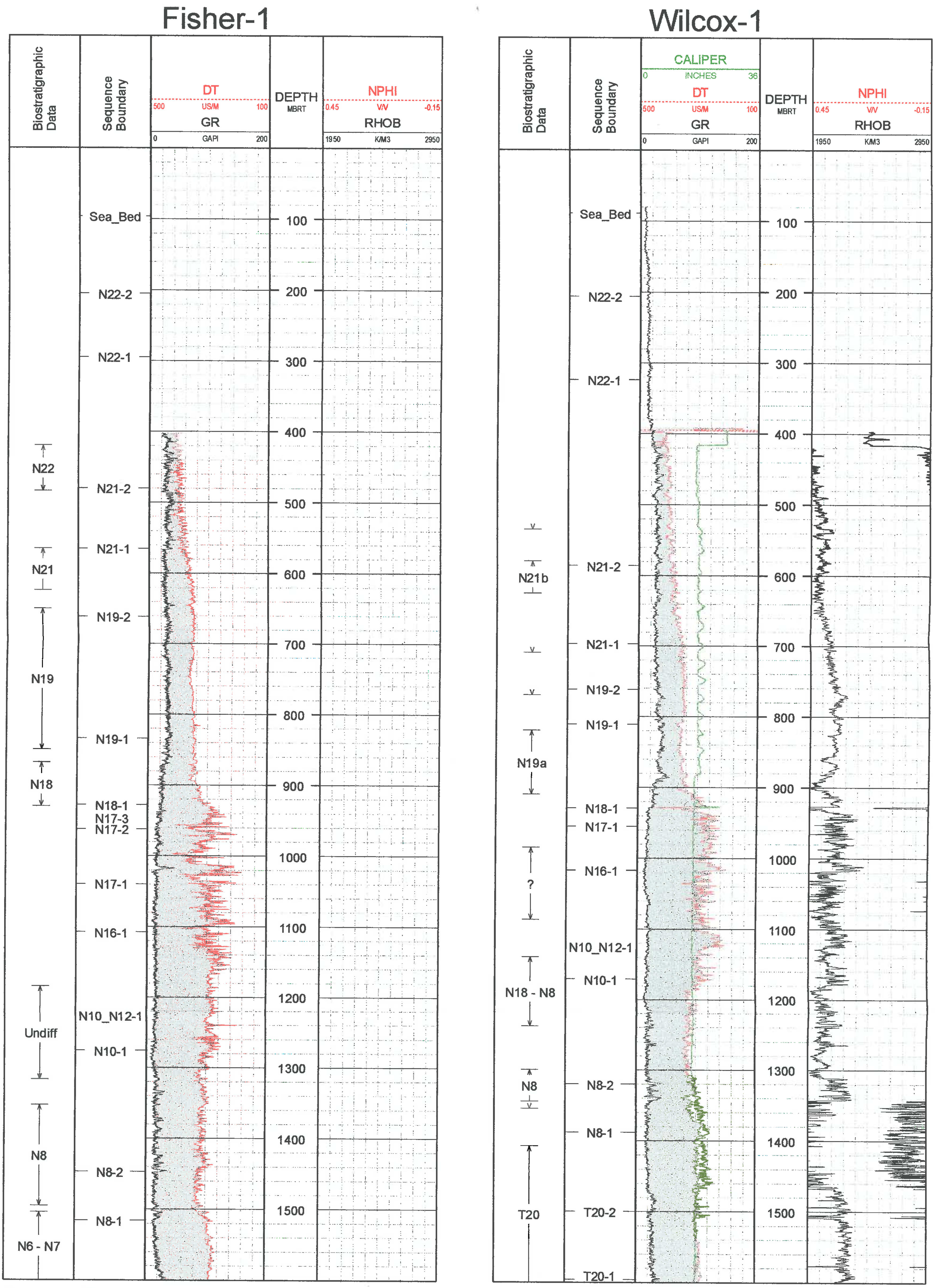

Figure 4.13 Wireline log response of the mid Miocene (N8) to Recent section of Fisher-1 and Wilcox-1 (Scale 1:5000).

4.4 Sequence stratigraphic analysis of carbonate wireline log motifs

The basin-wide events defined by missing section provided a framework within which a high-resolution subdivision of the section was defined. This subdivision was required to delineate the genetically-related packages of sediment that would be mapped on seismic and used in the quantitative analysis of accommodation space. To achieve this high-resolution subdivision, it was necessary to devise a model for the sequence stratigraphic interpretation of carbonate wireline logs as none existed in the literature.

From an initial inspection of the log characteristics of the C9-1, C13-1, T1-1, T7-1, T15-1 and N8-1 events it was apparent, that with the exception of C13-1, they were represented by an abrupt increase upward in the gamma and sonic readings (Figure 4.4). Using this observation and combining it with sequence stratigraphic principles, biostratigraphic constraints, wireline log motifs and theoretical considerations for carbonate systems, a model was developed for the sequence stratigraphic interpretation of carbonate wireline log motifs. The model as it is proposed is outlined below and has also been published in a paper (Hull *et al.*, 1998), which has been included in this thesis as Appendix B. The wireline log response of the major sequence boundaries as defined using the biostratigraphic data showed an abrupt increase upward in the gamma and sonic values across five of the six major sequence boundaries defined for this study (Figure 4.4). Across boundaries T7-1 and N8-1 this increase in log readings is noticed immediately above the boundary but away from the boundary the logs exhibit an identical characteristic carbonate response (low gamma and density, high sonic and neutron readings). This would suggest that the sediment deposited directly on top of the boundary is not pure carbonate. Both T7-1 and N8-1 regained the homogeneous carbonate signature relatively quickly, C13-1 and T1-1 saw a change in lithology across the boundary whilst C9-1 and T15-1 showed a gradual change in lithology.

In developing a model for the wireline response of carbonate system to changes in relative sea level, it is necessary to understand how changes in sedimentation style and type affect the log suite. Gamma logs record the abundance of naturally radioactive isotopes of potassium, thorium and uranium within a lithology. These elements are most commonly found in illites, heavy minerals and organic matter respectively. Sandstones and carbonates contain these minerals to a lesser degree than mudrocks with the exception being arkosic sandstones, which are rich in potassium-bearing feldspars. Consequently, the gamma log can often be used as a measure of mud content. Pure carbonates have very low clay content and so will be represented on wireline logs by low and constant gamma values.

Sonic logs record the interval transit time through a formation. They measure the time it takes for a compressional wave to travel between a source and receiver 30 to 60 cm apart on a logging tool. The velocity of the compressional wave depends on the elastic properties of the rock matrix and the fluids in the pore space. Therefore, for any given lithology, the velocity of the compressional wave is a function of porosity and matrix type. As porosity decreases with depth due to compaction the interval velocity will be seen to increase. The nature of the porosity-depth curve and correspondingly, the sonic curve, is controlled by the burial history of the sediment. A boundary that separates two sequences with differing burial histories will be represented by a change in the interval transit time recorded by the sonic log. Sequences as defined in sequence stratigraphy have undergone a different burial history purely by the nature of their formation. Thus, sequence boundaries can be identified on sonic logs as an abrupt shift in the interval transit time separating two packages of sediments, which, although they may be lithologically similar, will have experienced a different burial history.

The neutron and density logs can also be used in lithology determination and are commonly cross-plotted against each other for this purpose. The neutron log measures porosity of a formation via the hydrogen index and the density log measures the bulk density of a formation; this combination can be used to characterise sediments. The neutron log will be strongly affected by the burial history, as compaction will reduce porosity so that sequence boundaries separating sediments of differing burial history will be easily identified on log data. In the Tertiary section of the Dampier Sub-basin, it is practical only to run a skeleton logging suite of gamma and sonic logs and as such the model developed for the sequence stratigraphic interpretation of carbonate wireline log motifs has concentrated on gamma and sonic logs.

Combining this knowledge of wireline log response with an understanding of carbonate depositional systems and their response to changes in relative sea level, as outlined in Chapter 2, a model was proposed for the sequence stratigraphic interpretation of carbonate wireline logs. It was proposed that highstand systems tracts, which are characterised by high production rates of clean homogeneous carbonates and low siliciclastic input rates, would be represented on wireline logs by a relatively consistent low gamma reading. Sequence boundaries would be represented by a break at the top of this clean carbonate package, on top of which a more clay-rich, higher gamma reading, lowstand package would sit. The boundary would also be identified by a shift to lower interval transit times, marking the change from homogeneous prolific carbonate sedimentation of the highstand to mixed carbonate-clastic lowstand deposition. Due to low carbonate production rates under lowstand conditions, and the relative increase in siliciclastic sediments, the lowstand systems tract would be expected to be thin, contain more clay-rich sediments and have a higher gamma reading. The transgressive systems tract would consist of an upward-cleaning carbonate section in response to the landward relocation of siliciclastics. On the gamma log this would be represented by an upward-decreasing log signature, which is mirrored by a corresponding decrease in the interval transit time of the sonic log as it records a change to the more homogeneous carbonate lithologies of the highstand systems tract. The initial flooding surface at the base of the transgressive systems tract is identified by the change in log trend from the increasing gamma trend of the lowstand systems tract to a trend of decreasing gamma values of the transgressive systems tract. The maximum flooding surface at the top of the transgressive systems tract represents the maximum landward retreat of any siliciclastic sediments present in the system. The cleanest carbonate sediments of the relative sea level cycle will be deposited during this time. These will be represented by minima on the gamma and sonic logs at the top of the upward-cleaning trend of the transgressive systems tract and the base of the highstand systems tract with a flat response. Figure 4.14 shows the model that has been used to subdivide the intervening section between the major events defined from biostratigraphic data.

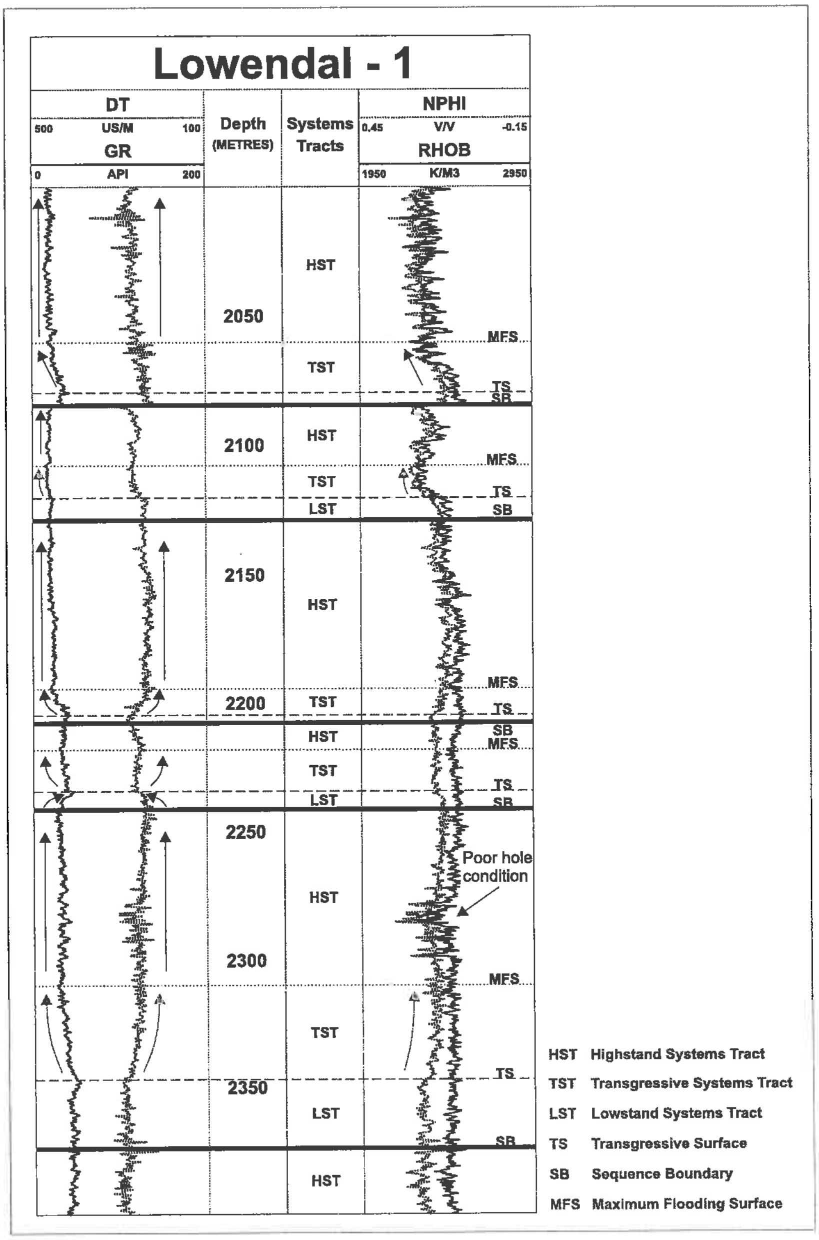

Figure 4.14 Model developed for the sequence stratigraphic interpretation of carbonate wireline log motifs (Hull et al., 1998)

The log responses presented above are for ideal situations at the shelf break. Within a single sequence lateral variations in log response will occur according to the contrasting nature of the sediments on either side of the boundary. For example, on a shelf top no lowstand and very thin transgressive systems tract sediments will exist and consequently the margin will predominantly consist of stacked highstand deposits. The log response to this will be a short lived upward increase in gamma reading at the sequence boundary before returning to the low gamma and low sonic values typical of the highstand systems tracts (Figure 4.14). In the distal setting, the toes of a series of prograding clinoforms will be represented by higher gamma values and irregular sonic values. This pattern represents the mix of sediment redeposited at the toe of a clinoforms, clastic sediment transported to the edge of a clinoform and basinal muds. Figure 4.15 summarises the variation in wireline log response that can be expected across a carbonate margin.

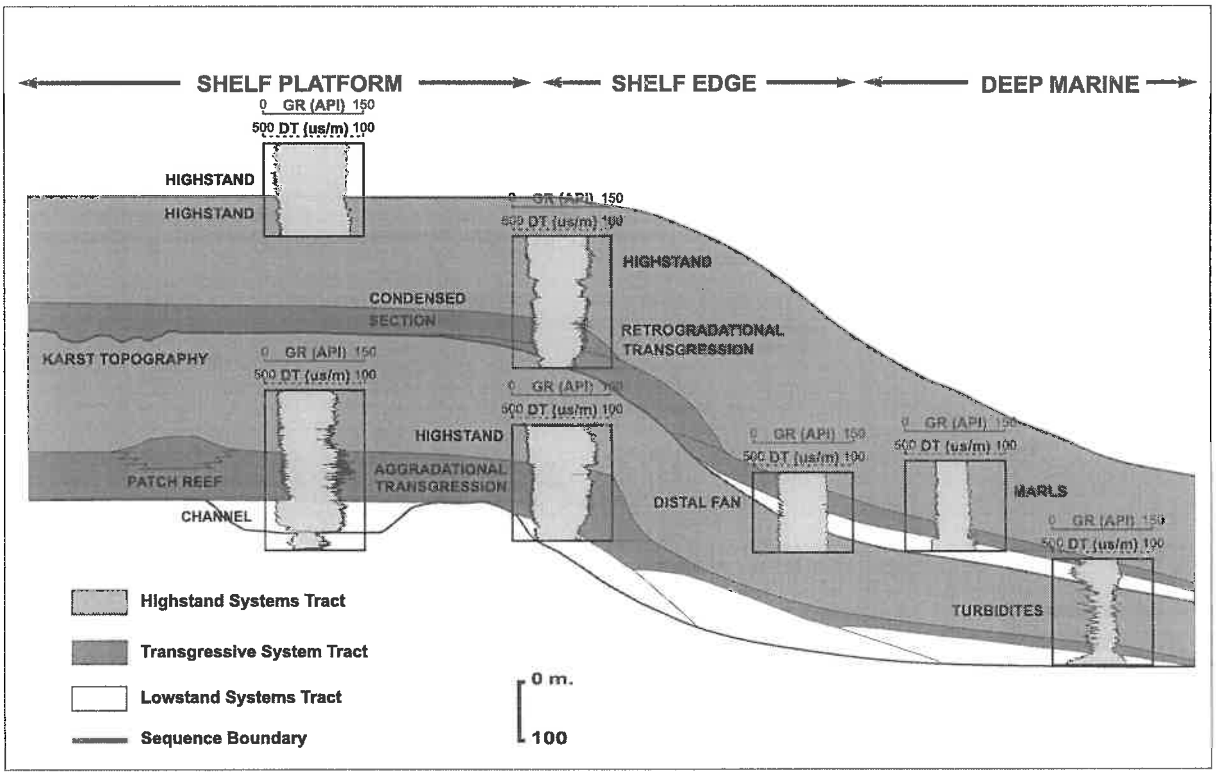

Figure 4.15 Log response of sequence stratigraphic events with variation in location on a carbonate margin (Hull, 1998).

Albian to Recent chronostratigraphic framework

From the initial gross subdivision of the Albian to Recent sediments of the Dampier Sub-basin, which was made from biostratigraphic data, the section has been further subdivided using the sequence stratigraphic model as outlined in Section 4.4. Events defined using this model have been correlated throughout the study area using all available biostratigraphic constraints. From this integrated biostratigraphic and wireline log study, thirty basin-wide events were identified and these define a chronostratigraphic framework for the study area with a higher resolution than has previously been published (Figure 4.16). Error bars, which have been defined from available biostratigraphic data, have been placed on the sequence stratigraphic events to indicate the range of possible ages. A list of sequence picks in the study wells is included as Appendix C.

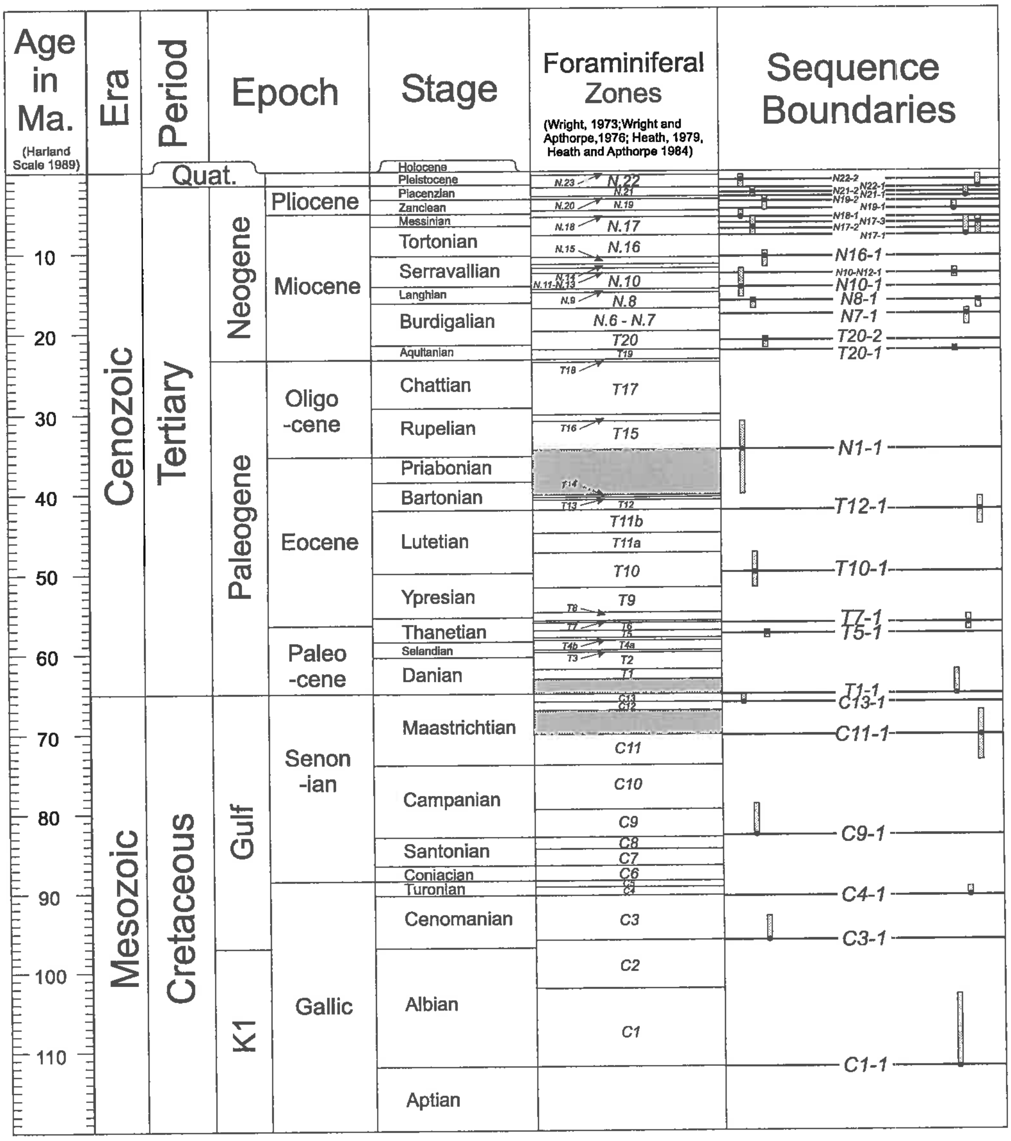

Figure 4.16 Chronostratigraphic framework for the Albian to Recent section of the Dampier Sub-basin.

CHAPTER 5 SEISMIC INTERPRETATION

5.1 Introduction

The chronostratigraphic framework defined from the biostratigraphic and wireline log analysis was used to initially subdivide the Albian to Recent section of the Dampier Sub-basin into a series of genetically-related units separated by time correlative boundaries. These boundaries were then identified on seismic and those represented by strong seismic reflectors were mapped throughout the dataset using all available biostratigraphic constraints. From these mapped horizons a series of time-depth and time-thickness maps have been generated. These maps have been used to describe the spatial distribution and variations in sediment thickness of the defined sequences.

5.2 Database

The seismic grid used in this study was derived primarily from the Dampier section of AGSO's Carnarvon Cretaceous-Tertiary Tie seismic survey (Survey 136), (Figure 3.1). This survey was designed specifically to acquire a high-quality, high-resolution, seismic dataset for the Cretaceous and Tertiary sediments of the Northern Carnarvon Basin encompassing the Barrow, Dampier and Beagle Sub-Basins. In the Dampier Sub-basin, there are seven dip lines in Survey 136 (lines 136-10–16), with two further dip lines in the Beagle Sub-basin to the north (lines 136-17 & 136-18). These Beagle lines have been included in this study to investigate changes in sediment distribution patterns at the northern end of the Dampier Sub-basin and also to constrain the northern ends of the three strike lines 110-08, 136-19 and 136-24, which have been used in this study. In addition to the nine 136 survey dip lines, an extra six dip lines have been included to reduce the line spacing and errors which may be associated with interpreting between them (101-08 & 09; 86-3104; PG93-1032 & 1046 and 110-03). Survey 136 has three strike lines (136-19, 20 & 24) acquired along the length of the Dampier Sub-basin and into the Beagle Sub-basin. These lines have been complemented with other regional (110-08, 101-02) and prospect specific strike lines (PG93-1025 & 1029, 86-3150, 3155A & 3157 and 85-DB13).

5.3 Seismic expression of the wireline defined events.

The seismic response of the sequence boundaries defined in the chronostratigraphic framework were investigated by converting the wireline log depth to two-way time using checkshot data as described in Section 3.3.4. Events that corresponded to strong seismic reflections were then mapped throughout the extent of the seismic database utilising all biostratigraphic constraints. Thirty events have been defined from the wireline log and biostratigraphic analysis and were shown to correlate extremely well on seismic data. These events were also represented by the stratal termination patterns that would be expected to be associated with sequence boundaries. The nature of these picks will be discussed in further detail in conjunction with the two-way time maps later in this chapter. Figure 5.1 shows a systems tract interpretation of a composite line between Lowendal-1 and Malus-1 showing the strong correlation between log characteristics and seismic peaks and the lateral continuity of the events between wells.

For each of these mapped events, a time-depth and a time-thickness map have been created to investigate the nature of the basin-fill history on a sequence scale. The biostratigraphic and wireline log analysis has ensured that seismic events being mapped are geologically significant horizons separating packages of genetically-related strata. An interpretation of basin-fill history and accommodation space development based on this series of two-way time and time thickness maps can thus be attempted.

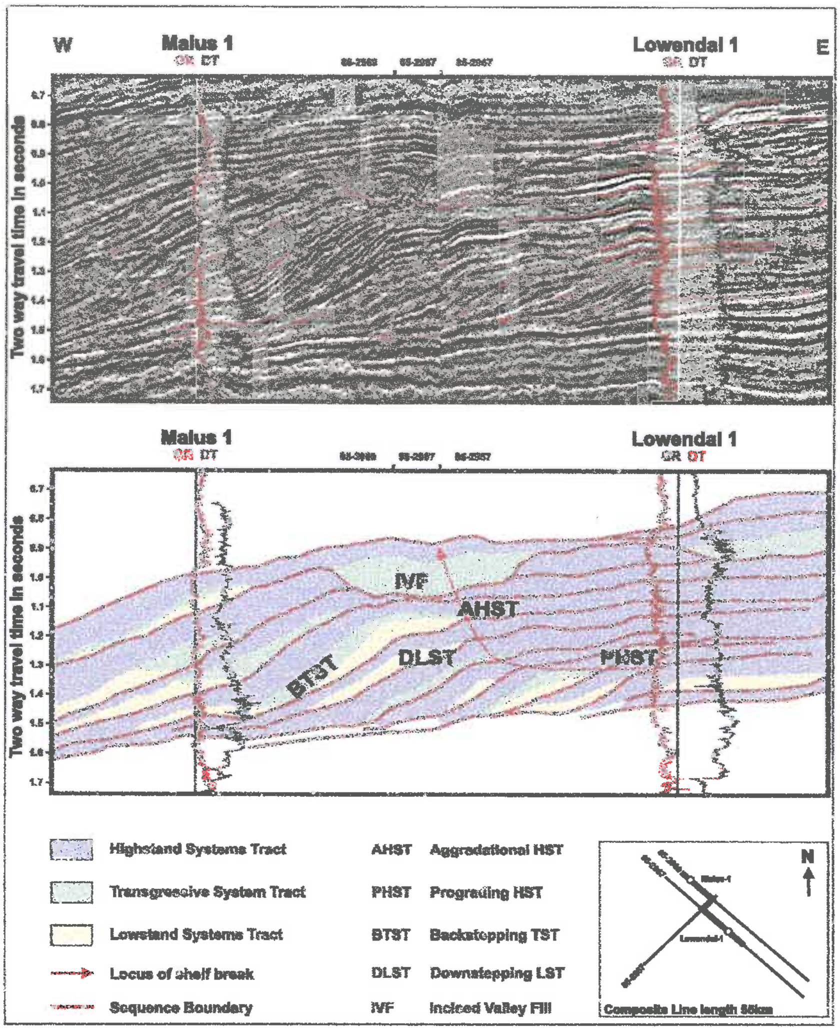

Figure 5.1 *Systems tract interpretation of prograding sequence and wireline logs (Hull et al., 1998)*

5.4 Stratal Architecture

Dip lines across the Dampier Sub-basin all exhibit similar stratal configurations with an upper section of strongly prograding clinoforms, a basal section characterised by extensional fault block and graben geometries and an intervening section of constant thickness with relatively low amplitude reflectors. Above the extensional fault block and graben structures, the section can be grossly subdivided into three basin-forming units on the basis of stratal architecture. These basin-forming units are bound by the horizons C1-1, T1-1, T15-1 and the seabed. The three basin-forming units are therefore Albian to base Paleocene, base Paleocene to base Oligocene and base Oligocene to Recent in age (Figure 5.2). The six major biostratigraphic events (C9-1, C13-1, T1-1, T7-1, T15-1 and N8-1) defined by regional episodes of missing section during the biostratigraphic analysis are also evident on seismic lines (Figure 5.2).

The base of this study has been taken as the Albian horizon (C1-1). Beneath this the section is characterised by a series of tilted fault blocks and grabens, which consist of laterally persistent high-amplitude internal reflections. The fault block and graben structure strongly controls sediment distribution and thickness patterns in the overlying middle to late Cretaceous section. Pronounced sediment thickening can be seen to occur over the Lewis Trough with associated thinning onto surrounding highs (Figure 5.2). Sediments of the C1-1 to T1-1 basin-forming unit are thickest in the area landward of the Rankin Trend and exist only as a thin veneer basinward of it. Within the C1-1 to T1-1 megasequence, five sequence boundaries have been identified and mapped: C3-1 (Cenomanian); C4-1 (Turonian); C9-1 (Campanian); C11-1 and C13-1 (both Maastrichtian). A basin-wide high-amplitude event at the base of the Tertiary (T1-1) marks the beginning of the second megasequence which persists until the Oligocene T15-1 event.

Within the second megasequence, sequence boundaries of T5-1, T7-1 (both Thanetian), T10-1 (Lutetian) and T12-1 (Bartonian) have been identified. The top of this unit and the base of the third megasequence are represented by the high-amplitude Oligocene T15-1 reflector. Above this event, the section is characterised by a series of strongly prograding, sigmoidal, high-amplitude reflectors. The toes of these sigmoidal reflectors downlap onto the underlying T15-1 reflector and in the proximal direction they are seen to onlap the T15-1 and younger regional events. Within the third basin-forming unit, seventeen sequence boundaries have been identified and mapped throughout the basin. (T20-1 – Aquitanian; T20-2 & N8-1 – Burdigalian; N8-2 & N10-1 – Langhian; N10-N12-1 & N16-1 – Serravallian; N17-1, N17-2, N17-3 – Tortonian; N18-1 – Messinian; N19-1 & N19-2 – Zanclean; N21-1 & N21-2 – Piacenzian and N22-1 & N22-2 – Pleistocene).

Strike lines in the Dampier Sub-basin show predominantly horizontal reflectors and some along-strike variations in depositional style, such as a change in the orientation of the stratal geometries across the N17-1 horizon (Figure 5.3). The presence of this event is suggested in the biostratigraphic data but lack of data resolution prevented its previous identification (Figure 4.2). On line PG93-1025 and many other of the strike lines used in the study, high frequency channeling can be seen on the front of the clinoforms (Figure 5.3 - horizons N10-1, N10-N12-1 N16-1). Line PG93-1025 runs slightly oblique to strike in a northeasterly direction and shows lateral changes along the front of the clinoforms with the channeling being restricted to beyond the shelf break on the slope. Thus on more landward located strike lines, the channeling is seen to involve older sequences. The origin of these features is not clear, it may be the result of small-scale channeling caused by current action, slumping due to incoherent substrate or slumping caused by oversteepening of carbonate build-ups. The upper slope of the Little Bahama Bank is cut by a series of gullies, which are approximately 100 m deep and up to 2 km wide whilst the lower slope has been smoothed by efficient along-strike redistribution of sediment (Austin, 1986; Harwood and Towers, 1988). This morphology appears similar to that observed on dip lines across the Dampier Sub-basin (Figure 5.2). A closer-spaced seismic grid, ideally a 3D seismic grid, would be required to map the distribution of these features and may confirm the morphology of these features and provide insights into their origin.

5.5 Two-way time maps

The two-way time maps generated for the 30 horizons mapped throughout the study area show a series of northeast-southwest striking horizons, which are seen to dip in a northwesterly direction (Enclosure 1). Many of the horizons show considerable deepening of reflectors to depths of 2500-3000 ms in the northwest corner of the sub-basin (lines 110-08, 101-08, 136-10 and 136-11). This rapid increase is in part due to a significant increase in water depth over the shelf edge from 200-400 ms depth over most of the basin to 1400 ms beyond the shelf edge at the southwest end of line 110-08. Water has a much slower interval velocity (1500 ms^{-1}) than sediments ($\cong$3500 ms^{-1}) and consequently the travel time for a seismic pulse through water will be two to three times slower than through sediments. As a result of this longer travel time, a reflector would appear deeper in two-way time if it is overlain by a significant thickness of water than if it was overlain by only a small amount of water. On examination of the lines in the study area, it was noted that the major increase in horizon depths begins further onshore than the location of the shelf break. Figure 5.2 shows the reflectors of the Brigadier Trend being elevated above the reflectors of the Rankin Platform, if this section were to be depth converted and the thickness of water accounted for then it would actually increase the elevation of the Brigadier Trend relative to the Rankin Platform. A depth map for the Albian C1-1 horizon has been created using the process described in Section 3.4.3 to verify that the time maps are representative of true features. A comparison of the two-way time and depth for horizon C1-1 (Figure 5.4 and Figure 5.5 respectively) shows this to be the case.

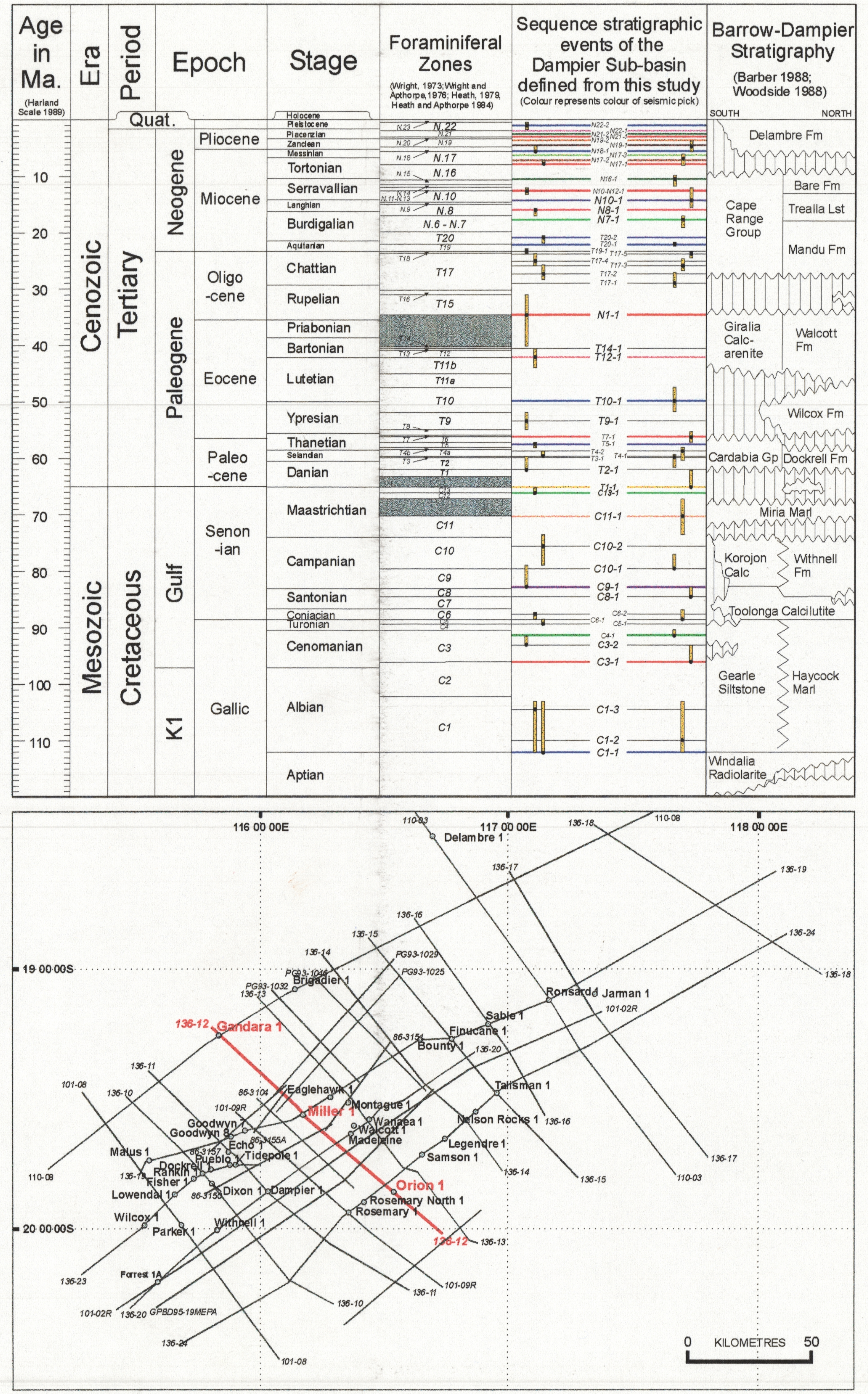

Figure 5.2 Line 136-12 showing the typical stratal architecture of the Albian to Recent section of the Dampier Sub-basin. (Line length 131.5km)

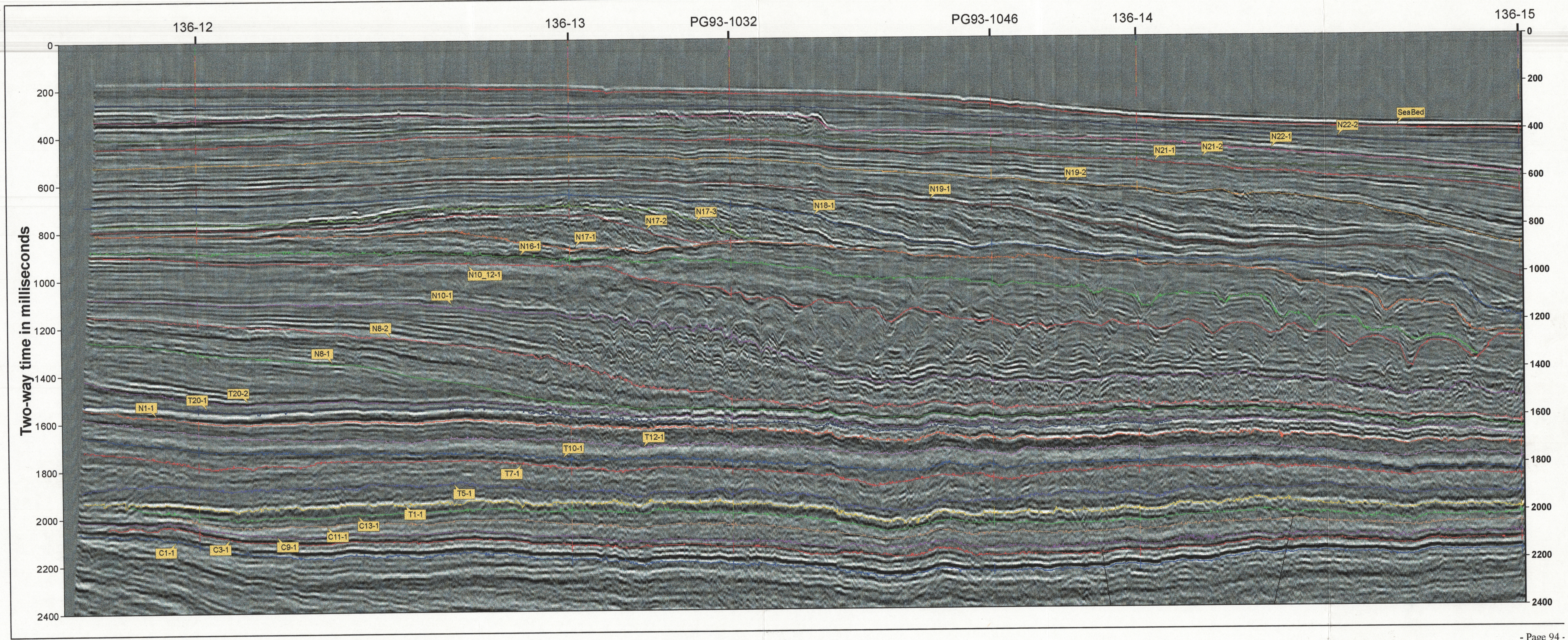

Figure 5.3 Strike line PG93-1025 showing along strike variation in sequence geometry and change in depositional style across the Messinian N17-1 sequence boundary. (Line length 78.9 km)

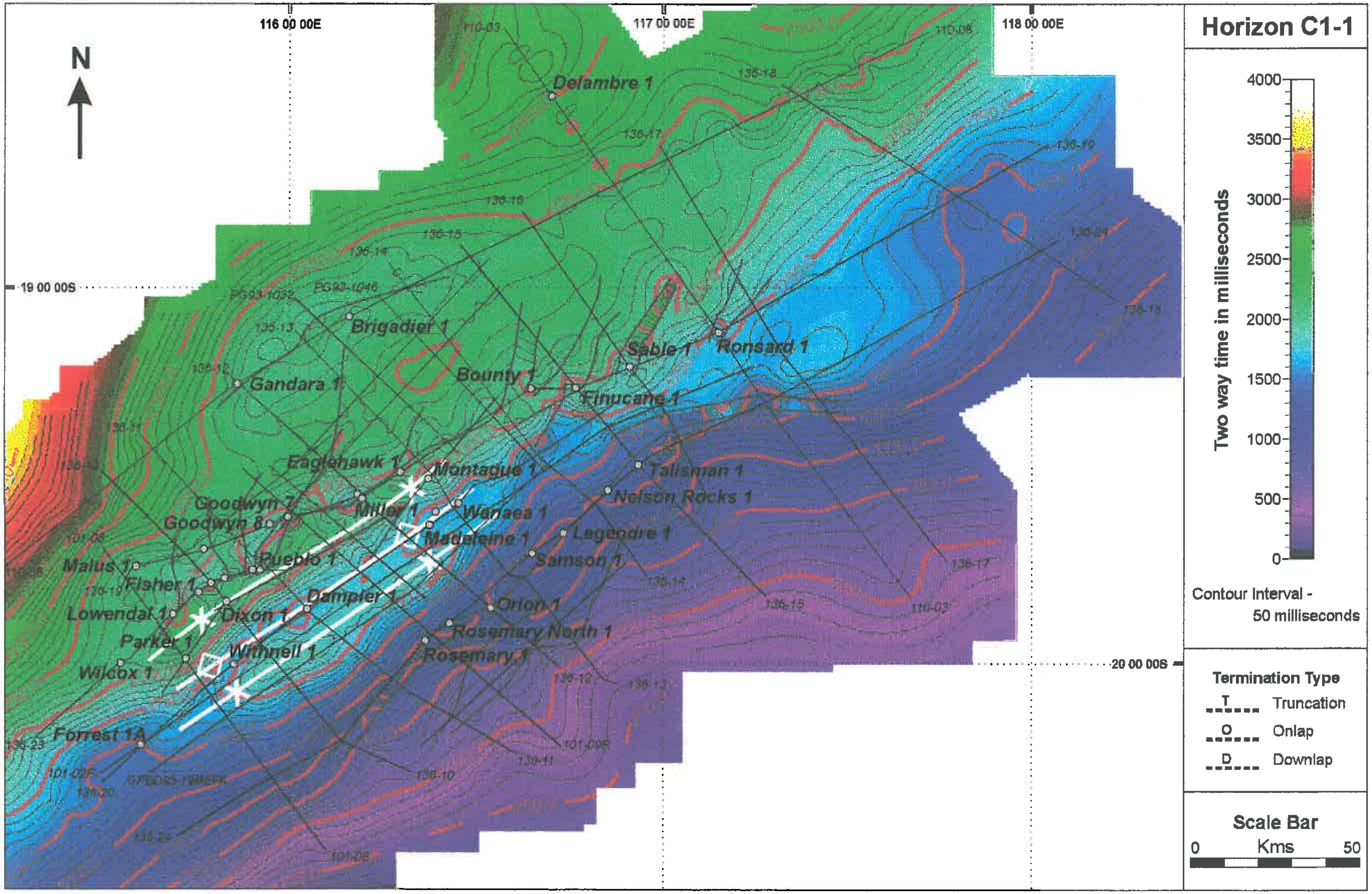

Figure 5.4 *Two-way time map for Albian horizon C1-1.*

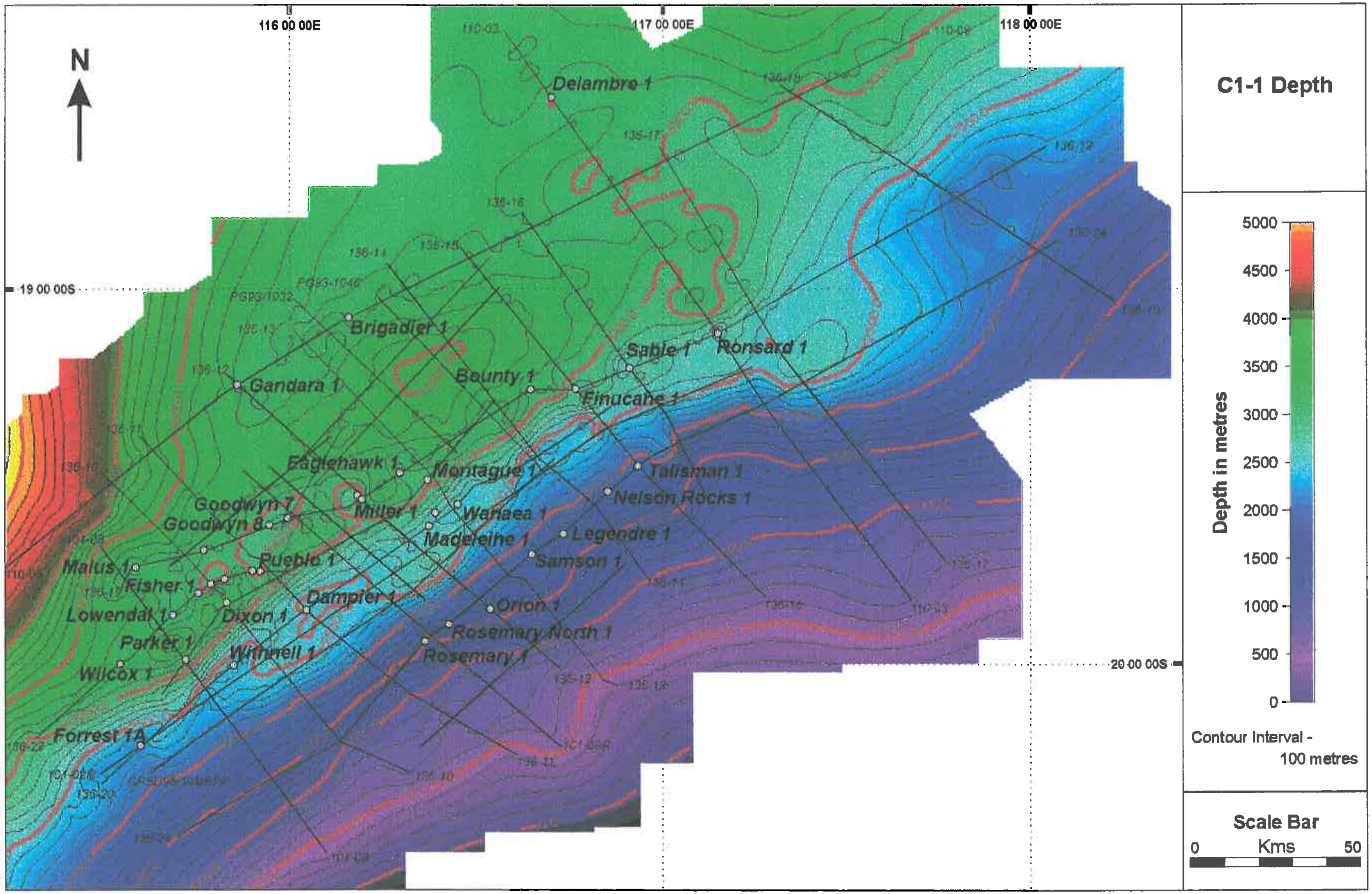

Figure 5.5 *Depth map for Albian horizon C1-1.*

5.5.1 Cretaceous sequences C1-1–C13-1 (Albian – Maastrichtian)

General Description

The two-way time maps presented in Enclosure 1 for the Cretaceous horizons C1-1 (Albian), C3-1 (Cenomanian), C4-1 (Turonian), C9-1 (Campanian), C11-1 and C13-1 (both Maastrichtian) demonstrate a series of northeast-southwest-striking, northwest-dipping horizons. These horizons are intersected by a series of faults along the Rankin Trend (line 136-19), Legendre Trend (line 136-24) and Brigadier Trend (line 110-08). Whilst most of these faults persist through the Cretaceous section, several Rankin Trend and Legendre Trend faults are seen to terminate in Campanian and Maastrichtian sediments. In the area contained within lines 110-08, 136-12, 136-16 and PG93-1025, the contours on the two-way time maps indicate a structural high, which is evident on all Cretaceous maps. To the southwest of this feature, along line 110-08, horizons are seen to dip steeply away to depths of 2500-3000 ms. A change in dip of the Cretaceous reflectors can be seen across the Rankin Trend from steeply dipping on the landward side to gently dipping on the basinward side (Figure 5.2).

In the southwestern corner of the basin, a northeast–southwest-trending folded synform-antiform-synform configuration is apparent on the maps of C1-1 to C9-1 age. These structures are most easily identified and have been marked on the two-way time map for horizon C1-1 (Figure 5.4). The first synform is aligned northeast-southwest, adjacent to the southern edge of the Rankin Trend and is represented by the dark green shading south of line 136-23 and line 136-19. The darker blue shading along line 136-20 between lines 101-08 and 136-13 marks the antiformal axis of this structure. The light blue-green shading around line 101-02R between lines 101-08 and 136-13 denotes the presence of a second synform. The two-way time map for horizon C1-1 shows these structures to die out in both northeasterly and southwesterly directions. This synform-antiform-synform trend is clearly visible as the Kendrew Trough, Madeleine Trend and Lewis Trough in Figure 5.2. These structural elements can be seen to control the stratal architecture until the C11-1 horizon. This can be seen in both the two-way time maps and Figure 5.2.

The Albian horizon C1-1 has been defined from wireline log and biostratigraphic data and is represented on seismic data as a high amplitude peak / trough pair. The horizon is present across the whole extent of the Dampier Sub-basin. The Cenomanian horizon C3-1 is a strong seismic peak, which has been defined from biostratigraphic and wireline data. It is present over the whole of the Dampier Sub-basin but in the Beagle Sub-basin (northeast of line 136-16) it is seen to onlap horizon C1-1. The Turonian C4-1 horizon is a high amplitude seismic peak in the vicinity of the Madeleine Trend and Lewis Trough. Over the Legendre Trend and Enderby Platform the amplitude of the reflector decreases significantly making it more problematic to map over this area. The basinward and landward edges of C4-1 both onlap on to horizon C3-1 along the Rankin Trend and Enderby Platform respectively as shown on Figure 5.2 and 5.6.

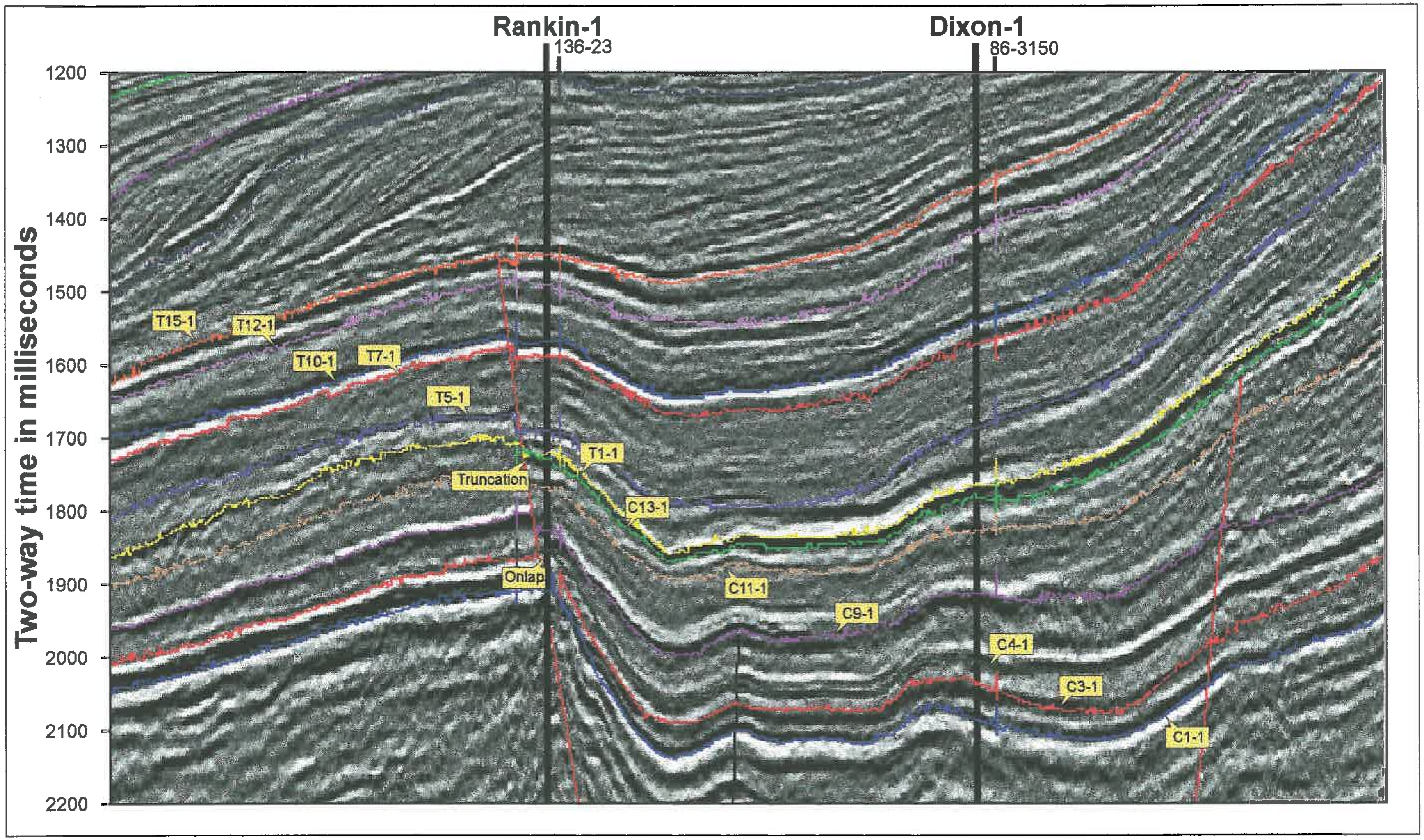

Figure 5.6 Seismic line 136-10 showing onlap of the Turonian C4-1 event against the Cenomanian C3-1 event along the Rankin Trend and truncation of the late Maastrichtian C13-1 event by the basal Tertiary T1-1 event. (Line length 22km)

The Campanian C9-1 event has been defined from both biostratigraphic and seismic data. Biostratigraphic reports indicate that Santonian sediments of C8 age are absent throughout much of the basin (Figure 4.2). The C9-1 event can easily be identified on wireline data, where it marks the top of a low gamma and sonic package On seismic it corresponds to one of the highest amplitude seismic events in the basin (Figure 5.2).

The Maastrichtian C11-1 horizon has been picked primarily from seismic data and with reference to a similar study of the Cretaceous - Tertiary evolution of the neighbouring Barrow Sub-basin (Young, in prep). The seismic picks have been constrained by all available biostratigraphic data in the study wells. On seismic, C11-1 is represented as a persistent medium to low amplitude peak with no associated trough (Figure 5.7). The two-way time map for C11-1 shows the horizon to be truncated both in a landward direction and basinward direction (distal portion of line 110-03) by the overlying Maastrichtian event. The effects of the Lewis Trough on the distribution nature of the sediments appear to have been greatly reduced at this stage as evident from the lack of associated structure on the C11-1 two-way time map and also from the nature of C11-1 in Figure 5.2.

The Maastrichtian C13-1 horizon has been defined primarily from biostratigraphic data, which recorded the absence of C12 sediments across all wells in the basin with the exception of Bounty-1 and Montague-1 (Figure 4.2). In the area basinward of the Madeleine Trend, C13 sediments are commonly in the order of 25-30 m thick. This is below seismic resolution and consequently the C13-1 and base Tertiary T1-1 horizons coalesce to form a single high amplitude reflector (Figure 5.7). In these situations, biostratigraphic and wireline data indicate that C13-1 is represented by the trough / peak crossover underneath the high amplitude reflector. Landward of the Madeleine Trend, in the area south of line 136-13, bifurcation of horizons C13-1 and T1-1 occurs and up to 70 m of C13 sediment has been preserved in Withnell-1 and Rosemary North-1. In this region it is possible to identify C13-1 as a seismic peak (Figure 5.7). Along the Enderby Trend, the proximal edge of horizon C13-1 is truncated by horizon T1-1.

At the southwestern end of line 136-19, biostratigraphic data in Wilcox-1, Dockrell-1, Echo-1 and Goodwyn-7 & 8 has confirmed the absence of C13 sediments. This results in Paleocene sediments resting directly on Lower Maastrichtian and Campanian sediments (Figure 4.2). In this situation the biostratigraphic relationships require C13-1 to be truncated by the overlying T1-1 horizon but, due to the coincident nature of these events, it is hard to differentiate on seismic where this truncation occurs. A combination of biostratigraphic data, horizon mapping and a decrease in the amplitude of the C13-1/T1-1 reflector (Figure 5.6) has been used to define the truncated edge of horizon C13-1 as mapped on the two-way time map although there is still some residual uncertainty.

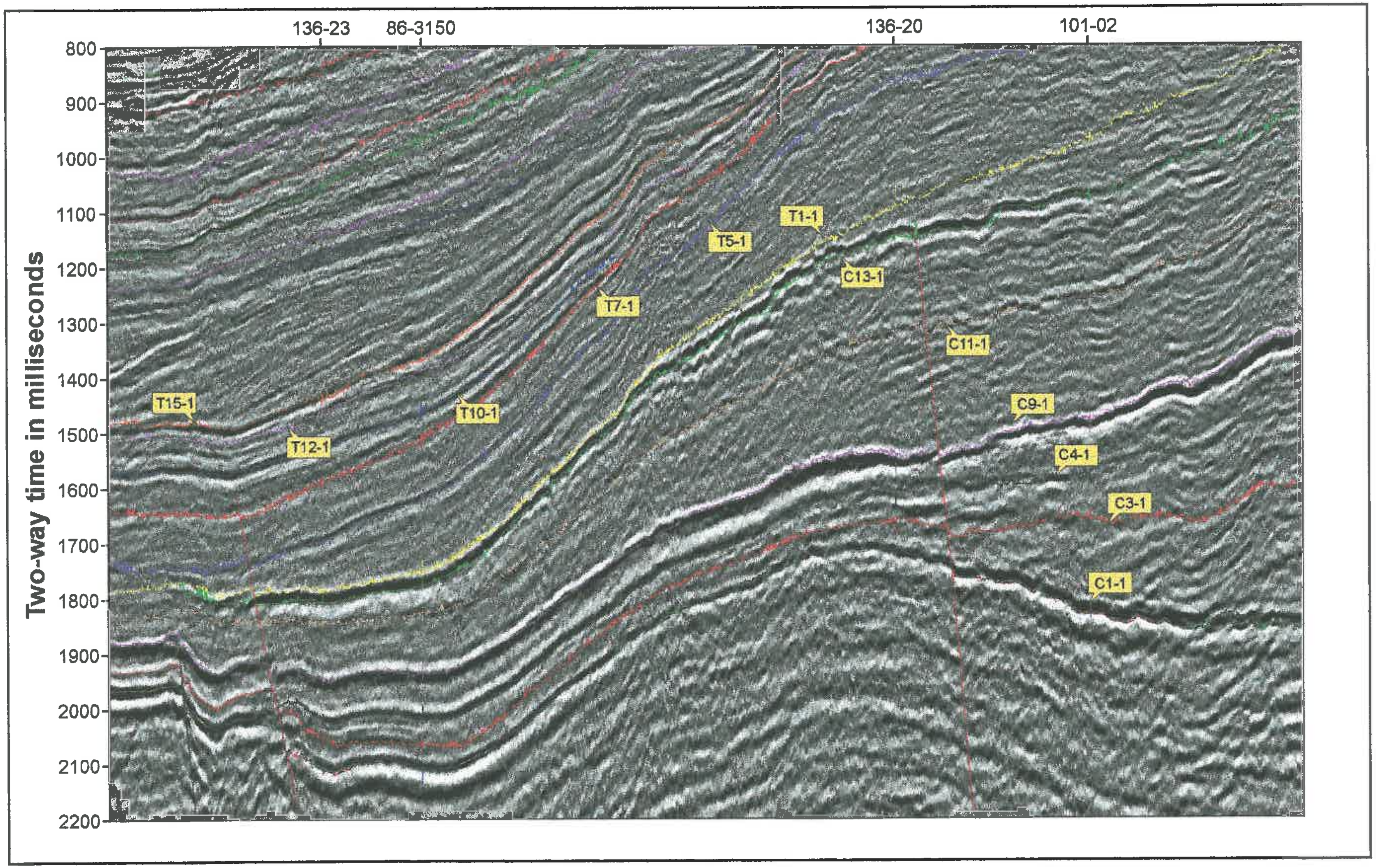

Figure 5.7 Line 136-11 showing the weak seismic reflection associated with the Maastrichtian C11-1 event and the bifurcation of coalescing Maastrichtian C13-1 and base Tertiary T1-1 horizons. (Line length 35 km).

5.5.2 Tertiary sequences T1-1–T12-1 (Danian – Bartonian)

General Description

Within the Paleocene and Eocene section, sequence boundaries of T1-1 (base Paleocene-Danian), T5-1 (Thanetian), T7-1 (base Eocene-Thanetian), T10-1 (middle Eocene-Lutetian) and T12-1 (late Eocene-Bartonian) age have been identified. The two-way time maps for these horizons (Enclosure 1) again show a series of northeast-southwest-striking, northeasterly-dipping horizons, which dip more steeply landward of the Rankin Trend than they do basinward of it. The major escarpment fault of the Rankin Trend and faults of the Rosemary Fault system can be seen to offset these horizons. The structural high in the vicinity of Gandara-1 and Brigadier-1, which was clearly evident on the Albian to Maastrichtian series of maps, is not as apparent on maps younger than horizon T1-1 (base Paleocene).

Horizon Description

As described previously, sediments of C13 age are extremely thin across much of the study area, resulting in the coalescence of the Maastrichtian C13-1 and the regionally extensive base Paleocene T1-1 reflectors in the area basinward of the Madeleine Trend. Biostratigraphic data and depth converted wireline log data have defined the T1-1 horizon as the crossover between the high amplitude peak and the trough above it. Landward of the Madeleine Trend, the horizons bifurcate and T1-1 is picked as a trough above a medium amplitude seismic reflector. Two Thanetian sequence boundaries T5-1 and T7-1 have been defined from characteristic log signatures which are easily identifiable across the study area. On seismic, T5-1 is represented by a low amplitude reflector which in some areas of the basin is relatively discontinuous. The proximal edge of the T5-1 event is truncated by the overlying T7-1 event approximately along the line of the Legendre Trend, as demonstrated on the two-way time map for horizon T5-1. The younger T7-1 event is associated with a major biostratigraphic disconformity, which removes much of T6 and some T5 sediment from the basin (Figure 4.2). This major basin-forming event was one of those initially used to subdivide the section (Figure 4.4). The proximal edge of T7-1 is itself truncated by the base Oligocene T15-1 reflector along the Enderby Trend (Figure 5.8). The distal edges of both T5-1 and T7-1 extend to the basinward edge of the seismic dataset. On seismic, T7-1 is picked as a low amplitude trough/peak crossover. The wireline and seismic expression of both T5-1 and T7-1 are displayed in Figure 5.9. In some wells in the study area there is little missing section associated with T7-1 and the wireline logs exhibit similar gamma/sonic and neutron/density values on either side of the T7-1 event (Figure 4.4). This lack of missing section results in little acoustic impedance contrast across the boundaries and consequently a small seismic response. The converse is true for those study wells with missing section.

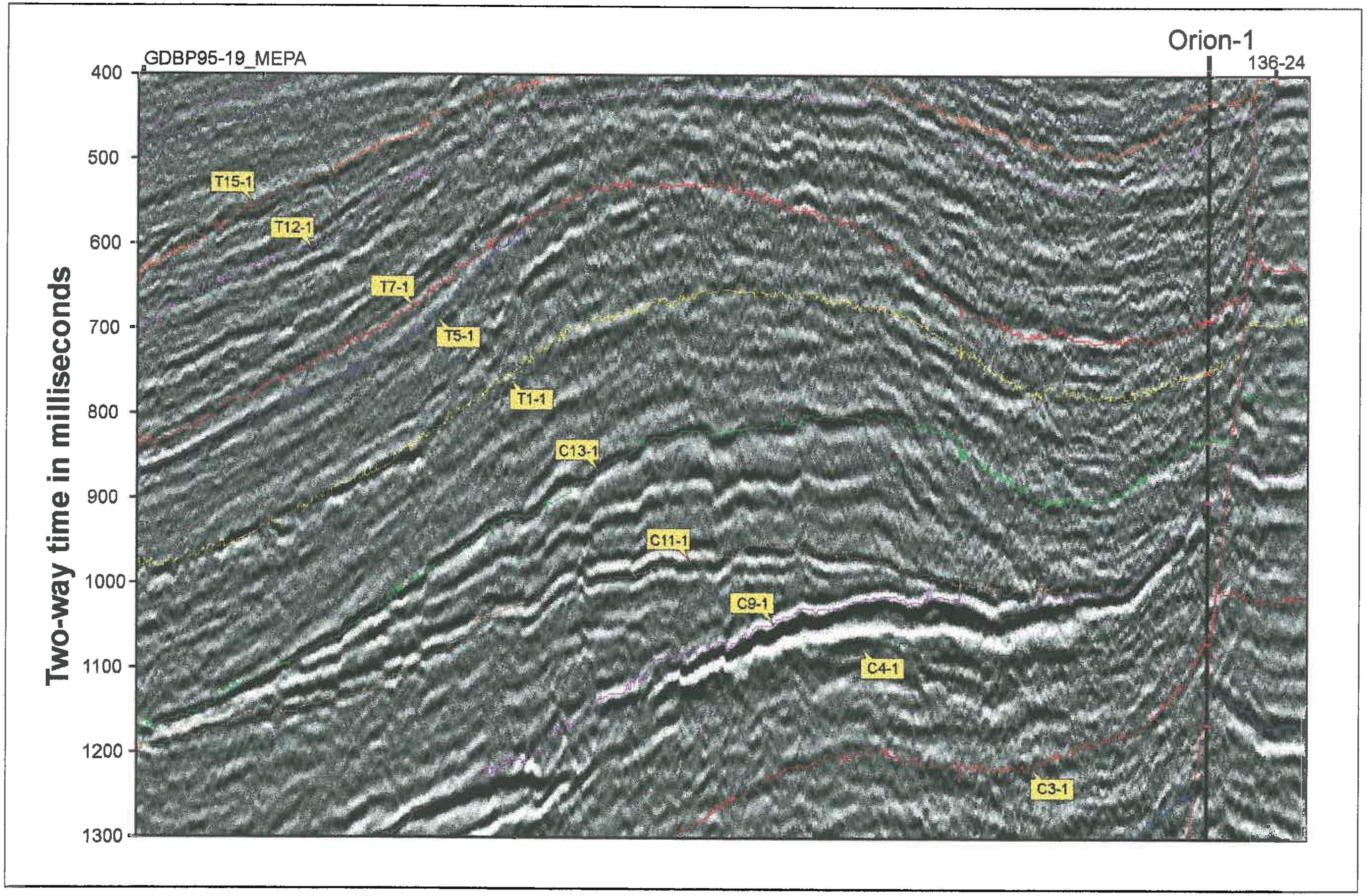

Figure 5.8 Line 136-12 displaying truncation of the Paleocene T5-1 event by the base Eocene T7-1 event. (Line length 21.7 km)

The T10-1 Lutetian event has been identified from biostratigraphic data in some of the study wells (Figure 4.2). This evidence has been combined with a persistent log break at the base of the T10 biozone, which shows a shift to higher gamma and sonic readings and a very distinctive shift to lower porosities and higher densities on the neutron-density logs. This sharp log break can be correlated to a strong seismic peak, which is readily identifiable across the distal portion of the basin. In the proximal region of the basin, T10-1 onlaps the underlying base Eocene T7-1 horizon as demonstrated on the T10-1 two-way time map (Enclosure 1) and in Figure 5.2. The final Eocene event mapped in the study is a Bartonian aged T12 event although the biostratigraphic data suggest the possibility of a T14 aged event (Figure 4.2). The T12 event corresponds to a small shift to lower gamma values and an abrupt shift to lower porosities and higher densities on the neutron-density tool. Moving across this boundary, the separation in the neutron-density logs decreases to zero (Figure 5.10). This feature was noted on wells across the basin and corresponds to a seismic peak that can be mapped throughout the area across the basin. The two-way time map for horizon T12-1 shows a proximal onlap edge where the T12-1 horizon onlaps against the base Eocene T7-1 event.

5.5.3 Tertiary sequences T15-1–SeaBed (Oligocene – Recent)

General Description

Seismic dip lines across the Dampier Sub-basin show the base Oligocene to Recent section to be composed of a strongly basinward-prograding package of clinoforms. Within this section a combination of stratal architecture, wireline log character and biostratigraphic constraints have been used to identify and correlate 17 horizons across the study area. Sequence boundaries of T20-1 (Aquitanian), T20-2 & N8-1 (Burdigalian), N8-2 & N10-1 (Langhian) N10-N12-1 & N16-1 (Serravallian), N17-1, N17-2, N17-3 (Tortonian), N18-1 (Messinian), N19-1 & N19-2 (Zanclean) N21-1 & N21-2 (Piacenzian) and N22-1 & N22-2 (Pleistocene) age have been defined. The two-way time maps for these horizons again show a series of northeast-southwest-striking, northwest-dipping horizons (Enclosure 1). Faulting in the section is restricted to movement on the Rosemary Fault System along the Legendre Trend with displacement observed in sediments as young as Pliocene (N19-2) in age. There is no evidence of movement on any faults along the Rankin or Brigadier Trends in this section.

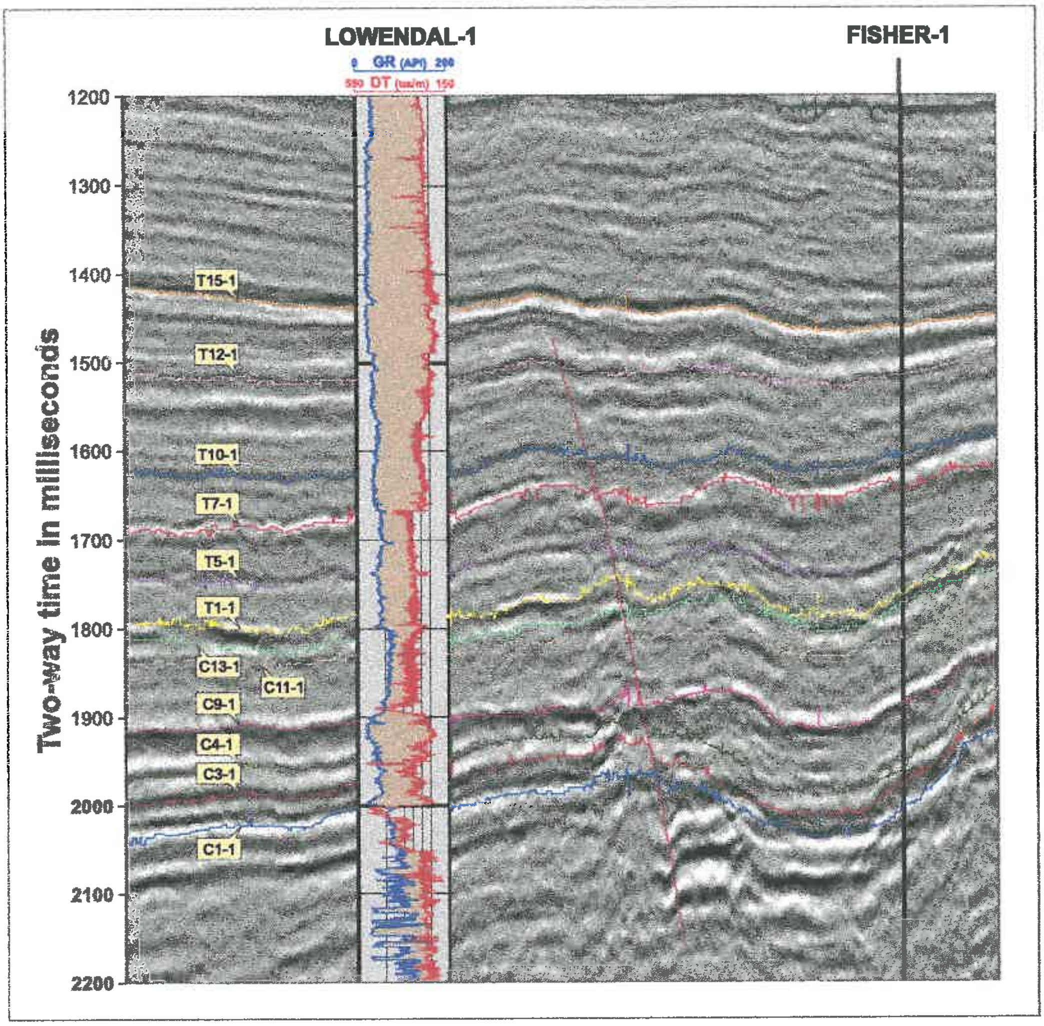

Figure 5.9 *Line 136-23 showing the log and seismic characteristics of the Paleocene T5-1 and base Eocene T7-1 events.*

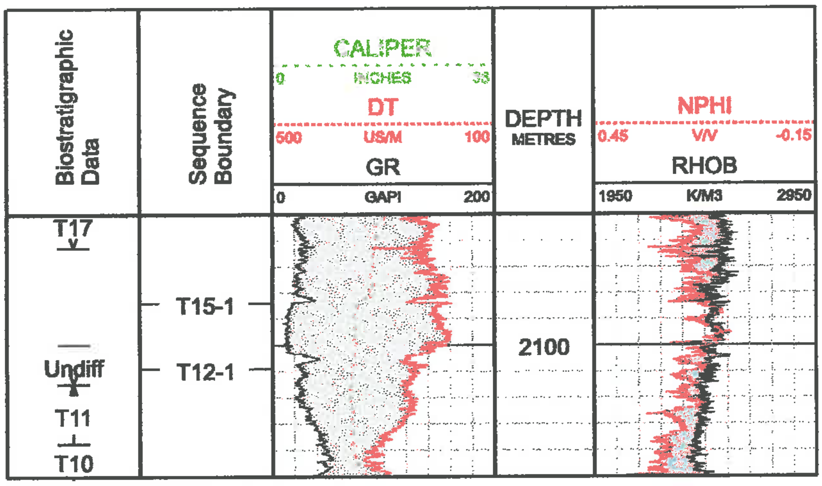

Figure 5.10 *T12-1 log characteristic showing minimal separation of density and neutron logs.*

Horizon Description

Horizon T15-1 is a distinct biostratigraphic discontinuity, a record of a process that apparently removed the majority of the Lower Oligocene sediments from the basin (Figure 4.2). On wireline logs, sharp increases in the gamma, sonic and neutron values are recorded across the boundary with a corresponding decrease in density (Figure 4.4). A marked separation in the neutron and density tools is also re-established after the minimal log separation that characterises the underlying T12-1 sequence (Figure 5.10). On seismic, T15-1 is represented by a very high amplitude regional reflector, which dips gently on the Enderby Platform, more steeply between the Legendre and Rankin Trends, becomes relatively flat-lying over the Rankin Platform and finally increases in dip over the Brigadier Trend (Figure 5.2). Due to the considerable amount of missing section, distinct log characteristics and significant change in seismic character across the horizon, T15-1 has been defined as one of the major basin-forming events that was initially used to subdivide the section.

Sequence boundaries T20-1, T20-2, N8-1, N8-2, N10-1, N10-N12-1, N16-1 and N17-1 have all been defined from biostratigraphic data and wireline log character using the model described in the previous chapter. The wireline expressions of these events are not significant but they are persistent throughout the study area and have been constrained by biostratigraphic data. The two-way time maps for horizons T20-1 – N17-1 clearly illustrate the clinoform geometries with relatively shallow-dipping tops and toes separated by the steep fore-sets, which are represented by the narrowly spaced northeast-southwest-trending contours (Enclosure 1). In a basinward direction, the toes of the clinoforms downlap the underlying horizons and in a landward direction they are seen to onlap the underlying horizons. T20-1 onlaps and downlaps the underlying T15-1 horizon at its proximal and distal ends respectively. The Burdigalian T20-2 event proximally onlaps T20-1 and distally downlaps on to T15-1. The second Burdigalian event, N8-1, distally downlaps on to T15-1 and is seen to extend over the remainder of the study area as demonstrated on the two-way time map. The two-way time map for N8-2 shows this horizon to be restricted to an area less than that of the underlying N8-1 horizon and as such N8-2 will onlap and downlap N8-1 in a proximal and distal sense respectively. The two-way time map for the N10-1 horizon shows it to be regionally more extensive than the underlying N8-2 horizon. In a proximal direction N10-1 onlaps N8-1, while in a distal direction, N10-1 is seen to extend over the whole of the study area. The subsequent N10-N12-1 event has been named as such because the biostratigraphic evidence is inconclusive whether this event is of N10 or N12 age. The two-way time map for the N10-N12-1 event shows it to be less extensive than the underlying N10-1 horizon, which it onlaps in a proximal direction and downlaps in a distal direction at the ends of line 110-03, 110-08, 136-10 and 136-11. The proximal end of the subsequent Serravallian N16-1 event onlaps the underlying N10-N12-1 horizon. The distal end of N16-1is truncated by the overlying N17-1 horizon at the northwest end of lines 136-10, 11, 14, 15, 16 and 110-08; on line 110-03 it is seen to downlap onto N10-1 and on other dip lines its termination is not seen. The N17-1 horizon, which caps this series of events is regionally extensive in nature which has been defined from wireline log and biostratigraphic data and mapped as a high-amplitude seismic reflector. A change in stratal architecture can be seen across the N17-1 horizon. This is especially evident on strike lines through the basin (Figure 5.11).

The two-way time maps for the T15-1 to N17-1 sequences show a series of laterally-extensive northwest-dipping horizons, which show no significant along strike variation (Enclosure 1). The two-way time maps for the subsequent N17-2, N17-3, N18-1, N19-1, N19-2, N21-1, N21-2, N22-1 and N22-2 horizons show a departure from this linear nature of the mapped horizons. Biostratigraphic data in this section is of poor quality (Figure 4.2) and as such these events have been primarily defined by stratal architecture and constrained by wireline log character and all available biostratigraphic data. The distal termination of most of these sequences is basinward of the limit of the seismic data, but information on distribution style and proximal termination type is still available for these sequences.

The two-way time maps for N17-2 and N17-3 show these sequences to be both spatially restricted clinoforms in the area between dip lines 101-08 and 136-14 and have steep fore-sets in the vicinity of line 110-08 (Enclosure 1). Both these sequences have been assigned N17 age on the basis that they are located beneath the overlying N18-1 sequence boundary, rather than on direct biostratigraphic evidence alone. On dip lines through this section, they appear to be yet another clinoform similar to all other post Oligocene sequences (Figure 5.2). However, strike lines through this section show N17-2 and N17-3 to be truncated by the overlying N18-1 event to the southwest, downlapping onto the underlying N17-1 horizon to the northwest and northeast, and onlapping N17-1 to the southeast, (Figure 5.12). The structural configuration of the remaining Tertiary sequences in the Dampier and Beagle Sub-basins appears to be related to the position of N17-1 & 2 as the subsequent sequences deepen to the northeast and southwest of it. Seismic lines through the distal portion of the Pliocene sequences show considerable sediment thinning onto the mound created by the N17-1 to N18-1 sediments (Figure 5.13).

The N18-1 event defined in the study is a high amplitude seismic reflector. The wireline log character of this event varies throughout the basin and a combination of seismic mapping, limited biostratigraphic data and log character have been used to constrain its location. The proximal edge of N18-1 onlaps N17-1 as demonstrated on the two-way time map. The following Pliocene sequences have been primarily defined from seismic data and their age has been determined from the limited biostratigraphic data that is available. The two-way time maps show the N19-1 event to onlap the underlying N18-1 sequence. N19-1 is followed by the regionally extensive N19-2 event, which is succeeded and onlapped by the N21-1 event. The second N21 event, N21-2 has approximately the same onlap edge as N21-1 and it too onlaps the underlying N19-2 event. N22-1 is a regionally extensive event that persists to the edge of the data and is followed by the N22-2 horizon, which is truncated by the present day seabed.

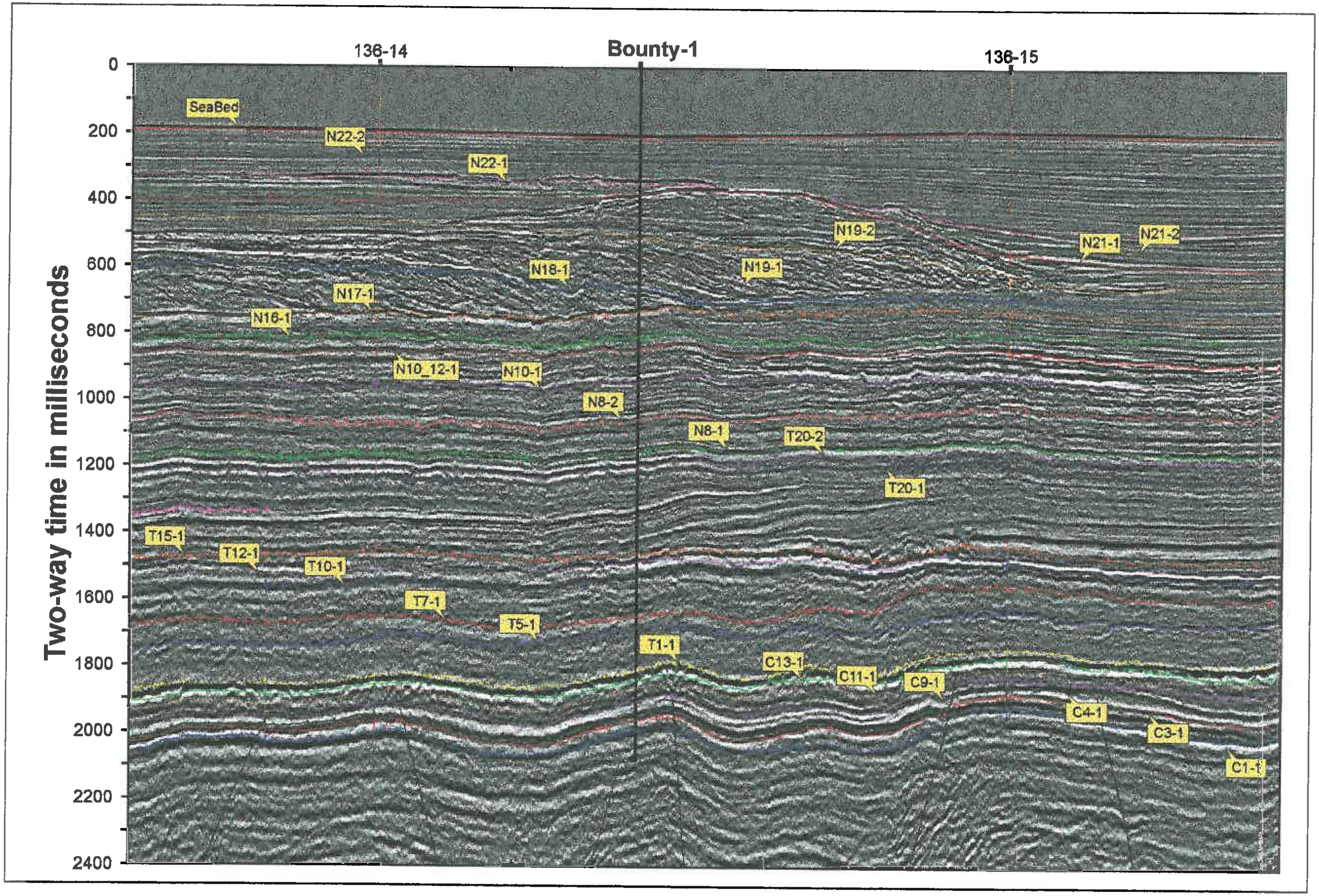

Figure 5.11 *Line 136-19 showing the change in stratal architecture across horizon N17-1. (Line length 39.8 km)*

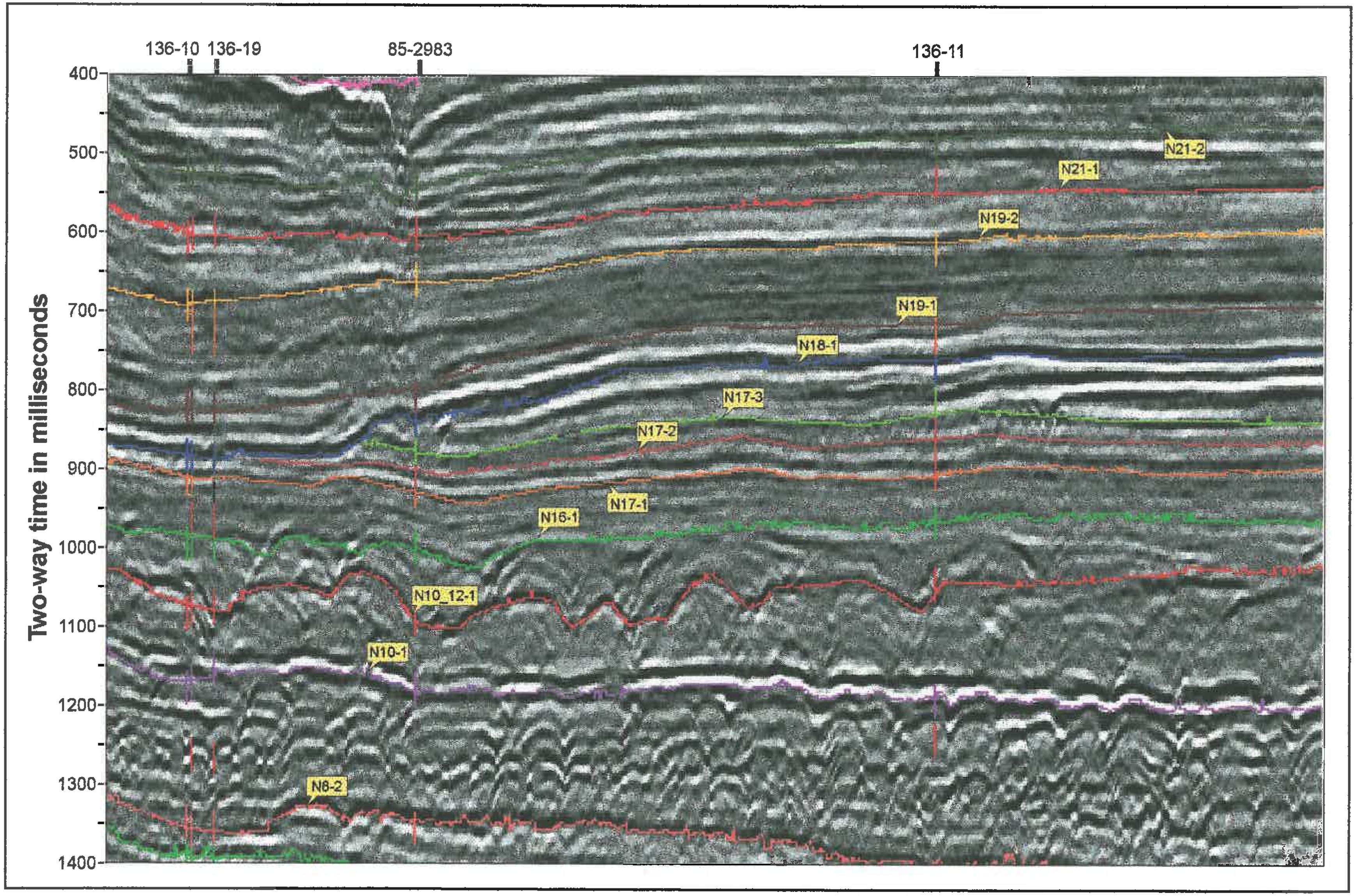

Figure 5.12 Strike line 86-3157 showing the southwestern truncation of the N17-2 and N17-3 horizons by the overlying N18-1 horizon. (Line length 23.3 km)

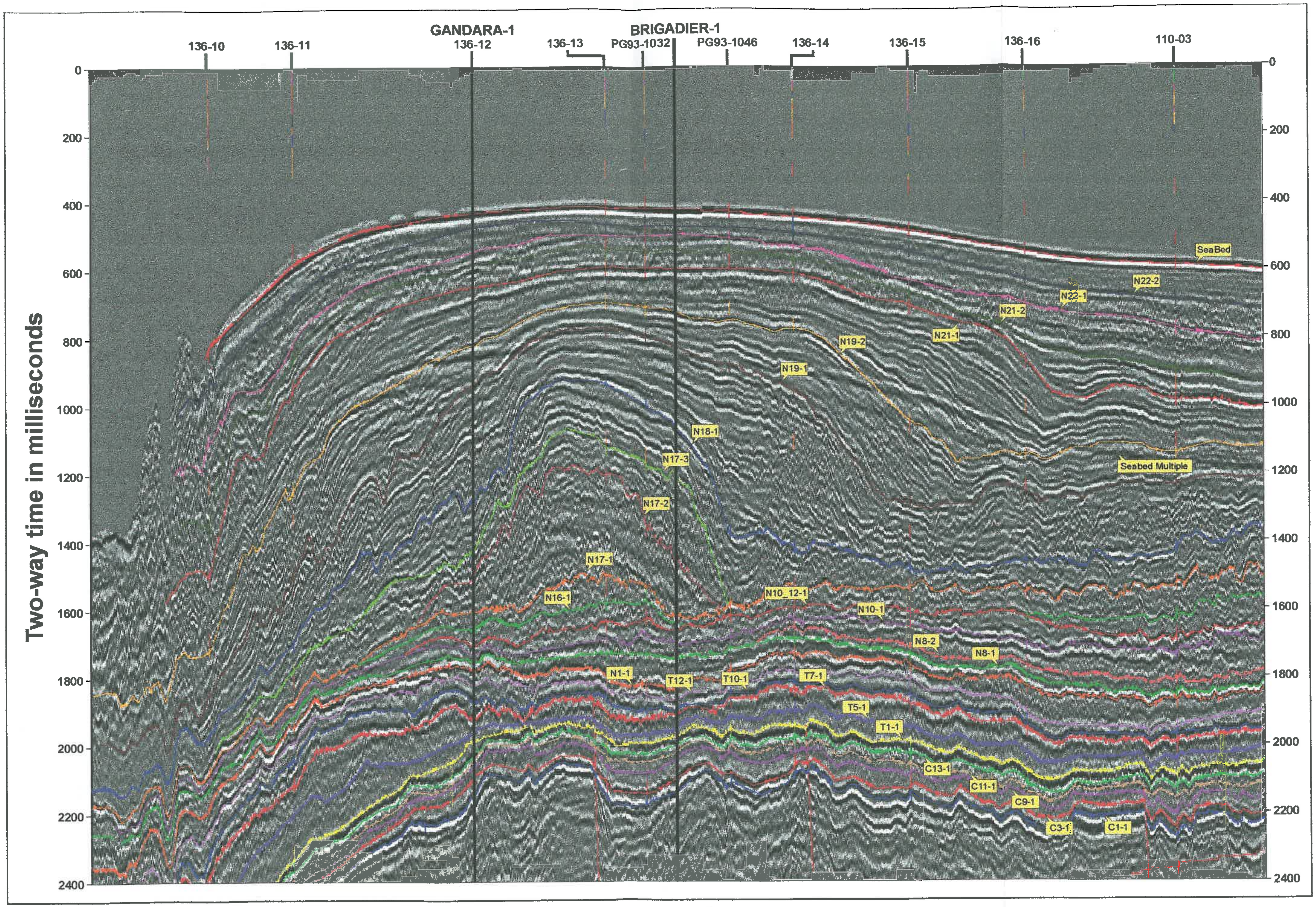

Figure 5.13 *Highly compressed display of line 110-08 showing development of thick N17 (Messinian) sediments and thining of the subsequent Pliocene (N19-1) to seabed sediments onto the N17 sediments. (Line length - 310 km)*

5.6 Isochron Maps

Isochron maps of "time thickness" distributions between the horizons described above have been produced to investigate the sedimentary architecture of the sequences defined between adjacent horizons. The isochron maps produced for each sequence are presented as Enclosure 2.

These maps have a colour palette that is automatically scaled so that it is equally distributed between the highest and lowest values contained on each grid. In the seismic interpretation package it is possible to customise a colour palette for the maps but it is not possible to set the range of values to which the colours correspond. In the case where there are large differences in sediment thickness between sequences a particular thickness will be represented by a different colour on each map. This can be a benefit in that it clearly shows the location of the sediment depocentre for each sequence but it can also be a problem in that it is not immediately evident where the thickest sediment accumulation within the whole suite of maps occurs. The maps illustrate the distribution of the thickest sediment preserved within each sequence, which can then be related to the development of accommodation space. Relative thicknesses for each sequence can be easily evaluated by referring to the contours and scale bars provided at the right hand side of each map.

5.6.1 Cretaceous sequences C1-1–T1-1 (Albian – Maastrichtian)

Isochron maps for the Cretaceous sequences bound by the C1-1 to T1-1 events all show the maximum sediment accumulation to be recorded in the southwest corner of the study area with thin sedimentation (<50 ms) being recorded over the remainder of the basin.

The isochron maps for the C1-1–C3-1 and C3-1–C4-1 sequences show the location of the thickest sediment to be restricted to a northeast-southwest-trending region to the southeast of line 136-20 and laterally restricted by line 136-15 at the northern end of the Dampier Sub-basin. In this area, sequence C1-1–C3-1 is up to 300 ms thick whilst C3-1–C4-1 is up to 180 ms thick. The location of these depocentres corresponds closely to the position of the underlying Lewis Trough, suggesting that accommodation space was being preferentially created in this location. In both these sequences, no significant thickness of sediment has been recorded in the region northwest of the Lewis Trough (approximated by line 136-20), implying that the creation of accommodation space was a localised phenomenon in response to sediment loading and compaction in the Lewis Trough. If the accommodation space were tectonic in origin, then it would be expected that other elements of the linked tectonic system, such as the Kendrew Trough, would also show development of accommodation space and sedimentation at this stage. The maps show this not to be the case. Erosion may have removed sediment deposited contemporaneously outside the Lewis Trough but this is considered unlikely as seismic lines through this section show no evidence of truncation and also show depositional thickening of the sequences into the Lewis Trough (Figure 5.2). At the northeast end of line 136-24 thickening of C3-1–C4-1 sediment is evident. The seismic reflectors are seen to separate at this location but due to the large line spacing at the northeastern end of the grid it is not possible to determine the nature or extent of this thickening with any confidence.

The Turonian to Campanian, C4-1–C9-1 isochron map again shows the thickest sediment accumulation to occur along the axis of the Lewis Trough. This map shows the first evidence of significant sediment accumulation outside the Lewis Trough, with 120 ms of sediment being recorded in the Kendrew Trough and Madeleine Trend and 150 ms of sedimentation recorded at the southeast ends of lines 136-15, 110-03 and 136-17. By this stage, the development of accommodation space is no longer restricted to the Lewis Trough as it was during the Albian and Cenomanian. The isochron map for the subsequent Campanian to Maastrichtian C9-1–C11-1 sequence also shows significant sedimentation centered on, but extending beyond the Lewis Trough (700 ms on line 101-08). The sediment depocentre is contained between line 136-14 and the southern end of the study area and is bounded to the northwest by the Rankin Trend against which the sequence thins rapidly. A further accumulation of C9-1–C11-1 sediment (100-180 ms) is evident in the Beagle Sub-basin (within the area bounded by dip lines 136-16 & 18 and strike lines 136-19 & 24). The presence of significant thicknesses of both C4-1–C9-1 and C9-1–C11-1 sediments outside the limits of the Lewis Trough is evident in Figure 5.2.

Sediment depocentres of the Maastrichtian C11-1–C13-1 and C13-1–T1-1 sequences are also restricted to the southwest corner of the basin. At the intersection of lines 101-09R and GPBD95-19_MEPA, a maximum of 250 ms of C11-1–C13-1 sediment is recorded. A similar maximum of C13-1–T1-1 sediment is recorded further northeast on line GPBD95-19_MEPA. For the first time since the Albian, the location of the thickest sediment has moved outside the confines of the underlying Lewis Trough, signaling the end of the Lewis Trough as a dominant control on sediment distribution during the Maastrichtian.

Isochron maps for the Cretaceous sequences show the point of thickest sediment accumulation in each sequence to migrate laterally along the axis of this basin through time. In the first sequence, C1-1–C3-1, the thickest point is located in the Lewis Trough between lines 136-10 and 136-12. In the following C3-1–C4-1 sequence it migrates northeastwards along the axis of the Lewis Trough to be situated between lines 136-13 and 136-16. In sequence C4-1–C9-1 it is located between lines 136-10 and 136-11 and by sequence C9-1–C11-1 it has migrated further to the southeast to be situated on line 101-08. By sequence C11-1–C13-1 the thickest point has migrated in northeasterly direction to be located at the intersection of lines 101-09R and GPBD95-19_MEPA and by the final Cretaceous C13-1–T1-1 sequence it has moved further northeast along line GPBD95-19_MEPA. The isochron maps for the C3-1–C4-1 to C9-1–C11-1 sequences also show a thickening of depocentres to the southeast.

5.6.2 Tertiary sequences T1-1–T12-1 (Danian – Bartonian)

Isochron maps for the Paleocene and Eocene sequences in the study area also show thickness variations which are seen to vary in both dip and strike directions. The Paleocene-Eocene section of the Dampier Sub-basin is a relatively thin section, compared to the late Cretaceous and post-Oligocene sediments, which show only minor variations in lateral thickness (Figure 5.14). However, isochron maps for these sequences have revealed thickness variations throughout the section.

The isochron map for the first Paleocene sequence, T1-1–T5-1 shows a northeast-trending body of sediment which attains maximum thickness (250 ms) over the area of the Kendrew Trough and the Madeleine Trend in the southwest of the study area. This sediment package is seen to thin laterally in a northwesterly direction to where more isolated thicknesses of the sequence are seen on line 136-19 between Miller-1 and Ronsard-1. The development of further thicknesses of this sequence is also recorded at the distal ends of lines 136-10 & 11, along line 110-08 and at the northeast end of line 136-14. Compared to the underlying C13-1–T1-1, sequence the point of thickest sedimentation has migrated southwest along the axis of the basin to be located on line 136-20 and between lines 136-10 and 101-08. The isochron map of the second Paleocene sequence (T5-1–T7-1) shows a sequence of relatively constant thickness (≅80 ms) with isolated thickening to 120 ms. There appears to be no pronounced depocentre in this sequence. The early Eocene T7-1–T10-1 sequence is also a thin, relatively homogeneous sequence but the isochron map does define a maximum thickness of approximately 100 ms along line 136-19. Figure 5.2 shows the nature of the T5-1, T7-1 and T10-1 reflectors and demonstrate the laterally consistent nature of these thin homogenous sequences.

The isochron map for the Eocene T10-1–T12-1 sequence demonstrates two distinct areas of sediment thickening in the study area, on what is another thin sequence (≅50 ms). In the area bounded by lines 101-09R, 136-20, 136-14 and 85DB-13, this sequence attains a thickness of 200 ms, though it is seen to thin rapidly in a northeasterly and southwesterly direction (Figure 5.15). The other area of the study where this sequence is seen to thicken to 100 ms is in the southwest, in the vicinity of line 136-23.

The final Eocene sequence T12-1–T15-1 shows further thickening in a similar location to the underlying T10-1–T12-1 sequence both along line 136-23, where approximately 100 ms of sediment has accumulated and also in the centre of the basin in an area bounded by lines 136-13, 136-20, 110-03 and 136-24. In this second location, sedimentation of 200 ms is recorded in a northeast-trending depocentre and the point of thickest deposition has migrated in a northeasterly direction along line 101-02R.

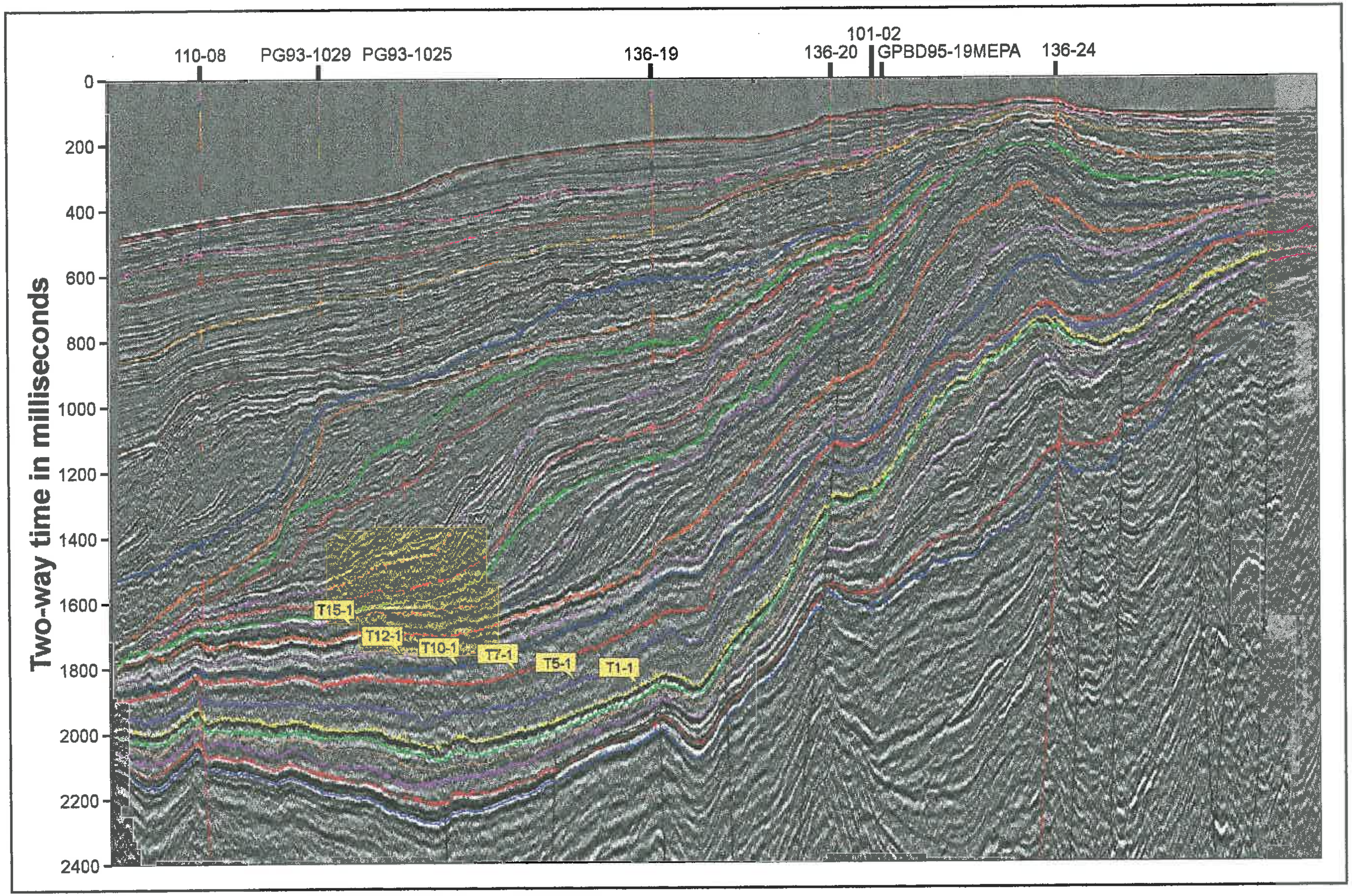

Figure 5.14 *Highly compressed display of line 136-14 showing the minor thickness variation in the Paleocene and Eocene sequences (T-1 to T15-1). (Line length 119 km)*

5.6.3 Tertiary sequences T15-1–SeaBed (Oligocene – Recent)

Isochron maps for the Oligocene to Recent section can be subdivided into distinct groups on the basis of sequence geometry. Sequences T15-1–T20-1 to N16-1–N17-1 are seen to be northeast-southwest-trending linear sediment bodies which have thickest sediment accumulation along a central axis and thin to zero at both the proximal and distal ends. Sequences of N17-1–N18-1 to N22-2–Seabed age also trend in a generally northeast-southwest direction and show thinning in a proximal and distal direction. However, these sequences show significant along-strike variation in sediment thickness with thickest sedimentation being restricted to an area at the distal ends of the dip lines in the Dampier Sub-basin and only thin sedimentation to the northwest and southeast areas of the study. Seismic lines through the Oligocene to Recent section show a series of strongly progradational clinoforms which thin in both a proximal and distal direction (Figure 5.2).

The isochron for the late Oligocene T15-1–T20-1 sequence shows thick axial sedimentation, which thins to zero in proximal and distal directions as is typical of clinoforms. The map shows the sediment thickness to remain fairly constant along the length of the basin with a maximum of 250 ms of sediment at the southwestern end of the study area on line 136-23 and 220 ms of sediment on lines 136-15, 16, 17, 18 & 110-03. The isochron map shows the sequence to increase in width with the thickest part of the sequence increasing from 10km width on line 101-08 to 50km width on line 136-18. The following base Miocene (Aquitanian) T20-1–T20-2 sequence is a much thinner sequence, which is not much greater than 100 ms thickness on the dip lines in the Dampier Sub-basin lines 101-08 to 136-15. It does however, represent a significantly shorter period of time than the underlying base Oligocene sequence. The isochron map for sequence T20-1–T20-2 also shows this sequence to thicken in a northeasterly direction towards the Beagle Sub-basin (lines 110-03 – 136-18). The isochron maps for both the T15-1–T20-1 and T20-1–T20-2 sequences are seen to thin at the northern end of the Dampier Sub-basin in the area between lines 136-14, 136-20, and 136-16. The isochron for the T20-1–T20-2 sequence also shows some thickening landward of the main clinoform on line 136-20.

The Burdigalian T20-2–N8-1 sequence also shows the northeast-southwest-trending clinoform which attains a maximum thickness of 200 ms throughout the Dampier Sub-basin and is seen to be thinner in the Beagle Sub-basin. Unlike the previous two sequences, the width of the thickest part of the clinoform remains constant along the length of the basin. Landward of the main T20-2–N8-1 clinoform, up to 100 ms thickness is recorded in a northeast-southwest trending depocentre on line 136-20. The N8-1–N8-2 isochron map shows thin sequence development (≅50 ms) at the southern and northern ends of the study area with 100 ms or more of sediment being recorded in the intervening area. Compared to the previous Oligocene and Miocene sequences, the sedimentation persists over a wider area which is not restricted to a linear band on the clinoform front. Seismic lines through this section show significant aggradation of top-sets between N8-1 and N8-2 (Figure 5.16).

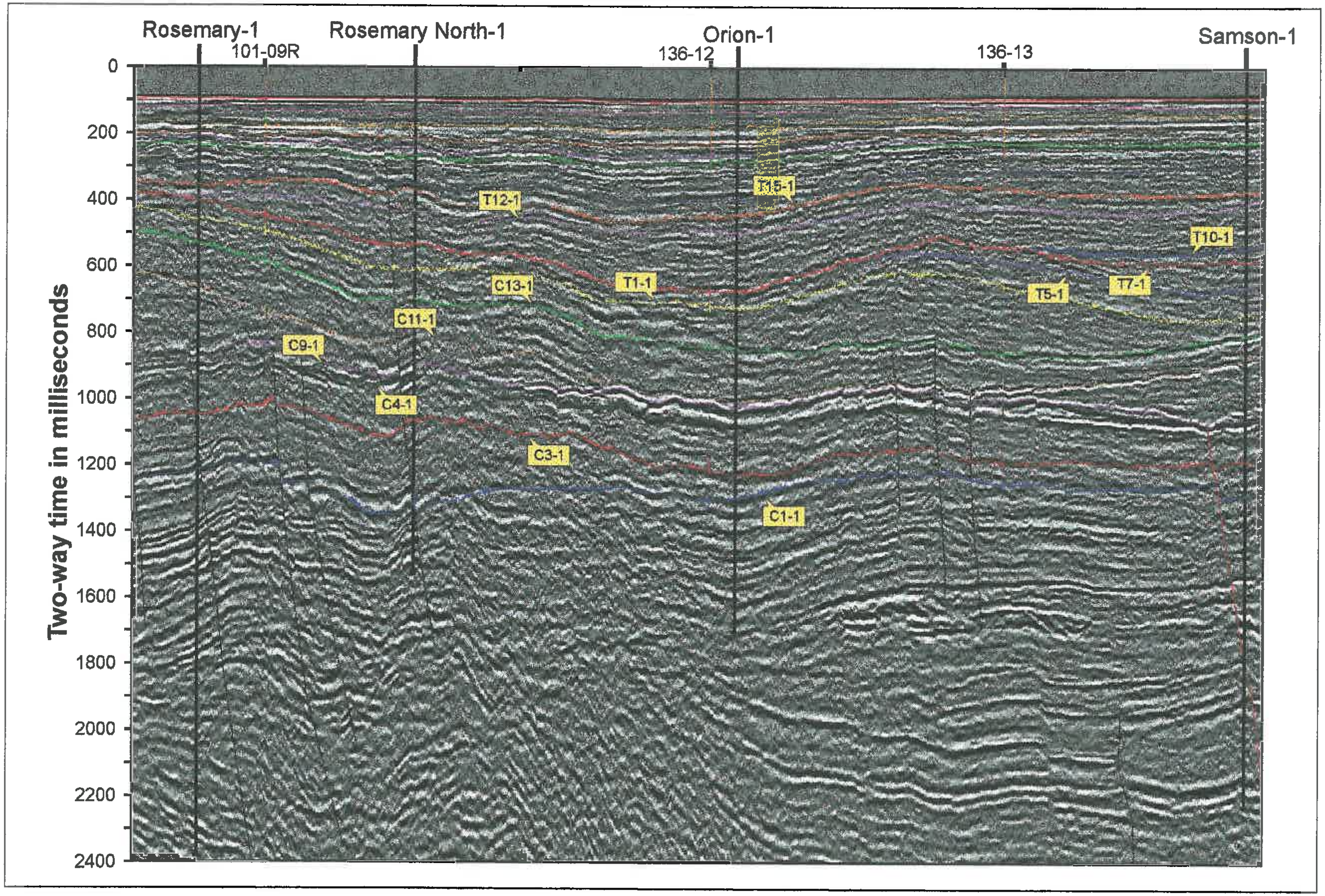

Figure 5.15 *Line 136-24 showing thinning of the Eocene T10-1 to T12-1 sequence. (Line length 43.5 km)*

The Langhian N8-2–N10-1 sequence also shows thick sediment distribution along an axis through the length of the basin. Considerable thickening of the vertical and lateral extent sequence is seen in a northerly direction. On line 136-10, the main section of the clinoform is no more than 5-10 kms wide and up to 150 ms thick, whilst on line 136-18, the clinoform is up to 50 km wide and up to 400 ms in thickness. The grid shading also indicates a significant increase in the volume of sediment towards the Beagle Sub-basin at the northern end of the study area. The isochron map for the subsequent Serravallian N10-1–N10-N12-1 sequence shows a northeast-trending clinoform, which thins to both the northern and southern ends of the study area. The maximum accumulation of 350 ms of this sequence occurs on line 136-13; this decreases to ≅100 ms on line 136-18 at the northern end of the study area. The N10-1–N10-N12-1 isochron map shows a considerable thickness of sediment to have accumulated landward of the main clinoform front, with 150 ms of sediment recorded on line 136-12. Seismic data through this section confirms significant accumulation of top-sets in this area (Figure 5.2). The Serravallian to Tortonian N10-N12-1–N16-1 sequence is thickest in the centre of the Dampier Sub-basin along lines 136-12 & 13 where it attains a thickness of 200-250 ms. The sequence thins rapidly in a landward direction, implying that the primary site of sediment deposition in this sequence is on the slope front. In the study area northeast of line 136-14, the isochron map for the N10-N12-1–N16-1 sequence shows very thin sediment deposition with the exception of the end of lines 110-03 and 136-17. The subsequent Tortonian N16-1–N17-1 sequence demonstrates a similar sediment distribution with thickest sediment accumulation occurring in an area between lines 101-08 and 136-15. The northeast-trending linear nature of the clinoforms is still evident in this map.

The isochron map for the Messinian N17-1–N18-1 sequences shows a marked change from the linear sequence geometries which characterised the N1-N16 sediments. The isochron map shows a thick accumulation of sediment (≅600 ms) in the area contained within lines 136-10, 136-19 and 136-15. Away from this accumulation, the sequence thins in all directions to be less than 100 ms. At the northern end of the study area, the sequence is no more than 50 ms thick across most of the Beagle Sub-basin. This pronounced lateral variation in sediment thickness suggests a change to a localised point source for this sequence rather than a linear source that typified the underlying T15-1 to N17-1 sequences. A landward extension of the N17-1–N18-1 sequence is seen between lines 136-12 & 14 where up to 200 ms of sediment is preserved along line 136-19.

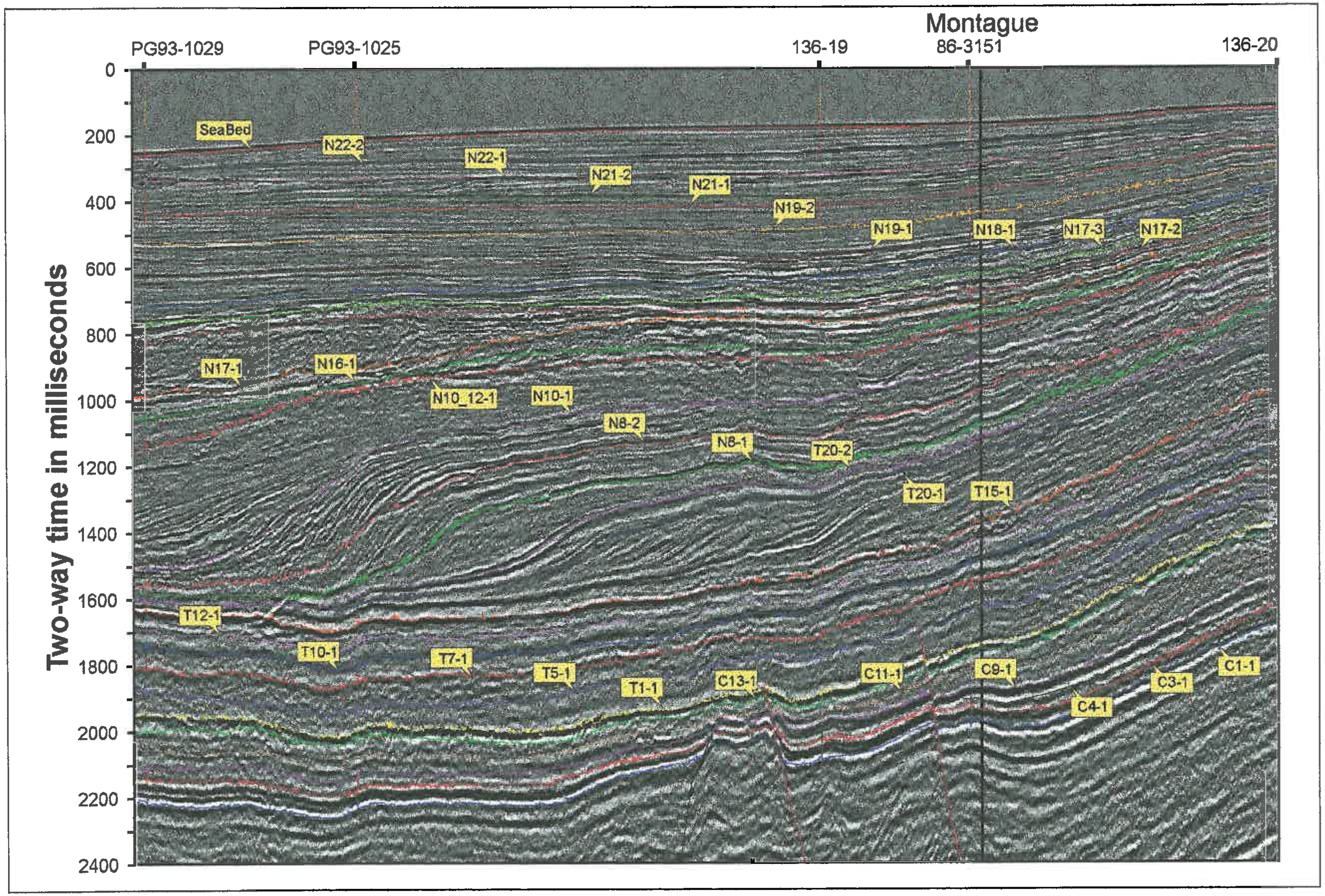

Figure 5.16 Line 136-13 showing significant top-set development of sequences N8-1 to N10-N12-1. (Line length 43.5 km)

The isochron map for the subsequent Pliocene N18-1–N19-1 sequence shows sediments to thicken away from the location of thickest N17-1–N18-1 sedimentation. Two main depocentres can be seen in this sequence, one centered on Gandara-1 (300 ms thick) and the other northeast of Brigadier-1 (300-400 ms thick). Between these two depocentres, only 150 ms of N18-1–N19-1 sediment exists in a location which corresponds to the thickest accumulation of the underlying N17-1–N18-1 sequence. This pattern of sedimentation persists through the N19-1–N19-2, N19-2–N21-1 and N21-1–N21-2 sequences as displayed on the respective isochron maps. On these maps, the two depocentres around Gandara-1 and Brigadier-1 are seen to migrate from the underlying N17-1–N18-1 sediments in a northeast and southwest direction respectively. The Pliocene sediments at this stage are primarily located basinward of the seismic dataset and so caution must be taken when interpreting sedimentation patterns. However, lines 110-08, 136-10,11, 14,15 &16 all show thickening of these sequences in the locations depicted on the maps. Stratal geometries on line 110-08 clearly show sedimentation patterns migrating away from the thick N17-1–N18-1 sequence (Figure 5.17).

An overall reduction in the thickness of the Messinian - Pliocene sequences can be seen through time beginning with an initial thickness of 600 ms in sequence N17-1–N18-1. The subsequent N18-1–N19-1 sequence has a maximum of 500 ms, N19-1–N19-2 has a maximum of 350 ms, N19-2–N21-1 shows a slight increase to a maximum of 400 ms and N21-1–N21-2 shows a maximum thickness of 100 ms. It would appear from this observation that accommodation space is gradually decreasing through time from a maximum at the beginning of the Messinian. In practice it is most probable that accommodation space is being filled from the southeast and migrating in a basinward direction.

The isochron map for N21-1–N21-2 sequence shows a thickening of the sediments towards the southern end of the Dampier Sub-basin and the adjacent Barrow Sub-basin and only minor accumulation in the two depocentres at either side of the N17-1–N18-1 depocentre. This change in depocentre location signifies the final major change in sedimentation style in the Dampier Sub-basin. At this stage significant accommodation space is being created in the Barrow Sub-basin to the southwest and sediments preferentially accumulate in this direction. Isochron maps for the Pleistocene and Holocene N21-2–N22-1, N22-1–N22-2 and N22-2–Seabed sequences all show thickening to the southwestern end of the study area, where 300 ms, 250 ms and 150 ms are recorded respectively. Remnants of the Pliocene northeastern depocentre, which was initially situated around Brigadier-1 after the N17-1–N18-1 sequence, can still be seen on these maps now situated around Delambre-1 and extends south on lines 136-15, 16 & 19 towards Finucane-1, Sable-1 and Ronsard-1.

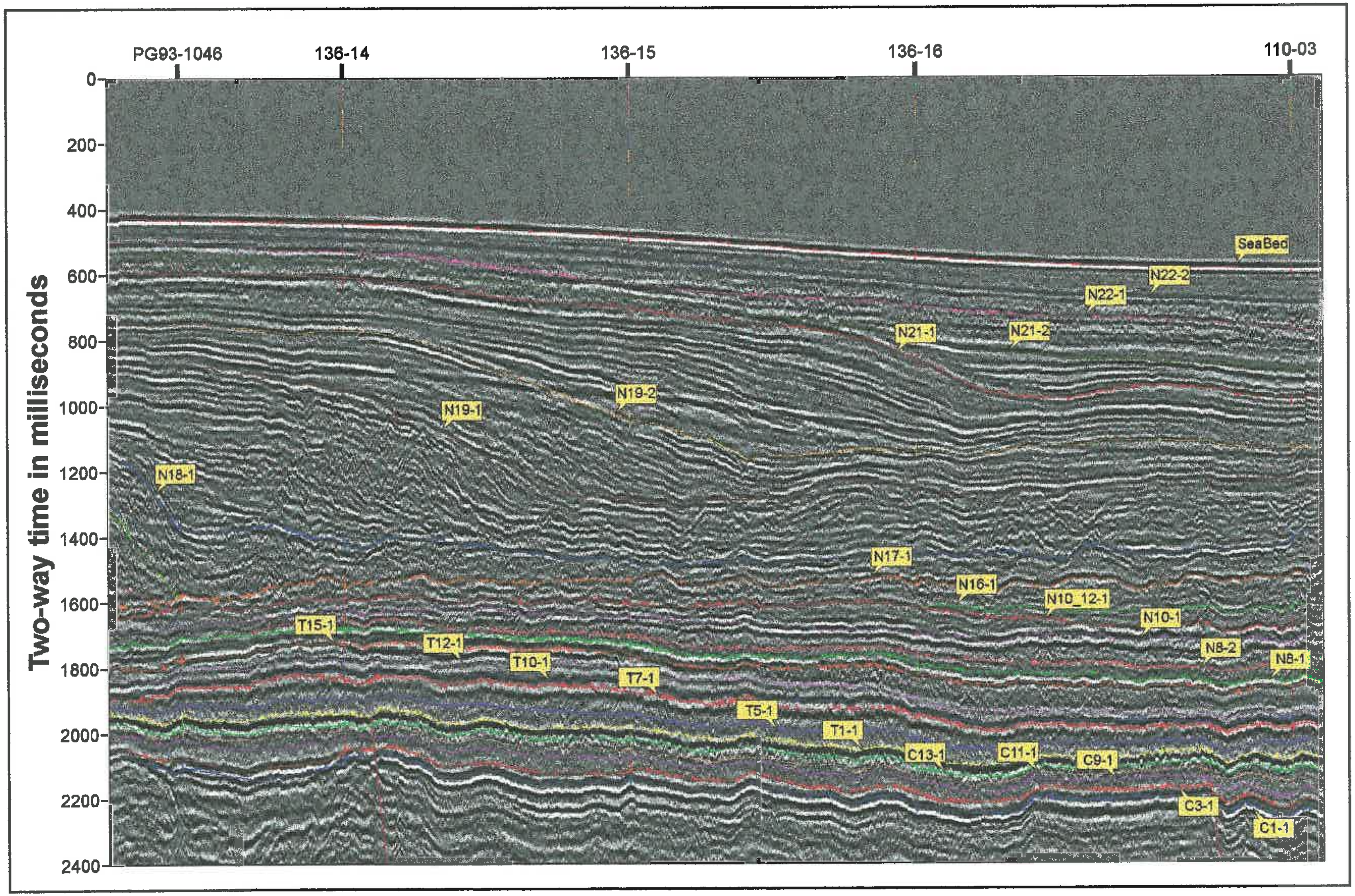

Figure 5.17 *Line 110-08 showing onlap of Pliocene (N18-1 to Seabed) sequences onto Messinian aged (N17-1 - N18-1) sediments to the south west. (Line length - 84 km)*

5.7 Fault Patterns

5.7.1 Introduction

The Dampier Sub-basin is a Jurassic-aged failed rift system (Hill, 1994), which is bound to the east by the Enderby Platform and the west by the Rankin Platform. The Rankin Trend and Rosemary Fault System mark the western and eastern margins between the Dampier Sub-basin and these adjacent platforms (Figure 5.18). The Rankin Trend is a series of tilted fault blocks bounded by north-northeast to south-southwest-trending faults. The Rosemary Fault System is a northeast-southwest-trending basin-forming fault. These two tectonic elements exert an overriding control on fault orientation in the basin.

Faults within this study have been identified and mapped on seismic data and have then been correlated between adjacent seismic lines. The seismic grid which has been used in this study is not of sufficient density to correlate accurately between adjacent lines as line spacing of 10-35 km is common (Figure 5.19). The fault interpretation was therefore conducted using a combination of seismic character, dip line information and published fault interpretations (AGSO North West Shelf Study Group, 1994; Driscoll and Karner, 1998; Hill, 1994; Keep *et al.*, 1998; Miller and Smith, 1996; Stein, 1994; Veenstra, 1985; Woodside Offshore Petroleum, 1988). Uncertainties in the fault interpretation exist due to the nature of the dataset used. However, many of the major basin-forming faults do not penetrate the Albian to Recent section and those which do are not seen to induce major changes in structural or stratal architecture. The upper age of the faulting, which is significant in terms of basin evolution, can be accurately defined from the age of the sediments that the faults disrupt.

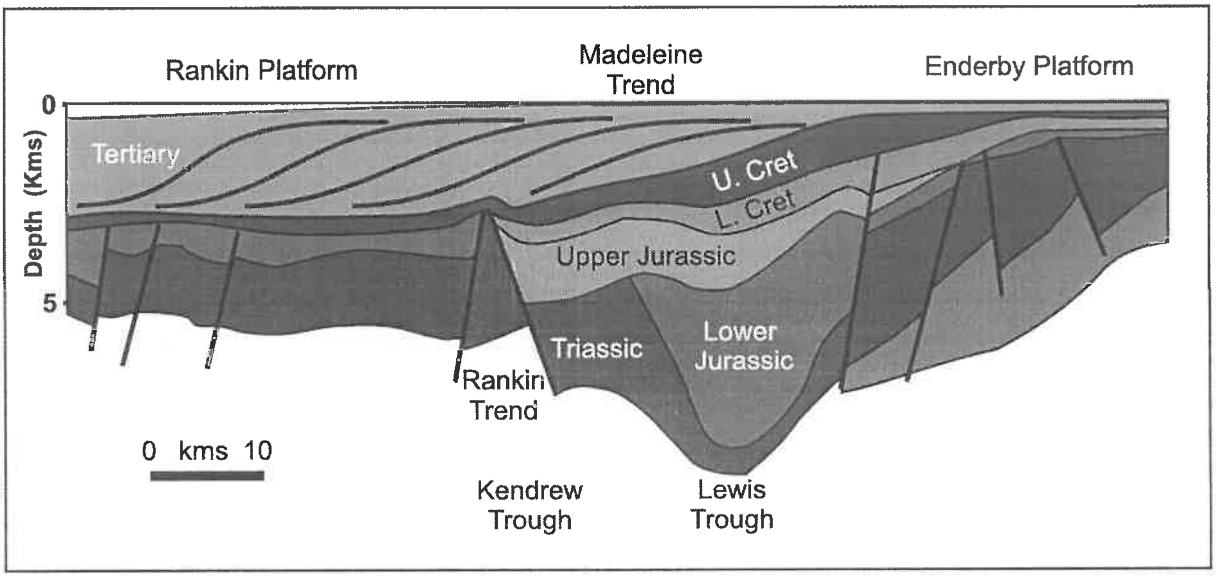

Figure 5.18 Schematic section across the centre of the Dampier Sub-basin.

5.7.2 Rankin Trend and Rankin Platform Faults

Two-way time maps for the Cretaceous horizons C1-1, C3-1, C4-1, C9-1, C11-1 and C13-1 (Enclosure 1) all show intersection of these horizons with the faults of the Rankin Trend (approximated by line 136-19). The Rankin Trend is composed of a series of en-echelon, tilted normal fault blocks with predominantly north-northeast to south-southwest trending bounding faults and a northwest-southeast-trending, southeast-dipping normal escarpment fault. This escarpment fault persists along the whole of the length of the Rankin Trend. The Rankin Trend forms the elevated eastern edge of the Rankin Platform and is separated from the adjacent Kendrew Trough to the southeast by a major escarpment fault, (Figure 5.18). On the northwest edge of the study area, the Rankin Platform is elevated to form the Brigadier Trend and faulting is clearly evident on the two-way time maps of Cretaceous - Tertiary age (C1-1 – T1-1).

En-echelon faults of the Rankin Trend are clearly visible on the two-way time map for the Albian C1-1 event (Figure 5.4). The subsequent Cretaceous two-way time maps (C3-1, C4-1, C9-1, C11-1 and C13-1 Enclosure 1) show these faults to die out at two specific ages. The first group of faults is seen to dislocate sediments of Albian to Campanian age (C1-1 – C9-1) but not the overlying Maastrichtian sediments (C11-1 – C13-1). The second group of en-echelon faults is seen to persist into the Maastrichtian C11-1 and C13-1 events and terminate against the base Tertiary T1-1 event (Figure 5.20).

The main northeast-southwest-trending escarpment fault of the Rankin Trend shows evidence of movement through the Paleocene and Eocene section (as shown on the two-way time maps in Enclosure 1) and is seen to terminate against the base Oligocene T15-1 event (Figure 5.20). The termination of the en-echelon faults in the Maastrichtian section suggest that tectonic movement on the Rankin Trend ceased at the end of the Cretaceous as no later reactivation of these faults has been identified in any part of the dataset. However, dislocation of some Paleocene and Eocene sediments above the escarpment fault suggests the possibility of early Tertiary movement of the Rankin Trend. With no evidence for early Tertiary fault block movement, it is thought that tectonic activity of this age is unlikely. These dislocations were interpreted to be a result of fault propagation caused by differential compaction across the Rankin Trend and adjacent Kendrew Trough, as shown schematically in Figure 5.21.

Faulting on the Rankin Platform is also evident on the Brigadier Trend in the vicinity of Brigadier 1 and Gandara 1. These normal faults have little associated stratigraphic displacement but cause the base Tertiary T1-1 and older sediments of Brigadier Trend to be structurally raised above equivalent sediments on the adjacent Rankin Platform. Most of these faults do not displace the Cretaceous section and so are not evident on the two-way time maps for horizons C1-1, C3-1, C4-1, C9-1, C11-1 and C13-1. However, there is a major northeast-southwest-trending, southeast-dipping normal fault, which offsets sediments of Eocene and older age in the area between lines 136-12 and 136-15. This fault is evident on the two-way time maps for horizons C1-1 – T15-1 and has a displacement in the order of 30 ms on line 136-14 (Figure 5.22). The Albian C1-1 to Tertiary T1-1 sediments are seen to thicken into the centre of the Rankin Platform from adjacent structural highs of the Brigadier and Rankin Trends as also shown in Figure 5.22.

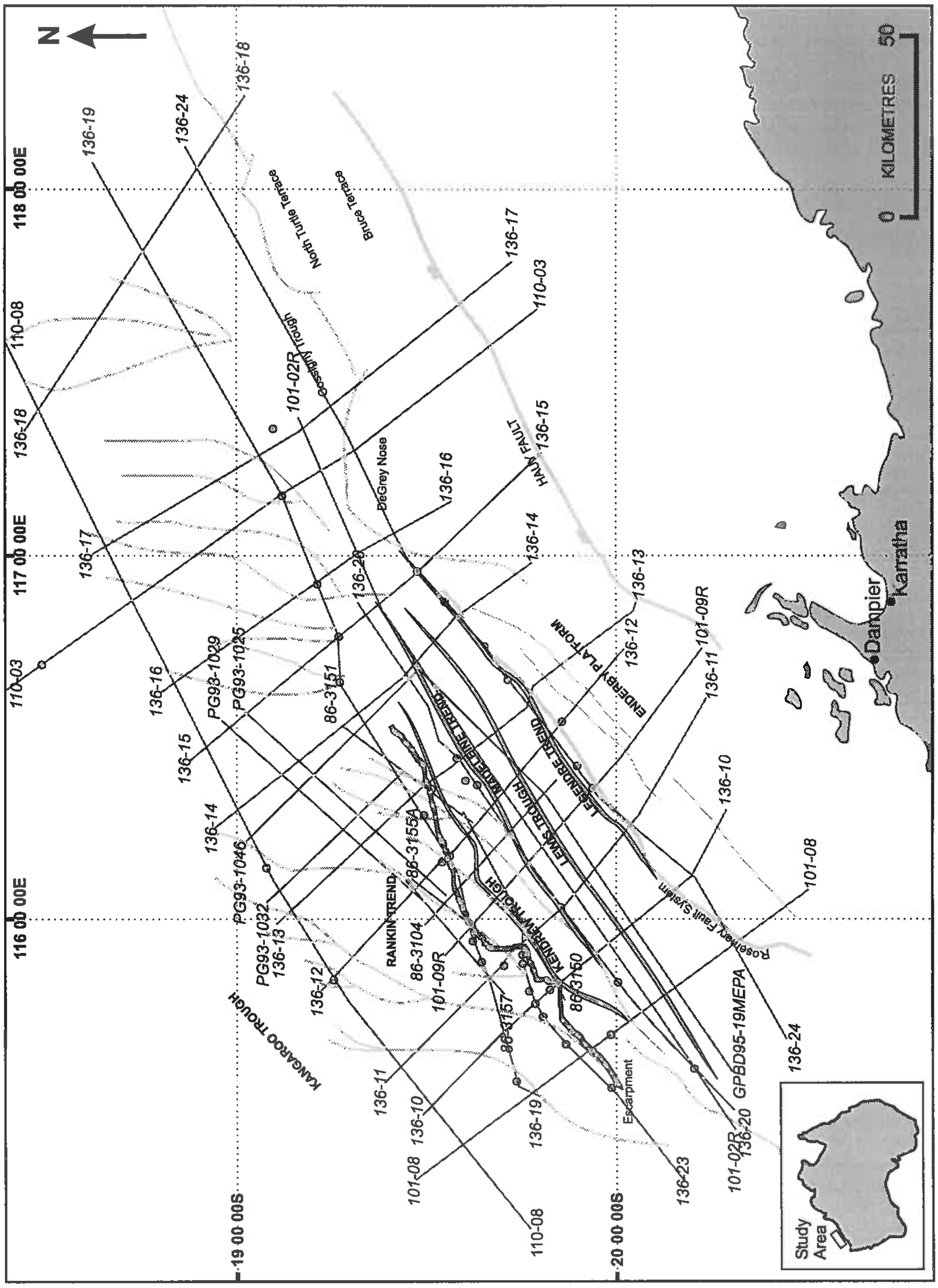

Figure 5.19 Base map showing the location and orientation of the major fault sets in the study area.

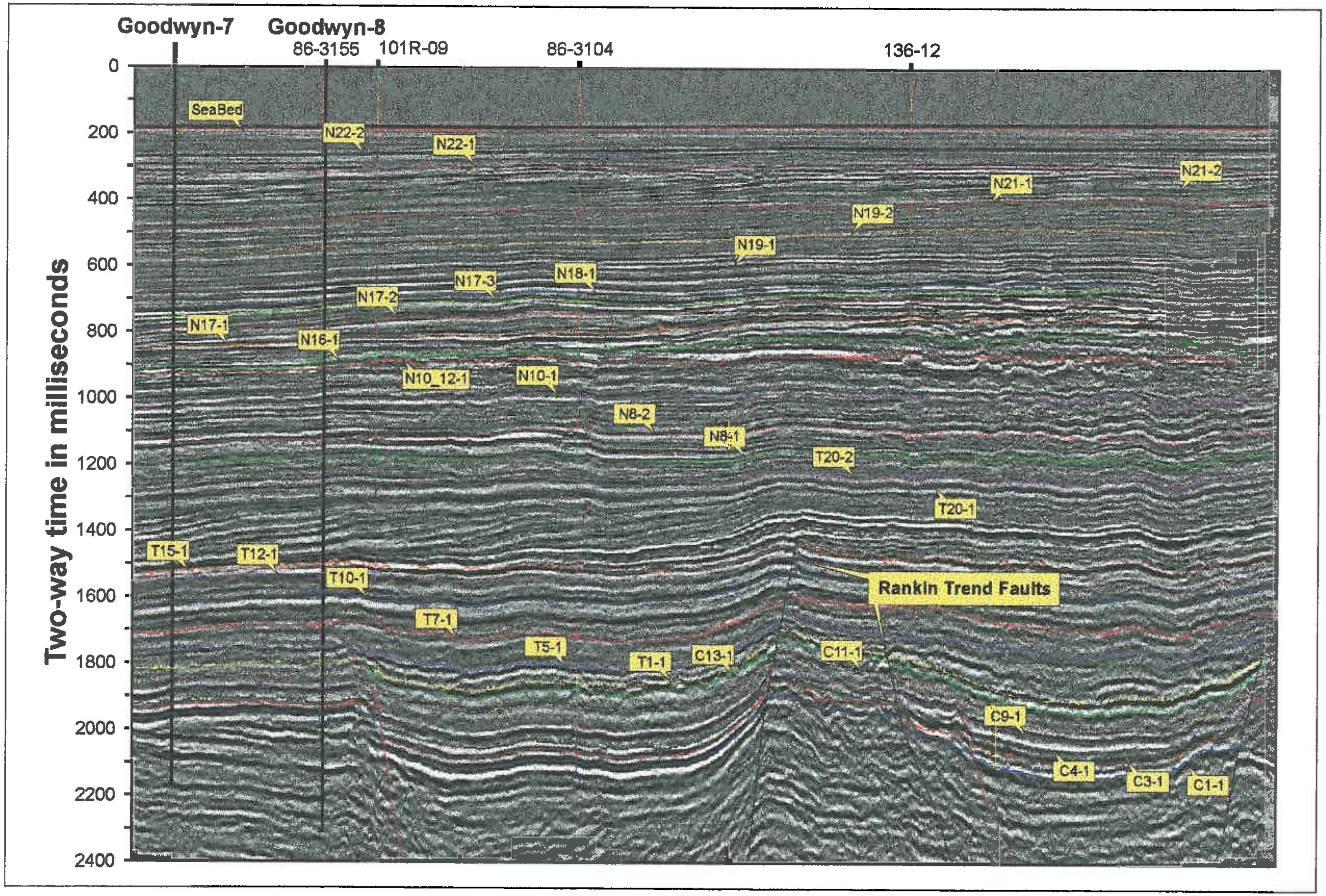

Figure 5.20 *Line 136-19 displaying termination of the Rankin Trend faults against the Campanian (C9-1), base Tertiary (T1-1) and base Oligocene (T15-1) events. (Line length 43.5 km)*

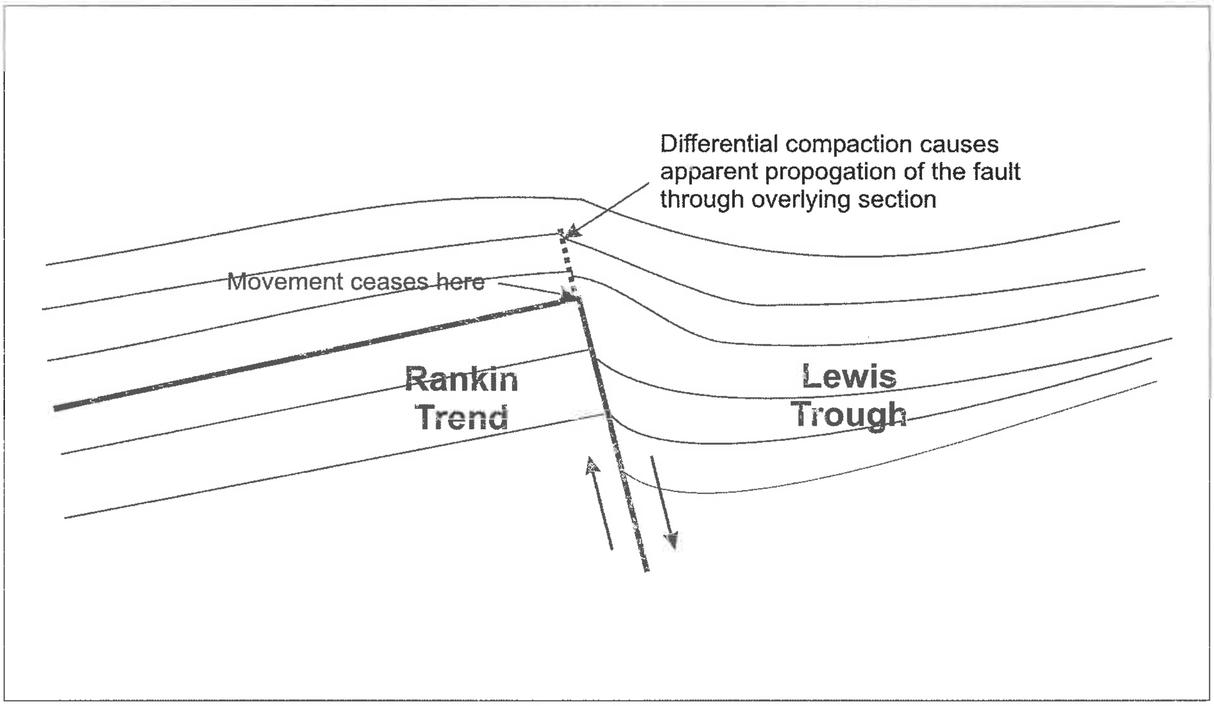

Figure 5.21 *Schematic of differential compaction across Rankin Trend causing fault propagation in the overlying sediments*

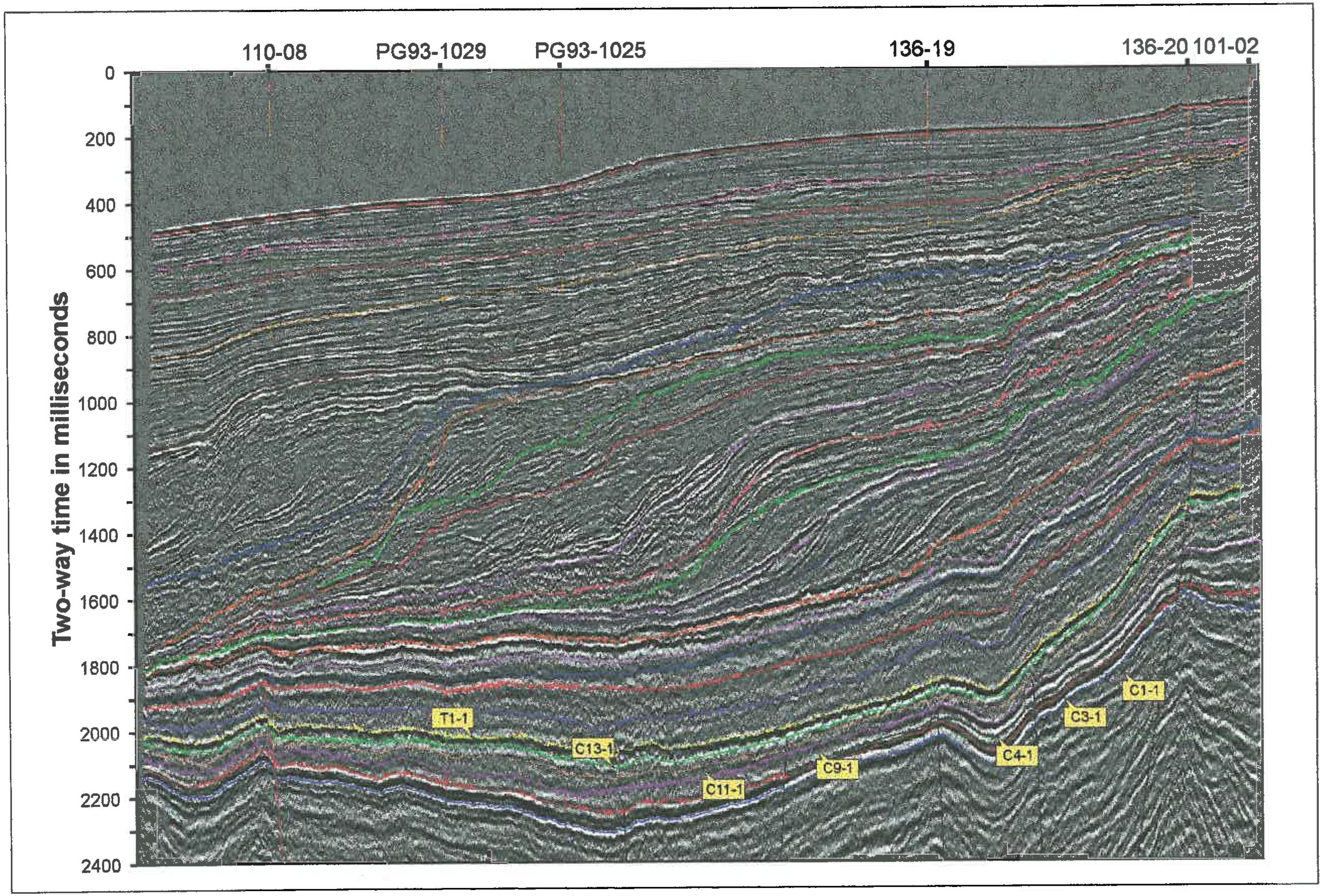

Figure 5.22 *Line 136-14 showing fault displacement associated with the Brigadier Trend and thickening of the Cretaceous sequences (C1-1 to T1-1) into the centre of the Rankin Platform. (Line length 88.5 km)*

5.7.3 Rosemary Fault System, Legendre Trend and Enderby Platform

The Rosemary Fault System, which marks the eastern edge of the Dampier Sub-basin (Figure 5.18), is a northeast-southwest-trending, northwest-dipping normal fault which shows an element of strike slip reactivation and can be dated to be as young as Recent in age (Figure 5.23). In the northern end of the Dampier Sub-basin, the trend of the fault changes to become approximately east-west in the Beagle Sub-basin. The Rosemary Fault System has a complex geological history involving a change from normal to strike slip movement through time. The seismic data used does not permit detailed analysis of this complex fault system. The Rosemary Fault System has been mapped as a single entity with many associated faults; the nature of this association is not clearly defined and consequently only major faults have been correlated on adjacent seismic lines.

The Enderby Platform to the south east of the Rosemary Fault System forms the footwall block to the fault. Little or no deformation of footwall sediments has been recorded in the Albian to Recent sediments of the study area. The Rosemary Fault is a major structural element, which separates the stable inner margin of the Carnarvon Basin from the subsiding outer margin during the Tertiary. Stratal geometries show the distribution of the Albian to Maastrichtian sediments to be controlled by the underlying structural grain as discussed in Section 5.6.1. In contrast, the Rosemary Fault System controls the distribution of Tertiary sediments within the basin with significant sedimentation occurring on the hanging wall and minor sedimentation on the footwall (Figure 5.2). These geometries suggest that the Rosemary Fault acted as a hinge line during the Tertiary, which separated the stable footwall block of the Enderby Platform, on which little accommodation space was developed, from the subsiding hanging wall block on which significant accommodation space was created (Figure 5.24).

The style of the deformation of the hanging wall sediments changes along the length of the Rosemary Fault System. It appears that this change is related to a change in the orientation of the fault from northeast-southwest to east-west trending. Where the Rosemary Fault trends northeast-southwest, as approximated by line 136-24 south of line 136-16, the hanging wall is a folded anticline with its axis offset approximately 10 km from the fault plane. This anticline is termed the Legendre Trend and it is seen to invert the reflectors in the order of 150-200 ms on line 136-13 (Figure 5.25). At the northern end of the Dampier Sub-basin in the area of lines 136-24 and 136-15 & 16, the height of the Legendre Trend anticline decreases significantly and it has considerably less lateral influence on the stratal geometries. The nature of the Rosemary Fault becomes extremely complex at this point and develops a flower structure typical of compressional strike slip regimes (McClay and Dooley, 1995) (Figure 5.26). The anticlinal Legendre Trend is not apparent in the Beagle Sub-basin and instead the displacement is taken up with an additional normal fault parallel to the Rosemary Fault System (lines 110-03 and 136-17). This change from a folded to faulted deformation style coincides with the change to an east-west-trending axis of the Rosemary Fault System in the Beagle Sub-basin, as can seen in the two-way time maps (Enclosure 1).

The major structural complexities of the east shoulder of the rift basin, the Enderby Platform, appear to be restricted to the section underlying the Albian C1-1 event (Figure 5.25). Two of the major normal faults of the Enderby Platform show displacement of the mid-Cretaceous and Tertiary reflectors. These faults have been interpreted to be reactivated pre-existing faults as the displacement in the Cretaceous and Tertiary reflectors are less than the displacement seen in the pre-Albian sediments. They have been mapped throughout the basin and can be identified on the two-way time maps in Enclosure 1.

Dip-slip movement of the Rosemary Fault appears to be of Eocene age or older. Dip lines across the fault show a constant throw in the order of 50-100 ms affecting each of the Albian (C1-1) to Eocene (T7-1) sequences (Figure 5.25). This would suggest that an Eocene event has displaced these sequences, as the displacement is constant throughout all C1-1 to T7-1 strata. Sediments younger than Eocene in age only show minor dip-slip displacement in the order of 10 ms, but they do show considerable flower structure development on line 136-24 (Figure 5.26). This suggests that the post-Eocene deformation is predominantly strike-slip in nature. The seismic coverage only allows identification of the presence and timing of this structure but it does not permit any detailed analysis on fault geometry. It has been concluded that the Rosemary Fault was predominantly a normal fault until the end of Eocene when the last normal fault movement was recorded, deformation since then has been strike slip in nature. It is not possible to define the timing of the initiation of strike-slip movement but dislocation of the N22-2 reflector demonstrates movement of the fault has continued until the Recent, (Figure 5.26).

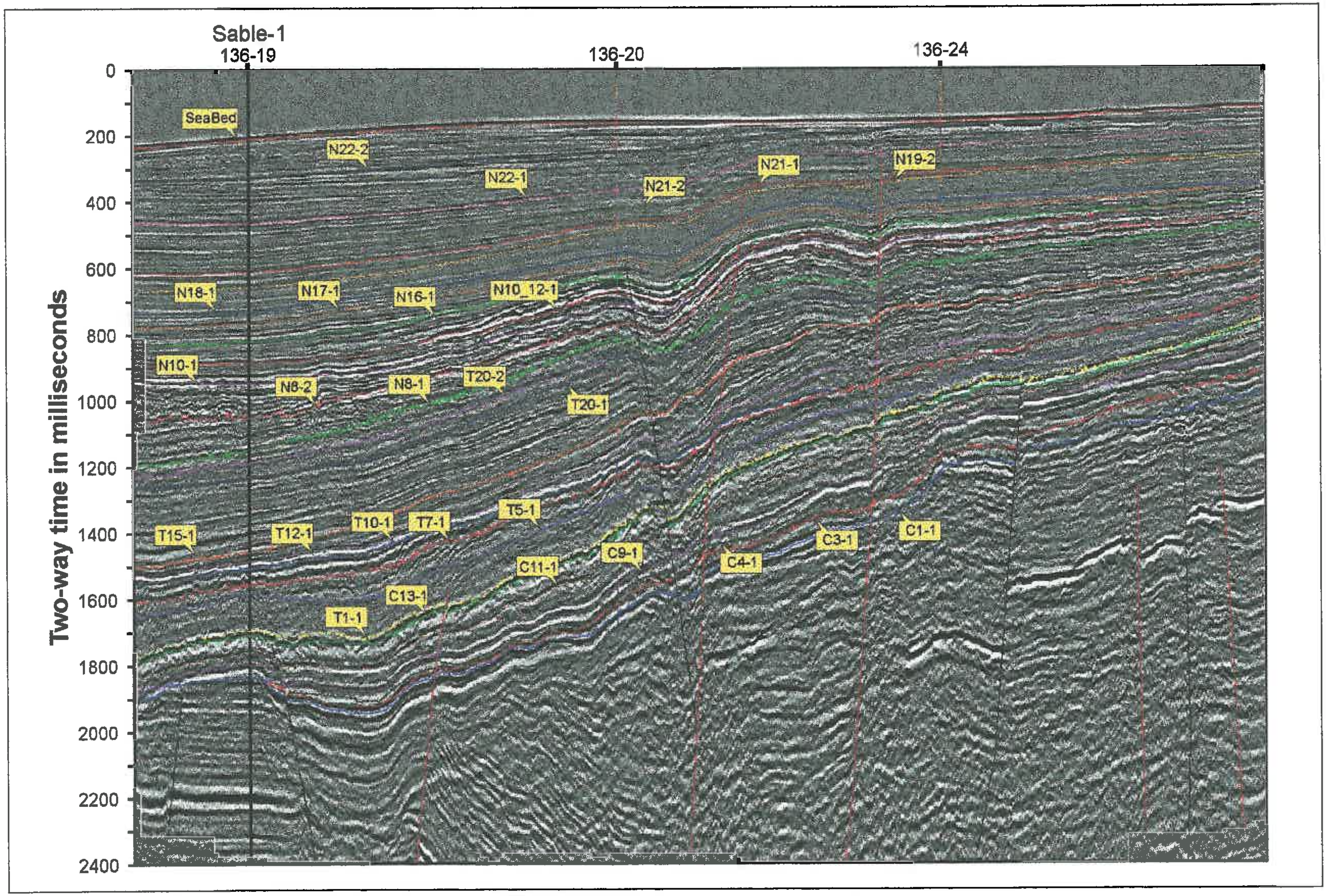

Figure 5.23 *Line 136-16 showing the normal faulted nature of the Rosemary Fault at the northern end of the Dampier Sub-basin. (Line length 43.5 km)*

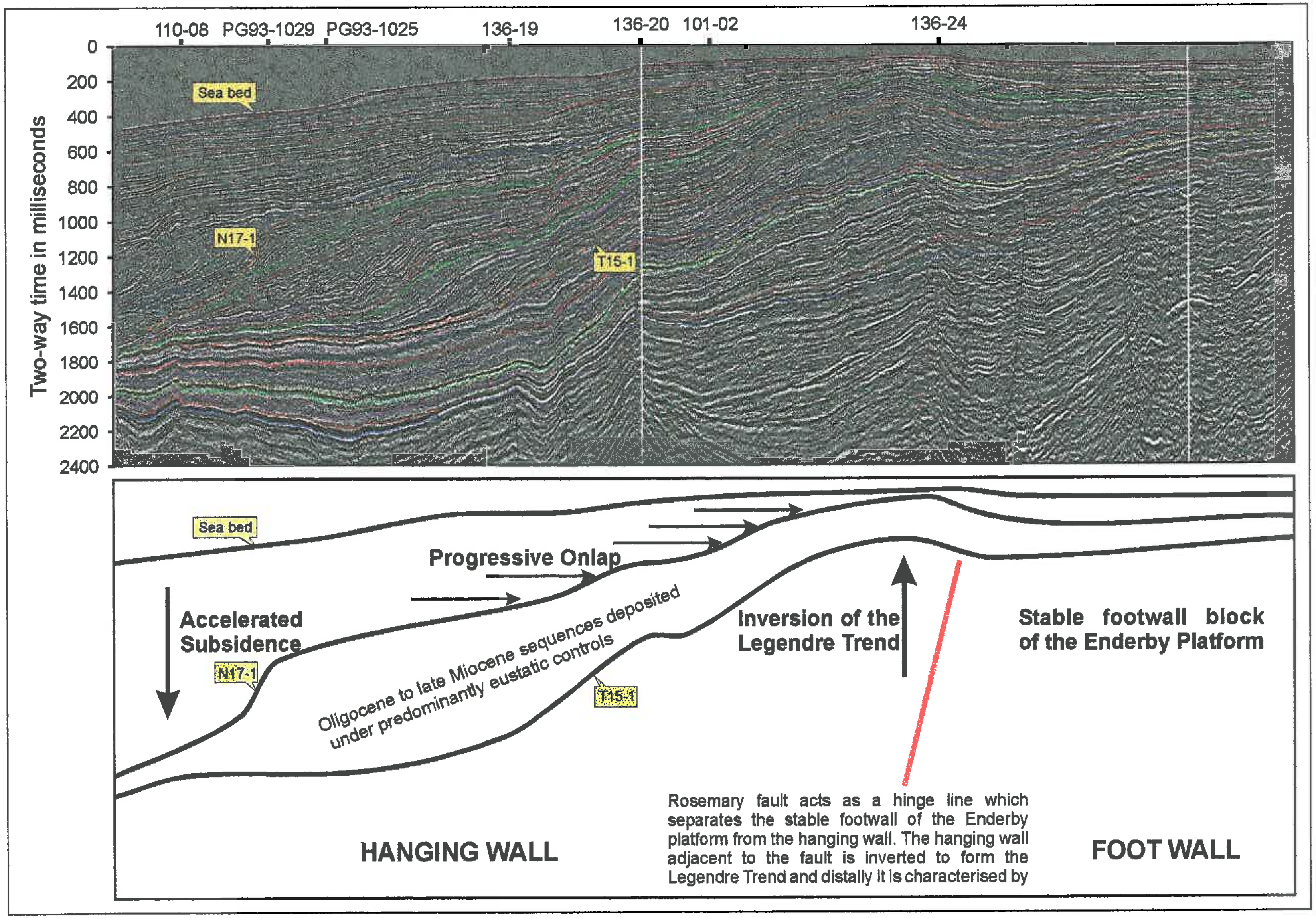

Figure 5.24 Line 136-14 demonstrating the nature of post N17-1 subsidence across the Rosemary Fault. (Line length 118.8 km)

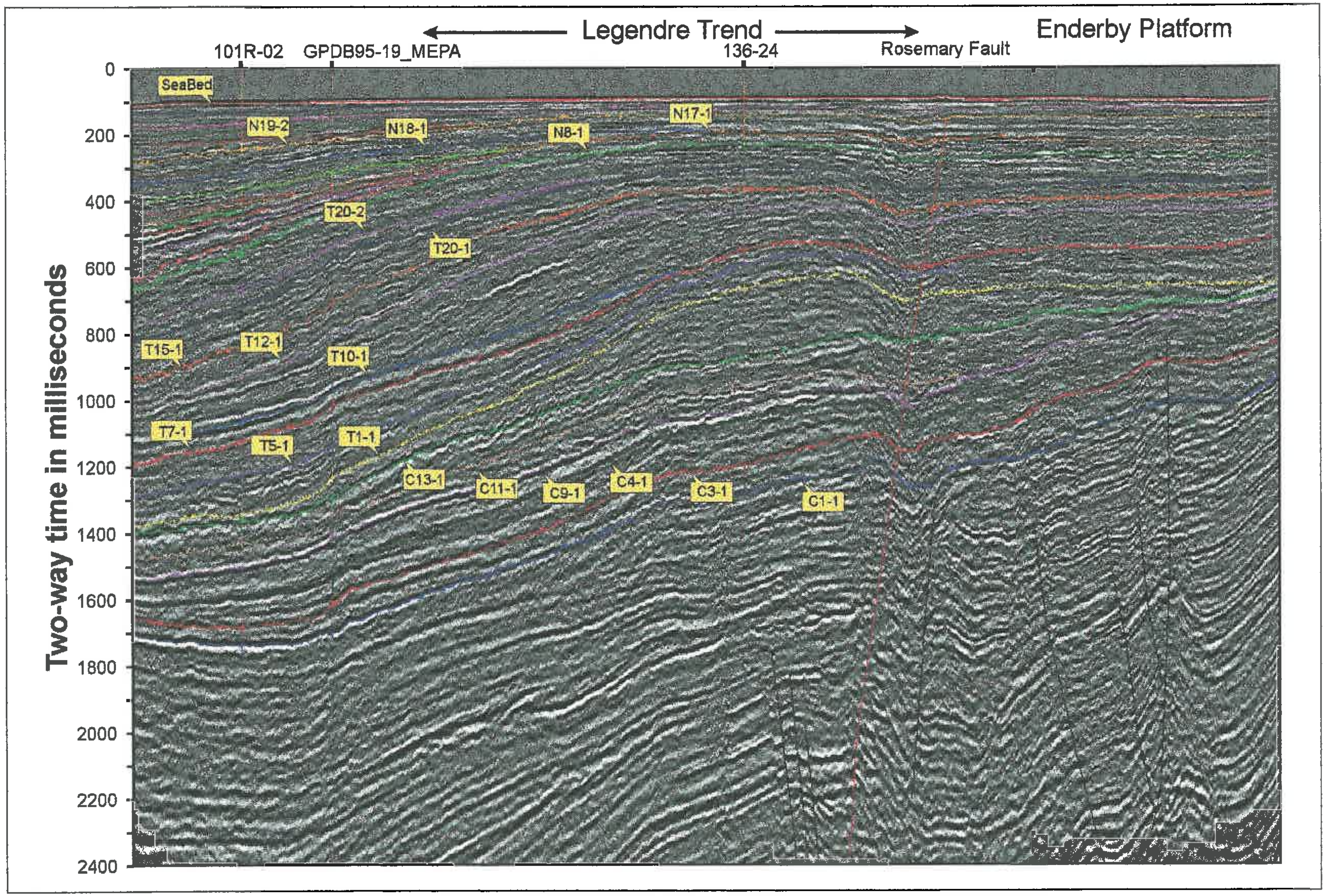

Figure 5.25 *Line 136-13 displaying the Legendre Trend (inversion of horizons C1-1 to N17-1 between the Rosemary Fault and line GPDB95-19_MEPA). Line length 43.5 km*

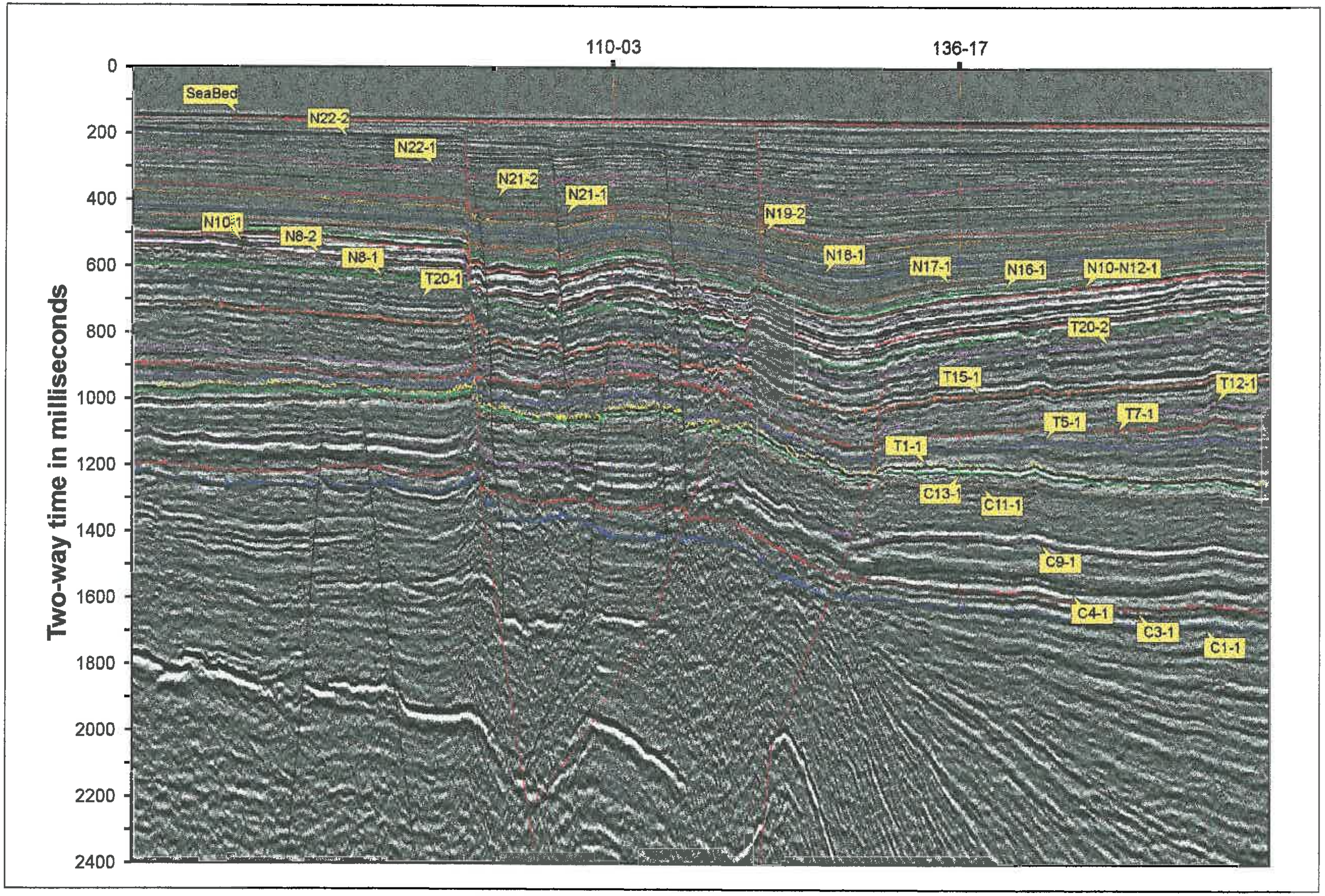

Figure 5.26 *Line 136-24 showing complex nature of the Rosemary Fault with movement of Recent age (N22-2) at the junction of the Beagle Sub-basin. (Line length 43.5 km)*

5.7.4 Tectonic relationship to faulting

The above discussion has shown the extent of faulting in the Albian to Recent section of the Dampier Sub-basin to be restricted to two zones related to the underlying basin-forming faults of the failed Jurassic rift and a third zone basinward of this rift termed the Brigadier Trend. Faults of the Rankin Trend are seen to dislocate the mid to late Cretaceous sediments and have been interpreted to die out at the Cretaceous-Tertiary boundary. The Rosemary Fault system has a complex history of normal and strike-slip movement, which has been active up to the Recent. From stratal relationships, it has been concluded that prior to the Eocene, movement on the Rosemary Fault was predominantly normal in nature and since the Eocene stratal geometries suggest that it has been predominantly strike-slip as was discussed in Section 5.7.3.

Collision of the northward-moving Australian plate occurred with the westward-moving Pacific Plate and the Eurasian Plate during the mid-Miocene. The interaction of these three plates resulted in an anti-clockwise rotational torque on the Australian continent causing dextral transcurrent movements along pre-existing fractures near the continent-ocean boundary (Veevers and Powell, 1984). The response of the North West Shelf to this Miocene collision has been shown to vary along the length of the shelf depending on the orientation of the reactivated basement structures relative to the dextral strike-slip moment (Keep *et al.*, 1998). In the Dampier Sub-basin it would seem that the northeast-southwest-trending Rosemary Fault System was preferentially orientated to be reactivated by the dextral strike-slip stresses rather than north-northeast-south southwest-trending faults of the Rankin Trend. It is also interpreted that the dextral strike-slip movement has given rise to the Legendre Trend in the Dampier Sub-basin and the flower structure identified at the boundary of the Dampier and Beagle Sub-basins (Figure 5.25 and Figure 5.26). The change in orientation of the Rosemary Fault from northeast-southwest-trending in the Dampier Sub-basin to east-west-trending in the Beagle Sub-basin (lines 110-03 and 136-17) corresponds to a transition from folded deformation of the Legendre Trend to faulted deformation in the Beagle Sub-basin. This change was interpreted to be related to the change in the angle of incidence between the dextral strike-slip stresses and the orientation of the Rosemary Fault. Figure 5.27 below summarises the orientation of basement structures and their response to the Miocene collision.

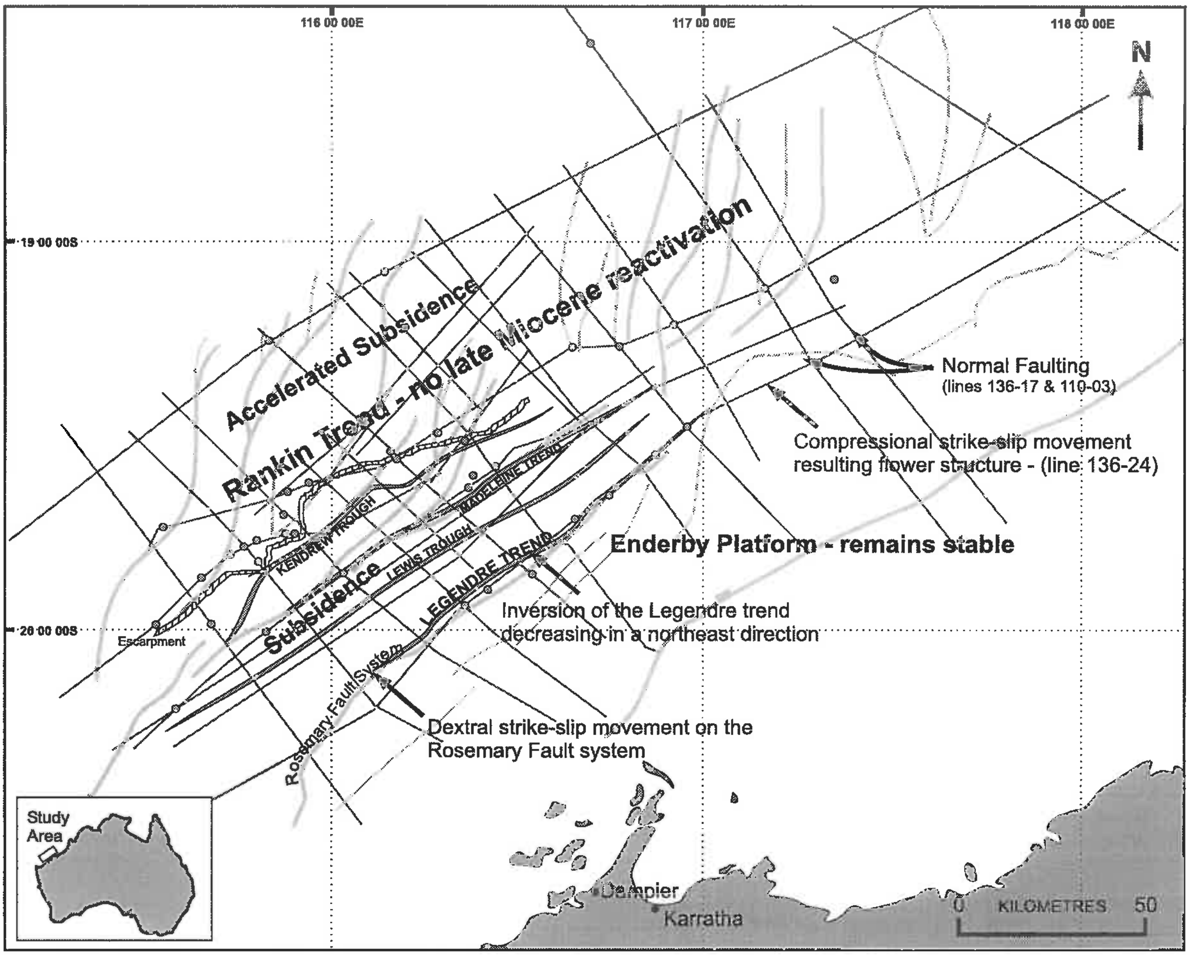

Figure 5.27 *Orientation of basement structures and their response to the dextral strike slip stresses caused by the late Miocene collision of the Australian, Eurasian and Pacific plates.*

5.8 Progradational seismic geometries

5.8.1 Introduction

The style and nature of progradational stratal geometries can be used to reveal important information on the controls of sediment deposition. The interaction between sediment supply rates and relative sea level controls the nature of the accommodation space created and consequently the stratal geometries developed in response to that accommodation space. Rates of progradation and aggradation will give quantitative information on the nature and rate of creation of the accommodation space. However, calculation of progradation rates using a single seismic dip line is meaningless, as these rates will be biased according to the sequence thickness on that particular line. This sediment thickness may or may not be the maximum sediment thickness in the basin. A sequence which thins in a strike direction will give varying rates of progradation depending on which dip line is used to calculate the progradation rate. Quantitative analysis of sedimentation rates has been conducted as part of the 3D-Chronostrat analysis and will be discussed in Chapter 6.

5.8.2 Oligocene to Recent section of the Dampier Sub-basin

The Oligocene to Recent (T15-1 – Seabed) section of the Dampier Sub-basin is characterised by a series of prograding clinoforms which have been described in Section 5.4. Within these clinoforms, differing styles of progradation can be seen to occur across the shelf at discrete time intervals. Sediments of Oligocene to early Miocene age (T15-1 to N8-1) show a series of strongly prograding clinoforms which have steeply dipping fore-sets and exhibit minor aggradational top-set development (Figure 5.2). Isochron maps for the T15-1–T20-1, T20-1–T20-2 and T20-2–N8-1 sequences (Enclosure 2) all show development of a linear sediment body which trends northeast-southwest, parallel to the depositional strike in the basin. These sediment bodies thin rapidly in the up and down dip directions to a thickness of not more than 80 ms. This sediment distribution pattern is indicative of clinoforms in which the slope front has been the principal site of sediment accumulation. During deposition of this type of clinoform, the sedimentation rate is greater than the rate of creation of accommodation space and so the shelf top becomes saturated with sediment and the remainder is transported off the shelf top and deposited on the slope front. During this scenario the margin will build vertically to sea level and then prograde basinwards. It can therefore be inferred that, during the Oligocene to early Miocene, the depth of water into which the margin was prograding was no greater than the decompacted height of the clinoforms.

In contrast to the progradational T15-1 to N8-1 clinoforms, the N8-1–N10-N12-1 clinoforms have a much greater aggradational component (Figure 5.2). Isochron maps for the N8-1–N8-2, N8-2–N10-1 and N10-1–N10-N12-1 sequences (Enclosure 2) also illustrate the preservation of significant thicknesses of top-set sediment (100-200 ms). During this period of the shelf growth, there is an apparent increase in the height and decrease in slope angle of the foresets (Figure 5.2). This change in stratal architecture implies there has been a rise in relative sea level as a result of the rate of accommodation space creation being greater than or equal to the rate of sediment supply. At this point it is not possible to delineate whether accelerated tectonic subsidence, a decrease in sediment supply or an eustatic rise in sea level has caused this rise in relative sea level. Independent of the cause the shelf responded to these conditions by aggrading vertically with some associated progradation.

Sequences N10-N12-1 to N17-1 show predominantly progradational geometries with a pronounced slope break, which have thin top-set accumulation and steeply dipping fore-sets (Figure 5.2). Isochron maps for these sequences (Enclosure 2) indicate 400 ms of sediment accumulation on the clinoform front, which thins rapidly to 50 ms on the top. These stratal geometries are also interpreted to represent a scenario where the sediment supply rate is greater than the rate of creation of accommodation space and the shelf has responded by prograding.

The N17-1 sequence boundary represents a significant change in depositional style in the Dampier Sub-basin. Below N17-1, the sequences are characterised by a prograding linear geometry which persists along the length of the shelf (Enclosure 2). Above the N17-1 sequence boundary, a thick (600 ms) localised accumulation of N17-2 and N17-3 age sediments occurs and the deposition of the remaining late Miocene to Recent sediments appears to have been controlled by this underlying topography (Enclosure 2). However, variations in progradational and aggradational geometries, relating to the interaction of the rates of sediment supply and accommodation space creation can still be seen in this section.

A return to predominantly aggradational seismic geometries is seen in sequences N17-2–N17-3, N17-3–N18-1, N18-1–N19-1 and N19-1–N19-2 (Figure 5.2). Sequences from N19-2 to Recent show mixed aggradational and progradational stratal geometries which have gently dipping foresets and no pronounced slope break, as with the present day sea floor profile (Figure 5.2).

It appears that through the Oligocene to Recent section of the Dampier Sub-basin, the slope angle of the clinoforms is related to the style of stratal stacking patterns of the individual sequences. This is in turn related to relative sea level and the rate of creation of accommodation space. When the sediment supply rate was greater than the rate at which accommodation space was being created, strongly progradational sequences with steeply-dipping foresets were developed. In contrast, when the rate of accommodation space creation was greater than the rate of sediment supply, aggradational sequences with gently dipping foresets were developed. The relationship of slope angle to stratal architecture and grain size criteria will be discussed further in Chapter 6 as part of the 3D-Chronostrat analysis.

Wheeler diagram analysis of progradation

Wheeler diagrams are commonly used to display the relative distribution of sediment packages in geological time and thus are extremely important when analysing the stacking patterns of a progradational sequence. Wheeler diagrams are produced as part of the 3D-Chronstrat analysis that has been conducted on this dataset, the results of which are presented in Chapter 6. A Wheeler diagram included at this point is used to illustrate the periods of predominantly progradational and aggradational growth of the Oligocene to Recent section of the Dampier Sub-basin (Figure 5.28). The chronosomes displayed between T15-1 and N8-1 on the Wheeler diagram are seen to prograde strongly towards the basin. The chronosomes between sequence boundaries N8-1 and N10-N12-1 are seen to be predominantly aggradational and those chronosomes between N10-N12-1 and N17-2 are seen to be strongly progradational once again. Above N17-2 the N17-3 to N19-2 sequences are seen to aggrade though it is not as clearly displayed as the underlying sequence as the line does not cover the whole cross section of the clinoform.

From an examination of the relative duration of the prograding and aggrading units, it is apparent that the prograding units are of longer duration than the aggrading units. From an examination of the seismic section of the Oligocene to Recent section the aggrading packages are seen to be thicker than prograding units. Thus the aggrading units appear to be volumetrically more significant yet occupy a smaller time scale.

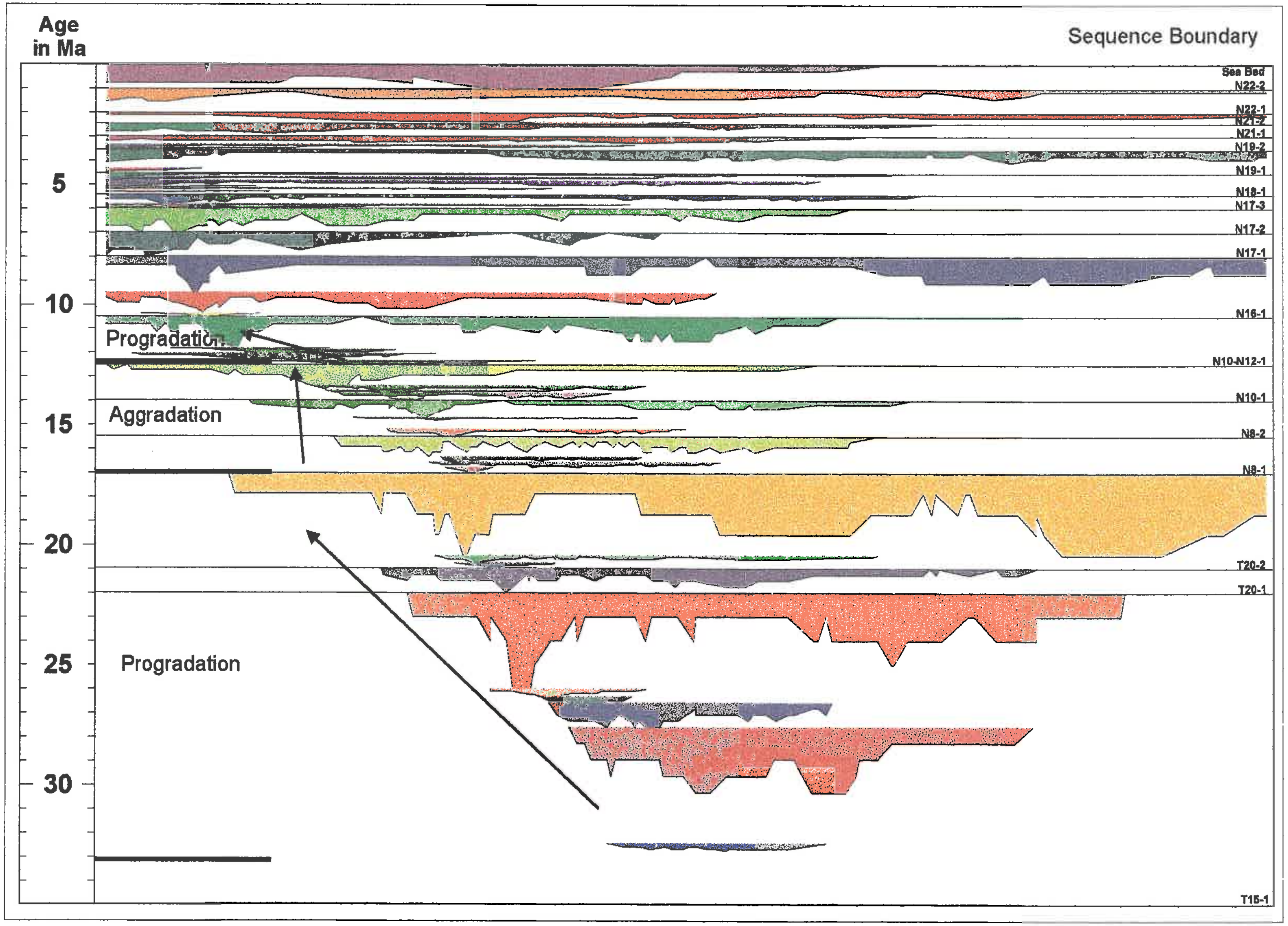

Figure 5.28 *Wheeler diagram for line 136-12 showing the progradational and aggradational nature of the Oligocene (T15-1) to late Miocene section (N17-1).*

CHAPTER 6 RESULTS – 3D CHRONOSTRAT

6.1 Introduction

3D-Chronostrat has been used to investigate the nature of the internal stacking architecture for each of the defined sequences and also to provide quantitative information on the rates of sedimentation and morphology of the shelf. By mapping every correlatable reflector between each of the thirty sequence boundaries defined in the seismic interpretation phase of the project, it was possible to construct a three-dimensional chronostratigraphy for the Albian to Recent section of the Dampier Sub-basin. This three-dimensional chronostratigraphy subdivides the basin fill history into a series of genetically-related three-dimensional units which describe the evolving nature of the basin.

6.1.1 Interpretation Procedure

The majority of seismic lines utilised during the seismic interpretation phase of the project were loaded into the 3D-Chronostrat database. Several lines at the centre of the study area were omitted due to a physical limit in the number of lines within a 3D-Chronostrat database. 3D-Chronostrat also cannot deal with lines that change orientation along their length and in such cases the line must be subdivided into straight sections which are then treated as separate lines. Figure 6.1 shows a map of the seismic database and illustrates which lines have also been used in the 3D-Chronostrat database.

The sequence stratigraphic events defined and mapped during the biostratigraphic, wireline and seismic interpretation were identified on the 3D-Chronostrat database. Their spatial distribution was once again mapped throughout the 3D-Chronostrat database as unfortunately there is no facility to import picks generated from another interpretation package into the 3D-Chronostrat database. These 30 sequence stratigraphic events provided the framework within which the remainder of the 3D-Chronostrat interpretation was constrained. All reflectors between these thirty sequence boundaries, which could be loop-tied on four lines, were subsequently mapped throughout the database. These events defined the high-resolution architecture of the basin fill that was used to construct the three-dimensional chronostratigraphy and analyse variations in sedimentation patterns through time.

6.2 Chronosome distribution patterns

The thirty sequence boundaries that were mapped during the seismic interpretation phase of the project were identified and digitized in 3D-Chronostrat. Further mapping of all correlatable reflectors in DIGITIZE has subdivided the 29 sequences into 98 constituent chronosomes. Table 6.1 lists the sequences defined and mapped during the biostratigraphic, wireline and seismic phases of the project, their age defined from biostratigraphic data and the corresponding chronosomes as defined during the 3D-Chronostrat analysis.

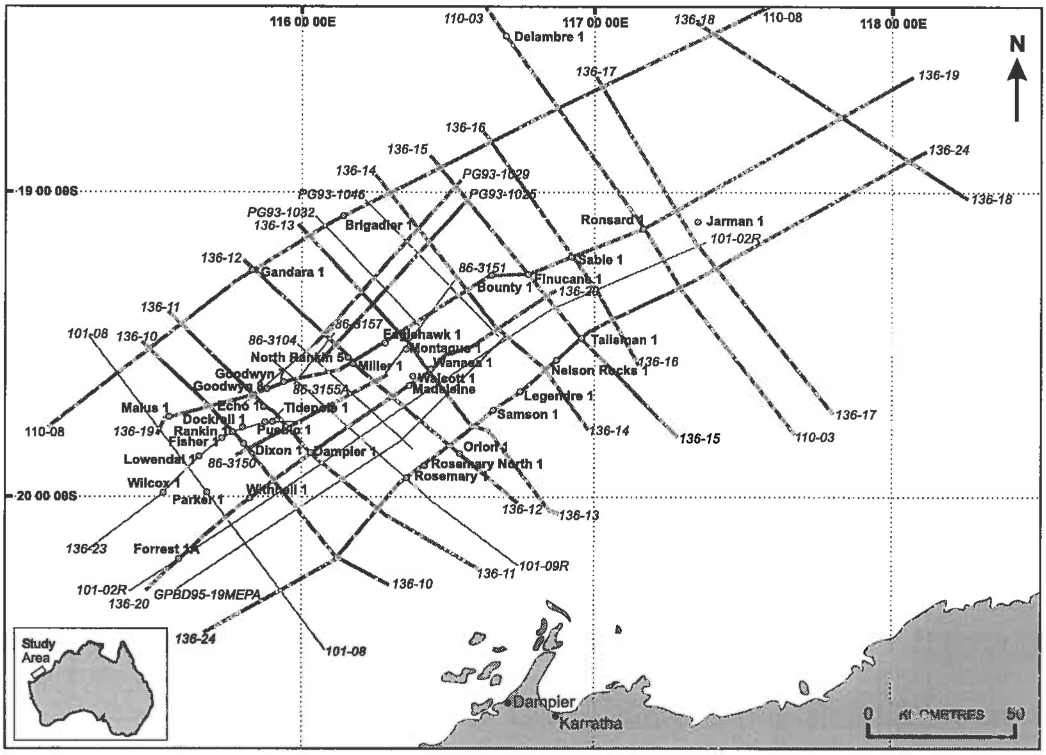

Figure 6.1 3D-Chronostrat data set (thick lines) in comparison to the seismic interpretation data set.

Sequence Name	Age (Ma)	Chronosome Numbers
N22-2 - Sea bed	1 - 0	98
N22-1 - N22-2	2 - 1	94 - 97
N21-2 - N22-1	2.5 - 2	92 - 93
N21-1 - N21-2	3 - 2.5	90 - 91
N19-2 - N21-1	3.5 - 3	83 - 89
N19-1 - N19-2	4.5 - 3.5	79 - 82
N18-1 - N19-1	5.5 - 4.5	69 - 78
N17-3 - N18-1	6 - 5.5	66 - 68
N17-2 - N17-3	7 - 6	65
N17-1 - N17-2	8 - 7	64
N16-1 - N17-1	10.5 - 8	61 - 63
N10_12-1 - N16-1	12.5 - 10.5	53 - 60
N10-1 - N10_12-1	14 - 12.5	48 - 52
N8-2 - N10-1	15.5 - 14	44 - 47
N8-1 - N8-2	17 - 15.5	40 - 43
T20-2 - N8-1	21 - 17	37 - 39
T20-1 - T20-2	22 - 21	36
T15-1 - T20-1	35 - 22	25 - 35
T12-1 - T15-1	42 - 35	23 - 24
T10-1 - T12-1	50 - 42	21 - 22
T7-1 - T10-1	56 - 50	19 - 20
T5-1 - T7-1	57.5 - 56	17 - 18
T1-1 - T5-1	65 - 57.5	15 - 16
C13-1 - T1-1	66 - 65	14
C11-1 - C13-1	70 - 66	12 - 13
C9-1 - C11-1	83 - 70	7 - 11
C4-1 - C9-1	92.5 - 83	5 - 6
C3-1 - C4-1	96 - 92	4
C1-1 - C3-1	112 - 96	1 - 3

Table 6.1 List of sequences and corresponding chronosome numbers

The 3D-Chronostrat sections created for each seismic line that has been included in the 3D-Chronostrat analysis are presented in Enclosure 3. These sections display the 98 chronosomes that have been defined from the interpretation of 99 correlatable reflectors throughout the seismic database. The chronosomes are numbered sequentially from the base up. The two-way time thickness of each of these chronosomes has been gridded to produce a series of isochron maps as presented in Figure 6.2 to Figure 6.6. The colour shading of these maps is scaled between the maximum (in red) and minimum (in blue) thicknesses on each individual map according to the colour bar displayed at the bottom left hand corner of each figure. The corresponding values for the maximum and minimum thicknesses are displayed at the top right hand corner of each individual isochron map on the figure. Also displayed at bottom left and bottom right hand corners on each individual chronosome map is the calculated chronosome area and volume.

The ages of the individual chronosomes have been calculated using the biostratigraphic age of the sequence boundaries and by making assumptions regarding chronosome shape, duration and sedimentation rates. The procedure for calculating chronosome ages is outlined later in Section 6.3.3.1. Wheeler diagrams for key dip and strike lines output from 3D-Chronostrat have been re-scaled from relative time to absolute time using these calculated ages. The Wheeler diagrams and associated 3D-Chronostrat sections for lines 136-12, 110-03, 136-19 and 110-08 are presented as Figure 6.7, Figure 6.8, Figure 6.9 and Figure 6.10 respectively.

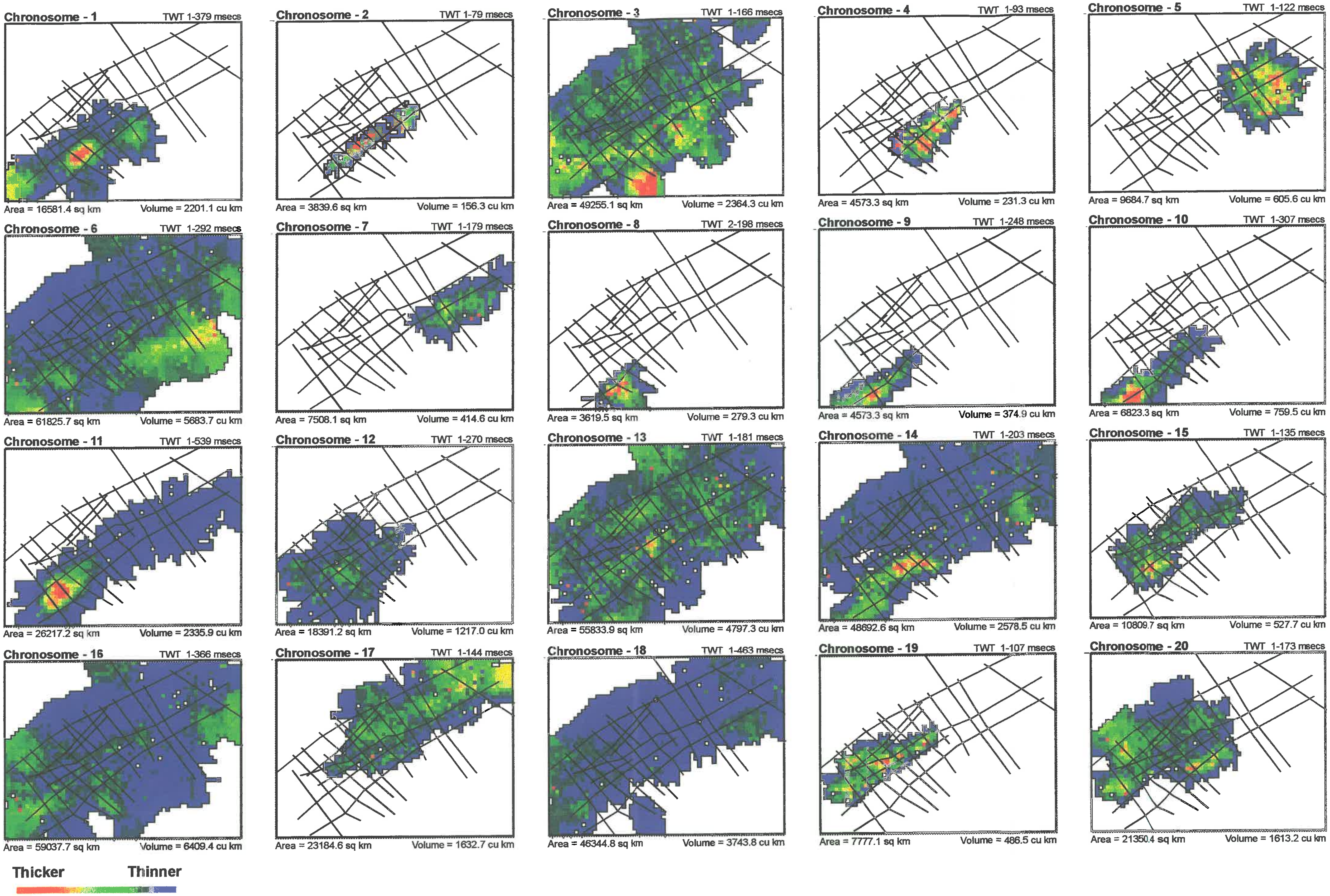

Figure 6.2 Two-way time thickness maps for chronosomes 1-20

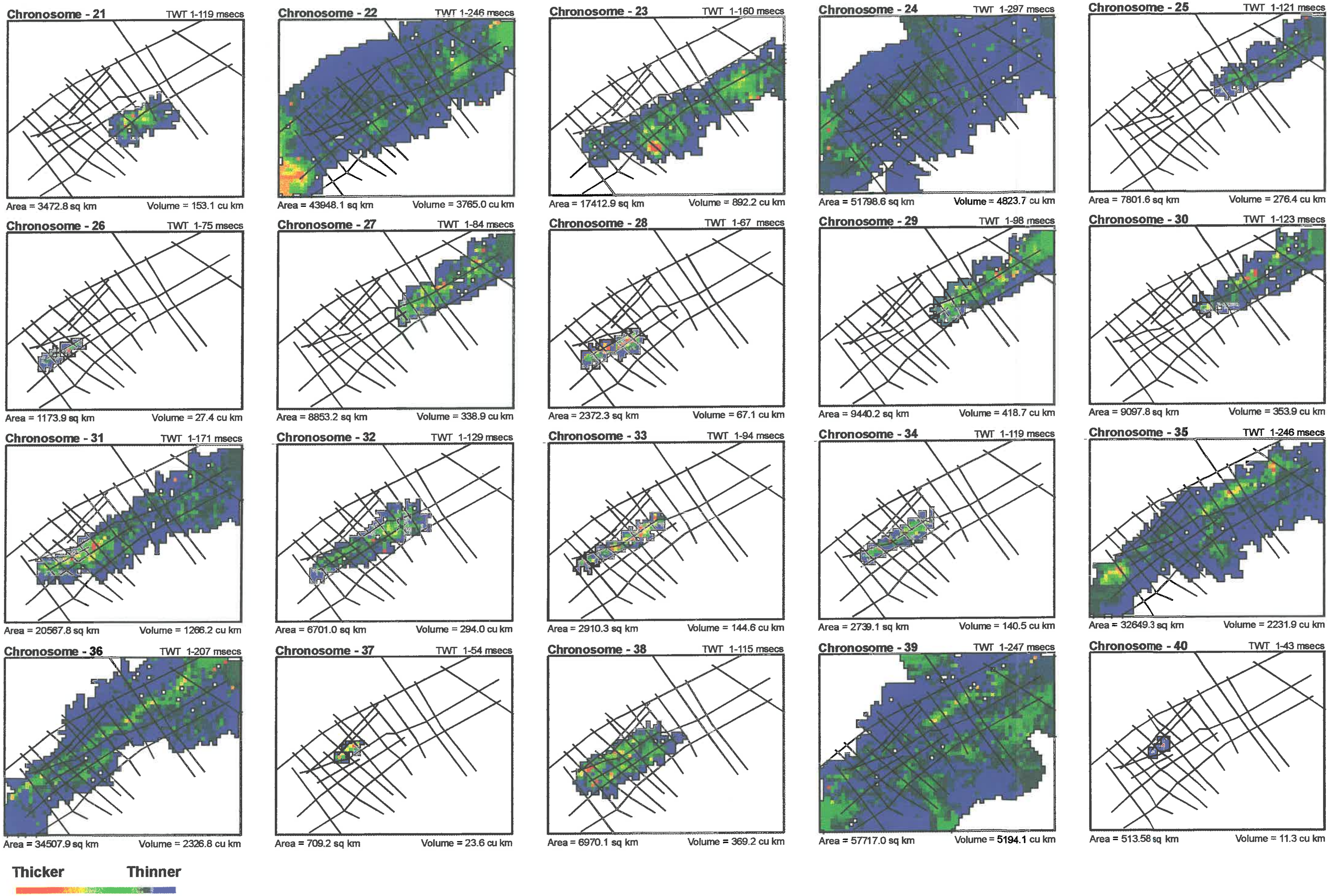

Figure 6.3 Two-way time thickness maps for chronosomes 21-40

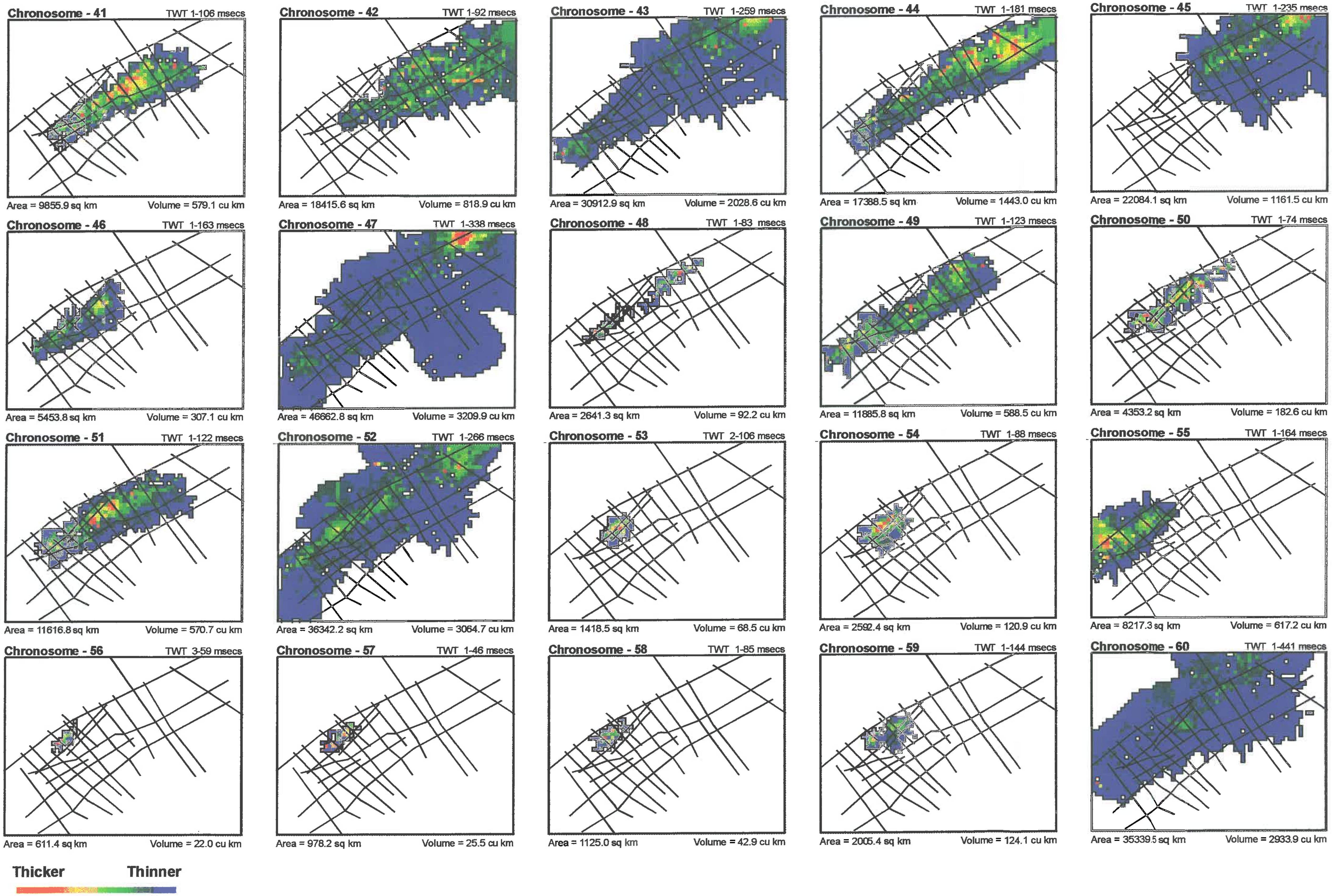

Figure 6.4 Two-way time thickness maps for chronosomes 41-60

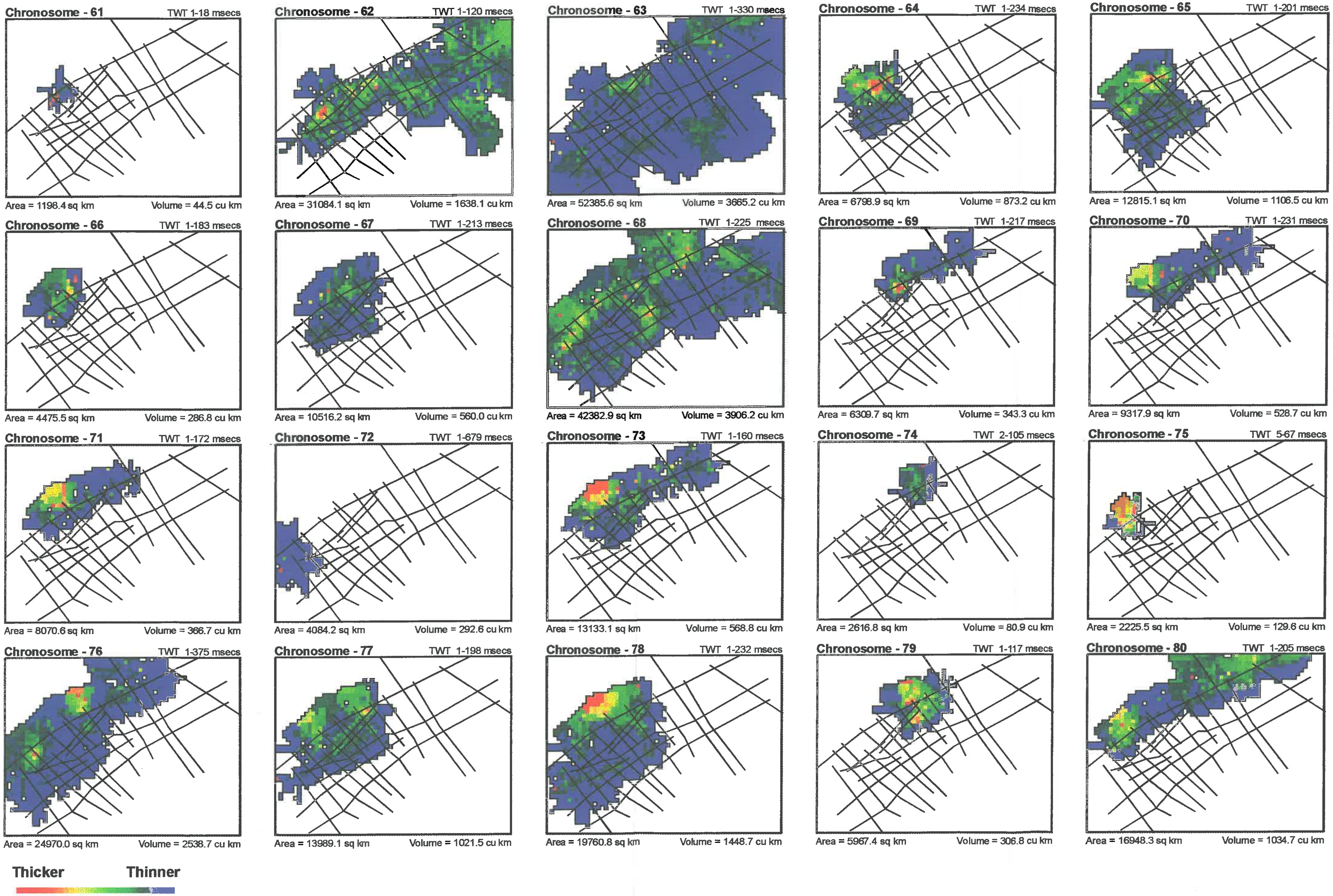

Figure 6.5 Two-way thickness maps for chronosmes 61-80

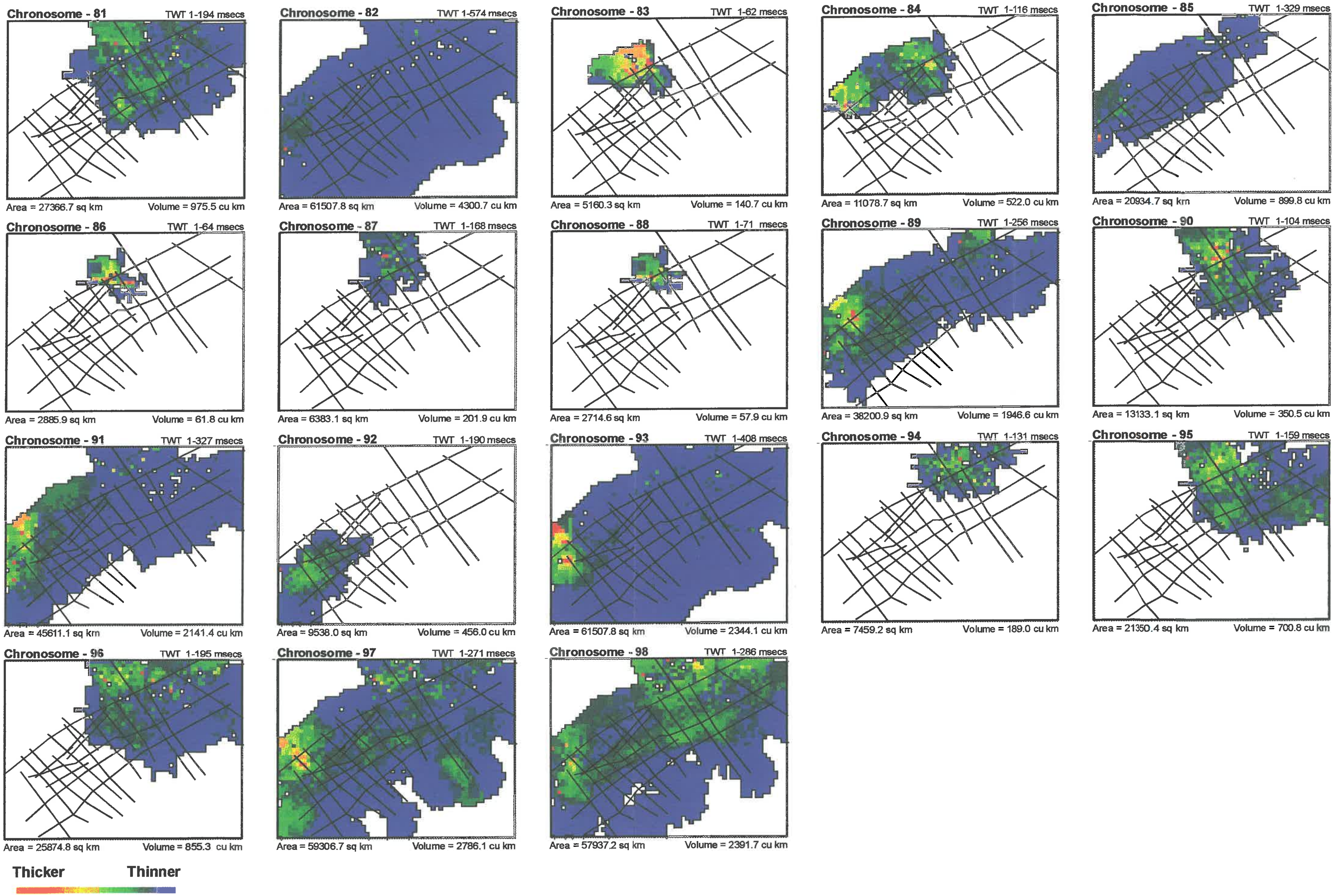

Figure 6.6 Two-way time thickness maps for chronosomes 81-98

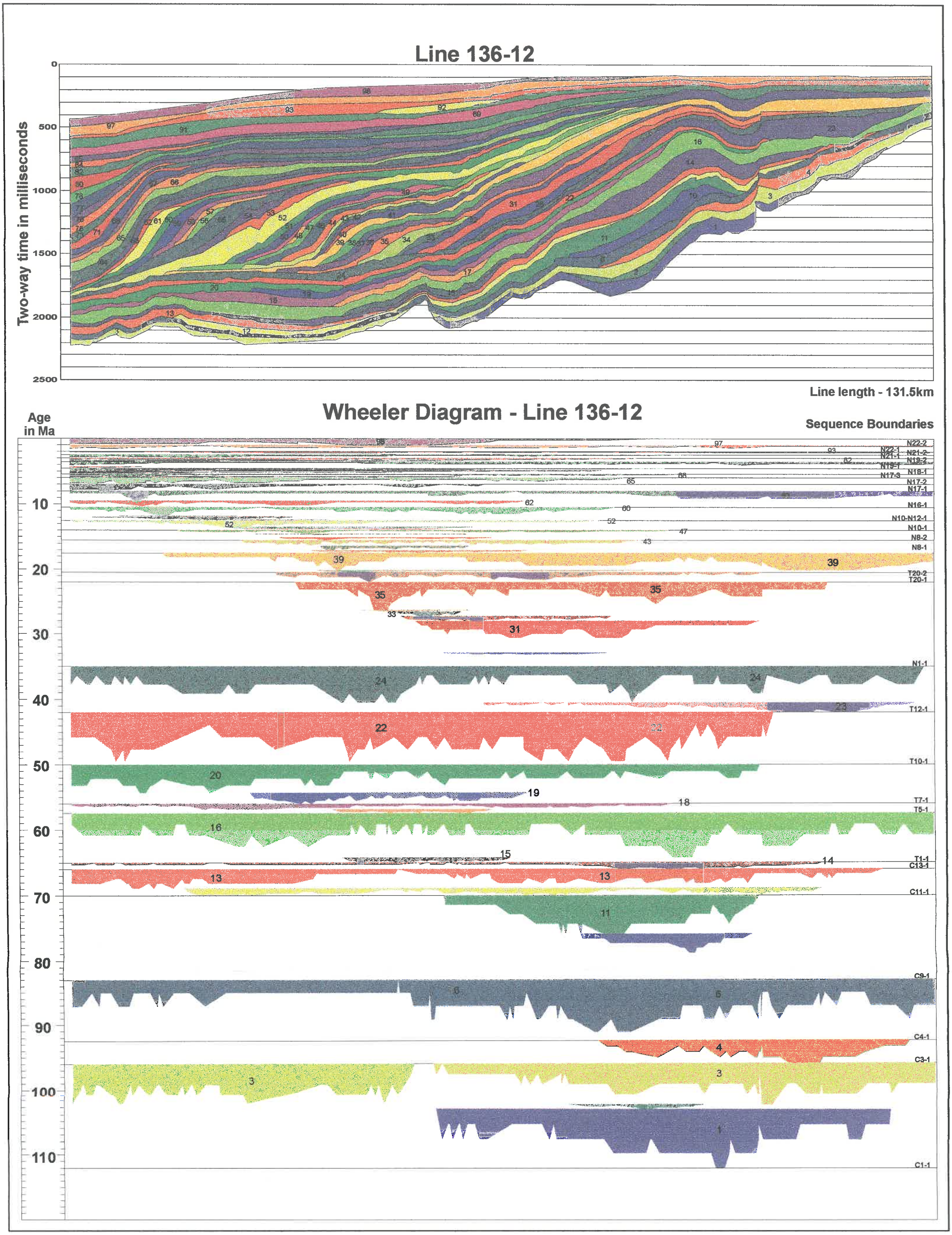

Figure 6.7 3D-Chronostrat section and Wheeler diagram for line 136-12

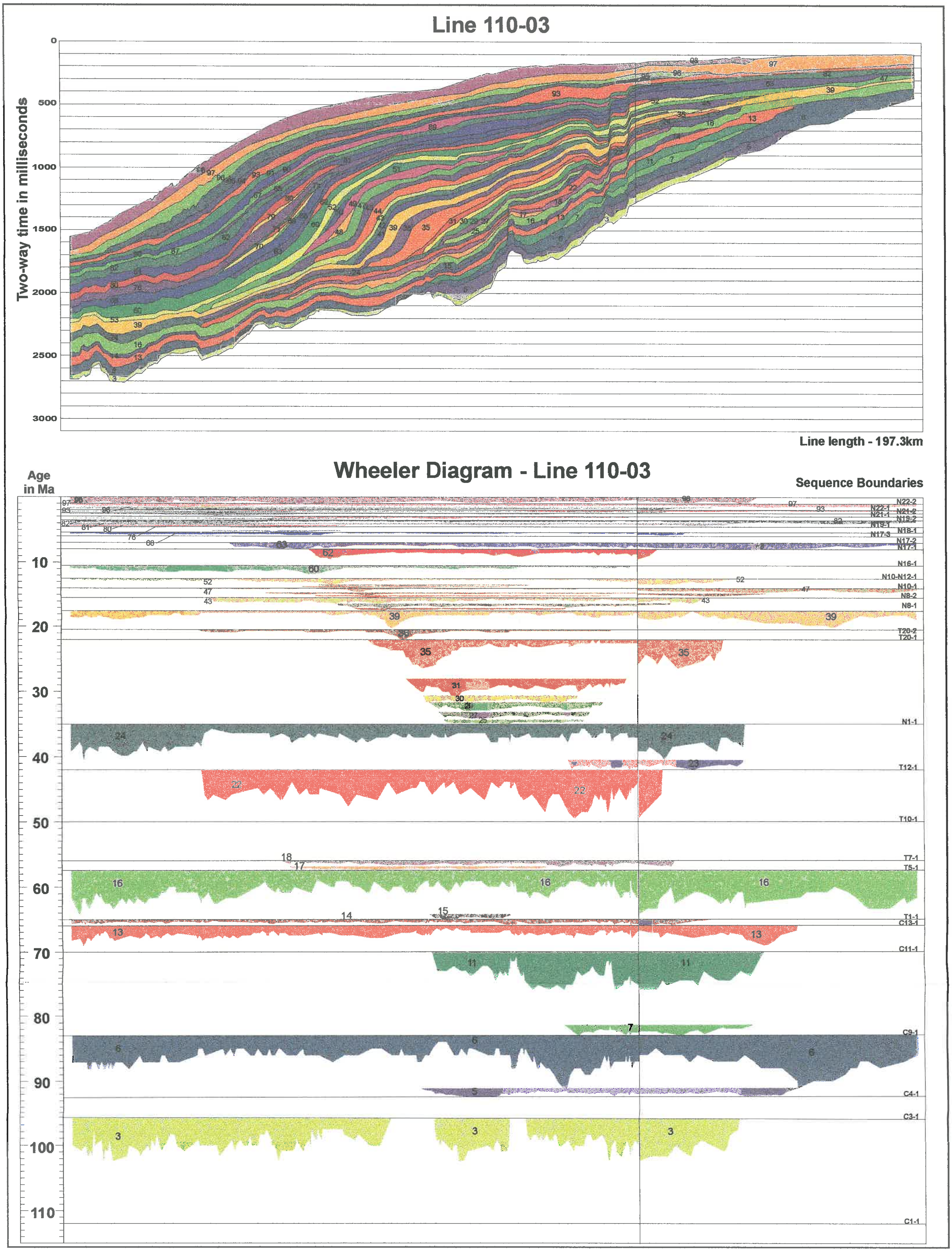

Figure 6.8 3D-Chronostrat section and Wheeler diagram for line 110-03

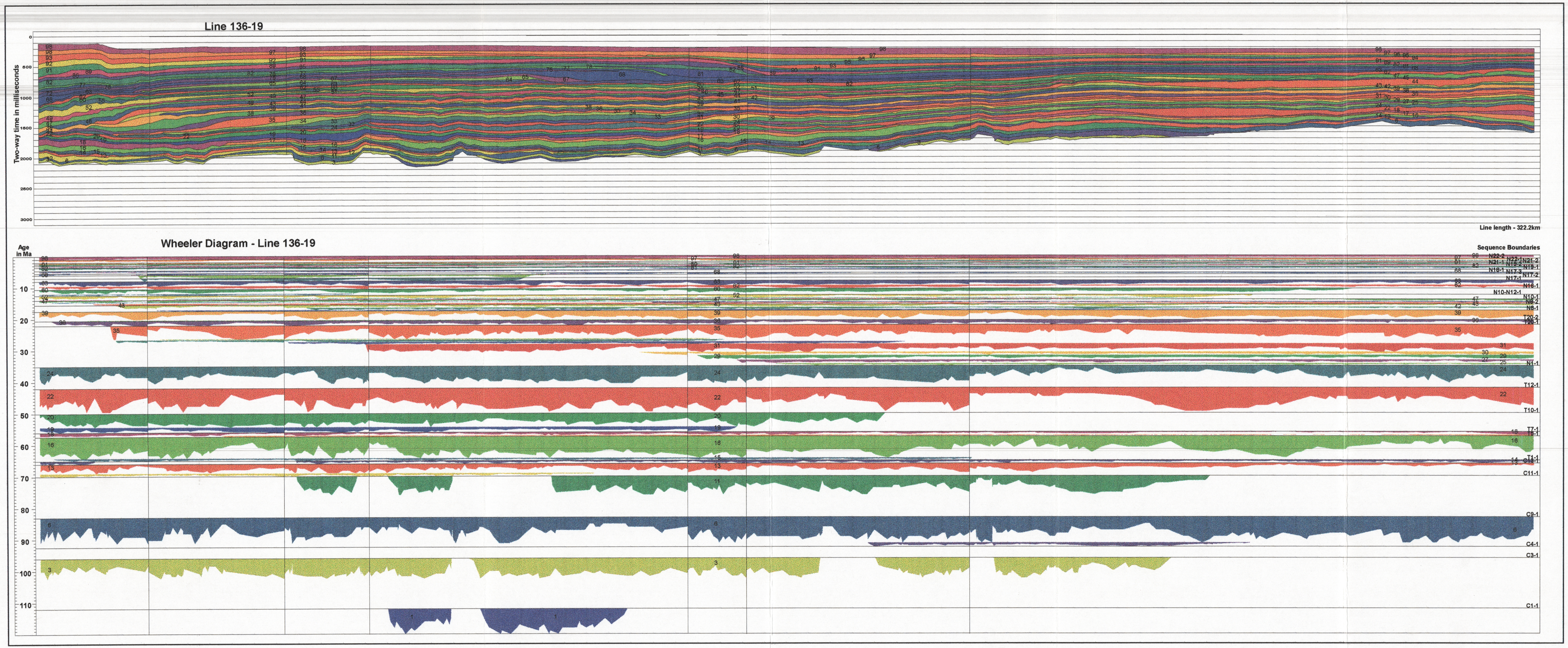

Figure 6.9 3D-Chronostrat section and Wheeler diagram for line 136-19.

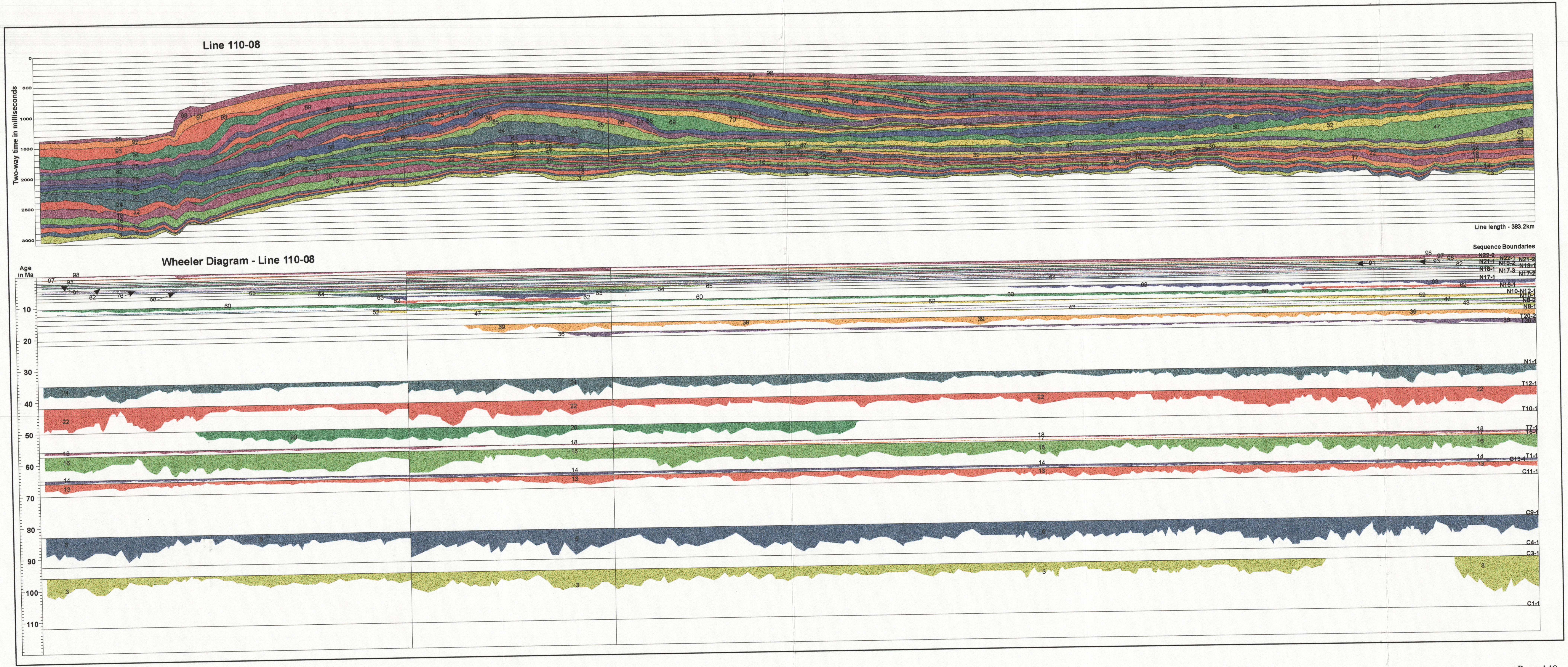

Figure 6.10 *3D-Chronostrat section and Wheeler diagram for line 110-08*

6.2.1 Sedimentation patterns - general

The sequence stratigraphic events defined from the seismic and wireline analysis have provided the framework within which the internal stacking architecture of the Albian to Recent sediments of the Dampier Sub-basin have been further analysed. As a result of this framework, the 3D-Chronostrat analysis shows the same general variations in sediment thickness as those defined from seismic sections and isochron maps produced during the seismic interpretation. In addition, the 3D-Chronostrat analysis has provided a high-resolution quantitative understanding of the evolutionary nature of the Albian to Recent section of the Dampier Sub-basin. This quantitative information has enabled the controls on the nature and distribution of sediment to be investigated.

The 3D-Chronostrat sections (Enclosure 3) and Wheeler diagrams (Figure 6.7 to Figure 6.10) demonstrate that the major units defined during seismic interpretation (C1-1–T1-1, T1-1–T15-1 and T15-1–Seabed) can easily be identified on the 3D-Chronostrat database. In the 3D-Chronostrat study, these major units correspond to chronosomes 1-14, 15-24 and 25-98 respectively. It is immediately evident from both the dip and strike 3D-Chronostrat sections (Enclosure 3) that, within the thick prograding T15-1–Seabed section, significantly more chronosomes (seventy four) have been defined than in the underlying thin laterally extensive C1-1–T15-1 section (twenty four). The Wheeler diagrams, which have been scaled to absolute age (Figure 6.7 to Figure 6.10), demonstrate that the prograding T15-1–Seabed section is in fact of much shorter duration, (35 Ma), than the underlying C1-1–T15-1 section (77 Ma). Thus the deposition of each of the Albian to mid-Oligocene chronosomes (1-24) had a significantly longer geological duration, in the scale millions of years, than the mid-Oligocene to Recent chronosomes (25-98) which were 100 000s of years in duration.

6.2.2 Cretaceous sediments (chronosomes numbers 1-14)

Chronosomes 1-14 correspond to the Cretaceous section of the study bound by the Albian C1-1 and base Tertiary T1-1 events. The relatively thin nature of Albian to base Tertiary sediments in the study area has precluded many chronosomes from being defined within the section. The isochron maps for the Albian to Maastrichtian chronosomes (Figure 6.2) display similar sediment distribution patterns to the isochron maps generated from the seismic data (Enclosure 2). Both sets of maps show the thickest sediment to be restricted to a linear northeast-southwest-trending area in the southwest corner of the study. The dip sections of lines 101-08, 136-10, 136-11, 136-12 and 136-13 all clearly show thickening of the individual Albian to base Tertiary chronosomes at the proximal ends of the lines. The Wheeler diagrams for line 136-12 (Figure 6.7) and to a lesser extent 110-03 (Figure 6.8) show that the thickest Cretaceous sedimentation is landward of the underlying Rankin Trend with only thin sedimentation (100-200 ms) beyond it. As was noted in the seismic interpretation, sediment thickening of chronosomes 1-10 is restricted to the location of the Lewis Trough (Figure 6.2 & Figure 6.7). Chronosomes 11-14 are also seen to thicken basinward of the Lewis Trough.

The isochron map for the C9-1–C11-1 sequence (Enclosure 2) demonstrates two areas of sediment thickening. In the southwest corner of the study area, sediment thicknesses of up to 700 ms are evident on the isochron map. The other area of significant sediment accumulation is in the northeast of the study area where 200 ms of sediment are recorded. The chronosome maps for this interval show that the sediment accumulation in the northeast of the study area (chronosome 7) predate the thick accumulation in the southeast. Chronosomes 8-11 prograded in a northeasterly direction from the south east of the basin (Figure 6.2).

6.2.3 Paleocene and Eocene sediments (chronosomes numbers 15-24)

Due to the thin nature of the Paleocene and Eocene sediments in the basin as discussed in Section 5.6.2, it has only been possible to subdivide each of the defined Tertiary sequences into two constituent chronosomes. The Tertiary T1-1–T5-1 sequence has been subdivided into chronosomes 15 and 16, T5-1–T7-1 into 17 & 18, T7-1–T10-1 into 19 & 20, T10-1–T12-1 into 21 & 22 and T12-1–T15-1 into chronosomes 23 & 24 as shown in Figure 6.2 and Figure 6.3. As a result of this inability to identify more than two chronosomes within each sequence, it has only been possible to delimit the location of the primary phase of sedimentation within the sequence rather than analyse the sequence evolution.

In contrast to the underlying Albian to base Tertiary chronosomes (1-14), which show pronounced thickness variations across the basin, the base Tertiary to mid-Oligocene chronosomes (15-24) are seen to be of relatively constant thickness throughout the basin. The contrast in thickness variation between chronosomes 1-14 and 15-24 is clearly evident on the Wheeler diagram for line 136-12 (Figure 6.7) which is one single Chronostrat file as line 136-12 is a straight line. These variations are also evident on all dip 3D-Chronostrat sections presented in Enclosure 3. A pronounced thickening of the base Tertiary to mid-Oligocene chronosomes in a southwesterly direction is visible on line 110-08 (Figure 6.10) and on the associated chronosome thickness maps (Figure 6.2 & Figure 6.3).

6.2.4 Oligocene – Recent sediments

Within the thick prograding Oligocene to Recent section of the Dampier Sub-basin, 74 chronosomes have been identified and mapped throughout the study area. Isochron maps showing sediment distribution and thickness for these chronosomes are presented in Figure 6.3 to Figure 6.6. The strongly progradational nature of chronosomes 25 to 98 can be clearly seen on the dip sections of Enclosure 3 (lines 101-08 & 09, 136-10–18, and 110-03).

On the strike sections of Enclosure 3 (lines 136-19, 20, & 24, 110-08, 86-3150 & 3157), it can be seen that the Oligocene to Recent section has been subdivided into two distinct packages on the basis of stratal architecture; chronosomes 25-63 and 64-98. On strike lines, chronosomes 25-63 are represented by flat-lying reflectors which show minor lateral variations in thickness, whilst chronosomes 64-98 show significant along-strike thickness variation especially on line 110-08 (Figure 6.10). A distinct change in the nature and distribution of chronosome thicknesses is also evident across this boundary on the chronosome thickness maps (Figure 6.4 & Figure 6.5). This change in stratal architecture corresponds to the N17-1 sequence boundary, which was also identified as a significant event in the seismic interpretation in Chapter 5. Lines PG93-1025 & 1029 are oblique to strike and the flat-lying reflectors of chronosomes 25-63 are expressed as dipping reflectors.

6.2.4.1 Oligocene – late Miocene (chronosomes numbers 25 – 63)

The strongly progradational nature of the mid-Oligocene to late Miocene sediments (chronosomes 25-63) of the Dampier Sub-basin is clearly evident on all dip lines in Enclosure 3. Chronosomes 25–63 correspond to the period of shelfal growth defined by sequence boundaries T15-1 to N17-1. These progradational sediments are also clearly evident on Wheeler diagrams for lines 136-12 (Figure 6.7) and 110-03 (Figure 6.8) which show the location of the thickest point of the chronosome moving progressively basinward through the section.

Within the mid-Oligocene to late Miocene sediments (chronosomes 25-63), a distinctive evolutionary pattern of chronosomes within a single sequence can be observed. The first chronosome above a sequence boundary tends to be spatially restricted and located slightly basinward of the thickest section of the underlying chronosome. The areal extent of the subsequent chronosomes within a sequence increases progressively until it reaches a maximum in the final chronosome prior to the subsequent sequence boundary. Above this sequence boundary is deposited another laterally restricted chronosome. This pattern of chronosome evolution is evident in the T20-2–N8-1 (chronosomes 37-39), N8-1–N8-2 (chronosomes 40-43), N8-2–N10-1 (chronosomes 44-47), N10-N10-N12-1 (chronosomes 48-52), N10-N12-1–N16-1 (chronosomes 53-60) and N16-1–N17-1 (chronosomes 61-63) sequences as shown in Figure 6.3, Figure 6.4 and Figure 6.5. These small, spatially-restricted chronosomes are interpreted to represent reduced carbonate growth under lowstand conditions. As relative sea level rises and begins to flood the margin, carbonate growth becomes re-established and the resulting chronosomes become progressively larger. Under highstand conditions the carbonate production is at a maximum, resulting in deposition of laterally extensive chronosomes. When relative sea level falls, the underlying laterally extensive highstand deposits are exposed and carbonate production is significantly reduced to a small area on the underlying slope.

Chronosome distribution patterns

Following the mid-Oligocene T15-1 sequence boundary at the top of chronosome 24, sedimentation resumes in an area restricted to the northern end of the study defined by the distribution of chronosome 25 (Figure 6.3). The 3D-Chronostrat section and Wheeler diagram for line 136-19 shows the subsequent chronosomes 25-39 to progressively build in a southwesterly direction through the basin, downlapping on to the late Eocene chronosome 24 (Figure 6.9). This southwesterly growth direction is also evident on the chronosome isochron maps, although these maps do reveal a more complex evolution with sedimentation of chronosomes 26 and 28 occurring in the southern end of the study area (Figure 6.3). The 3D-Chronostrat section and Wheeler diagram for the southwest end of line 136-19 demonstrate a thickening and downlapping of chronosomes 32-39 on to the underlying chronosome 24 (Figure 6.9). However, the isochron maps record no thickening of the respective chronosomes in this location (Figure 6.3). This stratal geometry is considered to be a result of the changing orientation of line 136-19 from initially running parallel to a linear sediment body and then cutting obliquely across it as demonstrated on the isochron map for chronosomes 36 (Figure 6.3).

During the deposition of chronosomes 25-39, basinward localities would have been starved of sediment and a condensed section would have formed. The Wheeler diagram for line 110-08 clearly indicates a long period of non-deposition following the T15-1 sequence boundary at the top of chronosome 24 with sedimentation resuming in chronosome 36 (Figure 6.10). This has been interpreted as a condensed section rather than missing section as there is evidence of clinoform sedimentation of chronosome 25-35 age landward of line 110-08. The clinoforms imply a marine environment and the height of these clinoforms also defines a minimum possible water depth, which in this case is approximately 300 ms for chronosome 39 on line 136-12. The isochron maps for chronosomes 36, 39, 41-47, 52 and 60 (Figure 6.3 and Figure 6.4) display thickening of the chronosomes toward the northeast of the study area which is particularly evident on line 110-08 (Figure 6.10). This thickness variation implies that the rate of accommodation space creation throughout chronosomes 36, 39, 41-47, 52 and 60 was greater at the northeastern end of the study area towards the Beagle Sub-basin than it was at the in southwestern end in the Dampier Sub-basin.

Progradational and aggradational nature of chronosomes 25-63

The periods of predominant aggradation and progradation, which were identified in the mid-Oligocene to late Miocene sediments during the seismic interpretation, are evident on both 3D-Chronostrat sections and Wheeler diagrams for lines 136-12 and 110-03 (Figure 6.7 and Figure 6.8). A curve joining the thickest point of each chronosome as identified from the Wheeler diagram for line 136-12 has been created to investigate the progradational and aggradational nature of chronosomes 25-63. An enlargement of the Wheeler diagram for the Oligocene to Recent section of line 136-12 displaying this curve is presented in Figure 6.11.

The progradational episodes of the T15-1 to N8-1 sequences and the N10-N12-1 to N17-1 sequences (chronosomes 25-39 and 53-63) and aggradational episode of the N8-1 to N10-N12-1 sequences (chronosomes 40-25), which were identified during the seismic interpretation, are clearly identifiable on Figure 6.11. Progradational sequences are characterised by concave-up portions of the curve joining the thickest point of the chronosomes whilst aggradational periods are characterised by convex-up portions of the curve. This concave/convex shape of the curve is most probably a result of the long-term rate of creation of accommodation space, which controlled the development of the aggradational and progradational sets of sequences. In the early stages of an aggradational set of sequences, the rate of accommodation space creation on the shelf top is high and sediments deposited will aggrade vertically to fill the accommodation space. As the rate of relative sea level rise decreases towards the end of the aggradational set of sequences, the rate of accommodation space creation on the shelf top decreases correspondingly. The primary location of sedimentation then migrates from the shelf top to the slope, resulting in sediments becoming deposited in a more basinward direction. The evolution from aggradation to progradation in the aggradational set of sequences gives rise to the convex-up nature of the curve. The concave-up portions of the curve have formed by the opposite of this process when the long-term rate of accommodation space creation has been low and progradational sets of sequences have formed. Initially minimal shelf top accommodation space is created and the resultant chronosomes prograde strongly basinward. In the later stages of a progradational set of sequences, shelf top accommodation space will be created and an aggradational component to the progradational set of sequences will occur. The inflection point between the concave and convex portions of the curve represents the change from an aggradational to progradational set of sequences as seen in Figure 6.11.

Figure 6.11 (On opposing page) Wheeler diagram of the Oligocene to late Miocene section of line 136-12. The thickest point of each chronosome has been identified and a line joining these points has been drawn. The curve is concave-up in the progradational sequences (T15-1 to N8-1 and N10-N12-1 to N17-1) and convex-up in the aggradational sequences N8-1 to N10-N12-1. The convex-up aggradational sequences are seen to correspond to the periods when the short and long term eustatic curves are coincident whilst the concave up progradational sequences corresponds to periods when the short and long term eustatic curves are separated.

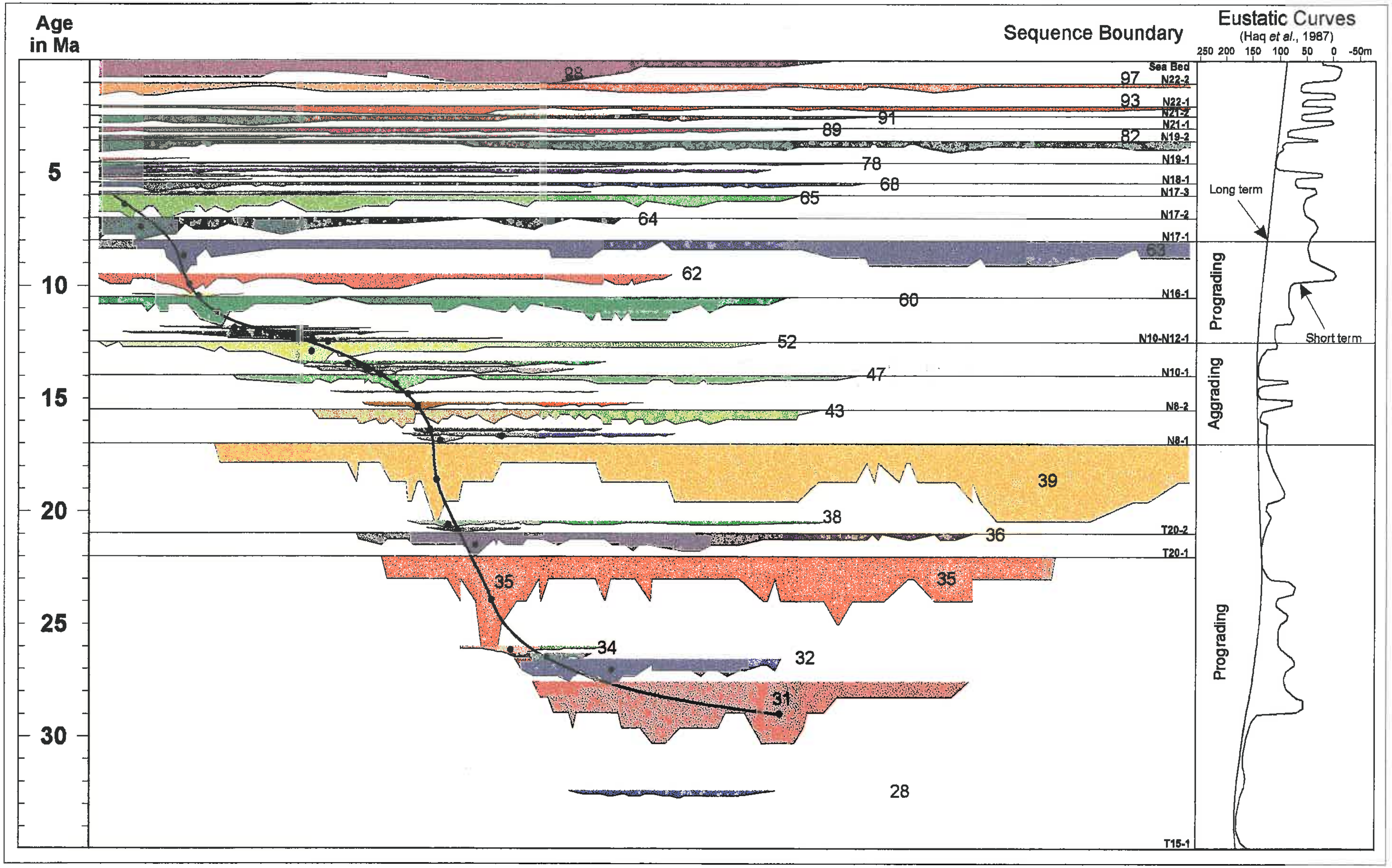

Sequence stratigraphic evolution of the Albian to Recent section of the Dampier Sub-basin

6.2.4.2 Late Miocene – Recent (chronosomes numbers 64 – 98)

The late Miocene N17-1 event that was defined during the seismic and wireline log interpretation phase of the project marks a distinct change in sedimentation patterns in the Dampier Sub-basin. Below N17-1, the section is characterised by northeast-southwest-trending linear clinoforms which exhibit little along-strike variations in thickness. Above the N17-1 sequence boundary, the seismic interpretation has defined a thick (up to 600ms) point-sourced wedge of sediment of late Miocene age (N17-1–N18-1) which builds out into the centre of the Dampier Sub-basin. This thick wedge of sediment has a profound influence on the subsequent sediment distribution patterns of the late Miocene to Recent sequences of the Dampier Sub-basin as was discussed in Chapter 5.

The wedge of N17-1–N18-1 sediments corresponds to chronosomes 64 to 68 in the 3D-Chronostrat interpretation. Chronosomes 64–67 record restricted sedimentation in the centre of the study area, whilst chronosome 68 records the resumption of basin-wide sedimentation (Figure 6.5). This wedge of sediment formed by chronosomes 64–68 can be clearly identified on line 110-08, where it attains a thickness of approximately 600 ms, and on the corresponding Wheeler diagram, where the restricted nature of chronosomes 64–67 is particularly evident (Figure 6.10). On dip sections, such as line 136-12, chronosomes 64 to 68 appear to be no more than part of the prograding mid-Oligocene to Recent sequences (Figure 6.7). On line 136-19, the up-dip expression of this wedge can be seen where chronosomes 64-68 are seen to progressively onlap the underlying chronosome 63 (Enclosure 3).

The distinct change in stratal architecture across the N17-1 sequence boundary (chronosomes 63–64) can be clearly seen on all 3D-Chronostrat sections (Enclosure 3). On line 136-14, chronosomes 25-63 show the development of strongly prograding clinoforms above a series of flat-lying Albian to mid-Oligocene chronosomes (1-14). In a landward direction, the dip of the Albian to mid-Oligocene chronosomes is seen to increase before becoming relatively flat-lying at the landward end of the line. No pronounced thickness variations are recorded within chronosomes 25-63. The late Miocene to Recent chronosomes (68, 77, 78, 81, 82, 93 and 97) are seen to progressively onlap chronosome 63 in a landward direction. This progressive onlap and steepening of dips in chronosomes 25-63 has been interpreted to represent accelerated subsidence following the N17-1 sequence boundary. As chronosomes 1-24 are flat-lying over the Rankin and Enderby Platforms, it is inferred that the bulk of the subsidence has occurred in the vicinity of the underlying Jurassic-Cretaceous Dampier rift with the Rankin Platform subsiding as a stable block and the Enderby Platform remaining stable.

Late Miocene to Recent chronosomes that were deposited during the phase of accelerated subsidence following chronosome 68, are seen to onlap and thin on to the sediment wedge formed by chronosomes 64–68 in both a northeasterly and southwesterly direction. Thinning of chronosomes 69–98 on to the underlying thickened section of chronosomes 43,45,47 & 52 is also evident at the northern end of line 110-08 (Figure 6.10). These variations in chronosome thickness and stratal architecture are evident on the Wheeler diagram for line 110-08 but are hard to distinguish due to the short duration of each chronosome. The Wheeler diagram output from 3D GRID prior to re-scaling to absolute time demonstrates these patterns more clearly and is presented in Figure 6.12. The chronosome thickness maps for chronosomes 69-98 (Figure 6.5 and Figure 6.6) record a change from chronosomes characterised by linear clinoform geometries (25-63) to chronosomes characterised by pronounced lateral thickness variations in response to the sediment wedge formed by chronosomes 64 to 68. Chronosome 76 typifies the style of sedimentation of the late Miocene to Recent chronosomes as sediment infills the remnant low topography of chronosomes 64-68. The isochron map for chronosome 76 (Figure 6.5) records thin sedimentation (10s ms) over the thickest point of the wedge formed by chronosomes 64-68 and pronounced sediment thickening (up to 375 ms) on either side of the underlying wedge.

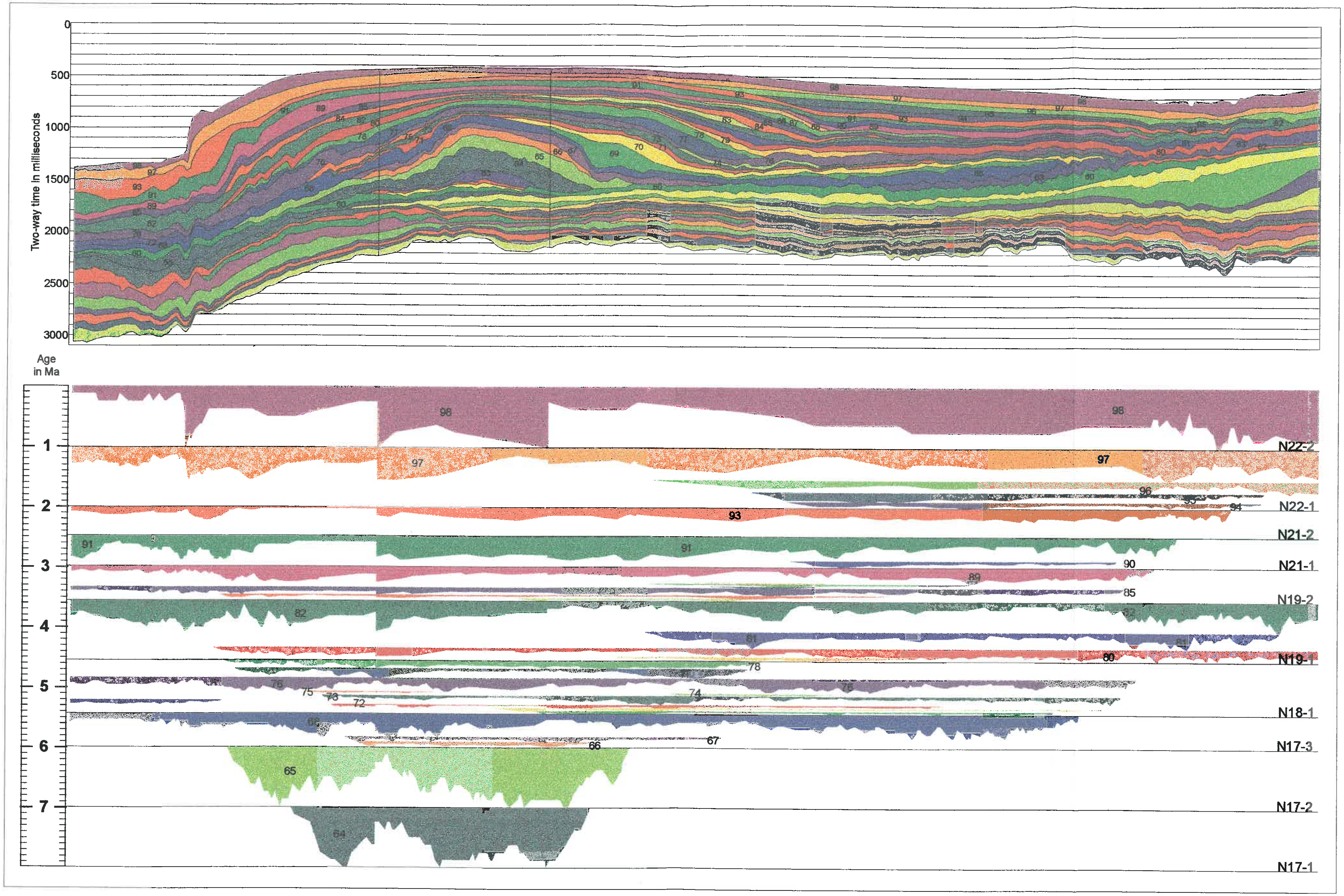

Figure 6.12 3D-Chronostrat section and Wheeler diagram of the late Miocene to Recent section of line 110-08 (chronosomes 64-98).

6.2.5 Migration of depocentres

The location of the thickest point of each chronosome, termed the 'depocentre' was identified from the chronosome thickness maps and plotted on a map to investigate the evolutionary nature of the sedimentary depocentres through time. For reasons of clarity, the map showing the locus of sediment depocentres has been subdivided into a series of maps on the basis of the major basin-forming units that have been defined in this study (Figure 6.13). These units are Albian – base Tertiary (chronosomes 1-14), base Tertiary–mid Oligocene (chronosomes 15-24), mid-Oligocene–late Miocene (chronosomes 25-63) and late Miocene – Seabed (chronosomes 64-98). The mid-Oligocene to late Miocene and late Miocene to Seabed sequences have been further subdivided into periods of predominant progradation and aggradation on the basis of observed seismic geometries as was discussed in Section 5.8.2 and 6.2.4

The maps of the locus of sediment depocentres through time demonstrate a systematic variation in the location of the thickest sediment of subsequent chronosomes (Figure 6.13). This is especially true of the Albian to mid-Oligocene sediments (chronosomes 1-24) in which the sediment depocentre can be seen to migrate laterally along the strike length of the basin. The map for the Albian to base Tertiary chronosomes shows the depocentre to originate in the southwest corner of the study area and then to migrate in a northeast direction during chronosomes 1-5, a southeast direction during chronosomes 6-10 and return to a northeasterly migration direction in chronosomes 10-13. This style of migration is again evident in the Paleocene and Eocene sediments (base Tertiary to mid-Oligocene) where northeasterly migration is observed chronosomes 16-17 and 20-22 and southeasterly migration is evident in chronosomes 14-16, 17-20 and 22-24.

Following the mid-Oligocene T15-1 event at the end of chronosome 24, the lateral migration of depocentres along the strike length of the basin becomes less pronounced though is still evident. Two distinct clusters of depocentres can be defined on the map for sequences T15-1 to N8-1, one in the northeast of the study area (chronosomes 25, 27, 29, 30 and 35) and the other in the centre of the study area (chronosomes 26, 28 and 31-34). In the early part of the T15-1 to N8-1 sequences, successive chronosome depocentres alternate between these two clusters whilst in the later part of the sequences, groups of chronosomes tend to cluster in these two areas. Within the initial chronosomes of the subsequent aggradational N8-1 to N10-N12-1 set of sequences, this pattern of switching depocentres is again evident. Chronosomes 36 and 39 group together in the northeast cluster whilst chronosomes 37, 38 and 40 are located cluster in the southwest. From chronosome 40, the long term northeast and southwest migrating nature of depocentres that was evident in chronosomes 1-24 is again apparent. Chronosomes 46-47 and 40-45 demonstrate northeasterly migration of the depocentres whilst chronosomes 45-46 and 47-52 demonstrate southwesterly migration of the depocentres. The southwesterly and northeasterly migrating pattern continues into sequences N10-N12-1 to N17-1 with chronosomes 53-55 & 60-62 demonstrating southwesterly migration and chronosomes 55-60 & 62-63 demonstrating northeasterly migration of sediment depocentres. The following N17-1–N19-2 sequences show northeasterly migration of the depocentres in chronosomes 64-68, 70-71 and 73-76 and southwesterly migration in 68-70 and 71-73. The location of the depocentre in chronosomes 77-82 alternates between the southern and central regions of the study area but, for the first time, the successive location of the depocentres migrates landward in a southeasterly direction as opposed to basinward in a northwesterly direction. The final set of sequences (N19-2 to Seabed) shows two distinct clusters of sediment depocentres on either side of the underlying cluster of N17-1 to N19-2 depocentres. Within these two geographically-defined clusters of depocentres, groups of chronosomes of 86-88 & 94-96 can be identified in the northeastern geographical area and 84-85, 91-93 and 97-98 in the southeastern area.

The migrating pattern of depocentres indicates that the nature of accommodation space creation and its use varies along the shelf through time. This is especially evident in the Albian to mid-Oligocene section where the depocentre is seen to migrate progressively along the strike direction of the basin. This lateral progression of sediment depocentres implies differential subsidence along the shelf during this time, resulting in the changing location of sediment deposition. Thickening of the chronosomes in the direction of migration of the depocentres as displayed on the maps of Figure 6.13 is evident on the 3D-Chronostrat section for these chronosomes (Enclosure 3). For example, thickening of chronosomes 14-16 can be clearly seen in a southerly direction on line 110-08 (Figure 6.10). This corresponds to the locus of sediment depocentre for these chronosomes as displayed on Figure 6.13.

The progressive thickening of chronosomes 41-47 in a northerly direction, as has been previously described from the chronosome thickness maps (Figure 6.4) and line 110-08 (Figure 6.10), is also clearly defined by clustering of depocentres at the northern end of the basin (Figure 6.13). The sections of the prograding mid-Oligocene to late Miocene sequences which do not show pronounced thickening in a specific direction as described from the chronosome thickness maps, are represented by the alternating location of sediment depocentres. During deposition of these chronosomes, the rate of accommodation space creation is considered to be consistent across the shelf.

The thickest sections of chronosomes 69-98 are seen to flank the underlying wedge of sediment formed by chronosomes 64-68 and they are also seen to progressively migrate away from this wedge in both a southwesterly and northeasterly direction. It is interpreted that this pattern of depocentres is recording the progressive infilling of the remnant topography left after the deposition of the thick wedge of formed by chronosomes 64 –68.

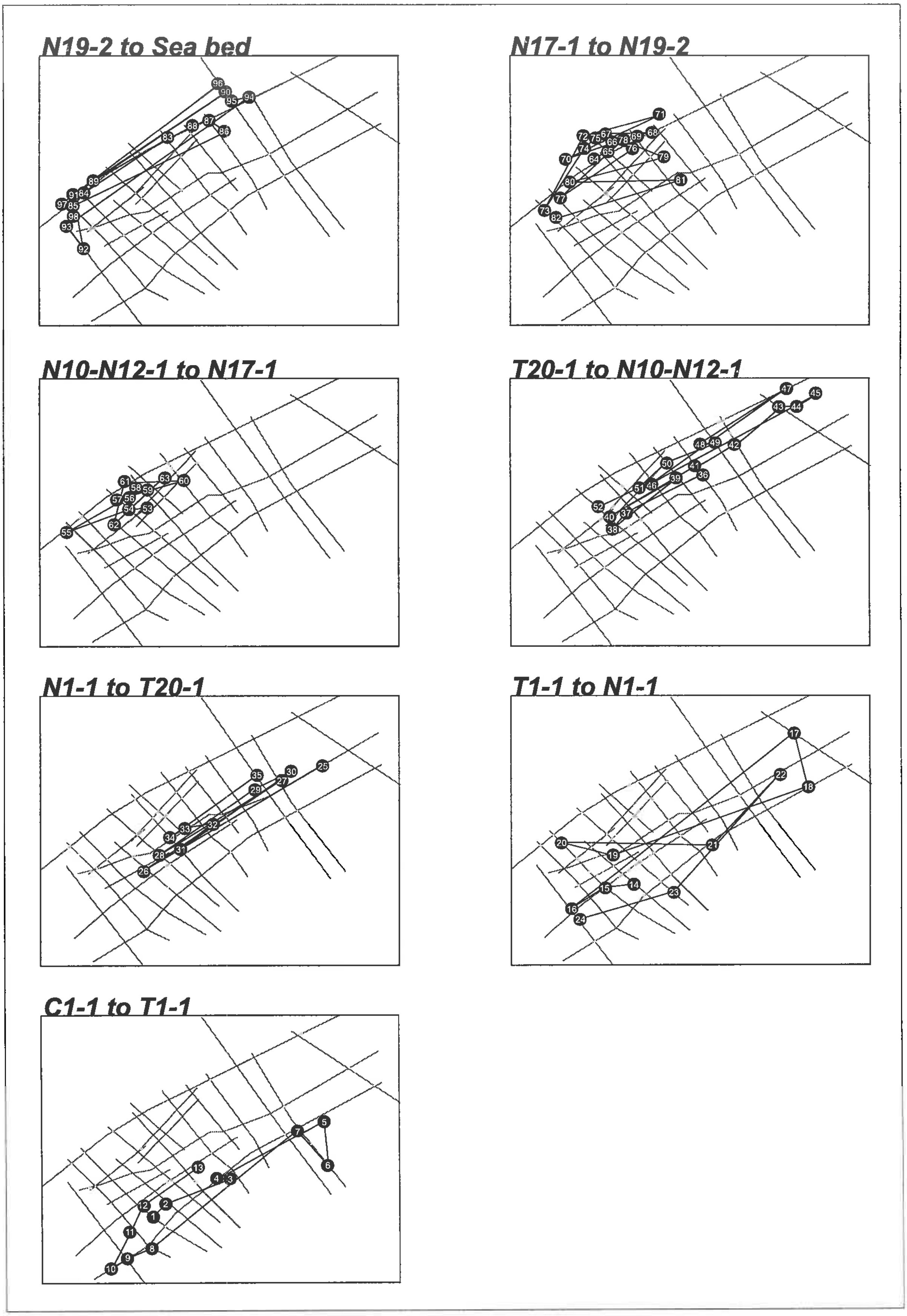

Figure 6.13 Migration of chronosome depocentres by major basin-forming units.

6.3 Sedimentation rates

Many carbonate platforms consist of shallow water facies that build to sea level in response to developing accommodation space. Calculated sedimentation rates for these sequences reflect the changing accommodation space which is controlled by subsidence and eustatic sea level changes rather than reflecting the intrinsic growth potential of a carbonate platform (Tucker *et al.*, 1990a). A study of the sedimentation rates throughout a platform's evolution will therefore reveal important insights into the development of accommodation space during that time.

Sedimentation rates for the Albian to Recent section of the Dampier Sub-basin have been calculated on three scales to investigate the nature of accommodation space development and filling in the Dampier Sub-basin. These three scales are chronosome scale (defined from 3D-Chronostrat), sequence scale (defined from biostratigraphic and seismic data) and 'sets of sequences' or basin scale (defined from seismic data). The sedimentation rates over each of these scales have been calculated by dividing the volume of the body of interest by its duration. The volume of each chronosome has been calculated using the process described in Section 3.5.2. The volumes of the sequences and sets of sequences have been calculated by summing the volumes of the constituent chronosomes. The duration of the sequences and sets of sequences can be calculated from the biostratigraphic ages of the sequence boundaries. The duration of each individual chronosome is somewhat more problematic but can be estimated by making certain assumptions on sedimentation rates and chronosome geometries. This process will be discussed in Section 6.3.3.

The accuracy of the calculated sedimentation rate will be dependent on the accuracy of the calculated sediment volumes and biostratigraphic age of the sequence boundaries. To address the inaccuracies in the biostratigraphic data significant analysis of cuttings and sidewall core data is required. A rigorous depth conversion of this dataset is not a trivial matter and is a considerable undertaking, as was previously discussed in Chapter 5. Even if a depth conversion were conducted, it would not be possible to integrate it into the 3D-Chronostrat data set and utilise it for calculation of chronosome volumes. Although the sedimentation rates which have been calculated for this project are subject to error, the values are still of interest in that this is one of the first volumetric analyses of this resolution undertaken in a carbonate environment. The nature and timing of changes in sedimentation rates are more critical to the interpretation, as they will reveal the controls on the late stage evolution of the Dampier Sub-basin.

6.3.1 Basin scale sedimentation rates – Oligocene to Recent sediments

As has been previously discussed in Section 6.2.4, the mid-Oligocene to Recent section of the Dampier Sub-basin is characterised by distinct periods of progradation and aggradation. It was also observed that the aggrading units appeared to be volumetrically more significant and of shorter duration than the prograding units, suggesting that sedimentation rates in the aggrading sequences were higher than in the prograding sequences. To test this theory sedimentation rates were calculated for the progradational and aggradational sets of sequences.

The section was subdivided into packages of progradational and aggradational sequences on the basis of the position of the slope break and the nature of the top-set accumulation. Progradational sequences were defined where the slope break migrated progressively basinwards with only a minor component of vertical migration; these sequences are characterised by strongly progradational units with thin top sets and have formed in response to a low rate of accommodation space creation. Aggradational sequences were defined where the locus of the slope break through the sequence had a major vertical component; these sequences are characterised by strongly aggradational units with significant top set accumulation and will have formed in response to a high rate of accommodation space creation. Figure 6.14 shows periods of predominant progradation and aggradation on line 136-12 that have been defined using the relative position of the slope break and the thickness of top sets.

The Oligocene to Recent section has been subdivided into predominantly progradational periods of T15-1–N8-1, N10-N12-1–N17-1 and N17-1–N17-3 age and predominantly aggradational periods of N8-1–N10-N12-1 and N17-3–N19-2 age. On dip lines (e.g. Figure 6.14), the N17-1–N17-2 sequence appears to be part of the progradational N10-N12-1–N17-1 package but it is considered to be separate from this package due to the change in stratal architecture that occurs across the N17-1 sequence boundary as discussed in Section 6.2.4. The volumes of these progradational and aggradational packages were calculated by summing the volumes of the constituent chronosomes within each package calculated in 3D-Chronstrat using the process described in Section 3.5.2. Sedimentation rates could then be calculated for long-term progradational and aggradational packages by dividing the calculated sediment volumes by the duration of the sequences. Table 6.2 presents the duration, volume and sedimentation rates calculated for the prograding and aggrading sets of sequences in the Oligocene to Recent section of the Dampier Sub-basin.

Sequence	Stacking Patterns	Duration (Ma)	Volume (Km^3)	Sed Rate (Km^3Ma^{-1})
N19-2 – Seabed	**Mixed – Aggrade**	**3.5**	**16045**	**4585**
N17-2 N19-2	**Aggradation**	**3.5**	**19800**	**5650**
N17-1 – N17-2	**Progradation**	**1**	**875**	**875**
N10-N12-1 – N17-1	**Progradation**	**4.5**	**9302**	**2065**
N8-1 – N10-N12-1	**Aggradation**	**4.5**	**14050**	**3125**
T15-1 – N8-1	**Progradation**	**18**	**13475**	**750**

Table 6.2 Packages of progradational and aggradational sequences defined for the Oligocene to Recent section of the Dampier Sub-basin.

From Table 6.2 it can be seen that the progradational and aggradational packages have differing sedimentation rates with generally higher rates in the aggradational sequences compared to the progradational sequences. If we equate the aggradational packages to low frequency (10 Ma) highstands of relative sea level and the progradational packages to low frequency (10 Ma) lowstands of relative sea level, it can be concluded that the gross stacking geometries of the Oligocene to Recent section of the Dampier Sub-basin support the current models for carbonate sedimentation. These models, which are outlined in Chapter 2, argue that carbonate sedimentation rates are higher during highstand conditions when the shelf top is flooded than they are under lowstand conditions when the shelf top is exposed and the carbonate production factory is significantly reduced in size (Emery, 1996; Handford and Loucks, 1993; Schlager, 1992; Schlager *et al.*, 1994; Tucker *et al.*, 1990b).

Within the Oligocene to Recent section, sedimentation rates of approximately 750 km^3Ma^{-1}, 2065 km^3Ma^{-1} and 875 km^3Ma^{-1} were calculated for the prograding T15-1–N8-1, N10-N12-1–N17-1 and N17-1–N17-2 sequences respectively. Sedimentation rates of approximately 3125 km^3Ma^{-1} and 5650 km^3Ma^{-1} were calculated for the aggradational N8-1–N10-N12-1 and N17-2–N19-2 sequences. A rate of 4585 km^3Ma^{-1} was calculated for the mixed aggradational N19-2–Seabed sequences. Whilst uncertainty may exist in the calculation of the absolute rates of carbonate sedimentation due to uncertainties in the biostratigraphic dating and inaccuracies in the depth conversion, there is a significant difference in the sedimentation rates between the progradational and aggradational sequences.

6.3.2 Sequence scale sedimentation rates – Albian to Recent sediments

The sedimentation rate for each sequence defined and mapped in the biostratigraphic, wireline and seismic interpretation phases of the project was calculated from the volume of the constituent chronosomes and duration of each sequence. The calculated sedimentation rates were then plotted against time to investigate the nature and timing of variations in sedimentation rate during the evolution of the basin (Figure 6.15).

Three distinct periods of high sedimentation rates have occurred in the Dampier Sub-basin since the Albian as demonstrated on Figure 6.15. The first is Maastrichtian to base Eocene in age (C13-1–T7-1) and the second is of Miocene age (T20-2–N17-1). Both these periods have sedimentation rates in the order of 2000-3000 km^3Ma^{-1}. The third period of high sedimentation rates is of late Miocene to Pliocene age (N18-1–Recent) and has calculated sedimentation rates which are initially as high as 9000 km^3Ma^{-1} but are seen to decline steadily through a range of 5000-7000 km^3Ma^{-1} (Figure 6.15). In between these periods of high sedimentation rates the background sedimentation rate has typically been less than 1000 km^3Ma^{-1}. Sedimentation rates of this magnitude typify the Albian to Campanian (C1-1–C11-1), Lutetian to Burdigalian (T10-1–T20-1) and late Miocene (N17-1–N17-3) sections.

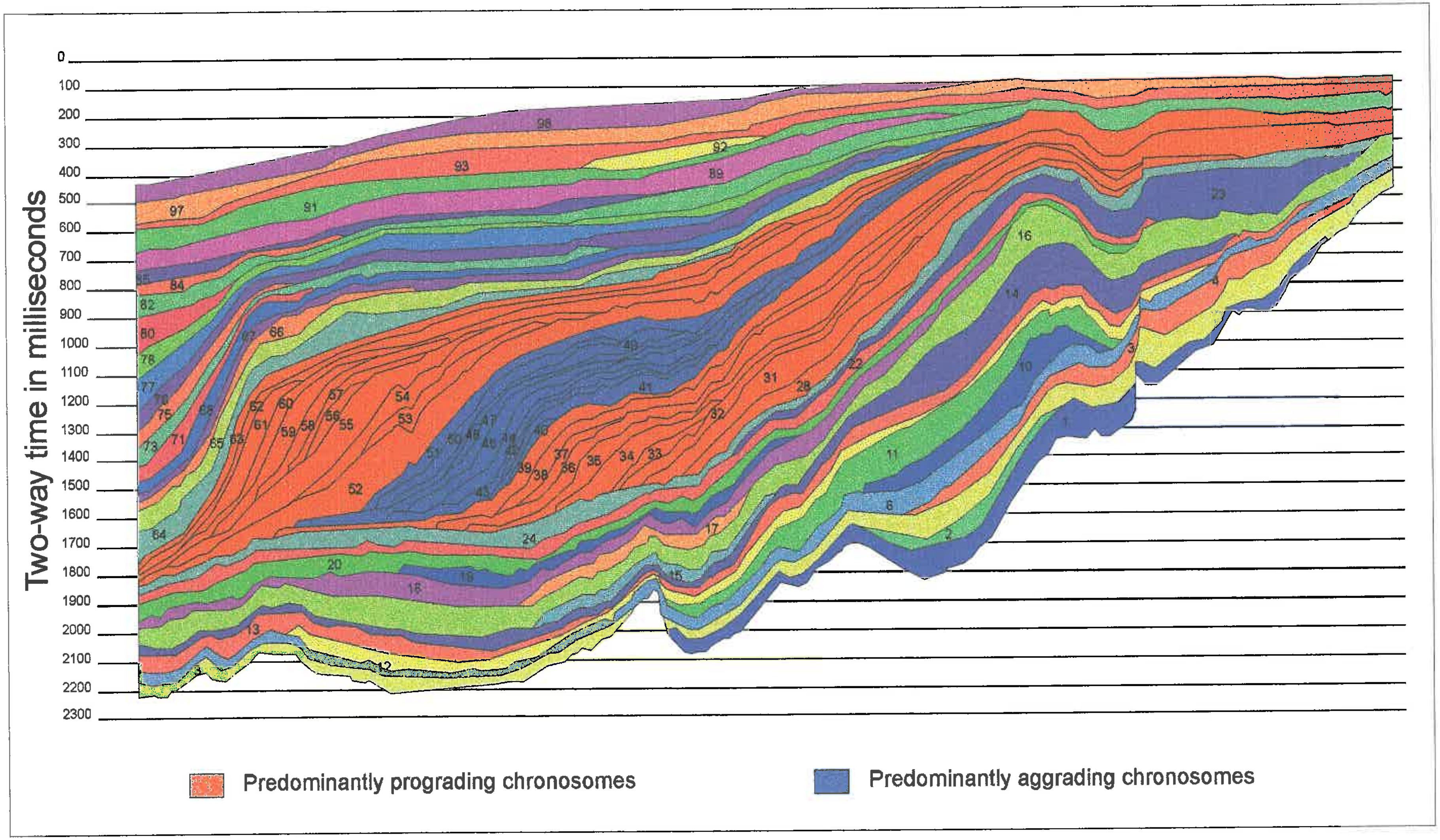

Figure 6.14 *3D-Chronostrat section of line 136-12 showing predominantly progradational and aggradational chronosomes. (Line length 131.5 km)*

Maastrichtian-Paleocene (C13-1–T7-1)

The late Cretaceous C11-1–C13-1 and C13-1–T1-1 and Eocene T7-1–T10-1 sequences have relatively high sedimentation rates (calculated to be 1500, 2500 and 3500 km^3Ma^{-1} respectively). The intervening Paleocene sequence has a much lower calculated sedimentation rate of 900 km^3Ma^{-1}.

Miocene (T20-2–N17-1)

Both progradation and aggradation-dominated periods have been observed in the Oligocene to Recent section of the Dampier Sub-basin. The T15-1 to N8-1 prograding set of sequences demonstrates an overall increase in sedimentation rate with time. Within this set of sequences, the calculated sedimentation rate can be seen to evolve from approximately 430 to 1165 to 1865 km^3Ma^{-1} in sequences T15-1–T20-1, T20-1–T20-2 and T20-2–N8-1 respectively. Observations made on the sequence scale predict that the highest sedimentation rate during a prograding set of sequences would occur at the end set of the sequences. Accommodation space is being created on the margin top at this time and the carbonate production factory is increasing in size. The calculated sedimentation rates for the T15-1–T20-1, T20-1–T20-2 and T20-2–N8-1 sequences support this observation.

The aggrading set of sequences, N8-1 to N10-N12-1, exhibit an overall increase in calculated sedimentation rate through time (Figure 6.15). Calculated rates increase from 2200 km^3Ma^{-1} in sequence N8-1–N8-2 to 4000 km^3Ma^{-1} in sequence N8-2–N10-N12-1 and then decrease in the last aggrading sequence N10-N12-1–N16-1 to 3000 km^3Ma^{-1}. By analogy with transgressive and highstand systems tracts, this pattern of sedimentation rates is to be expected for an aggrading set of sequences. Through time, the sedimentation rate will increase as both the rate of relative sea level rise and accommodation space development increase to a maximum. As the rate of relative sea level rise begins to decrease towards the end of the relative sea level rise, so does the rate of creation of accommodation space and consequently so does the sedimentation rate. This pattern of sedimentation rates is observed in the aggrading set of sequences where the final aggrading sequence, N10-N12-1, has a lower sedimentation rate than the underlying N8-2–N10-1 sequence.

The progradational N10-N12-1–N16-1 and N16-1–N17-1 sequences show a further decrease in sedimentation rates calculated for the final aggradational sequence (3000 km^3Ma^{-1}) to similar sedimentation rates of approximately 2000 km^3Ma^{-1} for either sequence.

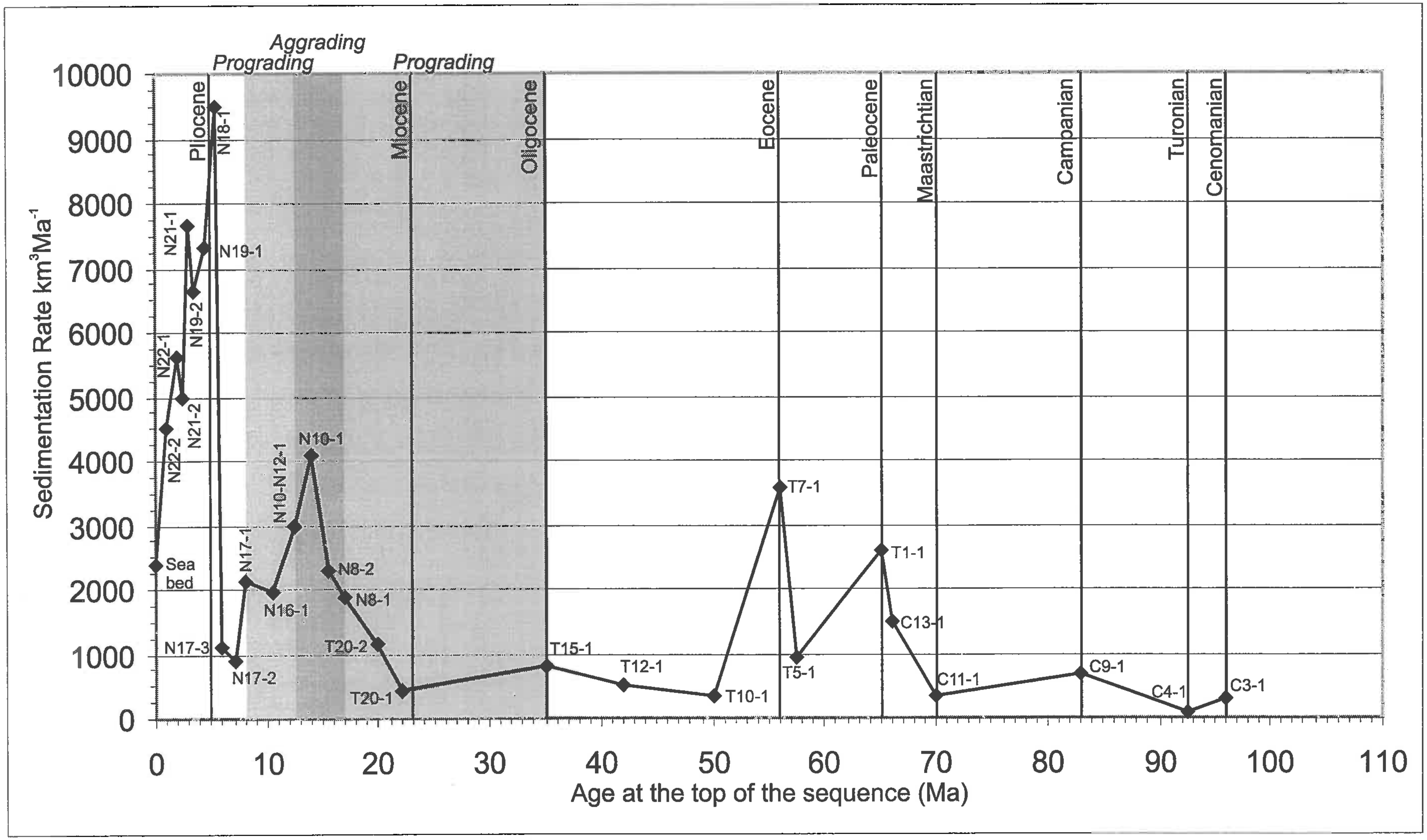

Figure 6.15 *Variations in sedimentation scale through time - sequence scale*

Miocene-Pliocene (N18-1–Recent)

The pronounced change in stratal architecture which has been identified across the late Miocene N17-1 sequence boundary from the chronosome distribution patterns (Section 6.2.4) also corresponds with a rapid increase in sedimentation rates as displayed on Figure 6.15. The N17-1–N17-2 and N17-2–N17-3 sequences, which were deposited immediately following the N17-1 sequence boundary, are areally restricted sequences (Figure 6.5) which have comparatively low calculated sedimentation rates of less than 1000 km^3Ma^{-1} (Figure 6.15). The subsequent N17-3–N18-1 sequence, which returns basin wide deposition to the study area, has the highest calculated sedimentation rate of the study at 9500 km^3Ma^{-1} (Figure 6.15). The subsequent N18-1 to Seabed sequences show a gradual decline in calculated sedimentation rate from a maximum of 9500 km^3Ma^{-1} in sequence N17-3–N18-1 to a present day calculated sedimentation rate of 2500 km^3Ma^{-1}. Within this overall decline, two minor increases in the calculated sedimentation rate are noted in sequences N19-2–N21-1 and N21-2–N22-1 (chronosomes 83-89 and 92-93 respectively). However, caution must be applied when interpreting this part of the curve as 3D-Chronostrat will underestimate chronosome volumes in instances where the chronosome extends beyond the bounds of the data set. From the chronosomes thickness maps (Figure 6.5 and Figure 6.6) and from line 110-03 (Figure 6.8) it can be seen that the majority of post-N17 chronosomes are not contained within the area of the data set.

6.3.3 Chronosome scale sedimentation rates – Albian to Recent sediments

In order to calculate sedimentation rates for each chronosome, both the volume of sediment and duration of each chronosome must be known. The volume of each of the chronosomes has been calculated using the process described in Section 3.5.2. but the age of the chronosomes is unknown and is only constrained by the biostratigraphic age of the thirty sequence boundaries mapped on seismic data. To calculate sedimentation rates on a chronosome scale it is important to proportion the total duration of a sequence to the constituent chronosomes adequately.

6.3.3.1 Calculating the duration of each chronosome

In the Outer Moray Firth in the North Sea, Griffiths and Hadler-Jacobsen (1995) have approached the problem of chronosome duration by making certain assumptions about chronosome dimensions and duration. They assumed that clay-rich sediments are more areally extensive and deposited more slowly than sand-rich sediments. The duration of a single chronosome was calculated as the total duration of the sequence multiplied by the proportion of the cross sectional area of the chronosome to the cross sectional area of the whole sequence on a dip line. Griffiths and Hadler-Jacobsen (1995) assume that there are no hiatuses in the section, which is known to be incorrect. The preserved volume of sediment will also have been subject to erosion and compaction and so the original sedimentation rate will have been greater than that calculated. The duration of the each chronosome calculated by this method will therefore be a maximum possible duration and therefore giving the minimum possible sedimentation rate (Griffiths and Hadler-Jacobsen, 1995).

Due to the nature of carbonate production, it may be incorrect to assume that small, laterally-restricted carbonate accumulations are deposited much more rapidly than large laterally-extensive accumulations. As discussed in Chapter 2, the in-situ carbonate production rate varies with changes in relative sea level. Under lowstand conditions, carbonate production rates will be at a minimum as the shelf is exposed and the carbonate production factory is relocated to a narrow band on the slope front. During highstand conditions, the whole shelf will be flooded and carbonate production rates will be at a maximum. Thus the lowstands will produce small, spatially-restricted chronosomes at slow rates and highstands will produce large spatially-extensive chronosomes at fast rates (Figure 6.3, Figure 6.4 and Figure 6.5). This is the opposite of the case described for siliciclastic sections in the Outer Moray Firth by Griffiths and Hadler-Jacobsen (1995).

In this study, a method has been devised to calculate the duration of individual carbonate-dominated chronosomes by applying the observations of varying sedimentation rates between aggrading and prograding sets of sequences as described in Section 6.3.1. The method assumes that the relationship between the sedimentation rates observed on a large scale between the prograding and aggrading sets of sequences also apply at a sequence scale. Periods of shelfal aggradation were equated to laterally extensive chronosomes with a shelf-top component, such as transgressive and highstand systems tracts, and periods of shelfal progradation were equated to laterally-restricted chronosomes with little shelf top component or lowstand systems tracts. By calculating the ratio of sedimentation rates in the aggrading and prograding sets of sequences and assuming that this ratio can be applied to the highstand/transgressive and lowstand systems tracts of individual sequences, it is possible to estimate the duration of the individual chronosomes.

The ratio of sedimentation rates between aggradational and progradational sequences was calculated using the values for the aggrading N8-1–N10-N12-1 set of sequences and the prograding N10-N12-1–N17-1 set of sequences (Table 6.2 and Figure 6.15). These sets of sequences were chosen because it appears that, at this time, carbonate growth was prolific and uninhibited by other factors (represented on the isochron maps by the linear nature of sediment bodies exhibiting minor along-strike variation in sediment thickness (Enclosure 2). The progradation rate calculated for the underlying T15-1 to N8-1 sequences was rejected in the calculation of the ratio because these sequences record the start-up of the strongly prograding section whilst the N10-N12-1 to N17-1 sequences record progradation during established growth. The post-N17-1 sequences were also rejected because of the large increase in sedimentation rates and change of stratal architecture across this boundary. This has been interpreted to represent a regional change in the controls on sediment distribution (Figure 6.15 and Section 6.2.4). Using the gross sedimentation rates calculated for the N8-1 to N10-N12-1 and N10-N12-1 to N17-1 sets of sequences of 3125 km^3Ma^{-1} and 2067 km^3Ma^{-1} respectively, it can be calculated that the sedimentation rate in an aggradational sequence is approximately 1.5 times that of a progradational sequence. It has therefore been assumed, for the purposes of calculating the duration of individual chronosomes, that the sedimentation rate in laterally-extensive highstand and transgressive systems tracts is 1.5 times that in the lowstand systems tracts. By making the further assumption that the sedimentation rate in all progradational or aggradational chronosomes within a single sequence is constant, it is possible to estimate the duration and therefore age of each individual chronosomes on the basis of chronosome volume. The age of each chronosome defined within this study has been calculated are presented in Table 6.3. The derivation of the formula to calculate the duration of each chronosome is presented as Equation 6.1

The assumption that the carbonate sedimentation rate will remain constant within a series of prograding or aggrading chronosomes is incorrect as the rate of carbonate sedimentation will increase with time as the carbonate production factory becomes established (Handford and Loucks, 1993). However, it is not possible to quantify how this sedimentation rate increases with time and so this assumption has been made.

Sequence	Chronosome	Age (Ma)	Sequence	Chronosome	Age (Ma)	Sequence	Chronosome	Age (Ma)
Sea Bed	98	0.00	N17-3	65	6.00	T20-1	32	27.22
N22-2	97	1.00	N17-2	64	7.00	T20-1	31	28.06
N22-2	96	1.52	N17-1	63	8.00	T20-1	30	30.76
N22-2	95	1.75	N17-1	62	9.48	T20-1	29	31.78
N22-2	94	1.95	N17-1	61	10.47	T20-1	28	32.97
N22-1	93	2.00	N16-1	60	10.50	T20-1	27	33.16
N22-1	92	2.39	N16-1	59	11.81	T20-1	26	34.13
N21-2	91	2.50	N16-1	58	11.90	T20-1	25	34.21
N21-2	90	2.90	N16-1	57	11.93	N1-1	24	35.00
N21-1	89	3.00	N16-1	56	11.94	N1-1	23	40.48
N21-1	88	3.23	N16-1	55	11.96	T12-1	22	42.00
N21-1	87	3.24	N16-1	54	12.37	T12-1	21	49.54
N21-1	86	3.27	N16-1	53	12.45	T10-1	20	50.00
N21-1	85	3.28	N10_N12-1	52	12.50	T10-1	19	54.13
N21-1	84	3.39	N10_N12-1	51	13.38	T7-1	18	56.00
N21-1	83	3.48	N10_N12-1	50	13.63	T7-1	17	56.91
N19-2	82	3.50	N10_N12-1	49	13.71	T5-1	16	57.50
N19-2	81	4.05	N10_N12-1	48	13.96	T5-1	15	64.18
N19-2	80	4.24	N10-1	47	14.00	T1-1	14	65.00
N19-2	79	4.44	N10-1	46	14.64	C13-1	13	66.00
N19-1	78	4.50	N10-1	45	14.73	C13-1	12	68.90
N19-1	77	4.67	N10-1	44	15.07	C11-1	11	70.00
N19-1	76	4.79	N8-2	43	15.50	C11-1	10	75.98
N19-1	75	5.09	N8-2	42	16.48	C11-1	9	78.90
N19-1	74	5.11	N8-2	41	17.07	C11-1	8	80.34
N19-1	73	5.13	N8-2	40	17.49	C11-1	7	81.41
N19-1	72	5.23	N8-1	39	17.50	C9-1	6	83.00
N19-1	71	5.28	N8-1	38	20.19	C9-1	5	91.19
N19-1	70	5.35	N8-1	37	20.48	C4-1	4	92.50
N19-1	69	5.44	T20-2	36	20.50	C3-1	3	96.00
N18-1	68	5.50	T20-1	35	22.00	C3-1	2	102.41
N18-1	67	5.88	T20-1	34	26.40	C3-1	1	103.05
N18-1	66	5.96	T20-1	33	26.80			

Table 6.3 Calculated chronosome ages and corresponding sequences

Assumming

T = Total duration of the sequence

t_{agg} = time spent aggrading

t_{pro} = time spent prograding

V_{agg} = volume of aggradational sediment

V_{pro} = volume of progradational sediment

$$T = \delta t_{agg} + \delta t_{pro}$$

$$V_{agg} = 1.5 \cdot V_{pro}$$ - *in unit time*

$$\frac{\delta V_{agg}}{\delta t} = \frac{1.5 \cdot \delta V_{pro}}{\delta t}$$ - *rate of aggradation = 1.5 x rate of progradation*

$$\frac{\delta V_{agg}}{\delta t_{agg}} = \frac{1.5 \cdot \delta V_{pro}}{\delta t_{pro}}$$

$$\frac{\delta t_{agg}}{\delta t_{pro}} = \frac{1.5 \cdot \delta V_{pro}}{\delta V_{agg}}$$

$$\delta t_{agg} = \frac{1.5 \cdot \delta V_{pro} \cdot \delta t_{pro}}{\delta V_{agg}}$$

Thus substituting into - $T = \delta t_{agg} + \delta t_{pro}$

$$\text{Gives } T = \frac{1.5 \cdot \delta V_{pro} \cdot \delta t_{pro}}{\delta V_{agg}} + \delta t_{pro}$$

$$\text{Gives } T = \left(\frac{1.5 \cdot \delta V_{pro}}{\delta V_{agg}} + 1 \right)$$

Equation 6.1 Derivation of the formula used to estimation chronosome duration in a mixed prograding and aggrading carbonate section.

6.3.3.2 Chronosome scale sedimentation rates

Sedimentation rates were estimated for each chronosome using the procedure outlined in Section 6.3.3.1 and then plotted against time as shown in Figure 6.16. As expected, the plot of sedimentation rates by chronosome is similar to the plot of sedimentation rate by sequence but it does show more detail in some of the longer duration sequences in which several chronosomes have been defined.

The nature of the sedimentation rates in the Maastrichtian (C11-1) to Eocene (T10-1) interval is more clearly defined on the chronosome scale (Figure 6.16) in contrast to the sequence-scale (Figure 6.15). The chronosome sedimentation rates show a gradual rise from 400 km^3Ma^{-1} to 2500 km^3Ma^{-1} between the C11-1 and T1-1 sequence boundaries; this is well represented on the sequence-scale plot of sedimentation rates (Figure 6.15). Following the base Tertiary T1-1, event the sedimentation rate drops rapidly to 650 km^3Ma^{-1} and remains low during the intervening Paleocene epoch before showing a sharp increase to around 4100 km^3Ma^{-1} between the late Paleocene T5-1 and base Eocene T7-1 sequence boundaries. On the plot of sedimentation rate by sequence (Figure 6.15), the T1-1–T5-1 sequence is represented by a consistently decreasing sedimentation rate. This is not the case on the plot of sedimentation rates by chronosomes (Figure 6.16). A further sharp drop in sedimentation rates to 260 km^3Ma^{-1} occurs across the subsequent base Eocene T7-1 sequence boundary which is followed by low but gradually increasing sedimentation rates until base Oligocene T15-1 event. Sedimentation rates in the Oligocene to earliest Miocene sediments (T15-1 to T20-1) remain consistent at around 350 km^3Ma^{-1}.

The shapes of the chronosome and sequence-scale sedimentation rate curves are similar in the following T20-1 to Seabed sediments. This is because the thick nature of the section has allowed more sequences to be defined for a given period of time than has been possible in the thin sediments of the Cretaceous and early Tertiary. Hence, there is a higher sample density and so variations in sedimentation rate are picked up by the sequence-scale sedimentation rate curve. Periods of low sedimentation rates directly above the interpreted sequence boundaries can be identified on the chronosome-calculated sedimentation rate curve (Figure 6.16). These represent the laterally-restricted chronosomes, which have been interpreted to be of lowstand origin.

6.4 Mid Oligocene to Recent chronosome morphology

The clinoform slope angle and heights were calculated for each clinoform in the prograding mid-Oligocene to Recent section of the Dampier Sub-basin to investigate variations in the slope angle and clinoform height through time and along shelf within a single chronosome. Slope and height calculations were performed for every clinoform on dip lines 136-10–18 and line 110-03 for which the shelf to toe transition could be identified.

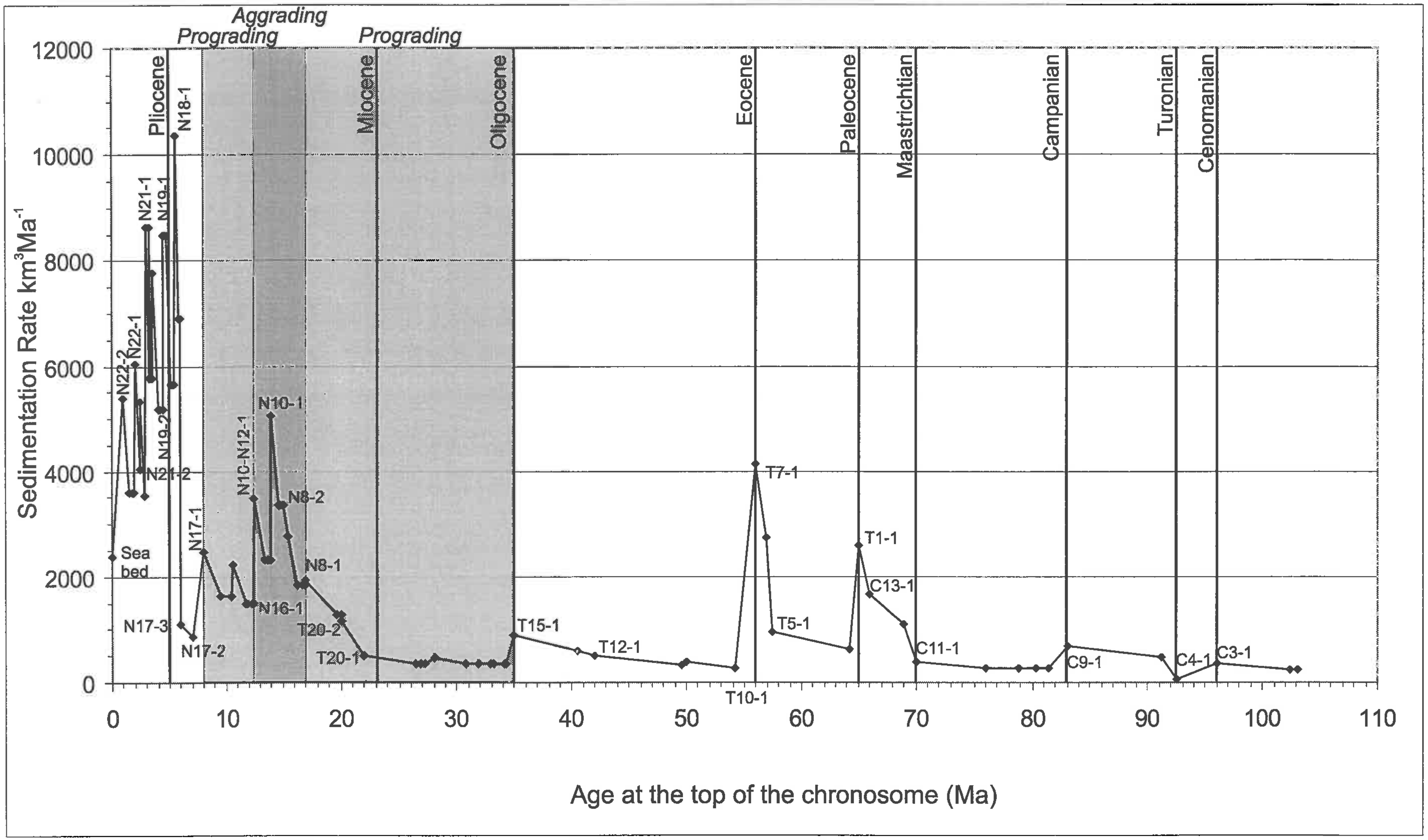

Figure 6.16 Variations in sedimentation scale through time - chronosome scale

6.4.1 Calculation Methodology

6.4.1.1 Calculation of clinoform slope angles

The angle of the clinoform slope has been calculated using the stacking velocities associated with the seismic data and the distance between two points at the base and top of the clinoform, which has been measured from the 3D-Chronostrat displays. The slope angle was calculated for the steepest point of each clinoform. A point at the top and bottom of this steepest section of the clinoform was defined and the two-way travel time and shot point location of each point was ascertained from the 3D-Chronostrat section. The stacking velocity associated with that two-way travel time was obtained from the nearest shot point for which stacking velocities have been calculated. It is commonplace to calculate stacking velocities for one in every hundred shot points on a line and for a particular shot point stacking velocities are typically calculated for every 500 ms of data. It is unlikely that a stacking velocity will have been calculated for the shot point and two-way time of interest. Therefore the stacking velocity must be estimated from the closest shot point for which stacking velocities have been calculated and from the velocities calculated for the two closest two-way times. In this study, the clinoform angles have been calculated using both the upper and lower velocities calculated for the nearest shot point to get a range of possible slope angles. The median of these calculated values for clinoform angle has been plotted graphically to investigate the changing nature of the slope angle during the evolution of the shelf. The slope angles have been calculated using the formula presented as Equation 6.2.

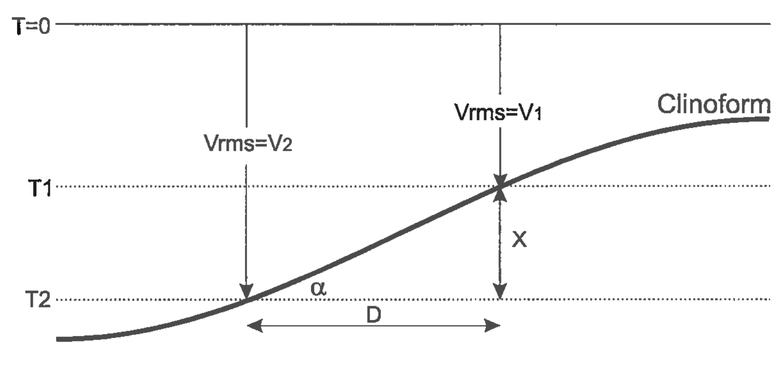

$$\alpha = \tan^{-1} X/D$$

where $X = ((V_2.T_2)-(V_1.T_1))/2$

Therefore $\alpha = \tan^{-1} (((V_2.T_2)-(V_1.T_1))/2D)$

Equation 6.2 Formula for the calculation of clinoform slope angles

It was noted that small variations in the stacking velocity (10%) could induce large differences in the resultant angle (up to 50% in some cases) whilst variations in the measured distance had only minor effects on the calculated clinoform angles. It must therefore be concluded that the accuracy of the calculated clinoform angles is dependent on the accuracy of the stacking velocities, which are interpreted during the processing of the raw seismic data. The clinoform slope angles calculated for this data set have also not been decompacted and so will not account for differential compaction due to lateral variations in sediment. However, in the Oligocene to Recent section of the Dampier Sub-basin, there is no evidence of significant reefal buildup and so differential compaction is not considered to be a critical problem within this data set. The clinoform angles have also not been corrected for regional dip, which has been calculated at less than one degree. Dip sections of Enclosure 3 show the regional dip of the T15-1 reflector (Chronosome 24) over the Rankin Platform to be minimal and in many cases mirrors the seabed profile and are thus interpreted to represent then difference in travel time through water than sediment rather than true depositional dip. The trends calculated in the clinoform angles show variations greater than one degree and will not be altered by a minor correction for depositional dip.

6.4.1.2 Calculation of clinoform height

The height of each clinoform for which the shelf-top to basin-floor profile could be defined on lines 136-10–18 and 110-03 was calculated using the stacking velocities associated with the seismic data. A point at the top and base of each clinoform was identified and depth converted using the associated stacking velocities. The difference between these two calculated depths was taken as the height of the clinoform. Similar to the calculation for slope angle, a maximum and minimum water depth was calculated for each point using the stacking velocities associated with two nearest two-way times for which velocities had been calculated. A median value for clinoform height has been calculated from these two values.

The points on each clinoform for which the depths have been calculated have been picked with reference to clinoform and overall stratal geometry. The lowest point has been picked as the flat section at the toe of a clinoform where the underlying stratal geometries are flat lying; such as at the end of line 136-15 (Enclosure 3). Where the dip of the underlying stratal geometries is seen to increase at the end of a line, such as on line 136-12 (Enclosure 3) the toe of the clinoform has been calculated at the point where the clinoforms parallel the underlying stratal geometry. Chronosomes 48-50 are restricted to the slope front of the underlying chronosome 47 and do not persist into the basin. In such a situation the basin floor has been assumed to be the flat-lying portion of the underlying chronosome and not the lowest point of the restricted chronosomes. The upper portion of the clinoform from which the upper height has been calculated has been picked as a flat-lying portion of the clinoform top parallel to the underlying stratal geometries (line 136-12 - Enclosure 3). In some cases it is problematic to define the top of the clinoform as the stratal geometries have associated tectonic dip associated with the loading of the shelf by the high sedimentation rates of chronosomes 64-98 (line 136-14 - Enclosure 3). In these cases a best estimate has been made at the inflection point where the underlying stratal geometries are seen to markedly increase.

6.4.2 Variations in clinoform slope angles through time

The median clinoform angles which have been calculated for the steepest sections of the mid-Oligocene to Recent clinoforms on lines 136-10–18 and 110-03 have been plotted against time to investigate the nature and timing of variations in clinoform slope angle (Figure 6.17). This plot demonstrates a progressive increase in calculated clinoform slope angles from a minimum at 35 Ma to a maximum around 12.5 Ma. This is followed by a decrease until 8 Ma after which a sharp increase is seen followed by a gradual decrease to the present day values. From Figure 6.17, it would appear that, in a general sense, the clinoform angle is following the sedimentation rate curve which shows steep clinoform angles occurring during periods of high sedimentation rates and low clinoform slope angles occurring during periods of low sedimentation rates. The calculated slope angle for a single chronosome on adjacent lines appears to vary along the length of the shelf as depicted by the large range in slope angles at a single chronosome age. The 3D-Chronostrat sections for lines 136-10 and 110-03 (Enclosure 3) show the present day slope to have differing morphologies along its length with line 136-10 showing a pronounced shelf break and 110-03 showing a gradual shelf to toe transition. There does not appear to be any systematic variation in the clinoform angles along the shelf for any particular clinoform. To resolve this uncertainty a higher density seismic grid with a closer line spacing than the current data set (15-25 km) would be required.

When Figure 6.17 is divided into periods of predominant shelfal progradation and aggradation, general trends in the data can be identified. The clinoform angles for the predominantly prograding set of sequences from T15-1 to N8-1 show a progressive increase in the range of clinoform angles from a narrow range of initially 2 – 4° to a range of 1.5–10° at the N8-1 sequence boundary. During the predominantly aggradational set of sequences between N8-1 and N10-N12-1, the range in clinoform slope angles is seen to decrease from a range of initially 2 – 11° to a range of 1.5 – 4° at the N10-N12-1 sequence boundary. The subsequent progradational set of sequences also shows a progressive increase in the slope angle of clinoforms as is especially evident on lines 136-12 & 13 (Figure 6.17). In this progradational phase of the shelf's growth, the range of clinoform slope angle increases from an initial range of 1.5–6° to a range of 2–10 ° at the N17-1 sequence boundary. The N17-1 event has been identified throughout the Dampier Sub-basin, and marks a pronounced change in the stratal architecture as has previously been discussed in Section 6.2.4. Associated with these changes in stratal geometry is a pronounced decrease in the clinoform angle where calculated angles can be seen to progressively decrease from a range of 2–10 ° at N17-1 to present day values of 1–2 ° (Figure 6.17).

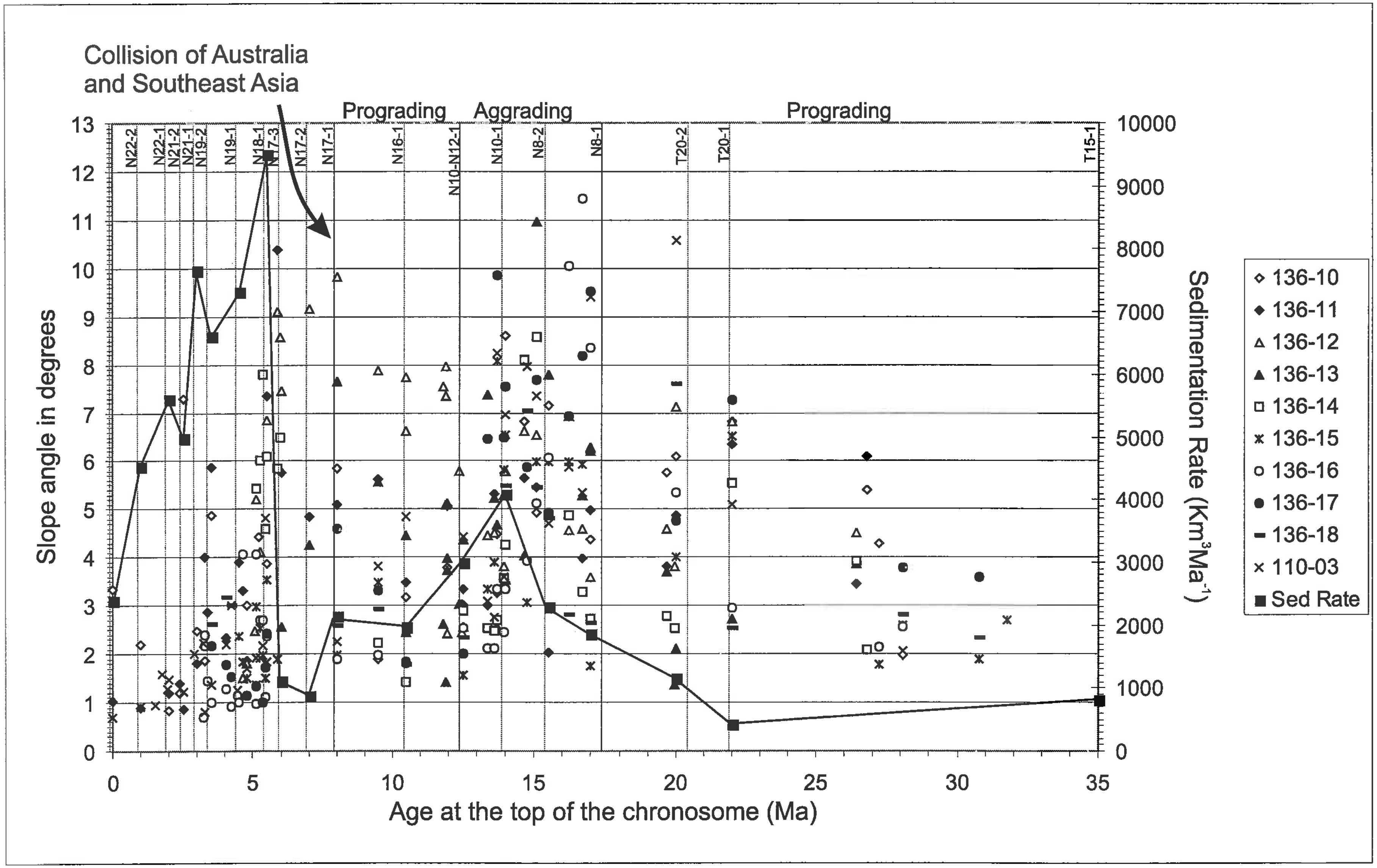

Figure 6.17 *Clinoform slope angles for the Oligocene to Recent section of the Dampier Sub-basin (lines 136-10 to 136-18).*

6.4.2.1 Controls on clinoform shape

The sequence-scale sedimentation rate calculated in Section 6.3.2 has also been overlain on Figure 6.17 to investigate the relationship between clinoform slope angle and calculated sedimentation rates and stratal architecture. Figure 6.17 shows a relationship between the angle of the clinoforms and the sedimentation rate curve. The two periods of high sedimentation rates at 6 Ma and 14 Ma correspond closely to the highest calculated slope angles in predominantly aggrading sections. Increasing sedimentation rates in the prograding sections correspond to increasing slope angles in both progradational sets of sequences whilst falling sedimentation rates correspond to decreasing slope angles as is seen in the later part of the N8-1--N10-N12-1 aggrading sequence and in the post N17-1 aggrading sediments.

It can be concluded that when the rate of accommodation space creation is low, the sequences deposited are predominantly progradational in nature and the slopes of the constituent clinoforms are seen to progressively increase through the sequence. In contrast, when the rate of accommodation space creation is high the sediments deposited are predominantly aggradational in nature and the slope of the constituent clinoforms is seen to progressively decrease. Kenter (1990) has shown that the angle to which a carbonate slope can build to and still remain stable is controlled by the nature of the carbonate sediment which builds the margin (Figure 6.18). However, the evidence presented in this thesis has shown that the style of margin developed is primarily controlled by the rate of creation of accommodation space. As we know that the type of carbonate sediment which builds low angle clinoforms is different from that which builds high angle clinoforms, it can be concluded that the rate of creation of accommodation space is controlling the type and nature of carbonate sedimentation in the Dampier Sub-basin.

6.4.3 Variations in clinoform height through time

Clinoform heights calculated for the mid-Oligocene to Recent chronosomes of the Dampier Sub-basin have been plotted against the age of the chronosomes to investigate variations in clinoform height through time (Figure 6.19). The predominantly progradational and aggradational periods of growth, which have been previously been identified from the stratal architecture, have again been indicated on the plot. Figure 6.19 demonstrates an overall increase in clinoform height from approximately 200-300 m during the mid-Oligocene to a maximum of 1200-1300 m at the end of the Miocene and a subsequent decrease in clinoform height until the present day values of 1000 m.

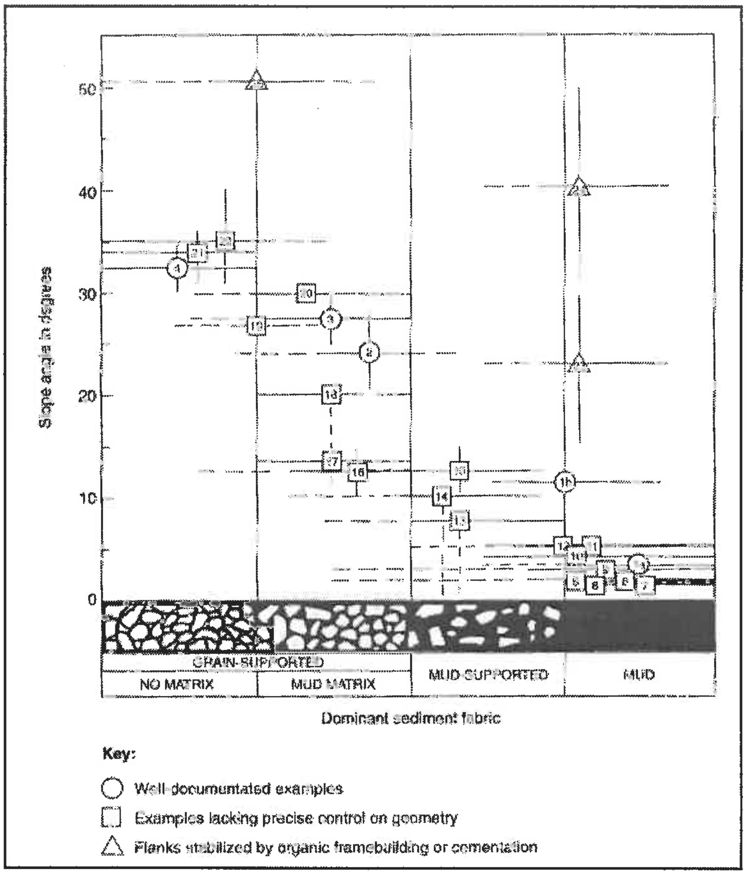

Figure 6.18 Relationship between slope angle and composition (Kenter, 1990).

The initial progradational section from 35 Ma to 17 Ma shows an initial rapid increase in clinoform height from 200-300 m at 35 Ma to 500-700 m at 26 Ma. This corresponds to the initial period of growth of the margin following the regional T15-1 mid-Oligocene event. The clinoform height remains in the order of 500-700 m throughout the remainder of the progradational T15-1–N8-1 sequence. During the aggradational N8-1–N10-N12-1 set of sequences, the clinoform height is seen to increase rapidly from 500-700 m at the start of the predominantly aggradational episode to 800-1200 m at the end of the set of sequences. Within this aggradational set of sequences some lower calculated clinoform heights have been recorded directly above the sequence boundaries, such as chronosomes 48-50. These correspond to the lowstand deposits following the sequence boundaries, which are clearly evident on the 3D-Chronostrat dip sections (Enclosure 3). There is a marked drop in calculated clinoform heights following the N10-N12-1 sequence boundary, again representing the deposition of a lowstand progradational unit following the deposition of chronosome 52, the last aggradational chronosome of the N10-1–N10-N12-1 set of sequences. The lowstand progradational nature of chronosomes 53-59 is evident on the 3D-Chronostrat section for line 136-12 (Figure 6.7).

In the portion of the Figure 6.19 representing clinoform growth following the N17-1 sequence boundary there is a wide variety of calculated clinoform heights. This is in part due to the large number of sequences and consequently lowstands that have been defined in the 3D-Chronostrat interpretation. However, it may also be due to inaccuracies in calculation of clinoform height due to an inability to define the basin floor correctly as many of the dip lines stop before the complete shelf top to basin floor profile is visible. The mean clinoform height for the late Miocene to Recent section a has been created and is presented on Figure 6.19. This plot clearly identifies lowstand sedimentation of chronosomes 69-71, 79-80, 87 and 94, which correspond to the N18-1, N19-1, N19-2 and N22-1 sequence boundaries respectively. The lowstand nature of these chronosomes can be confirmed from the 3D-Chronostrat section of line 110-03 (Figure 6.8). Figure 6.19 demonstrates a gradual decrease in clinoform height since the N17-1 sequence boundary with the tallest clinoforms occurring during sequences N18-1–N21-1 where heights of 1200 m have been calculated. This decreasing height of clinoforms corresponds to the decreasing sedimentation rate and decreasing slope angles also recorded over this period (Figure 6.19).

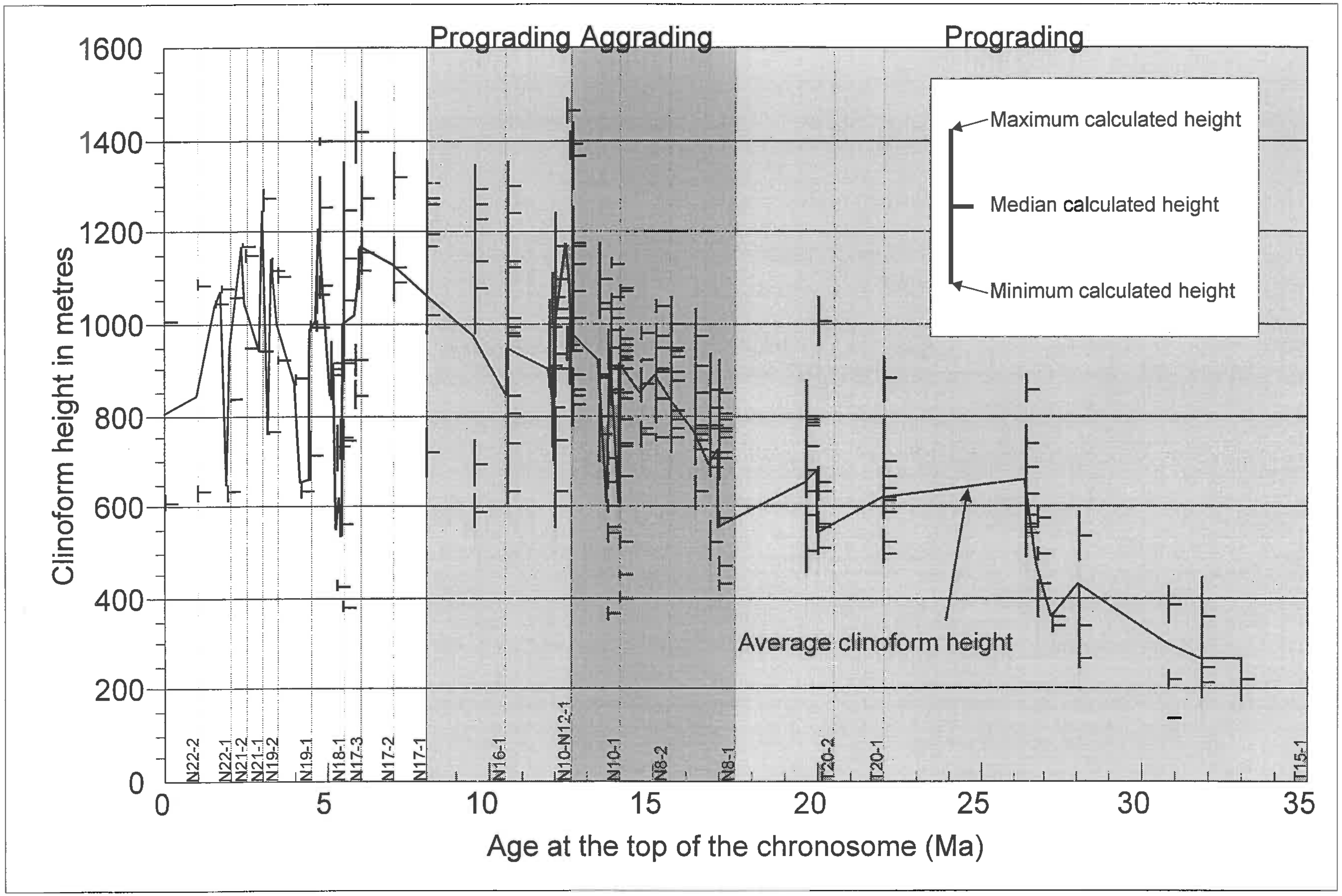

Figure 6.19 *Calculated clinoform height throught time for the Oligocene to Recent section of the Dampier Sub-basin (lines 136-10 to 136-18).*

CHAPTER 7 EVOLUTION OF THE ALBIAN TO RECENT SECTION OF THE DAMPIER SUB-BASIN

7.1 Introduction

The biostratigraphic, wireline, seismic and 3D-Chronostrat analysis has been used to subdivide the Albian to Recent section of the Dampier Sub-basin into a series of genetically-related units or sequences. For each of these sequences, a paleogeographic map has been produced as a means to summarise the environment at the time of deposition. These paleogeographic maps have been produced from a combination of sidewall core, cuttings, biostratigraphic and seismic data and are presented as Enclosure 4.

Figure 7.1 shows the chronostratigraphic framework detailing the sequence boundaries that have been defined for the Albian to Recent section of the Dampier Sub-basin from this study. Also indicated on Figure 7.1 are the eustatic curves of Haq *et al.* (1987) and the plate tectonic events which have affected the Australian Plate during this time, which have been summarised from Powell *et al.* (1988), Veevers *et al.* (1991), Baillie *et al.* (1994), Ross (1995), Mihut and Muller (1998) Muller *et al.* (1998).

7.1.1 Lithology determination

The lithology of each sidewall core is defined from the grain size of the constituent minerals and relative percentage of carbonate to siliciclastic grains within a sample. The lithologies used to describe sidewall cores samples in company reports in the Dampier Sub-basin are outlined in Table 7-1. Within the sand grain size in the carbonate regime, the percentage of quartz, skeletal, calcite and glauconite grains are defined where any of these grain types are present. Where these are significant these have been marked on the paleogeographic maps.

		>50%	>50%	>50%
% $CaCO_3$	Grain size	**Clay** (0 - 1/256mm)	**Silt** (1/256 - 1/16mm)	**Sand** (1/16 – 2mm)
>60%	**Carbonate**	Calcilutite	Calcisiltite	Calcarenite
40%<>60%	**Carb/clastic**	Marl		
<40%	**Siliciclastic**	Claystone	Siltstone	Sandstone

Table 7-1 Lithologies used to describe sidewall core samples for the Dampier Sub-basin.

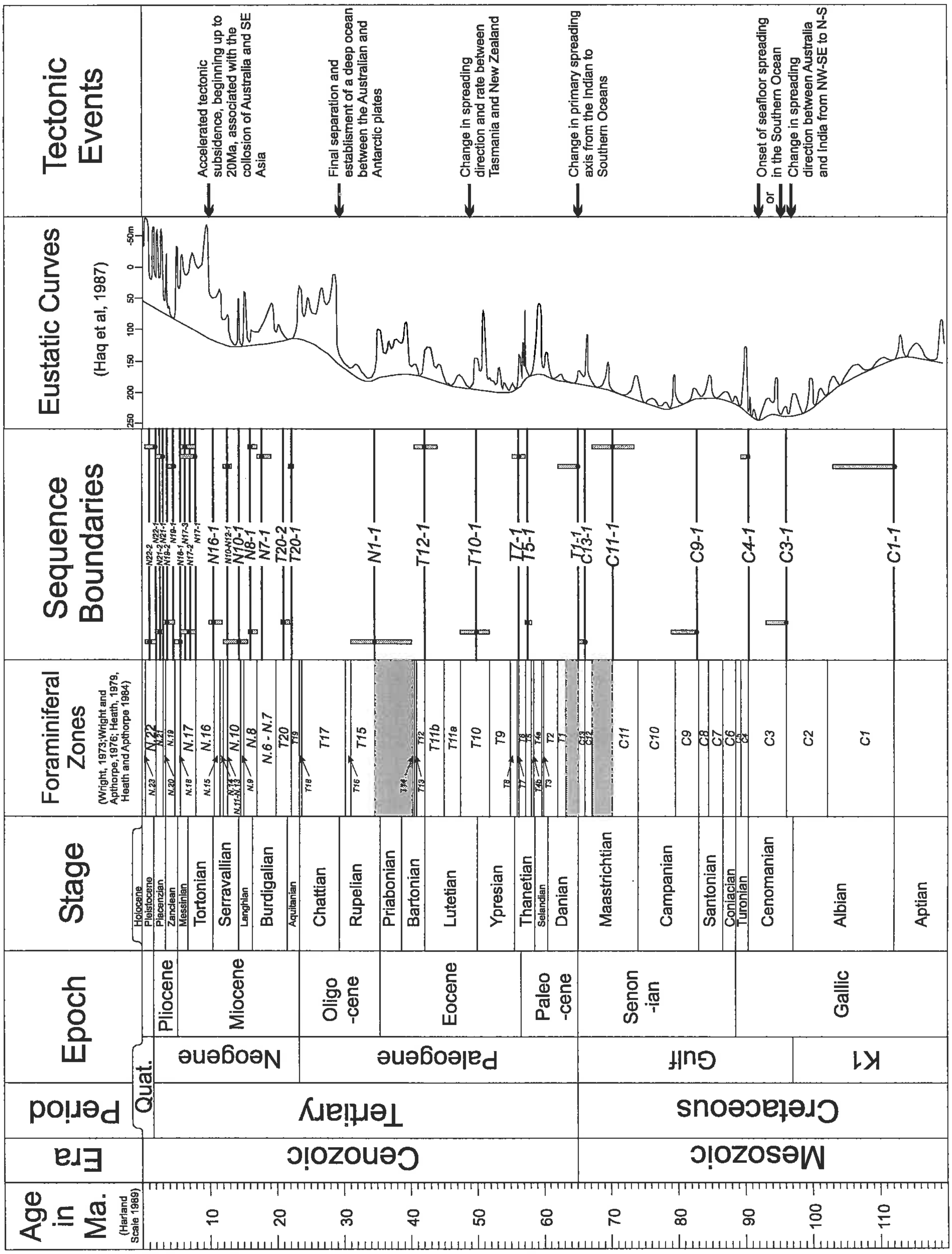

Figure 7.1 Chronostratigraphic framework for the Albian to Recent section of the Dampier Sub-basin with eustatic sea level curves and plate tectonic events. Error bars on sequence stratigraphic events have been defined from available biostratigraphic data.

The lithological description of the sidewall cores and the estimation of the relative percentage of the constituent minerals was conducted visually at the well site by several well site geologists. As the wells utilised in this study are of a range of ages, a variety of well site geologists have described the samples in the various wells and this has led to variation in sample description. Key sidewall cores from wells in this study area were described in the study and these descriptions compared with core reports. The correlation between the company sidewall core reports and the samples described independently was good and this increased confidence in the use of company core reports.

7.2 Cretaceous evolution

The Albian to Maastrichtian sediments of the Dampier Sub-basin were deposited during a period of thermal subsidence in a passive margin setting following the intra-Valanginian rifting of Greater India from Australia (Mihut and Muller, 1998; Muller *et al.*, 1998). Within Albian to Maastrichtian section of the Dampier Sub-basin, the following sequences have been defined - C1-1–C3-1, C3-1–C4-1, C4-1–C9-1, C9-1–C11-1, C11-1–C13-1 and C13-1–T1-1. Lithologically these sequences are composed of a series of fine-grained mixed clastic and carbonate sediments, the percentage of which can be seen to vary through the section.

7.2.1 Albian to Santonian sequences (C1-1 to C9-1)

The isochron maps for the Albian to Santonian sequences of the Dampier Sub-basin (C1-1 to C9-1) show pronounced sediment thickening along a northeast-southwest central axis between lines 101-02R and 136-24 (Enclosure 2), as has been discussed in Chapter 5. The thickest parts of these sequences correspond to the location of the underlying Lewis Trough with only thin sedimentation existing beyond it. Dip lines across the basin have been flattened on the base Tertiary T1-1 reflector to investigate the stratal architecture of the Cretaceous sequences without the complication of Tertiary structuring. Figure 7.2 displays line 136-11 flattened on the T1-1 horizon and demonstrates pronounced thickening of the C1-1 to C9-1 sequences into the Lewis Trough with only minor sedimentation extending beyond it. It is interpreted that during the deposition of these sequences, sediments were being trapped in the Lewis Trough as it continued to subside, possibly as a response to sediment loading and compaction. Within the area of the study, the Albian – Santonian sequences (C1-1–C9-1) have characteristic log signatures (Figure 7.3).

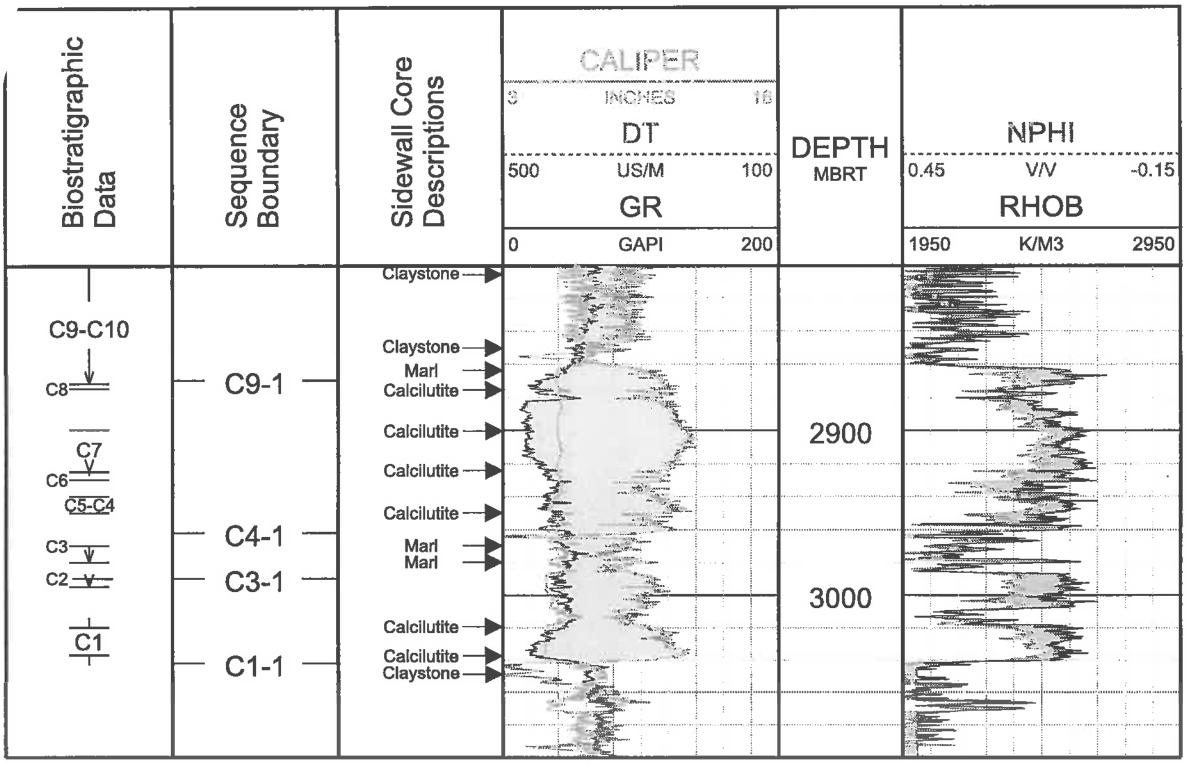

Figure 7.3 Wireline log signature and associated lithotypes for the Albian to Santonian sequences of the Dampier Sub-basin.

The oldest sequence of the study, C1-1–C3-1, is Albian to Cenomanian in age and represented by a mixture of fine-grained siliciclastic and carbonate lithologies. Along the Rosemary Fault, the sequence is dominated by claystones whilst further into the basin, the sequence is characterised by calcilutites which are overlain by marls towards the end of the sequence (Enclosure 4). Environmental interpretations for this sequence suggest the wells along the Rosemary Fault are of inner shelf depths whilst those in more basinward localities are of outer shelf to slope depths.

The subsequent C3-1–C4-1 sequence is also represented by predominantly fine-grained lithologies. As before, an increase in carbonate content of the mud rocks is evident in a basinward direction with claystones being typical of the proximal area along the Rosemary Fault System, and marls being typical of more basinal localities (Enclosure 4). Carbonate-dominated lithologies have been recorded within the C3-1–C4-1 sequence at Malus-1, Bounty-1 and Finucane-1. Without further information, it is not possible to decipher whether these are localised anomalies or regional features.

Both the C3-1 and C4-1 events are seen to bring increased concentrations of fine-grained siliciclastic muds into the basin. Biostratigraphic data suggest that outer shelf to upper slope environments existed in the area of the Rankin Trend during the Albian to Santonian. The Turonian C4-1 sequence boundary is seen to onlap onto the Rankin Trend (Figure 7.2). However, sediment of C3-1–C4-1 age has been identified in Brigadier-1 and Gandara-1 (Figure 4.2), suggesting that the C4-1 sequence boundary does exist in these locations and it merely falls below seismic resolution on the Rankin Trend. The apparent onlap of C4-1 along the Rankin Trend is therefore actually a condensed section, which appears to onlap as the sequence becomes thin and falls below seismic resolution. The alternative interpretation for this event is an erosional event which has removed the C3-1–C4-1 sequence, leaving only a thin remnant over the Rankin Trend. Romine *et al.* (1997) cite the presence of a Turonian angular unconformity on the Rankin Platform which they have interpreted to be related to a period of mild inversion and uplift within the area between the Barrow and Dampier Sub-basins. However, data from this study show no evidence of an angular unconformity at the C4-1 sequence boundary (Figure 5.3 and Figure 5.8) and biostratigraphic data indicate slope depths at this stage. The combination of these two lines of evidence suggests the presence of a condensed section rather than an angular unconformity.

The following C4-1–C9-1 sequence records a change to more carbonate-dominated fine-grained sediments. Many of the wells record an initial phase of fine-grained clastic sedimentation, which was progressively replaced by fine-grained carbonate deposition (in the form of calcilutites) across the whole basin (Enclosure 4). These widespread, fine-grained, carbonate lithologies are represented in some places by the lithotype described as the Toolonga Calcilutite.

Faulting on the Rankin Trend is seen to die out in two phases as has previously been discussed in Chapter 4 – one phase at the base Campanian C9-1 event and the other at the base Tertiary T1-1 event. Movement on the Rosemary Fault system and faults of the Enderby platform can also be seen to terminate against the base Campanian C9-1 event (Figrue 7.4). Fault movement of this age on both margins of the Lewis Trough supports the interpretation of active subsidence occurring in the Lewis Trough during the deposition of the Albian to Santonian sequences.

7.2.1.1 Summary

Overall, the Albian to Santonian sequences record an upward increase in carbonate content, reaching a maximum at the end of the Santonian with the widespread deposition of fine-grained carbonates, which are in some places represented by the Toolonga Calcilutite lithofacies. These lithological variations of an upward increase in carbonate content punctuated by short-lived siliciclastic-dominated episodes following interpreted sequence boundaries may indicate a period of prolonged relative sea level rise. Environmental interpretation from biostratigraphic data indicates a progressive deepening of the environment from shelfal depths (0-200 m) during Albian to outer shelf to continental slope depths (200-1000 m) at the end of the Santonian. During these sequences, the shoreline would have been located to the southeast of the study area and would have been progressively migrating in a landward direction on to the craton. The absence of any coarse-grained sediments or angular seismic unconformities suggest that no sub-aerial exposure was associated with the C1-1, C3-1, and C4-1 or C9-1 sequence boundaries in the region of this study.

The sequence boundaries of Cenomanian (C3-1) and Turonian (C4-1) age appear to correspond to regional plate tectonic events. Continental extension between Australia and Antarctica began in the late Jurassic but it was not until a major shift in spreading direction occurred in the Indian Ocean that sea-floor spreading began in the Southern Ocean (Baillie *et al.*, 1994; Powell *et al.*, 1988). Veevers *et al.* (1991) date this event to be of base Cenomanian age (96 Ma) whilst Ross (1995) favours a late Cenomanian – Turonian age (92 Ma). Romine *et al.* (1997) have identified a significant fall in relative sea level of Turonian age within the Northern Carnarvon Basin which they have associated with the initiation of spreading in the Southern Ocean thus favouring a Turonian age for the event. This study has identified two discrete events, one of base Cenomanian (96 Ma) and one of Turonian (92 Ma) age. It may be the case that the change in spreading direction identified in the Indian Ocean was not contemporaneous with the onset of sea floor spreading in the Southern Ocean, as has been assumed. The base Cenomanian event (C3-1) identified during this study may therefore represent the initial change of spreading direction in the Indian Ocean whilst the Turonian event (C4-1) may represent the initiation of spreading in the Southern Ocean.

7.2.2 Campanian and Maastrichtian sequences (C9-1 to T1-1)

At the end of the Santonian, a more extensive relative sea level fall caused the cessation of carbonate deposition and a return of clastic-dominated deposition to the Dampier Sub-basin. This event has been termed C9-1 and can be easily recognised on seismic data by a high amplitude reflector (Figure 7.2). Other studies of the Dampier Sub-basin have also identified an end-Santonian event (Apthorpe, 1988; Rasidi, 1995; Romine *et al.*, 1997). In the study by Romine *at al.* (1997), the end-Santonian event marks the boundary between the transgressive and regressive phases of the 'Cretaceous-Tertiary Megasequence'. Based on biofacies preserved on either side of this boundary, Apthorpe (1979) has interpreted a fall in relative sea level of 70-100m across the end Santonian boundary.

The Campanian and Maastrichtian sequences of the Dampier Sub-basin are composed of a series of progradational siliciclastic units that built into the basin following the end-Santonian relative sea level fall and associated sequence boundary. Within the Campanian and Maastrichtian sequences, sequence boundaries of Campanian (C9-1), mid-Maastrichtian (C11-1) and late Maastrichtian (C13-1) have been identified and correlated.

The first Campanian sequence, C9-1–C11-1, is composed of an area of thick, prograding clinoforms in the southwest corner of the study area (Enclosure 4). Seismic lines through this section show the progradational nature of the sequence with a series of downlapping foresets and parallel to sub-parallel topsets (Figure 7.4). Of the wells that have been drilled in the Dampier Sub-basin, the majority have only intersected the distal edge of the thick prograding section. Of the few wells that do penetrate the thick prograding section of this sequence, sample recovery has been extremely poor. The thickest sections of the prograding part of the C9-1–C11-1 sequence, which have been intercepted at Rosemary-1, are composed of glauconitic, argillaceous sandstones separated by a thin claystone section. The thickness of the progradational unit (up to 1000 m (Rasidi, 1995)) implies the water depth in the Dampier Sub-basin during deposition of this sequence was considerable. These progrades grade distally into thin claystones and become progressively marl dominated in a northerly direction. The isochron map for the sequence shows up to 700 ms of sediment on line 101-08 at the southern end of the study area (Enclosure 2). In some of the study wells, the fine-grained carbonates which characterised late-Santonian sedimentation are seen to persist into the lower part of the C9-1–C11-1 sequence. An upward decrease in carbonate content progressively replaces the calcilutites, firstly by marls and subsequently by claystones within the C9-1–C11-1 sequence. This change in lithotype has a characteristic wireline log signature, which is demonstrated in Figure 7.3.

Seismic dip sections through the C9-1–C11-1 sequence record thickening of the sequence into the Lewis Trough (Figure 7.2 and Figure 7.4), suggesting it still acted as a sediment sink during the Campanian. However, the isochron map for the C9-1–C11-1 sequence records the first significant accumulation of sediment beyond the confines of the Lewis Trough (Enclosure 2). The mid-Maastrichtian C11-1 event, which constitutes the upper limit of the C9-1–C11-1 sequence, has been defined primarily from wireline data and by correlation with the Barrow Sub-basin (Young, in prep). The wireline logs record an upward decrease in gamma values and a break in the sonic trends which represent an influx in coarser-grained sediments associated with an interpreted relative sea level fall (Figure 7.5). Biostratigraphic data shows this relative sea level fall does not remove significant amounts of section and occurs within sediments of the C11 biozone.

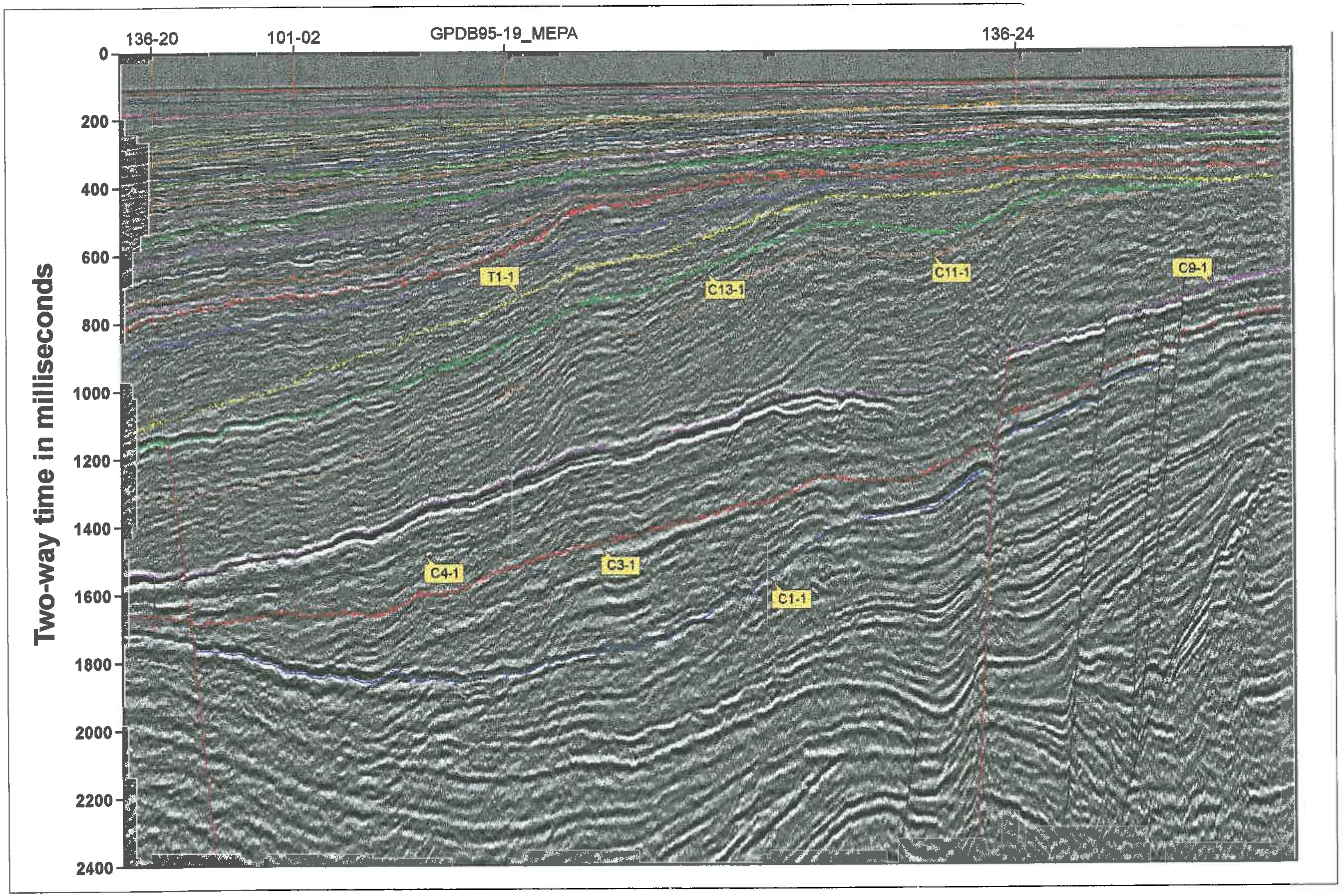

Figure 7.4 Line 136-11 showing the progradational nature of the Campanian C9-1 to C11-1 sequence. (Line length 43.5 km)

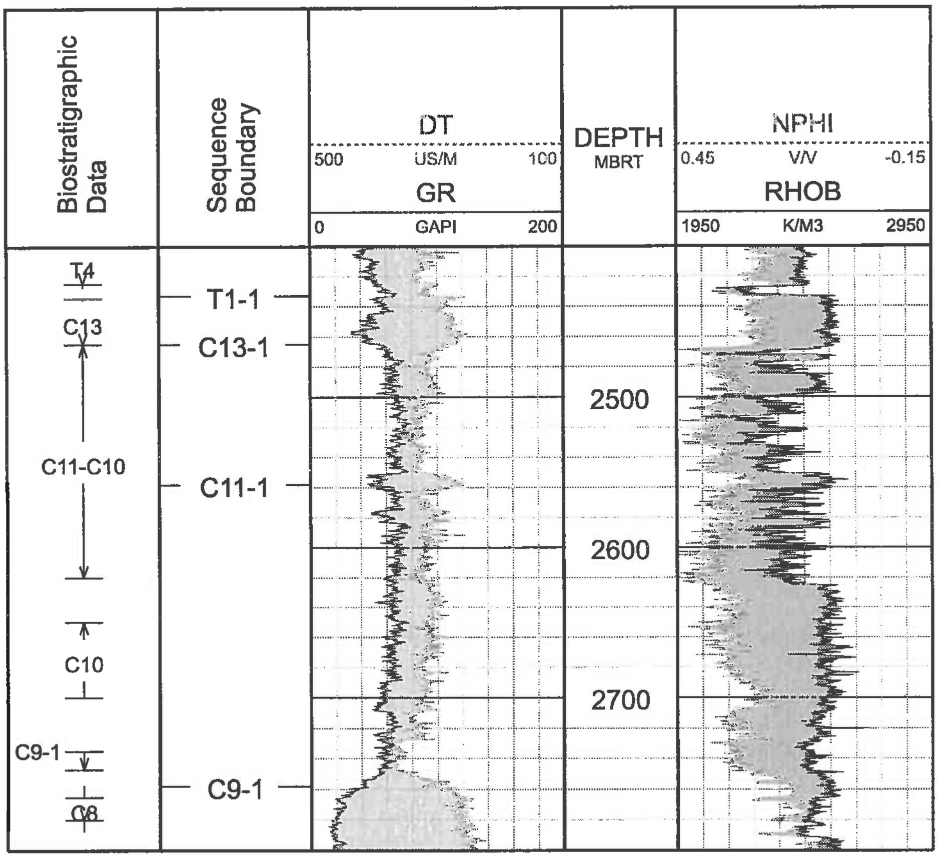

Figure 7.5 Wireline log response of the mid-Maastrichtian C11-1 sequence boundary

The isochron maps for the Maastrichtian C11-1–C13-1 and C13-1–T1-1 sequences (Enclosure 2) both show the thickest sediment accumulation in the southwest corner of the study area immediately adjacent to the C9-1–C11-1 progradational wedge. Similar to the C9-1–C11-1 sequence, the paleogeographic maps for both Maastrichtian sequences (Enclosure 4) show more clastic-rich sedimentation around the thickest part of the sequence with increasing carbonate content in a distal direction. The isochron and paleogeographic maps for both these sequences indicate that there are no other significant sediment input points into the basin at this time. However, siltstones encountered at Talisman-1 (Enclosure 4) may represent a secondary input point. The thickness and lithological distributions of the C9-1 to T1-1 sequences suggest that the siliciclastic source, which became established in the southwest corner of the study following the end-Santonian relative sea level fall, persisted throughout the Campanian and Maastrichtian. From the isochron maps of the C11-1–C13-1 and C13-1–T1-1, sequences it is apparent that the thickest parts of these sequences are located at the front of the thick prograding section of the underlying C9-1–C11-1 sequence. It is uncertain whether this sediment source is related to uplift at the southern end of the Enderby Platform or reorganisation of pre-existing drainage patterns associated with the relative fall in sea level. Romine *et al.* (1997) have identified a series of relay ramps which focussed sediment from the Robe, Fortescue and Yule rivers into the Barrow Sub-basin whilst by-passing the Dampier Sub-basin during the Valanginian to

Aptian (Figure 1.4). It is possible that this mechanism persisted until the Campanian when sediment input became focussed on the Dampier Sub-basin.

The Maastrichtian C11-1–C13-1 sequence is dominated by claystones in the area landward of the Rankin Trend and marls in area basinward of the Rankin Trend (Enclosure 4). In both Pueblo-1 and Talisman-1, coarser-grained siliciclastic sedimentation is recorded within the C11-1–C13-1 sequence. At Pueblo-1, the coarse sand occurs directly above the C11-1 sequence boundary and is therefore interpreted as a basin floor fan situated at the toe of the underlying C9-1–C11-1 prograding wedge. The possibility exists for other such fans along the front of the underlying prograding wedge.

The late Maastrichtian C13-1 event has been defined primarily from biostratigraphic data and a pronounced wireline log break where the majority of the wells in the study record the absence of sediments from biozone C12. (Figure 7.5). Romine *et al.* (1997) have identified a mid-Maastrichtian event which has been placed at the top of biozone C11. Ross (1995) also identifies a late Cretaceous event of mid-Maastrichtian age that has a poorly constrained age of 78.1 Ma and has been related to a change in spreading direction in the Indian and Southern Oceans. This age date in fact places the event in the middle of the Campanian and why this was interpreted by Ross (1995) as a mid-Maastrichtian event is unclear. The isochron map for the C13-1–T1-1 sequence records the absence of the sediments of these age from wells at the southern end of the Rankin Trend (Enclosure 2). The absence of C13-aged sediments at this location has been identified from biostratigraphic and wireline data (Figure 4.2). In this location, the base Tertiary T1-1 event has removed the late Maastrichtian C13 sediment. On seismic sections, the responses of the C13-1 and T1-1 events commonly coincide to form a single high amplitude reflector basinward of the Rankin Trend as the sequence is thin and below seismic resolution in this area. In the area where the C13-1–T1-1 sediments are absent, no high amplitude reflector is observed as is evident in Figure 7.2. Minor uplift on the Rankin Trend late in the Maastrichtian has been interpreted to cause the erosion of the C13-1–T1-1 sediments. Biostratigraphic data from Bounty-1, Delambre-1 and Talisman-1 in both the C13-1–T1-1 and the first Paleocene T1-1–T5-1 sequences indicate an outer shelf (120-200 m) environment. The absence of C13-1–T1-1 sediments at the southern end of the Rankin Trend is suspected to be result of submarine erosion and not subaerial erosion as sediments both above and below the boundary are of outer shelf origin.

7.3 Paleocene and Eocene evolution

In the Dampier Sub-basin, the base Tertiary is represented by a widespread erosional event which results from the collision between India and Asia and the associated relocation of the primary spreading axis from the Indian to the Southern Ocean (Mihut and Muller, 1998; Muller *et al.*, 1998). This change in primary spreading axis resulted in the northward migration of Australia into lower latitudes and the progressive change from siliciclastic to carbonate-dominated sedimentation in the

Dampier Sub-basin. From the late Eocene until the present day, sedimentation in the Dampier Sub-basin has been carbonate dominated. Within the Paleocene and Eocene sediments of the Dampier Sub-basin two Paleocene (T1-1–T5-1 and T5-1–T7-1) and three Eocene sequences (T7-1–T10-1, T10-1–T12-1 and T12-1–T15-1) have been defined.

Biostratigraphic evidence shows the base Tertiary event to be diachronous in age removing all T1 to T3 aged sediments in some wells, whilst other wells record Danian (T1) sediments directly above Maastrichtian (C13) aged sediments. It is interpreted that sedimentation resumed in some parts of the Dampier Sub-basin during the Danian (T1) but it was not until the Selandian that the first significant flood occurred over the whole basin and deposited widespread T4 sediments.

7.3.1 Paleocene sequences (T1-1 to T7-1)

The initial phase of Tertiary sedimentation within the Dampier Sub-basin occurred as a pulse of clastic-dominated deposition typified by fine-grained sand and siltstones in the inner margins which grade distally into claystones and minor marls (Enclosure 4). Glauconite has also been identified in the fine-grained siltstones and sandstones in both Legendre-1 and Talisman-1. These lithologies represent shallower water facies than those present in the underlying C13-1–T1-1 sequence. The isochron maps for the Paleocene T1-1–T5-1 sequence (Enclosure 2) show sedimentation concentrated in the southwestern corner of the study, suggesting the siliciclastic source which was present during the Campanian and Maastrichtian and persisted into the Paleocene. However, in contrast to the Campanian and Maastrichtian sequences, T1-1–T5-1 does show sediment thickening in other areas of the basin (Enclosure 2). Chronosome thickness maps for sequences C9-1 to T5-1 demonstrate the progressive accumulation of sediment in the southwest corner of the study area following an initial phase of sedimentation in the northeast of the study (chronosomes 7-16 on Figure 6.2). On these maps, the Paleocene T1-1–T5-1 sequence is represented by chronosomes 15 and 16. The chronosome maps demonstrate that the sequence thickening in the southwest of the study area identified from the isochron map predates the other episodes of T1-1–T5-1 thickening. This observation supports the theory of the continuation of the siliciclastic sediment source from the southwest corner of the study area.

The second Paleocene sequence, T5-1–T7-1, shows localised thickening along a northeast-southwest trend over the Rankin Platform (Enclosure 2). Some thickening does occur in the southwest corner of the study area but it would appear that the sediment source which has persisted in this area since the Campanian no longer supplies sediment to the Dampier Sub-basin. This sequence is characterised by siltstones and sandstones in wells on the Rosemary Fault and in Pueblo-1 and Miller-1, with claystones and marls deposited over the remainder of the basin. Overall, this sequence shows an increase in the percentage of fine-grained sediments compared to the preceding T1-1–T5-1 sequence.

Environmental interpretations which exist for Bounty-1, Gandara-1 and Talisman-1 all record an increase in water depth between the T1-1–T5-1 and T5-1–T7-1 sequences. The lithological and environmental data suggest an overall increase in water depth during the Paleocene of the Dampier Sub-basin.

7.3.2 Paleocene - Eocene boundary

The base of the Eocene section of the Dampier Sub-basin is marked by the T7-1 event. This event is a diachronous erosive surface, which removes variable amounts of Paleocene and Eocene sediments across the whole of the basin as has previously been discussed in Chapter 4. A base-Eocene event has been identified in all wells from the Northern Carnarvon to Browse basins on the North West Shelf by Apthorpe (1988). Romine *et al.* (1997) also identify a base-Eocene event on a summary diagram of sequence boundaries but its nature or presence is not discussed in the text. In the Dampier Sub-basin, slope faunas have been identified in claystones both above and below the boundary. Where the event has been cored in Dampier-1, it is marked by a hard-ground surface with large burrows filled with muddy sand containing planktonic foraminifera (Apthorpe, 1988). Biostratigraphic evidence from Bounty-1 defines the sediments of the T5-1–T7-1 sequence to be of slope origin and sediments of the overlying T7-1–T10-1 sequence to be of upper slope origin, implying water depths of more than 300 m in both cases. The combination of evidence from both the boundary itself and the nature of the faunal assemblages and lithotypes of sediment above and below the event suggest it is submarine in origin. However, it does bring an influx of coarser-grained sediments into the basin, suggesting it is associated with a relative sea level fall and is therefore defined as a sequence boundary.

7.3.3 Eocene sequences (T7-1 to T15-1)

Within the Eocene section of the Dampier Sub-basin, three sequences have been defined and been correlated throughout the basin on the basis of biostratigraphic, wireline log and seismic data: T7-1–T10-1; T10-1–T12-1 and T12-1–T15-1. These sequences record the change from clastic to carbonate-dominated sedimentation in the Dampier Sub-basin. The isochron maps for these sequences show them to be relatively thin and of constant thickness across most of the study area with some localised thickening (up to 200 ms) in the area between Madeleine-1 and Talisman-1 (Enclosure 2).

Sediments of the first Eocene sequence, T7-1–T10-1, are composed of a mixture of sandstones and siltstones along the Rosemary Fault and a mixture of claystones, marls and minor siltstones over the majority of the basin with calcilutites in distal wells (Enclosure 4). The isochron map for the T7-1–T10-1 sequence shows two episodes of thickening, one between Talisman-1 and Legendre-1 and the other on the Rankin Trend between Goodwyn-8 and Finucane-1 (Enclosure 2). The paleogeographic maps show the thickening around Talisman-1 to be composed predominantly of sandstones and siltstones, and the thickening along the Rankin Trend to be composed of marls, claystones and minor siltstones. The chronosome maps for the T7-1–T10-1 sequence, (chronosomes 19 & 20 in Figure 6.2) shows that thickening along the Rankin Trend predates the localised thickening between Talisman-1 and Legendre-1. Apthorpe (1988) has interpreted the siltstones and sandstones of Eocene age in Talisman-1, Nelson Rocks-1 and Legendre-1 to be part of an Eocene delta. The quality of seismic data through this section is not good but nevertheless, downlapping foreset and parallel topset beds can be identified on lines flattened on the underlying T7-1 sequence boundary (Figure 7.7). The stratal architecture, lithology and sediment thickness distribution of the T7-1–T10-1 sequence all support the interpretation of an Eocene delta.

Within the sediments of the T7-1–T10-1 sequence Apthorpe (1988) has identified a rapid cooling in oceanic temperatures of T9 age from the nature of the faunal assemblage present and an observed increase in continental-derived sediment. This pronounced change in sediment type is reflected by a characteristic log character, showing a decrease in the gamma and sonic values (Figure 7.6). The 3D-Chronostrat analysis showed the mud-dominated thickening on the Rankin Trend to predate the delta forming around Talsiman-1. It is probable that the delta formation is associated with the cooling and increase in terrestrial sediment identified by Apthorpe (1988).

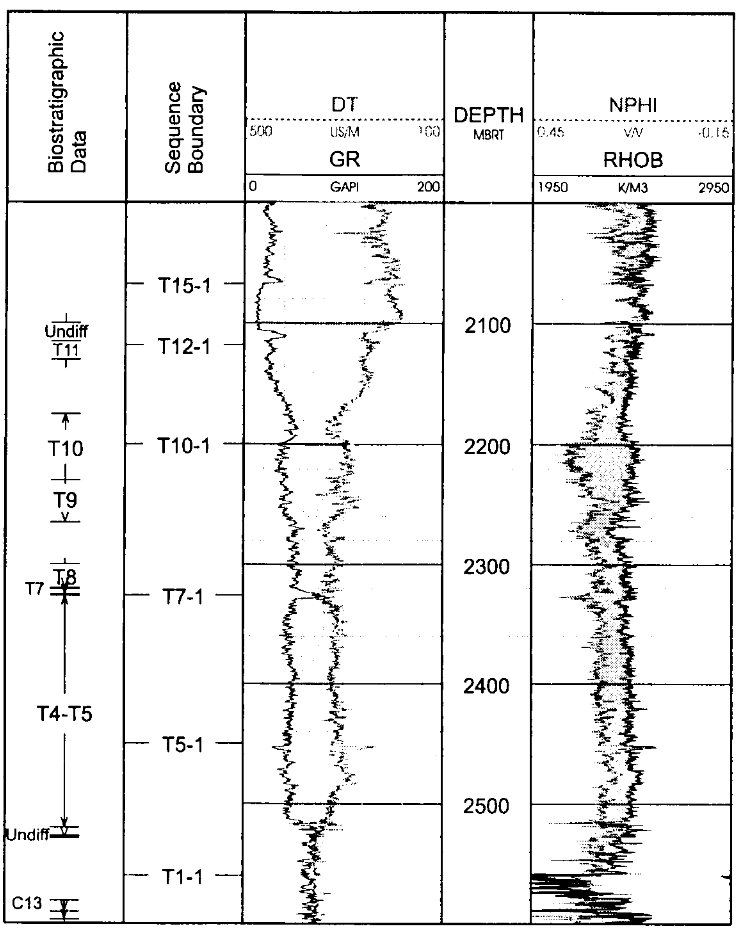

Figure 7.6 Paleocene and Eocene section of Miller-1.

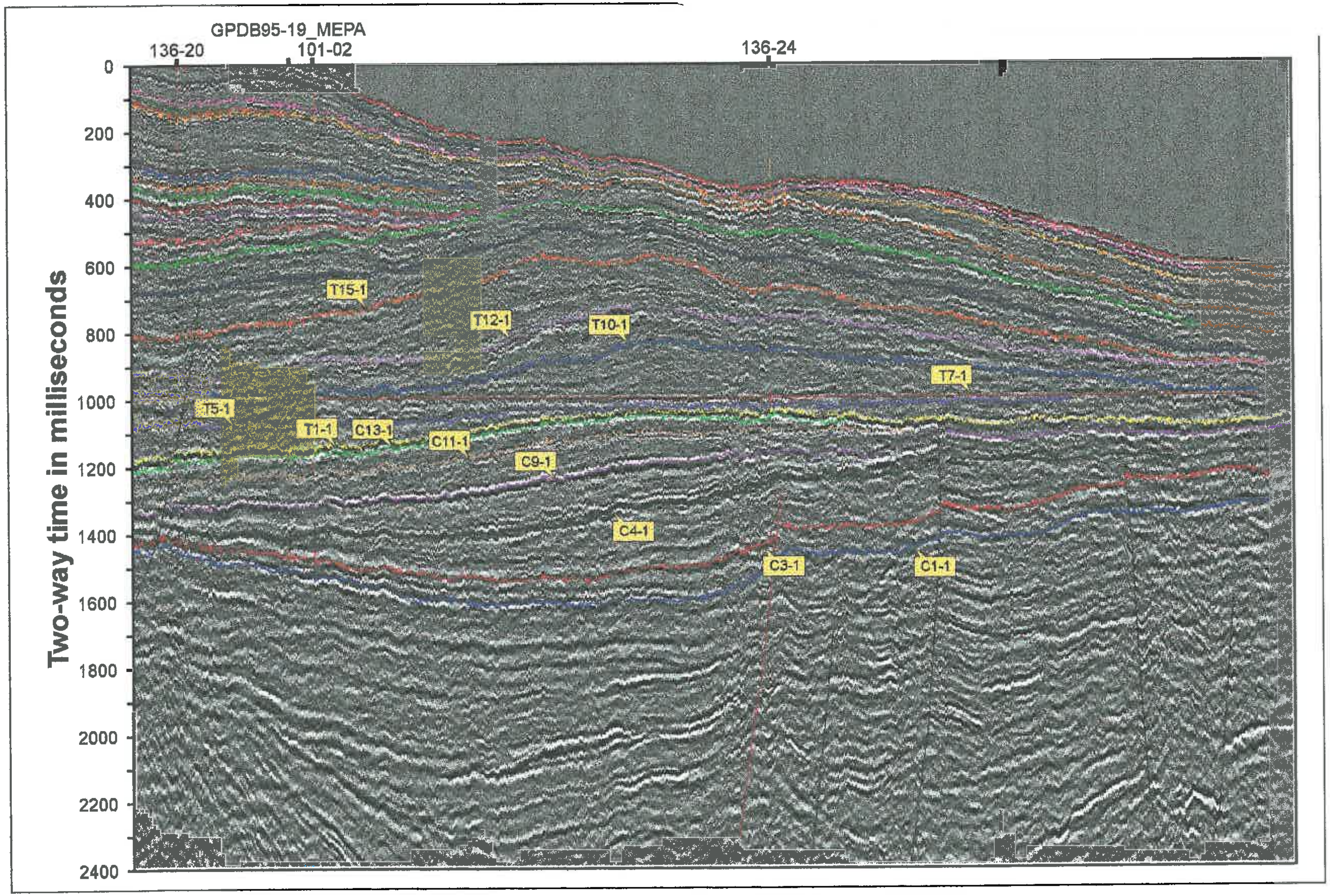

Figure 7.7 *Line 136-14 flattened on the base Eocene T7-1 sequence boundary displaying the progradational nature of the T7-1 to T10-1 sequence.*

The T10-1 event, which defines the top of the T7-1–T10-1 sequence, is of variable extent throughout the basin. In some wells, several of the mid-Eocene biozones are absent and a pronounced log break is evident, whilst in other wells, a complete Eocene section is preserved and no log break is evident. The varying nature of this event has been discussed in more detail in Chapter 3. Spreading between Tasmania and New Zealand began during the Paleocene and deposition of the T7-1–T10-1 sequence began and continued until a subsequent change in spreading direction and increase in spreading rates occurred at 49 Ma (Veevers, 1991). This change in spreading direction and rate corresponds to the mid-Eocene T10-1 sequence boundary that has been identified in this study.

The mid-Eocene T10-1–T12-1 sequence is characterised by an upward increase in carbonate content which is reflected in the gamma log profile of the wells of the study (Figure 7.8). Lithologically, the sequence is composed of siltstones and sandstones along the Rosemary Fault and a mixture of marls and calcilutites over the remainder of the basin with some additional siltstones and sandstones at the southern end of the Rankin Trend (Enclosure 4). The isochron map for the middle Eocene T10-1–T12-1 sequence records thickening immediately offset to the southwest of the underlying T7-1–T10-1 delta (Enclosure 2). The paleogeographic maps show the sequence to be characterised by siltstones inter-bedded with sandstone at this location. The thickest part of the sequence is intersected at Orion-1 but unfortunately, hole problems have prevented the recovery of samples from the majority of the Paleocene and Eocene section. The Eocene section of the gamma log from Orion-1 shows an upward-decreasing trend typical of that for a prograding delta (760-820 m, Figure 7.9). The chronosome maps for the T10-1–T12-1 sequence (chronosomes 21 & 22, Figure 6.3) suggest that the localised thickening around Orion-1 predates basin-wide sedimentation of chronosome 22. Progradational geometries can again be identified on seismic through the thickest section of the T10-1–T12-1 sequence (Figure 7.10). The thickening of the T10-1–T12-1 sequence in this location is therefore interpreted to be a continuation of the delta which began forming during the early Eocene. Chronosome 22 (Figure 6.3) shows minor thickening in the region of the interpreted delta, implying that the source of sediment for the delta either ceased or moved out of the study area towards the end of sequence T10-1–T12-1. Over the remainder of the basin, this sequence is characterised by fine-grained carbonate muds, marls and some siltstones and claystones at the southern end of the Rankin Trend (Enclosure 4). Both the isochron map (Enclosure 2) and the thickness map for chronosome 22 (Figure 6.3) display thickening of the T10-1–T12-1 sequence in Parker-1, Dixon-1, Lowendal-1 and Wilcox-1. Lithologically, the wells are represented by a series of claystones, marls, sandstones and siltstones. These thickness patterns suggest the possibility of another terrestrial input point to the basin at this location but without further information from the Barrow Sub-basin, the origin of these sediments must remain conjectural.

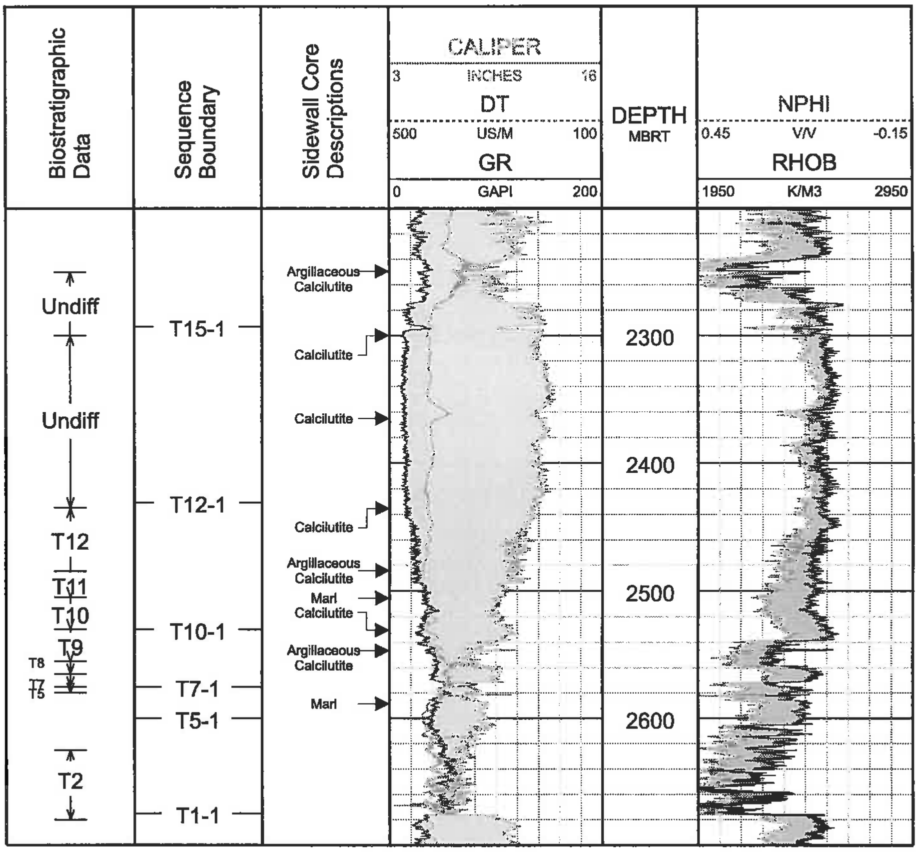

Figure 7.8 Wireline log and lithology response of T7-1 to T15-1 sequences in Gandara-1

The final Eocene sequence, T12-1–T15-1, records the transition from siliciclastic to carbonate-dominated sedimentation within the Dampier Sub-basin. Many of the wells in the study record initial siliciclastic-dominated sedimentation, which becomes progressively carbonate-dominated. The paleogeographic map for this sequence shows that it is composed of calcilutites in the outer shelf areas, a mixture of calcisiltites in the mid-shelf, and calcarenites in the inner shelf (Enclosure 4). The isochron map for the sequence shows a discrete episode of thickening in the area bounded by Wanaea-1, Finucane-1, Talisman-1 and Samson-1, which unfortunately none of the study wells intersect (Enclosure 2). On seismic, this early part of the sequence appears to downlap onto the basal T12-1 sequence boundary (Figure 7.10). The chronosome thickness maps show the sedimentation of the early part of the T12-1–T15-1 (chronosome 23) sequence to be restricted to an area landward of the Rankin Trend whilst sedimentation of the remainder of the sequence (chronosome 24) persists across the whole basin (Figure 6.3). It is interpreted that the early part of the sequence is a continuation of the siliciclastic deposition, which characterised the underlying Eocene sequences. A change in environmental conditions resulted in the deposition of carbonate-dominated lithologies for the remainder of the sequence. The absence of siliciclastic sediment in the later part of the T12-1–T15-1 sequence and the deposition of constant thickness carbonate sediment suggest a rise in sea level has accompanied the change to warmer latitudes.

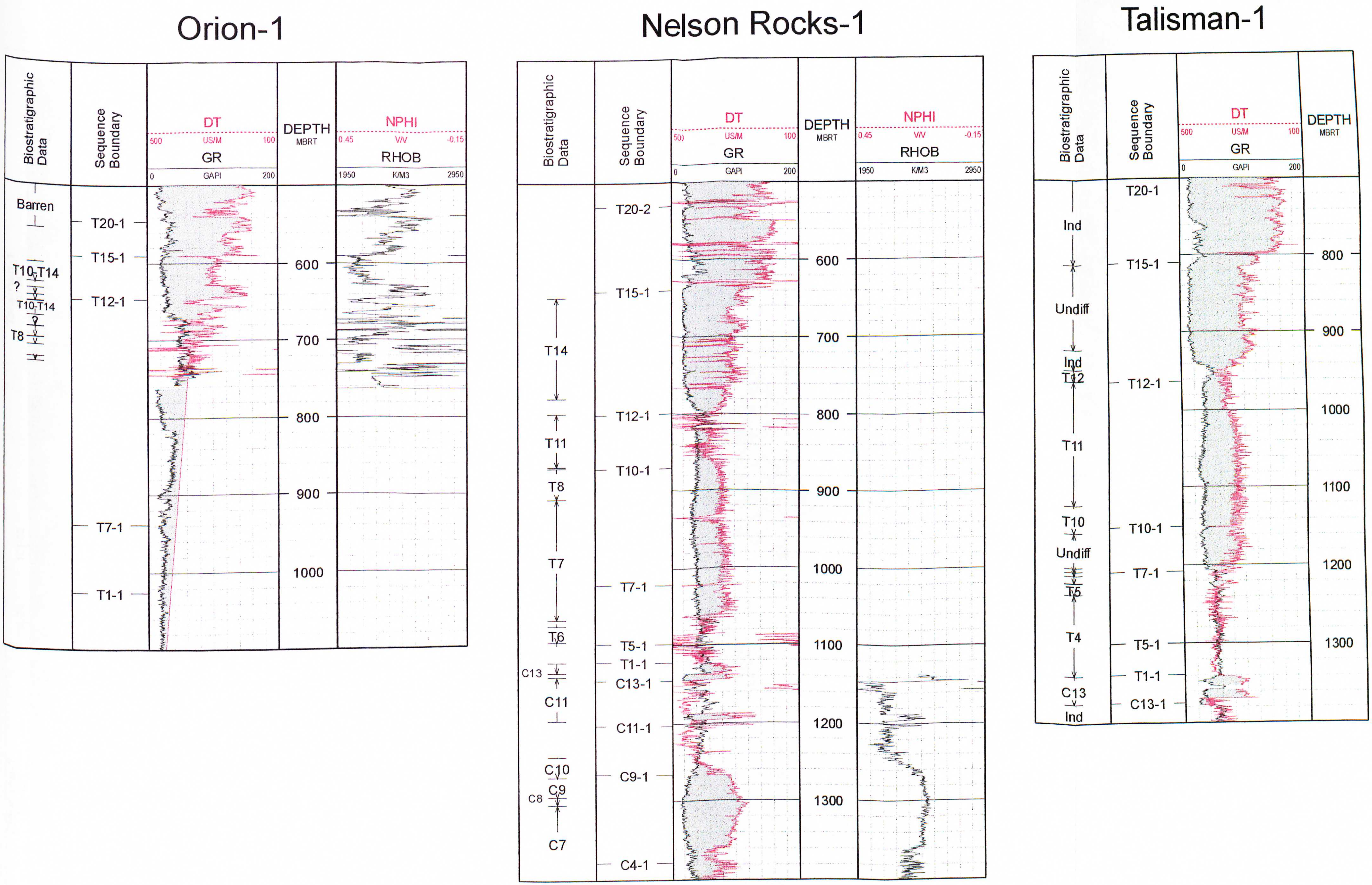

Figure 7.9 Wireline log response of the Paleocene and Eocene sections of Orion-1, Nelson Rocks-1 and Talisman-1 (Scale 1:5000).

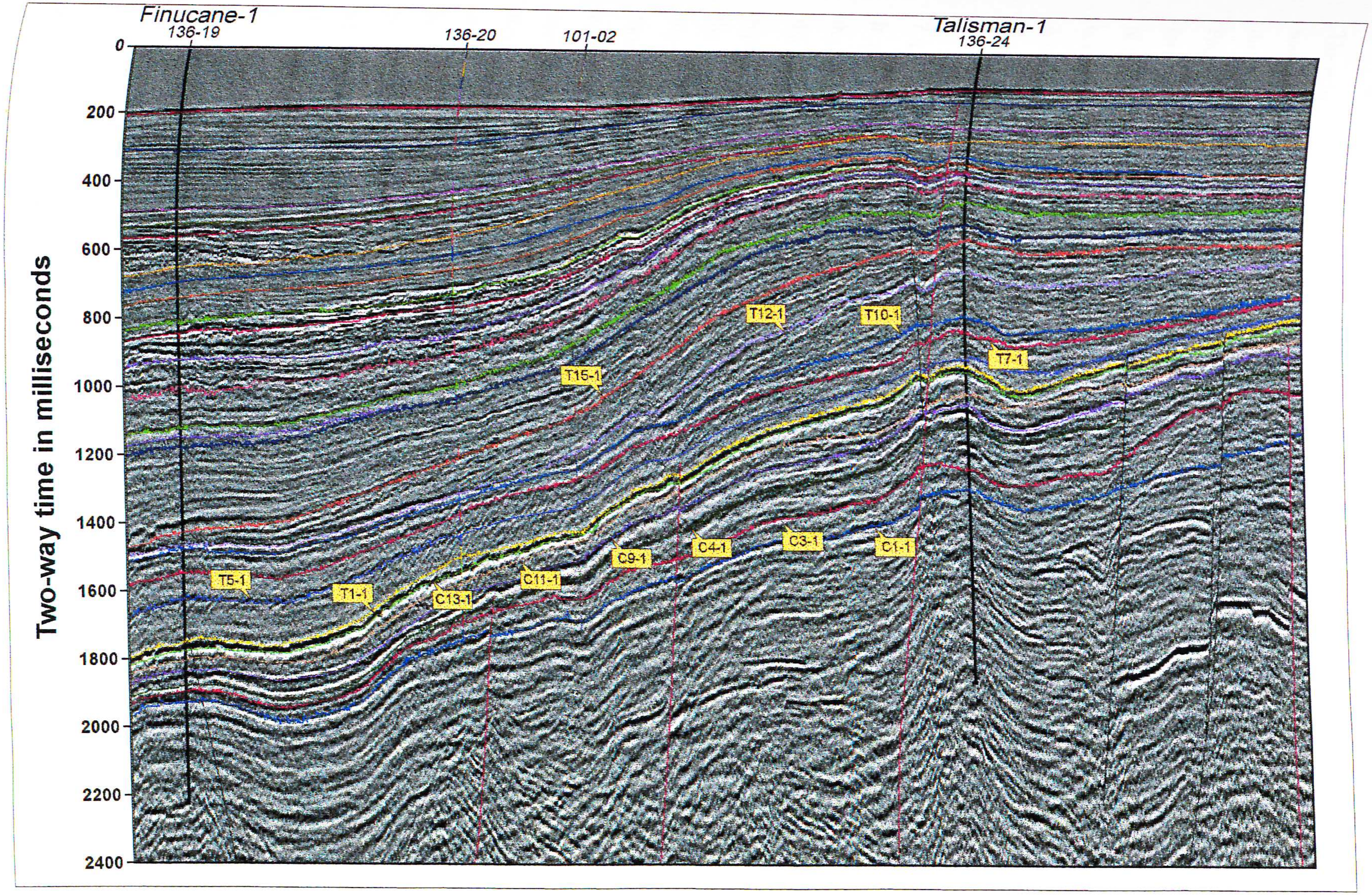

Figure 7.10 Line 136-15 showing progradational geometries of the T10-1 to T12-1 and T12-1 to T15-1 sequences.

7.4 Oligocene to Recent evolution

The primary sea-floor spreading axis affecting Australia during the Paleocene and Eocene trended east west in the Southern Ocean. This resulted in the northward migration of the Australian continent and the opening of the Southern Ocean. However, during this time, no deep ocean opened towards the Pacific as the movement between Antarctica and Tasmania was transform and no ocean floor was formed (Veevers et al., 1991). It was not until the beginning of the Oligocene that the final separation of the Antarctic and Australian plates occurred (Baillie *et al.*, 1994). With the establishment of a deep ocean between Australia and Antarctica, the circum-polar current which previously flowed around Antarctica and Australia, now moved south of Australia. This resulted in a buildup of continental ice sheets and an associated global fall in sea level (Romine *et al.*, 1997).

7.4.1 Eocene - Oligocene boundary

In the Dampier Sub-basin, there is a pronounced break in sedimentation with an associated break in the biostratigraphic record at the base of the Oligocene (Figure 7.1). The biostratigraphic reports for the majority of the wells investigated during this study record a hiatus of considerable duration, which separates late Eocene T14 faunas from middle Oligocene T17 faunas. However, three wells do record the presence of T15-aged sediment directly above this boundary (Bounty-1, Echo-1 and Montague-1, Figure 4.2 and Figure 4.11). The age dating of this event is confounded by the fact that the diagnostic faunas for the basal Oligocene are poorly defined for the North West Shelf as much of the sediment is commonly missing. The base-Oligocene event, termed T15-1 in this study, is evident on seismic sections where it separates the strongly progradational clinoform geometries of the Oligocene to Recent sediments from the underlying sediments (Figure 7.10). Studies by Apthorpe (1988), Romine *et al.* (1997) and Westphal and Aigner (1997) all recognise the significance of a base Oligocene event. Both Romine *et al.* (1997) and Westphal and Aigner (1997) date this event as base Chattian age (base biozone T17) whilst Apthorpe (1988) favours a late Rupelian age (base biozone T16). The three wells which have identified T15 aged sediments in the Dampier Sub-basin constrain this event to be older than the studies by Apthorpe (1988), Romine *et al.* (1997) and Westphal and Aigner (1997) suggest. There is the possibility that reworking of T15 faunas into T17 sediments may have occurred and it is hard to completely discard this possibility without thorough investigation of the faunas. However, the biostratigraphic reports do not discuss the presence of reworking in these samples and are confident in their interpretation of T15-aged sediment.

7.4.2 Oligocene to late Miocene sequences (T15-1 to N17-1)

The Oligocene to late Miocene sequences of the Dampier Sub-basin are characterised by a series of strongly prograding, sigmoidal clinoforms primarily composed of a mixture of coarse and fine-grained carbonates and some siliciclastic sediments. The Oligocene to late Miocene section has been subdivided into seven sequences based on biostratigraphic, wireline and seismic data. These sequences are T15-1–T20-1, T20-1–T20-2, T20-2–N8-1, N8-1–N8-2, N8-2–N10-1, N10-1–N10-N12-1, N10-N12-1–N16-1 and N16-1–N17-1.

7.4.2.1 Stratal architecture

The isochron maps for Oligocene to late Miocene sequences demonstrate a series of northeast-southwest-trending sediment bodies which have the thickest accumulation along a central axis and thin to zero in both a proximal and distal direction (Enclosure 2). The chronosome thickness maps (chronosomes 25-64 in Figure 6.4 to Figure 6.6), display the nature of the internal stratal architecture of each sequence. The first chronosomes within each sequence are laterally restricted and located on the slope of the underlying sequence boundary; subsequent chronosomes increase in areal extent progressively throughout the sequence until they reach a maximum prior to the next sequence boundary.

Within the Oligocene to late Miocene sequences, discrete episodes can be identified when the margin was predominantly progradational or aggradational. The margin is initially progradational during sequences T15-1 to N8-1, during which time the sequences deposited are seen to move basinward with little topset development. The following N8-1 to N10-N12-1 sequences have a predominantly aggradational nature, have significant topset development and display a lesser degree of progradation than the underlying sequences. The margin then returns to being predominantly progradational during sequences N10-N12-1 to N17-1. The 3D-Chronostrat analysis has shown that the sedimentation rate within the progradational sequences was significantly lower than in the aggradational sequences. Whilst no reference to published eustatic curves has been made during the interpretation of the data, the progradational and aggradational periods defined in this study closely correspond to the eustatic curves of Haq *et al.* (1987). Aggradational sequences correspond to periods when the low frequency (10 Ma) and high frequency (1-3 Ma) relative sea level curves are coincident and progradational periods correspond to periods when the curves are separated (Figure 7.1).

7.4.2.2 Lithological distribution

The paleogeographic maps for Oligocene to late Miocene sequences have been annotated with the location of the slope break to enable assessment of the variation in lithology with reference to clinoform morphology (Enclosure 4). The position of the slope break has been ascertained from the seismic database. The paleogeographic maps for the T15-1 to N10-1 sequences show a consistent pattern of sediment distribution of carbonate-dominated lithologies. In these sequences, fine-grained calcilutites occur on the slope, a mixture of calcisiltites and calcarenites at the slope break, calcarenites on the platform top and calcilutites and anhydrites at the proximal edge of the sequence. Calcarenites within these sequences are heterogeneous in nature and contain varying proportions of fine-grained, silt and sand-sized carbonate particles. In sequence T15-1–T20-1, the sand-sized particles identified within the calcarenites are predominantly composed of calcite. In the subsequent T20-2–N10-1 sequences, up to 80% of the grain-sized particles are composed of foraminiferal skeletal debris.

Miocene sequences N10-1–N10-N12-1, N10-N12-1–N16-1 and N16-1–N17-1 record a progressive increase in very fine to coarse-grained siliciclastic sediments on the shelf top (Enclosure 4). Sequence N10-1–N10-N12-1 is composed almost entirely of calcarenites across the whole shelf top with calcilutites on the shelf slope at Malus-1 and Echo-1 (Enclosure 4). The calcarenites of this sequence are a mixture of skeletal and calcite sand-sized grains. In addition to these carbonate sediments, fine to medium-grained quartz sands have been recorded in the southwestern region of the study area at Withnell-1 and Parker-1. This is the first significant accumulation of clastic sediment recorded in the Oligocene to Recent section of the Dampier Sub-basin.

The subsequent N10-N12-1–N16-1 sequence records fine to medium-grained sandstones in Parker-1, Pueblo-1 and Miller-1 with the remainder of the platform sediments being composed of calcite sand-sized grain-dominated calcarenites. Calcilutites are identified on the slope front at Malus-1, Gandara-1 and Delambre-1. The increase in fine to coarse-grained quartz sand, which was has been identified in both N10-1–N10-N12-1 and N10-N12-1–N16-1, continues into the next sequence N16-1–N17-1, as can be seen from the paleogeographic maps (Enclosure 4). Fine to very coarse grained sand, which is dominantly medium grained, is evident in Lowendal-1, Parker-1, Dockrell-1, Pueblo-1, Miller-1, and Madeliene-1. In the northern end of the study area (Bounty-1, Sable-1 and Ronsard-1), calcarenites still dominate and have a mixture of skeletal and calcite sand-sized grains. Calcisiltites are identified on the shelf top close to the slope break with fine grained carbonate sedimentation in the form of calcilutites again occurring on the slope.

7.4.2.3 Stratal architecture and sediment type

Quantitative measurements of clinoform slope angle and clinoform height were obtained from the 3D-Chronostrat analysis and the plots of angle and height through time show a close correspondence to the progradational and aggradational sequences defined from the seismic interpretation (Figure 6.17 and Figure 6.19). Figure 6.17 shows increasing clinoform angles during the progradational periods and decreasing clinoform angles during the aggradational periods. The clinoform slope angle also appears to closely match the sedimentation rate curves defined for the sequences from the volumes output from 3D-Chronostrat, with highest slope angles occurring at times of highest sedimentation rate (Figure 6.17). The height of the clinoforms is seen to increase at a much greater rate in the predominantly aggradational sequences than in the predominantly progradational sequences (Figure 6.19).

Studies by Kenter (1990) have demonstrated the slope angle of carbonate sediments to be related to the type of sediment from which the slope is composed (Figure 6.18). Low angle slopes tend to be composed of fine-grained mud-dominated carbonates whilst higher angle slopes tend to be composed of coarser-grained carbonate sediments. The lithological analysis of sidewall core data, which was conducted during this project, failed to reveal any relationship between the clinoform slope angle and sediment composition. Whether there is no relationship between sediment type and slope angle for the Oligocene to late Miocene section of the Dampier Sub-basin or whether the dataset was too limited is uncertain.

7.4.2.4 Depositional interpretation

The Oligocene to late Miocene sediments of the Dampier Sub-basin have been deposited during a phase of passive regional subsidence where the predominant control on stratal architecture was interpreted to be eustatic sea level. Evidence from biostratigraphic, seismic and 3D-Chronostrat data support this interpretation. Biostratigraphic and wireline data do not identify any significant regional or localised breaks in sedimentation throughout the Oligocene to late Miocene section. Isochron maps produced for the defined sequences demonstrate them to be laterally extensive in nature and show minor along-strike thickness variations. On dip sections, the sequences are characterised by prograding sigmoidal clinoforms, which thin to zero in both proximal and distal directions. There is no evidence of Oligocene to late Miocene aged tectonics affecting these clinoforms. All these factors suggest deposition on a gently subsiding margin under eustatic control and, while the possibility of large-scale high frequency tectonic events generating the preserved stratal geometries cannot be discounted, it is thought unlikely.

During the Oligocene to late Miocene, the style and nature of sedimentation of the Dampier Sub-basin was controlled by the development of accommodation space in response to variations in eustatic sea level. When the short and long-term eustatic sea level curves were in phase, they combined to produce significant accommodation space on the shelf top resulting in the deposition of predominantly aggradational sequences. Conversely, when the short and long-term eustatic sea level curves were out of phase, little shelf-top accommodation space was created and the sequences deposited were predominantly progradational in nature. When shelf-top accommodation space is being created during aggradational periods, the carbonate production rate will be higher than during progradational periods for two reasons. Firstly, the area of the carbonate production factory will be at a maximum and secondly, the large volume of water on the shelf top will allow effective circulation with the open ocean and thus ensure a constant supply of nutrients. This difference in sedimentation rates has been identified during the 3D-Chronostrat analysis.

The isochron maps for the Oligocene to late Miocene sequences of the Dampier Sub-basin demonstrate a series of linear basinward-progressing sequences with no significant along-strike variations in thickness or sedimentation style. This suggests that the predominant sediment transport direction during deposition of these sequences is perpendicular to the shelf edge with minor along-shelf sediment transport. This scenario is similar to the present day environment in which carbonate sediment is produced in a high-energy coastal environment and then transported offshore by prevailing currents and wind direction (Chapter 1).

7.4.3 Late Miocene to Recent sequences (N17-1 to Sea bed)

The wireline, biostratigraphic, seismic and 3D-Chronostrat analysis conducted during this project all identify a late Miocene (Messinian) aged event which marks a significant change in stratal architecture, sedimentation rates and clinoform angles of the prograding section of the Dampier Sub-basin. This event has been termed N17-1.

The isochron maps for the Oligocene to late Miocene sequences beneath the N17-1 sequence boundary are characterised by a series of northeast-southwest-trending, linear, prograding clinoforms which exhibit little along-strike variations in thickness (Enclosure 2). Above the N17-1 sequence boundary, a thick (up to 600 ms) point-sourced wedge of sediment of late Miocene age (N17-1 – N18-1) builds out into the centre of the Dampier Sub-basin (Enclosure 2). The stratal architecture of the subsequent Pliocene to Recent sequences of the Dampier Sub-basin is profoundly influenced by this wedge of sediment. The isochron maps for the subsequent Pliocene to Recent sequences (N18-1 to Seabed) are seen to thin on to the underlying Messinian-aged wedge and thicken away from either side of it as described in Chapter 4. This change in stratal architecture is also clearly evident in the 3D-Chronostrat analysis with chronosomes 25-63 representing sequences T15-1 to N17-1, chronosomes 63-68 representing the wedge of Messinian-aged sediment and chronosomes 69-99 represent the Pliocene to Recent sequences (Figure 6.5 and Figure 6.6). The quantitative analysis of sedimentation rates, clinoform angles and clinoform heights calculated as part of the 3D-Chronostrat analysis also indicate a significant change across the N17-1 sequence boundary. The 3D-Chronostrat analysis also clearly indicates that the chronosomes deposited after the Messinian wedge are seen to progressively backstep onto the N17-1 event (line 136-14, Enclosure 3). These geometries imply that the rate of creation of accommodation space was high at this time and relative sea level was progressively rising.

7.4.3.1 Lithological distribution

Paleogeographic maps of sediment distribution for the late Miocene to Recent sequences of the Dampier Sub-basin show the wedge of N17-1 to N18-1 aged sediment to be composed primarily of fine to very-coarse grained sandstone with minor calcarenites and calcilutites (Enclosure 4). The sandstones within these sequences are restricted to an area in the south west of line 136-14. Where these sequences have been identified northeast of line 136-14, they are represented by calcarenites in N17-1–N17-2 and N17-2–N17-3 and a mixture of calcarenites and calcilutites in N17-3–N18-1. These calcarenites are essentially composed of skeletal grains but have up to 20% glauconite in some cases (Bounty-1). Gandara-1 and Delambre-1 are the only wells that intersect the slope facies of these sequences, which are again represented by fine-grained calcilutite lithologies.

The N18-1–N19-1 sequence records fine to very coarse-grained sandstones across the majority of the shelf top as is identified in Dockrell-1, Pueblo-1, Miller-1, Madeleine-1 and Brigadier-1. In the southwestern corner of the study area, calcarenites are identified in wells Lowendal-1, Parker-1, Fisher-1 and Dockrell-1. Wells located basinward of the slope break are similarily composed of calcilutite. The subsequent N19-1–N19-2 sequence shows a marked reduction in the geographical extent of the sandstones, which are now only identified in Brigadier-1, Miller-1 and Madeleine-1. Over the remainder of the study area, sequence N19-1–N19-2 is typified by silt to sand-sized carbonates (calcisiltites - calcilutites) which are dominantly skeletal in the northeast with calcite grains in the southeast regions of the study area. The subsequent N19-2–N21-1 and N21-1–N21-2 sequences are characterised by very fine to coarse-grained sandstones in Madeleine-1 and Miller-1 and calcarenites over the remainder of the basin. Similar to the underlying sequence, the calcarenites in the southwest are composed predominantly of calcite grains whilst those in the northeast tend to have a significant skeletal component. In the northeastern area of the study, fine-grained calcilutites are also recorded at Sable-1 and Ronsard-1 in sequences N19-2–N21-1 and N21-1–N21-2.

The final three sequences defined within the Dampier Sub-basin, N21-2–N22-1, N22-1–N22-2 and N22-2–Seabed, are poorly defined lithologically due to a lack of available data. No samples can be collected at the well site until the marine riser has been installed, which commonly occurs at a depth of 500m. Of the samples that exist for these sequences, the sediments are redominantly calcarenites with some calcilutites and minor sandstones. As data for these sequences are scarce, the respective lithology maps have only identified the presence of individual lithologies and no attempt has been made to delineate trends in the data.

7.4.3.2 Late Miocene to Recent faulting

The Rosemary Fault system displays complex strike-slip reactivation during the late Miocene to Recent sequences of the Dampier Sub-basin. None of the other fault lineaments in the Dampier Sub-basin display movement of this age, suggesting the Rosemary fault system was preferentially orientated to accommodate stresses induced by the collision of Australia with Southeast Asia. Movement on the Rosemary Fault at this time has been described as dextral (Keep *et al.*, 1998; 1991; Veevers and Powell, 1984) but the large line spacing of the seismic grid used in this project has prevented the direction of fault displacement from being defined. A dextral displacement has been inferred from a consideration of plate motions and internal stresses.

The nature of the dextral strike-slip reactivation is seen to vary along the length of the Rosemary Fault System. In the Dampier Sub-basin, the displacement has been accommodated by inversion in the hangingwall producing the Legendre anticlinal trend. The amount of inversion and width of the Legendre Trend increases from a minimum at the southern end of the study to a maximum at line 136-14, and then progressively decreases in a northeasterly direction. At the northern end of the Dampier Sub-basin, the fold progressively becomes shorter in wavelength to the point where the displacement becomes faulted in the Beagle Sub-basin. The change from folded to faulted deformation style corresponds to a change in the orientation of the Rosemary Fault system from northeast-southwest in the Dampier Sub-basin to approximately east-west in the Beagle Sub-basin. Where line 136-24 cuts obliquely across the Rosemary Fault a flower structure can be clearly identified (Enclosure 3).

Minor thicknesses of flat-lying, late Miocene to Recent sediments are seen landward of the Rosemary Fault System whilst in a basinward direction, significant thicknesses of prograding clinoforms can be easily identified on seismic data. These geometries suggest that during the late Miocene to Recent, the Rosemary Fault acted as a hinge separating the stable footwall block of the Enderby Platform from the subsiding hanging wall block of the Dampier Rift and Rankin Platform. 3D-Chronostrat and seismic sections for the study show the Albian to Eocene sediments to be relatively flat lying over the Rankin and Enderby platforms and more steeply dipping over the Dampier rift (Enclosure 3). These geometries imply that most of the late Miocene deformation has been accommodated in the Dampier rift whilst the Enderby Platform has remained as a rigid block and the Rankin Platform has subsided as a stable block.

7.4.3.3 Depositional interpretation

It is evident from all the wireline, biostratigraphic, seismic, lithological and 3D-Chronostrat data sets that a major geological event occurs in the Dampier Sub-basin during the late Miocene. The sequences deposited since this event record an increase in accommodation space and relative sea level which, as previously mentioned, can be a result of a decreased sedimentation rate, increased subsidence rate or increase in eustatic sea level. The quantitative analyses of the sedimentation rates record a pronounced increase in sedimentation rates across the N17-1 boundary therefore ruling out the first possibility. The change in stratal architecture associated with the N17-1 sequence boundary would not be expected if this was purely an increase in eustatic sea level. It has therefore been concluded that the N17-1 event records a period of increased subsidence in the Dampier Sub-basin, which has resulted in increased sedimentation rates and a decrease in the clinoform slope angle.

As discussed in Chapter 1, the northward-moving Australian continent collided with the westward-moving Pacific Plate and the Eurasian Plate during the mid-Miocene. The interaction of these three plates resulted in an anti-clockwise rotational torque on the Australian continent causing dextral transcurrent movements along pre-existing fractures near the continent-ocean boundary (Veevers and Powell, 1984). The age of the collision of Australia and Southeast Asia has been dated as mid-Miocene (Keep *et al.*, 1998; Romine *et al.*, 1997; Veevers *et al.*, 1991; Westphal and Aigner, 1997). The change in stratal architecture, sedimentation rates and clinoform morphology that have been identified across the N17-1 boundary of this study have been interpreted to be the result of the collision of Australia and Southeast Asia. As this study has adopted a sequence stratigraphic approach, it is possible for the first time to accurately date the timing of the first effects of the collision as recorded in the Dampier Sub-basin. The age of sediments that first record the effects of the collision has been constrained to be of late Tortonian to Messinian (N17) age.

The collision of Australia with Southeast Asia resulted in reactivation of the Rosemary Fault, inversion of the Legendre Trend and the accelerated subsidence of the area basinward of the Rosemary Fault. This accelerated subsidence significantly increased the accommodation space available for the deposition of late Miocene to Recent sequences. Initial sedimentation associated with the increased subsidence rates was dominated by medium to coarse-grained clastic sediments that were restricted to the central area of the Dampier Sub-basin. These sediments are interpreted to be terrestrial in origin as the isochron map for the N17-1–N18-1 sequence shows a point sourced sediment body. The increased accommodation space also resulted in a significant increase in sedimentation rate (Figure 6.15). Highest sedimentation rates for the whole of the Albian to Recent section of the Dampier Sub-basin were recorded immediately after the collision of Australia and Southeast Asia. The calculated sedimentation rates appear to decrease to present day but this may be a result of an underestimation of chronosome volumes caused by chronosomes extending beyond the extent of the data set. Lithologically, the upward decrease in the proportion of siliciclastic sediments recorded in the post N17 sequences also suggests decreasing sedimentation rates, but poor recovery from the upper section prevents confirmation of this.

CHAPTER 8 CONCLUSIONS

8.1 Introduction

A integrated biostratigraphic, wireline, seismic, lithological and 3D-Chronostrat sequence stratigraphic study has been conducted to investigate the evolution of the Albian to Recent section of the Dampier Sub-basin on Australia's North West Shelf. Using the principles of sequence stratigraphy, the study has subdivided the section into a series of genetically-related units, termed sequences, which have been used to describe the evolution of the basin. These sequences are separated by time-correlative surfaces across which a lowering of relative sea level, a basinward shift in facies and commonly a break in sedimentation have occurred. These boundaries are termed 'sequence boundaries'.

8.2 Wireline log model

During the study, a model for the sequence stratigraphic interpretation of the carbonate wireline log motifs was developed as none previously existed in the literature. The model has been developed using biostratigraphic constraints, wireline log patterns and theoretical considerations. It is proposed that highstand systems tracts, which are characterised by high production rates of clean homogeneous carbonates with low siliciclastic input rates, are represented on wireline logs by a relatively consistent low gamma reading. Sequence boundaries are represented by a break at the top of this clean carbonate package, on top of which a more clay-rich, higher gamma reading, lowstand package sits. The transgressive systems tract consists of an upward-cleaning carbonate section in response to the landward relocation of siliciclastics, and is represented by upward-decreasing trends on the sonic and gamma logs. The maximum flooding surface at the top of the transgressive systems tract represents the maximum landward retreat of any siliciclastic sediments present in the system and the deposition of the cleanest carbonate sediments of the relative sea level cycle. This is represented by minima on the gamma and sonic logs at the top of the upward-cleaning trend of the transgressive systems tract and the base of the homogenous trace of the highstand systems tract.

The model has been used to successfully subdivide the Albian to Recent section of the Dampier Sub-basin into a series of genetically-related units.

8.3 Albian to Maastrichtian sequence development

The Albian to Maastrichtian sediments of the Dampier Sub-basin were deposited during a period of passive margin subsidence following the intra-Valanginian rifting of Greater India from Australia (Mihut and Muller, 1998; Muller *et al.*, 1998). The sequences deposited in the Dampier Sub-basin at that time are composed of a mixture of fine-grained clastic and carbonate sediments. Sequence boundaries of Cenomanian (C3-1) and Turonian (C4-1), Campanian (C9-1 & C11-1), Maastrichtian (C13-1) age have been identified and correlated within the Albian to Maastrichtian section.

The Albian to Santonian sequences are thin over the Rankin Trend and Enderby Platform and are seen to thicken into the centre of the Lewis Trough. Active faulting ceases at the Santonian–Campanian boundary and suggests that the Lewis Trough was actively subsiding during the deposition of these sequences. The Albian to Santonian sequences record an upward increase in carbonate content that reaches a maximum at the end Santonian with the widespread deposition of fine-grained carbonates, which are in some places represented by the Toolonga Calcilutite. Biostratigraphic data indicate a progressive deepening of the environment from initial shelfal depths (0-200 m) during Albian to outer shelf to continental slope depths (200-1000 m) at the end of the Santonian. The Albian to Santonian sequences have been deposited during a prolonged period of relative sea level rise, punctuated by short-lived relative sea level falls of Cenomanian and Turonian age.

At the end of the Santonian, a relative sea level fall termed C9-1, caused the cessation of carbonate deposition and a return of clastic-dominated deposition to the Dampier Sub-basin. The Campanian and Maastrichtian sequences of the Dampier Sub-basin, which were deposited subsequently, are composed of a series of progradational siliciclastic units that build into the basin. Immediately following the relative sea level fall at the end of the Santonian, a major siliciclastic source became established in the southwest corner of the study. This source resulted in the deposition of a thick progradational unit, up to 700 ms thick, composed of glauconitic argillaceous sandstones in the southwest corner of the study area. Over the remainder of the basin, the Campanian C9-1–C11-1 sequence is composed of claystones which grade into marls in a northerly direction. This clastic source continued to feed sediment into the Dampier Sub-basin throughout the deposition of the remainder of the Campanian and Maastrichtian sequences with fine-grained claystones and marls persisting over the remainder of the basin. A late Maastrichtian sequence boundary termed C13-1, removed the majority of late Maastrichtian C12 sediment from the basin and returned more carbonate-rich fine-grained sedimentation of late Maastrichtian C13 age to the Dampier Sub-basin.

8.4 Paleocene to Eocene sequence development

The collision of India with Asia at the beginning of the Tertiary and the associated relocation of the primary spreading axis from the Indian to the Southern Ocean heralded the onset of Tertiary deposition in the Dampier Sub-basin (Mihut and Muller, 1998; Muller *et al.*, 1998). This change in primary spreading axis resulted in the northward migration of Australia into lower latitudes and the progressive change from siliciclastic to carbonate-dominated sedimentation in the Dampier Sub-basin.

Within the Paleocene and Eocene section of the Dampier Sub-basin two Paleocene and three Eocene sequences have been defined.

A widespread erosional event of base-Tertiary age, associated with the collision of India with Asia, signified the end of Cretaceous sedimentation in the Dampier Sub-basin. In some areas along the Rankin Trend, submarine erosion has eroded the underlying Maastrichtian sediments. Sedimentation resumed in some parts of the Dampier Sub-basin during the Danian (T1) but it was not until the Selandian when the first significant flood occurred over the whole basin and deposited widespread T4 sediments. Sediments of the Paleocene section are characterised by fine-grained sand and siltstones in the inner margins of the basin grading into claystones and minor marls in more distal locations. The sediment source, which was established at the southern end of the Enderby Platform during the Campanian, persisted into the first Paleocene sequence T1-1–T5-1. Biostratigraphic data indicate a middle–outer shelf environment of deposition for the first Paleocene sequence. The second Paleocene sequence is characterised by an increase in the percentage of fine-grained sediments compared to the preceding sequence. Water depths of middle–outer shelf to slope depths are suggested from the biostratigraphic data. The lithological and environmental data suggest an overall increase in water depth in the Dampier Sub-basin during the Paleocene.

The relocation of the primary north-south spreading axis from the Indian to the Southern Ocean occurred at the end of the Paleocene. The base of the Eocene section of the Dampier Sub-basin is marked by the T7-1 event, which is a diachronous erosive surface which removed variable amounts of Paleocene and Eocene sediments from the basin. In the study area, this event has been interpreted to be a submarine event. During the Eocene, a delta composed of fine-grained sandstones and siltstones built out into the Dampier Sub-basin in the area between Talisman-1 and Legendre-1. During deposition of this delta, the remainder of the basin was in relatively deep water and is characterised by fine-grained claystones and marls. The final Eocene sequence (T12-1–T15-1) is characterised by calcilutites in the outer shelf areas, a mixture of calcisiltites in the mid-shelf, and calcarenites in the inner shelf. This sequence records the transition from siliciclastic to carbonate-dominated sedimentation within the Dampier Sub-basin.

8.5 Oligocene to late Miocene sequence development

At the beginning of the Oligocene, the final separation of the Australian and Antarctic plates occurred south of Tasmania (Baillie *et al.*, 1994). A deep oceanic link between the Southern and Pacific Oceans now existed and with Antarctica isolated at the South Pole, the circum–polar current, which had previously flowed around Australia and Antarctica, now flowed solely around the Antarctic continent. This resulted in a build up of continental ice sheets on the Antarctic continent and an associated global fall in sea level (Romine *et al.*, 1997).

8.5.1 Sequence description

The Oligocene to late Miocene sediments of the Dampier Sub-basin were deposited following the base Oligocene sea level fall, and during a phase of passive regional subsidence. Within this succession, seven sequences have been defined on the basis of biostratigraphic, wireline and seismic data. These sequences are characterised by a series of strongly-prograding, sigmoidal clinoforms composed of a mixture of coarse-grained carbonate and some siliciclastic sediments on the shelf top, silt-sized carbonates at the shelf edge and fine-grained carbonates muds and marls on the slope. The constituent sediment for these sequences was produced in two locations, in a high-energy coastal environment and as a pelagic foraminiferal-dominated deposit. These sediments were transported offshore by prevailing currents and winds, giving rise to the progradational geometries observed on seismic.

8.5.2 Stratal architecture

Within each sequence, the first chronosomes are laterally restricted and located on the slope of the underlying sequence boundary. Subsequent chronosomes increase in areal extent progressively throughout the sequence until they reach a maximum prior to the next sequence boundary. This observed pattern is a result of the control of relative sea level on carbonate production. Relative sea-level falls following a sequence boundary significantly reduce the area of the carbonate production factory resulting in small areally restricted chronosomes. As relative sea level rises and begins to flood the margin, carbonate growth becomes re-established and the resulting chronosomes become progressively larger. At highstand conditions, the carbonate production is at a maximum, resulting in deposition of laterally-extensive chronosomes.

Within the Oligocene to late Miocene section of the Dampier Sub-basin, episodes of predominantly progradational or aggradational sequences can be defined. Progradational clinoforms have steeply dipping fore-sets and exhibit minor aggradational top-set development. In contrast, aggradational clinoforms have progressively less steeply-dipping fore-sets and show the development of significant top-set thicknesses. Calculated sedimentation rates for the aggradational sequences were higher than those calculated for the progradational sequences by a factor of 1.5. The aggradational sequences correspond to periods when the high frequency (1-3 Ma) and low frequency (10 Ma) eustatic curves of Haq *et al.* (1987) are coincident and progradational periods correspond to periods when the curves are separated. When both the short and long-term eustatic curves combine to produce relative sea level highs and therefore significant shelf-top accommodation space, the margin responds by aggrading to fill the accommodation space. Associated with this aggradation are an increase in sedimentation rate and a progressive decrease in clinoform slope angle. When the short and long term eustatic curves are out of phase, relatively minor shelf-top accommodation space is created and sediment is transported off the margin and deposited on the clinoform slope, causing the margin to prograde. Higher sedimentation rates occur in the aggradational periods than in the progradational periods as a result of two factors. Firstly, the area of the carbonate production factory will be at a maximum and secondly, the large volume of water on the shelf top will allow effective circulation with the open ocean and thus a constant supply of nutrients.

Wheeler diagrams for the prograding Oligocene to late Miocene section of the Dampier Sub-basin clearly show the progradational and aggradational episodes that have been identified on the seismic sections. A curve drawn on the Wheeler diagrams which joins the thickest point of each chronosome demonstrates the progradational sequences to be characterised by concave-up portions of the curve whilst aggradational periods are characterised by convex-up portions of the curve. This concave/convex shape of the curve is a result of long-term rate of creation of shelf-top accommodation space. Initially, when the rate is low, the sediment is deposited on the clinoform front, resulting in predominantly progradational sequences. As the rate increases, progressively more sediment is deposited on the shelf-top and the sequences deposited have a larger aggradational component. This increase in rate of shelf-top accommodation space gives rise to the concave-up portion of the curve. The convex-up portions of the curve result from the inverse of this process, when the long-term rate of creation of shelf-top accommodation space has been initially high and has become progressively less.

8.5.3 Shelf morphology

The morphology of the clinoforms appears to be intricately related to the progradational and aggradational periods, which have been identified in the Oligocene to late Miocene section of the Dampier Sub-basin. The predominantly progradational sequences have increasing clinoform slope angles with only a minor associated increase in clinoform height. Conversely, the aggradational sequences are characterised by decreasing clinoform angles and a marked increase in clinoform height, corresponding to the coincidence of the short and long-term eustatic curves.

When the rate of accommodation space creation is low, the sequences deposited are predominantly progradational in nature and characterised by lower sedimentation rates, progressively increasing clinoform slope angles and relatively constant clinoform height. In contrast, when the rate of accommodation space creation is high, the sediments deposited are predominantly aggradational in nature and are characterised by high sedimentation rates, progressively decreasing clinoform slope angles and have a marked increase in clinoform height. It has therefore been concluded that the controlling factor on sequence development during the Oligocene to late Miocene in the Dampier Sub-basin was the rate of creation of shelf-top accommodation space, which is a result of relative sea level changes.

8.6 Controls on late Miocene to Recent sequence development

The wireline, biostratigraphic, seismic and 3D-Chronostrat analyses all identify a late Miocene event across which major changes in stratal architecture, sedimentation rates and clinoform angles of the prograding section of the Dampier Sub-basin are observed. This event has been termed N17-1 and is interpreted to be a result of the collision of Australia with Southeast Asia.

During the late Miocene, the northward-moving Australian continent collided with the Eurasian and westward-moving Pacific Plates. The interaction of these three plates resulted in an anti-clockwise rotational torque on the Australian continent causing dextral transcurrent movements along pre-existing fractures near the continent-ocean boundary (Veevers and Powell, 1984). In the Dampier Sub-basin, the Rosemary Fault System was preferentially orientated to accommodate the stresses associated with the collision which resulted in dextral compressional strike-slip movement on the Rosemary Fault. The nature of this movement is seen to vary along the length of the fault. In the Dampier Sub-basin, the displacement was accommodated by inversion in the hanging wall, producing the Legendre anticlinal trend. Towards the northern end of the Dampier Sub-basin, the anticline becomes progressively shorter in wavelength and at the boundary of the Dampier and Beagle Sub-basins, a flower structure developed. In the Beagle Sub-basin, the orientation of the fault plane changes to trend approximately east-west and the stresses induced by the collision are accommodated by normal faulting.

As discussed in Chapter 5, evidence has suggested that, in addition to the reactivation of the Rosemary Fault System and inversion of the Legendre and Madeleine Trends, the collision of Australia with Southeast Asia caused accelerated subsidence of the Dampier Rift and the Rankin Platform. During the late Miocene to Recent, the Rosemary Fault acted as a hinge, separating the stable footwall block of the Enderby Platform, from the subsiding hangingwall block of the Dampier Rift and Rankin Platform. The majority of the structural deformation associated with the accelerated subsidence of the hangingwall is taken up in the Dampier Rift. The Rankin Platform subsided homogeneously as a rigid block during this phase of accelerated subsidence. In gross terms, the rigid blocks of the Enderby and Rankin Platforms are separated by the ductile Dampier Rift in which the late Miocene to Recent deformation is accommodated.

The accelerated subsidence significantly increased the accommodation space available for the deposition of late Miocene to Recent sequences. Across the N17-1 boundary the isochron maps show a change from the linear prograding geometries that characterised the Oligocene to late Miocene sequences to an areally-restricted wedge of sediment onto which subsequent Pliocene to Recent sequences thin. Initial sedimentation associated with the increased subsidence rates was dominated by terrestrially-derived, medium to coarse-grained clastic sediments that were restricted to the central area of the Dampier Sub-basin. Following deposition of the late Miocene areally-restricted wedge, the highest sedimentation rates for the Albian to Recent section of the Dampier Sub-basin were recorded (9000 km^3Ma^{-1}). The subsequent Pliocene to Recent sequences backstep onto the N17-1 boundary and record a progressive decrease in sedimentation rate, siliciclastic content and clinoform slope angle.

8.7 Implications for hydrocarbon exploration

The study has identified several potential plays in this proven hydrocarbon bearing-basin and the detailed understanding of the timing and nature of the late Miocene section has implications for the timing of generation and migration of hydrocarbons.

The Albian to Santonian sequences of the Dampier Sub-basin are deposited during a long term rise in relative sea level and are composed of predominantly fine-grained sediments and therefore not perceived to have the potential for significant reservoir development. Some reservoir development in these sequences may be associated with Cenomanian and Turonian sequence boundaries. The sealing potential of these sequences, especially the basin-wide late Santonian calcilutites, is considered high.

The relative sea level fall at the end of the Santonian brought a large volume of prograding, siliciclastic dominated sediments into the southwest corner of the basin. This siliciclastic sediment source persisted from the Campanian into the early Paleocene. To date, very few wells have been drilled in this section, which has a high potential for reservoir development. The late Eocene fine-grained carbonates and Oligocene to Recent carbonates provide the seal for these Campanian to early Paleocene clastic sediments. However, the base-Oligocene event has removed a significant amount of the late Eocene sediment and over the Enderby Platform, where Oligocene to Recent sediments are thin, there would be risk associated with up-dip sealing potential. The Eocene delta at the northern end of the Dampier Sub-basin is also considered as a potential target though significantly smaller than the Campanian siliciclastic sediments at the southern end of the Dampier Sub-basin. The proximity of these potential reservoirs to the Rosemary Fault System, which may have acted as a conduit to hydrocarbon migration during the late Miocene, upgrades these play types. The Wandoo Field on the Enderby platform is interpreted to be sourced by migration of hydrocarbons along the Rosemary Fault as no mature source rocks exist on the Enderby Platform (Christiansen, 1992; Delfos and Boardman, 1994).

Within the Oligocene to Recent section of the Dampier Sub-basin, significant development of quartz sands are recorded above the late Miocene N17-1 sequence boundary. Further sand deposition is also recorded in the top-sets of the Miocene sequences. These accumulations are shallow, unconsolidated and lack a good regional seal and a pathway for hydrocarbon migration, as faults on the Rankin Trend show no post-Campanian movement.

Kopsen and McGann (1985) suggested that the generation and migration of hydrocarbons from late Jurassic and Triassic source rocks occurred in three phases during the Tertiary, with the main phase of oil generation occurring with a heat pulse associated with mid-Miocene tectonics. Woodside Offshore Petroleum (1988) believe that hydrocarbons have exploited these Miocene fractures and migrated vertically through the basin to be trapped in stratigraphically younger sections. More recent work by Kaiko and Tingate (1996) suggests that hydrocarbon generation from late Jurassic source rocks has been driven by loading of the passive margin wedge and actually began during the late Cretaceous and is still occurring at the present day. The maturation state of a source rock is dictated by the thermal regime and heat flow though the section. A quantitative understanding of the timing of sediment loading and the palaeowater depths is critical to the understanding of the thermal regime and therefore the timing of generation of hydrocarbon generation and migration. This study provides the quantitative data on sediment loading and water depths that can be used to constrain the hydrocarbon charge models for the Dampier Sub-basin.

8.8 Recommendations for future work

Lithological data for the Albian to Recent section of the Dampier Sub-basin are scarce and exist only in the form of cuttings and sidewall core data. These data are routinely described at the well site and the descriptions are included in the well completion report. Inconsistencies in descriptions between wells may exist as a result of the variety of well site geologists and mudloggers who have worked on the wells during the basin's exploration history. A re-examination of all available samples and a quantitative analysis of the carbonate to siliciclastic content of the samples may reveal a better understanding of lithological variations within each of the sequences. This study found no discernable relationship between sediment type and clinoform slope angle, whilst other workers propose the angle to which a carbonate margin can grow is intricately linked to the sediment type from which the margin is composed. Further investigation of lithological variations of the sequences would contribute to this debate.

The biostratigraphic data for the Dampier Sub-basin are of variable quality, especially in the Oligocene to Recent sediments along the Enderby Platform and Rosemary Fault, where seismic data are also of lower quality. In the Miocene section of the Dampier Sub-basin, the faunal ranges are poorly defined, making correlation more problematic. Further refinement of the biostratigraphic zonation in this section would greatly aid correlation and age dating of the mid-Miocene to Recent sequences defined in this project. Of the wells which have a biostratigraphic analysis of the Albian to Recent foraminiferal assemblages, only a handful have an environmental interpretation relating the species to water depth. An environmental analysis of samples in these wells would greatly aid in the paleogeographic reconstructions of the defined sequences.

The high-resolution subdivision of the Albian to Recent section of the Dampier Sub-basin provides a much better record of the late stage development of the sub-basin than previously existed. Combining this knowledge of sediment loading patterns with water depth analysis would help to better constrain thermal modelling studies of hydrocarbon generation. A comparison of results generated using the genetic subdivision, as presented in this study, and results produced using the broad ranging lithostratigraphic subdivision from the well completion reports, may well lead to radically different understanding of timing of oil generation. This could significantly upgrade or downgrade the prospectivity of certain areas of the basin.

The Oligocene to late Miocene sequences of the Dampier Sub-basin have been deposited on a tectonically quiescent margin under what have been interpreted to be eustatic sea level controls. In this section, predominantly progradational and aggradational sets of sequences have been identified and have been correlated with published eustatic sea level curves. Further studies on other margins of the Australian continent may identify such stacking patterns of a similar age and these may give support to the idea of globally synchronous relative sea level rises and falls.

The effects of the collision of Australia and Southeast Asia in the late Miocene are dramatic and cause significant changes in the stratal architecture and morphology of the sequences deposited in the Dampier Sub-basin. Further studies of the equivalent sequences along the North West Shelf will reveal important information of variations in the deformation style with distance from a subduction zone. Studies on the southern margin of the Australian continent may also reveal the nature of the collision of Australia and Southeast Asia and studies of style and timing may reveal important information on the transfer of intra-plate stresses across a continent.

APPENDIX A - SUGGESTED DEPOSITIONAL ENVIRONMENTS FOR WELLS ON THE NORTH-WEST SHELF, BASED ON FORAMINIFERAL REPORTS - LOUISE CHRISTIAN.

Nelson Rocks 1

Upper Eocene (T14 – approx. 647.6-777.5m) - Shallow inner to inner shelf, based on the presence of abundant fragmented *Discocyclina*, along with *Heterostegina* sp. and *Spiroclypeus* sp..

Mid Eocene (798-868m) - Mid to outer shelf.

Lower Eocene to Palaeocene (870-1117m) - No benthic data available.

Talisman 1

Pleistocene (155-230m) - Inner shelf, based on presence of abundant *Amphistegina* spp. and *Elphidium crispum*, with low plankton abundance.

Late Pliocene (230-275m) - Inner to mid shelf, based on increased abundance of planktonic faunas compared with Pleistocene deposits.

Undifferentiated Pliocene to Latest Miocene (305-425m) - Low planktonic abundances suggest inner shelf.

Latest Miocene (425-470m) - Mid shelf, based on high plankton abundances.

Age indeterminate zones and Mid to Early Miocene (470-805m) - Ranging from intertidal (barren, dolomitic) to shallow inner shelf deposits (based on *Nephrolepidina howchini* group and *Miogypsina* sp.).

Undifferentiated Late to Middle Eocene (810-920m) - Shallow inner to inner shelf deposition, based on presence of large symbiont-bearing forms such as *Asterocyclina* sp. and *Discocyclina* sp.

Early Eocene and Palaeocene(920-1225m) - No benthic data provided.

Eaglehawk 1

Mid Miocene to Burdigalian (4458-5230')- Inner shelf, based on entire assemblage, but particularly on the presence of larger symbiont-bearing forms such as *Amphistegina lessoni*.

Aquitanian (5350-5600') - Mid shelf (approx. 80-150m)

Lower Aquitanian to Upper Oligocene (5970-6950') - Outer shelf to shelf break.

Oligocene (5970-6950') - Insufficient benthic info.

Upper to middle Eocene (7030-7295') - Upper slope (down to 2000m water depth), based on presence of *Bathysiphon* and other deep-water agglutinates.

Lower Eocene (7426-7950') - As above.

Upper Palaeocene (7998-8360') - As above.

Miller 1

Undifferentiated Mid Miocene to Recent (465-660m) - Inner shelf to shallow inner shelf.

Age indeterminable (690-975m) - Beach or similar near-shore environment, based on deposits of quartz sandstone devoid of foraminifera.

Possible Mid Miocene (1005-1155m) - Inner shelf, based on presence of large symbiont-bearing foraminifera.

Undifferentiated Mid Miocene to Burdigalian (1185-1605m) - Inner shelf, as above.

Aquitanian (1635-1680m) - Mid-shelf, based on first appearance of abundant smaller benthic fauna, including *Cibicides* and *Anomalinoides*.

Oligocene (1680-2025m) - Possibly outer shelf?

Eocene and Palaeocene (2070-2590m) - No benthic data available.

Delambre 1

Pliocene (1254.5-1463m) - Outer shelf, tropical to sub-tropical conditions

Late Miocene (N17 – 1475-1606m) - Outer shelf to upper slope, tropical to sub-tropical conditions

(N16) - As above

(N15) - Sub-tropical, upper slope

(N10) - Sub-tropical, no benthic info

N4 - Upper to mid slope

Oligocene - No benthic info

Eocene - Slope (most likely upper)

Late Palaeocene (T4b) - Slope?

Fisher 1

Pleistocene to Late Miocene (420-930m) - No benthic data provided.

Age indeterminable (950-1150) - Intertidal, due to barren samples.

Mid Miocene (1185-1317m) - Shallow inner shelf to inner shelf, based on the presence of *Amphistegina* spp., *Operculina complanata* and *Elphidium* sp.. The sucession shallows up – at 1243m, a number of species attributed to slightly deeper water are apparent, those being *Nephrolepidina howchini* and *Cycloclypeus* sp.

Early Miocene (N8 - 1353-1495m) - No benthic data available.

Undifferentiated Early Miocene (1504-1615m) - Oscillating sea-level implied, based on interbedded suites of larger foraminifera (shallow, inner shelf) with mid-shelf benthic assemblages.

Aquitanian (1637-1714m) - Possibly mid-shelf?

Oligocene (1723-2107.5m) - No benthic data provided.

Eocene (2118-2415m) - As above.

Late Palaeocene to Early Palaeocene (2420-2605m) - As above.

Undifferentiated Palaeocene (2609-2647m) - Deep upper slope, possibly upper lower slope (approx 2000m water depth).

Lowendal 1

Pleistocene and Pliocene (500-965m) - No benthic data provided.

Age indeterminable (985-1150m) - Possible beach environment, based on absence of foraminifera in dolomitic, sandy sediments.

Mid Miocene to Burdigalian (1210-1600m) - Inner shelf, based on presence of large, symbiont-bearing faunas, plus other typical inner shelf forms. Plankton abundance increased down-hole, indicating the conditions shallowed through the succession.

Aquitanian (1615-1650m) - Inner to mid shelf conditions.

Basal Aquitanian to Oligocene (1680-1920m) - Mid to outer shelf.

Oligocene (1950-2060m) - No benthic data

Eocene and Palaeocene (2100-2710m) - As above.

Upper Maastrichtian (2717-2730m) - The presence of *Bathysiphon* and *Dorothia oxycona* indicate upper slope deposition.

Malus 1

Mid Miocene (6380-6705') - Transitional to possibly sub-tropical conditions, mid to outer shelf environment.

Burdigalian (6815') to Oligocene (7150') - No benthic info given

Upper to Middle Eocene (7240-7800') - Poor benthic fauna, including *Quinqueloculina*. Possibly mid-shelf, though could be outer shelf.

Lower Eocene (7825-8250') - The assemblage, but particularly with the presence of *Bathysiphon* suggests upper bathyal (ie. upper slope, down to 2000m)

Upper Palaeocene (8290-8515') - High specific diversity with species including *Bathysiphon*, *Cribrostomoides* and *Cyclammina* suggests deep upper slope.

Parker 1

Pleistocene (420-50m) - Outer shelf (150-200m water depth)

Pliocene (480-630m) - No benthic data

Undifferentiated Late Miocene to Base Pliocene (658-approx.710m) - Mid shelf, based on large *Cibicides*, abundant echinoid plates, with low diversity, moderate abundance planktonics.

Age indeterminate (725-1190m) - Possibly beach-nearshore environment?? This is based on samples barren of forams, plus section from 725-967m consisting of well-rounded, frosted quartz.

Mid Miocene to Burdigalian (1240m) - Inner shelf (down to max. 100m)

Aquitanian (1500-1565m) - No benthic data.

Upper Eocene (1635-1819m) - Outer shelf.

Middle Eocene (1839-1995m) - Possibly also outer shelf?

Early Eocene (2020-2160m) - Outer shelf?

APPENDIX B - HULL, J.N.F., SMITH, S.A. AND YOUNG, H.C., 1998. SEQUENCE STRATIGRAPHIC INTERPRETATION OF CARBONATE WIRELINE LOG MOTIFS: AN EXAMPLE FROM THE NORTH WEST SHELF OF AUSTRALIA, THE APPEA JOURNAL. AUSTRALIAN PETROLEUM PRODUCTION & EXPLORATION ASSOCIATION, 188-198.

Hull, N. F., Smith, S. A., & Young, H. C. (1998). Sequence stratigraphic evolution of the Albian to recent section of the Dampier Sub-basin, North West Shelf, Australia. *APPEA Journal*, 188-198.

NOTE:

This publication is included in the print copy
of the thesis held in the University of Adelaide Library.

APPENDIX C – SEQUENCE PICKS IN STUDY WELLS

Events	BOUNTY-1	BRIGADIER-1	DELAMBRE-1	DIXON-1	DOCKRELL-1	EAGLEHAWK-1	ECHO-1	FINUCANE-1	FISHER-1	GANDARA-1	GOODWYN-7	GOODWYN-8	LEGENDRE-1	LOWENDAL-1	MADELEINE-1
Sea_Bed	154.2	321	724	102	140	132	175	147	96	305	150	160	61	115	77.5
N22-2	254	381	873	190	226	200	382	287	205	383	248	252		188	127
N22-1	324	411	1003	273	314	266	512	505	295	440	305	314	117	270	212
N21-2		471	1150	411	478	315	657	545	480	481	438	479		485	241
N21-1	362	526	1230	485	552	352	713	599	565	556	484	518		616	284
N19-2	558	629	1355	567	625	469	815	660	661	726	586	613	176	680	372
N19-1		808	1454	680	757	602	959		834	900	688	739		832	440
N18-1	777	1183	1538	756	830	694	1025	754	928	1400	776	822		999	478
N17-3		1370		795	860	745	1073			1680	806	848			554
N17-2		1860		853	888	813	1109		962	1770	867	910			588
N17-1	883	2031	1620	894	990	857	1167	802	1040	1984	936	974	238	1047	609
N16-1	1016		1780	958	1060	987	1255	897	1108	2083	1057	1069		1117	678
N10_N12-1	1086	2084		1055	1190	1059	1351	978	1226	2167	1071	1107		1223	740
N10-1	1225	2170	1826	1180	1266	1247	1449	1103	1276	2220	1255	1285		1278	807
N8-2	1425			1355	1435	1457	1649	1262	1447		1440	1465		1445	855
N8-1	1556	2202		1442	1510	1573	1730	1441	1516		1516	1545	314	1516	920
T20-2	1634			1550	1617	1669	2090	1485	1624		1669	1711	397	1626	1129
T20-1	1680			1654	1665	1736	2163	1536	1692		1741	1788		1672	1222
T15-1	2103	2330	1860	1960	2107	2121	2284	1989	2110	2293	2062	2110	505	2085	1470
T12-1	2125	2440	1880	2126	2198	2232	2357	2035	2204	2431	2095	2146	610	2238	1627
T10-1	2181	2470	1940	2298	2295	2317	2440	2040	2360	2530	2210	2271	734	2412	1720
T7-1	2394	2511	1990	2365	2380	2431	2449	2170	2420	2575	2351	2385	883	2518	1779
T5-1	2441	2569	2010	2547	2519	2520	2535	2267	2565	2600	2450	2475	932	2620	1840
T1-1	2626	2607	2071	2651	2585	2581	2702	2456	2650	2675	2534	2550	1010	2718	1927
C13-1	2663	2640	2115	2682		2604		2479	2658	2715			1054	2730	2027
C11-1		2668		2740	2613	2701	2761	2540	2675	2735	2564	2584	1081	2762	2090
C9-1	2733	2705	2170	2897	2707	2718	2798	2587	2823	2782	2631	2651	1232	2870	2195
C4-1	2812	2762		3057	2818			2661	2962	2845	2732	2744	1355	2962	2369
C3-1	2828	2778	2240	3095	2830		2881	2683	2985	2854	2740	2760	1558	2990	2427
C1-1	2877	2811	2293	3156	2885	2739	2950	2738	3039	2917	2787	2810	1648	3042	2484

REFERENCES

AGSO North West Shelf Study Group, 1994. Deep reflections on the North West Shelf: Changing perceptions of basin formation. In: Purcell, P.G. and Purcell, R.R. (Eds), The Sedimentary Basins of Western Australia. Petroleum Exploration Society of Australia, 63-76.

Ahr, W.M., 1973. The carbonate ramp; an alternative to the shelf model, Today's New Technology, Tomorrow's New Targets. *Transactions - Gulf Coast Association of Geological Societies*. Gulf Coast Association of Geological Societies, 221-225.

Apthorpe, M.C., 1979. Depositional history and palaeogeography of the Upper Cretaceous of the North West Shelf based on foraminifera, The APEA Journal. Australian Petroleum Exploration Association, 74-89.

Apthorpe, M.C., 1988. Cainozoic depositional history of the North West Shelf. In: Purcell, P.G. and Purcell, R.R. (Eds), The North West Shelf. Petroleum Exploration Society of Australia, 55-84.

Austin, J.A., 1986. Proceedings of the ocean drilling program, initial reports, 101. Ocean Drilling Program.

Baillie, P.W., Powell, C.M., Li, Z.X. and Ryall, A.M., 1994. The tectonic framework of Western Australia's Neoproterozoic to Recent sedimentary basins. In: Purcell, P.G. and Purcell, R.R. (Eds), The Sedimentary Basins of Western Australia. Petroleum Exploration Society of Australia, 45-61.

Barber, P., 1994. Late Jurassic - Early Cretaceous depositional systems of the Dampier Sub-basin - Quo Vadis?, The APPEA Journal. Australian Petroleum Production & Exploration Association, 566-585.

Barber, P.M., 1988. The Exmouth Plateau deep water frontier: A case history. In: Purcell, P.G. and Purcell, R.R. (Eds), The North West Shelf. Petroleum Exploration Society of Australia, 173-187.

Berggren, W.A., Kent, D.V., Swisher, C.C., III and Aubry, M.P., 1995. A revised Cenozoic geochronology and chronostratigraphy. In: Berggren, W.A., Kent, D.V., Aubry, M.P. and Hardenbol, J. (Eds), Geochronology, time scales and global stratigraphic correlation. *Special Publication - SEPM (Society for Sedimentary Geology)*. SEPM (Society for Sedimentary Geology), 129-212.

Brown, L.F., Jr. and Fisher, W.L., 1977. Seismic-stratigraphic interpretation of depositional systems; examples from Brazilian rift and pull-apart basins. In: Payton, C.E. (Ed), Seismic stratigraphy; applications to hydrocarbon exploration. *Memoir - American Association of Petroleum Geologists*. American Association of Petroleum Geologists, 213-248.

Burchette, T.P. and Wright, V.P., 1992. Carbonate ramp depositional systems. In: Sellwood, B.W. (Ed), Ramps and reefs. *Sedimentary Geology*. Elsevier, 3-57.

Buxton, M.W.N. and Pedley, H.M., 1989. A standardized model for Tethyan Tertiary carbonate ramps. *Journal of the Geological Society of London*, **146,** 746-748.

Calvet, F., Tucker, M.E. and Henton, J.M., 1990. Middle Triassic carbonate ramp systems in the Catalan Basin, Northeast Spain; facies, systems tracts, sequences and controls. In: Tucker, M.E., Wilson, J.L., Crevello, P.D., Sarg, J.R. and Read, J.F. (Eds), Carbonate platforms; facies, sequences and evolution. *Special Publication of the International Association of Sedimentologists*. Blackwell, 79-108.

Chegwidden, A., Fisher, S.J., Alexander, R. and Kagi, R.I., 1993. The fate of hydrocarbons associated with drilling from the North Rankin "A" gas and condensate platform, Western Australia. In: O, M.G. (Ed), 1993 APEA conference; technical papers. *The APEA Journal*. Australian Petroleum Exploration Association, 386-394.

Christiansen, D.J., 1992. The hydrocarbon potential of a western portion of the Lambert Shelf, Dampier Sub-basin, Western Australia. B.Sc. (Hons) Thesis, University of Adelaide.

Commonwealth Bureau of Meteorology, 1972. Climatic Survey: Northwest Region 6, Western Australia. Aust. Pub. Serv., 144.

Curray, J.R., 1964. Transgressions and regressions, [Chapter] 10, Papers in marine geology--Shepard Commemorative Volume., 175-203.

Davies, P.J., Symond, P.A., Feary, D.A. and Pigram, C.J., 1989. The evolution of the carbonate platforms of Northeast Australia. In: Crevello, P.D., Wilson, J.J., Sarg, J.F. and Read, J.F. (Eds), Controls on carbonate platform and basin development. *Special Publication - Society of Economic Paleontologists and Mineralogists*. SEPM (Society for Sedimentary Geology), 233-258.

Delfos, E. and Boardman, M., 1994. Wandoo - a new trend, The APEA Journal. Australian Petroleum Production & Exploration Association, 658-601.

Dix, G.R., 1989. High-energy, inner shelf carbonate facies along a tide-dominated non-rimmed margin, northwestern Australia. *Marine Geology*, **89,** 347-362.

Driscoll, N.W. and Karner, G.D., 1998. Lower crustal extension across the Northern Carnarvon Basin, Australia: Evidence for an eastward dipping detachment. *Journal of Geophysical Research*, **103,** 4975-4991.

Driscoll, N.W., Weissel, J.K., Karner, G.D. and Mountain, G.S., 1991. Stratigraphic response of a carbonate platform to relative sea level changes; Broken Ridge, Southeast Indian Ocean. *AAPG Bulletin*, **75,** 808-831.

Droxler, A.W. and Schlager, W., 1985. Glacial versus interglacial sedimentation rates and turbidite frequency in the Bahamas. *Geology (Boulder)*, **13,** 799-802.

Eberli, G.P. and Ginsburg, R.N., 1989. Cenozoic progradation of northwestern Great Bahama Bank, a record of lateral platform growth and sea-level fluctuations. In: Crevello, P.D., Wilson, J.J., Sarg, J.F. and Read, J.F. (Eds), Controls on carbonate platform and basin development. *Special Publication - Society of Economic Paleontologists and Mineralogists*. SEPM (Society for Sedimentary Geology), 339-351.

Emery, D., 1996. Carbonate Systems. In: Emery, D. and Myers, K.J. (Eds), Sequence Stratigraphy. Blackwell Scientific Publications, 211-237.

Emery, D. and Dickson, J.A.D., 1991. The subsurface correlation of the Lincolnshire Limestone Formation in Lincolnshire. *Proceedings of the Geologists' Association*, **102,** 109-122.

Emery, D. and Myers, K.J., 1996. Sequence Stratigraphy. Blackwell Scientific Publications, 297.

Erlich, R.N., Longo, A.P., Jr. and Hyare, S., 1993. Response of carbonate platform margins to drowning; evidence of environmental collapse. In: Loucks, R.G. and Sarg, J.F. (Eds), Carbonate sequence stratigraphy; recent developments and applications. *AAPG Memoir*. American Association of Petroleum Geologists, 241-266.

Exon, N.F. and Colwell, J.B., 1994. Geological history of the outer North West Shelf of Australia; a synthesis. In: Exon, N. (Ed), Geology of the outer North West Shelf, Australia. *AGSO Journal of Australian Geology and Geophysics*. Australian Geological Survey Organization, 177-190.

Exon, N.F. and von Rad, U., 1994. The Mesozoic and Cainozoic Sequences of the Northwest Australian margin, as revealed by ODP core drilling and related studies. In: Purcell, P.G. and Purcell, R.R. (Eds), The Sedimentary Basins of Western Australia. Petroleum Exploration Society of Australia, 181-199.

Falvey, D.A. and Mutter, J.C., 1981. Regional plate tectonics and the evolution of Australia's passive continental margins. *Bureau of Mineral Resources Journal of Australian Geology and Geophysics*, **6,** 1-29.

Galloway, W.E., 1989. Genetic stratigraphic sequences in basin analysis; I, Architecture and genesis of flooding-surface bounded depositional units. *AAPG Bulletin*, **73,** 125-142.

Glenn, C.R., Kronen, J.D., Jr., Symonds, P.A., Wei, W. and Kroon, D., 1993. High-resolution sequence stratigraphy, condensed sections, and flooding events off the Great Barrier Reef; 0.1.5 Ma. In: McKenzie, J.A., Davies, P.J., Palmer, J.A.A., Betzler, C.G., Brachert, T.C., Chen, M.P.P., Crumbiere, J.P., Dix, G.R., Droxler, A.W., Feary, D.A., Gartner, S., Glenn, C.R., Isern, A., Jackson, P.D., Jarrard, R.D., Katz, M.E., Konishi, K., Kroon, D., Ladd, J.W., Martin, J.M., McNeill, D.F., Montaggioni, L.F., Muller, D.W., Omarzai, S.K., Pigram, C.J., Swart, P.K., Symonds, P.A., Watts, K.F., Wei, W., Stewart, S.K. and Marin, J.A. (Eds), Proceedings of the Ocean Drilling Program, scientific results, Northeast Australian Margin; covering Leg 133 of the cruises of the drilling vessel JOIDES Resolution, Apra Harbor, Guam, to Townsville, Australia, sites 811-826, 4 August-11 October 1990. *Proceedings of the Ocean Drilling Program, Scientific Results*. Texas A & M University, Ocean Drilling Program, 353-364.

Grammer, G.M. and Ginsburg, R.N., 1992. Highstand versus lowstand deposition on carbonate platform margins; insight from Quaternary foreslopes in the Bahamas. *Marine Geology*, **103,** 125-136.

Griffiths, C.M. and Hadler-Jacobsen, F., 1995. Practical dynamic modelling of basin fill. In: Steel, R.J. (Ed), Sequence stratigraphy on the Northwest European Margin. Norwegian Petroleum Society, 31-49.

Griffiths, C.M. and Nordlund, U., 1993. Chronosomes and quantitative stratigraphy. In: Nishiwaki, N. (Ed), Recent advances in geomathematics and geoinformatics. *Joho Chishitsu = Geoinformatics*. Japanese Society for Geological Data Processing [in cooperation with] Osaka City University, Department of Geosciences, 327-336.

Griffiths, C.M. and Nordlund, U., 1996. Chronosomes and quantitative stratigraphy. *Jianghan Shiyou Xueyuan Xuebao = Journal of the Jianghan Petroleum Institute*, **18,** 1-8.

Handford, C.R. and Loucks, R.G., 1993. Carbonate depositional sequences and systems tracts; responses of carbonate platforms to relative sea-level changes. In: Loucks, R.G. and Sarg, J.F. (Eds), Carbonate sequence stratigraphy; recent developments and applications. *AAPG Memoir*. American Association of Petroleum Geologists, 3-41.

Haq, B.U., Hardenbol, J. and Vail, P.R., 1987. Chronology of fluctuating sea levels since the Triassic. *Science*, **235,** 1156-1167.

Hardenbol, J., Vail, P.R. and Ferrer, J., 1981. Interpreting paleoenvironments, subsidence history and sea-level changes of passive margins from seismic and biostratigraphy. In: Anonymous (Ed), Colloque C3; Geologie des marges continentales; 26eme congres geologique international. *Oceanologica Acta*. Gauthier-Villars, 33-44.

Harland, W.B., Cox, A., LLewellyn, P.G., Picton, C.A.G. and Smith, A.G., 1989. A geological time scale. Cambridge University Press.

Harland, W.B., Cox, A.V., Llewellyn, P.G., Pickton, C.A.G., Smith, A.G. and Walters, R., 1982. A geologic time scale. Cambridge Univ. Press, 131.

Harwood, G.M. and Towers, P.A., 1988. Seismic sedimentologic interpretation of a carbonate slope, north margin of Little Bahama Bank. In: Austin, J.A., Jr., Schlager, W., Comet, P.A., Droxler, A.W., Eberli, G.P., Fourcade, E., Freeman, L.R.P., Fulthorpe, C.S., Harwood, G.M., Kuhn, G., Lavoie, D., Leckie, R.M., Melillo, A.J., Moore, A., Mullins, H.T., Ravenne, C., Sager, W.W., Swart, P.K., Verbeek, J.W., Watkins, D.K., Williams, C.F., Palmer, A.A., Rose, W.D. and Stewart, S.K. (Eds), Proceedings of the Ocean Drilling Program, Bahamas, covering Leg 101 of the cruises of the drilling vessel JOIDES Resolution, Miami, Florida to Miami, Florida, sites 626-636, 29 January 1985-14 March 1985. *Proceedings of the Ocean Drilling Program, Scientific Results*. Texas A & M University, Ocean Drilling Program, 263-277.

Heath, R.S., 1979. Neogene planktonic foraminifera: studies on Indo-Pacific oceanic sections. The University of Adelaide.

Heath, R.S. and Apthorpe, M.C., 1984. Late Cretaceous and Tertiary stratigraphy, southern Northwest Shelf. Woodside Petroleum Pty Ltd.

Hill, G., 1994. The role of the pre-rift structure in the architecture of the Dampier Basin area, North West Shelf, Australia., The APPEA Journal. Australian Petroleum Production & Exploration Association, 602-613.

Hine, A.C. and Neumann, A.C., 1977. Shallow carbonate-bank-margin growth and structure, Little Bahama Bank, Bahamas. *AAPG Bulletin*, **61,** 376-406.

Hocking, R.M., 1988. Regional geology of the Northern Carnarvon Basin. In: Purcell, P.G. and Purcell, R.R. (Eds), The North West Shelf. Petroleum Exploration Society of Australia, 97-114.

Holloway, P.E., 1983. Tides on the Australian northwest shelf. *Australian Journal of Marine Freshwater Research*, **34,** 213-230.

Hull, J.N.F., Smith, S.A. and Young, H.C., 1998. Sequence stratigraphic interpretation of carbonate wireline log motifs: An example from the North West Shelf of Australia, The APPEA Journal. Australian Petroleum Production & Exploration Association, 188-198.

Jablonski, D., 1997. Recent advances in the sequence stratigraphy of the Triassic to Lower Cretaceous succession in the Northern Carnarvon Basin, The APPEA Journal. Australian Petroleum Production & Exploration Association, 429-454.

Jacquin, T., Arnaud, V.A., Arnaud, H., Ravenne, C. and Vail, P.R., 1991. Systems tracts and depositional sequences in a carbonate setting; a study of continuous outcrops from platform to basin at the scale of seismic lines. *Marine and Petroleum Geology*, **8,** 122-139.

Jervey, M.T., 1988. Quantitative geological modeling of siliciclastic rock sequences and their seismic expression. In: Wilgus, C.K., Hastings, B.S., Ross, C.A., Posamentier, H., Van, W.J. and Kendall, C.G.S.C. (Eds), Sea-level changes; an integrated approach. *Special Publication - Society of Economic Paleontologists and Mineralogists*. SEPM (Society for Sedimentary Geology), 47-69.

Kaiko, A.R. and Tingate, P.R., 1996. Suppressed vitrinite reflectance and its effect on thermal history modelling in the Barrow and Dampier Sub-basins, The APPEA Journal. Australian Petroleum Exploration Association, 428-444.

Keep, M., Powell, C.M. and W, B.P., 1998. Neogene deformation of the North West Shelf, Australia. In: Purcell, P.G. and Purcell, R.R. (Eds), The Sedimentary Basins of Western Australia 2. Petroleum Exploration Society of Australia, 81-91.

Kendall, C.G.S.C. and Schlager, W., 1981. Carbonates and relative changes in sea level. In: Cita, M.B. and Ryan, W.B.F. (Eds), Carbonate platforms of the passive-type continental margins. *Marine Geology*. Elsevier, 181-212.

Kenter, J.A.M., 1990. Carbonate platform flanks; slope angle and sediment fabric. *Sedimentology*, **37,** 777-794.

Klootwijk, C.T., Gee Jeffrey, S., Peirce, J.W., Smith, G.M. and McFadden, P.L., 1992. An early India-Asia contact; paleomagnetic constraints from Ninetyeast Ridge, ODP Leg 121; with Suppl. Data 92-15. *Geology (Boulder)*, **20,** 395-398.

Kopsen, E. and McGann, G., 1985. A review of the hydrocarbon habitat of the eastern and central Barrow-Dampier Sub-basin, Western Australia, The APEA Journal. Australian Petroleum Exploration Association, 154-176.

Krumbein, W.C. and Sloss, L.L., 1963. Stratigraphy and sedimentation (2d edition).

Neumann, A.C. and MacIntyre, I., 1985. Reef response to sea level rise; keep-up, catch-up or give-up. In: Gabrie, C., Toffart, J.L. and Salvat, B. (Eds), Proceedings of the Fifth international coral congress. *Proceedings - International Coral Reef Symposium*. Rosenstiel School of Marine and Atmospheric Science, University of Miami, 105-110.

Newman, S., 1994. Clues to the structural history of the Rankin Trend, from 3D seismic data. In: Purcell, P.G. and Purcell, R.R. (Eds), The Sedimentary Basins of Western Australia. Petroleum Exploration Society of Australia, 497-507.

Nordlund, U., 1992. 3D-Chronostrat.

Nordlund, U. and Griffiths, C.M., 1993a. An example of the practical use of chronosomes in quantitative stratigraphy. In: Nishiwaki, N. (Ed), Recent advances in geomathematics and geoinformatics. *Joho Chishitsu = Geoinformatics*. Japanese Society for Geological Data Processing [in cooperation with] Osaka City University, Department of Geosciences, 313-325.

Nordlund, U. and Griffiths, C.M., 1993b. Automatic construction of two- and three-dimensional chronostratigraphic sections from digitized seismic data. *Computers & Geosciences*, **19,** 1185-1205.

Payton, C.E., 1977. Seismic stratigraphy; applications to hydrocarbon exploration, Memoir - American Association of Petroleum Geologists. American Association of Petroleum Geologists, 516.

Powell, C.M., Roots, S.R. and Veevers, J.J., 1988. Pre-breakup continental extension in East Gondwanaland and the early opening of the eastern Indian Ocean. In: Scotese, C.R. and Sager, W.W. (Eds), Mesozoic and Cenozoic plate reconstructions. *Tectonophysics*. Elsevier, 261-283.

Prosser, S., 1993. Rift-related linked depositional systems and their seismic expression. In: Williams, G.D. and Dobb, A. (Eds), Tectonics and seismic sequence stratigraphy. *Geological Society Special Publications*. Geological Society of London, 35-66.

Purdy, E.G. and Bertram, G.T., 1993. Carbonate concepts from the Maldives, Indian Ocean, AAPG Studies in Geology. American Association of Petroleum Geologists, 56.

Rasidi, J.S., 1995. Depositional sequence of the Withnell Formation, Dampier Sub-basin, The APPEA Journal. Australian Petroleum Production & Exploration Association, 296-306.

Read, J.F., 1982. Carbonate platforms of passive (extensional) continental margins; types, characteristics and evolution. In: Hales, A.L. (Ed), Geodynamics final symposium. *Tectonophysics*. Elsevier, 195-212.

Read, J.F., 1985. Carbonate platform facies models. *AAPG Bulletin*, **69,** 1-21.

Read, J.F. and Hodbury, A.D., 1993. Eustatic and tectonic controls on porosity evolution beneath sequence bounding unconformities and parasequence disconformities on carbonate platforms. In: Hodbury, A.D. and Robinson, A.G. (Eds), Diagenesis and Basin Development. *AAPG Studies in Geology*. American Association of Petroleum Geologists, 155-197.

Reijmer, J.J.G., Ten, K.W.G.H.Z., Sprenger, A. and Schlager, W., 1991. Calciturbidite composition related to exposure and flooding of a carbonate platform (Triassic, eastern Alps). *Sedimentology*, **38,** 1059-1074.

Romine, K.K., Durrant, J.M., Cathro, D.L. and Bernardel, G., 1997. Petroleum play element prediction for the Cretaceous-Tertiary basin phase, Northern Carnarvon Basin, The APPEA Journal. Australian Petroleum Production & Exploration Association, 315-339.

Ross, M.I., 1995. Influence of plate tectonic re-organisations and tectonic subsidence on the Mesozoic stratigraphy of Northwestern and Southeastern Australia: Implications for sequence stratigraphic analysis, The APPEA Journal. Australian Petroleum Production & Exploration Association, 253-279.

Ross, M.I. and Vail, P.R., 1994. Sequence Stratigraphy of the Lower Neocomian Barrow Delta Exmouth Plateau. In: Purcell, P.G. and Purcell, R.R. (Eds), The Sedimentary Basins of Western Australia. Petroleum Exploration Society of Australia, 435-438.

Saller, A.H., Barton, J.W. and Barton, R.E., 1989. Slope sedimentation associated with a vertically building shelf, Bone Spring Formation, Mescalero Escarpe Field, southeastern New Mexico. In: Crevello, P.D., Wilson, J.J., Sarg, J.F. and Read, J.F. (Eds), Controls on carbonate platform and basin development. *Special Publication - Society of Economic Paleontologists and Mineralogists*. SEPM (Society for Sedimentary Geology), 275-288.

Sarg, J.F., 1988. Carbonate sequence stratigraphy. In: Wilgus, C.K., Hastings, B.S., Ross, C.A., Posamentier, H., Van, W.J. and Kendall, C.G.S.C. (Eds), Sea-level changes; an integrated approach. *Special Publication - Society of Economic Paleontologists and Mineralogists*. SEPM (Society for Sedimentary Geology), 155-181.

Schlager, W., 1981. The paradox of drowned reefs and carbonate platforms. *Geological Society of America Bulletin*, **92,** I 197-I 211.

Schlager, W. and Camber, O., 1986. Submarine slope angles, drowning unconformities, and self-erosion of limestone escarpments. *Geology (Boulder)*, **14,** 762-765

Schlager, W., 1989. Drowning unconformities on carbonate platforms. In: Crevello, P.D., Wilson, J.J., Sarg, J.F. and Read, J.F. (Eds), Controls on carbonate platform and basin development. *Special Publication - Society of Economic Paleontologists and Mineralogists*. SEPM (Society for Sedimentary Geology), 15-25.

Schlager, W., 1992. Sedimentology and sequence stratigraphy of reefs and carbonate platforms, AAPG Continuing Education Course Note Series. American Association of Petroleum Geologists. Education Department, 71.

Schlager, W., Reijmer, J.J.G. and Droxler, A., 1994. Highstand shedding of carbonate platforms. *Journal of Sedimentary Research, Section B: Stratigraphy and Global Studies*, **64,** 270-281.

Schultz, E.H., 1982. The chronosome and supersome; terms proposed for low-rank chronostratigraphic units. *Bulletin of Canadian Petroleum Geology*, **30,** 29-33.

Southgate, P.N., Kennard, J.M., Jackson, M.J., O'Brien, P.E. and Sexton, M.J., 1993. Reciprocal lowstand clastic and highstand carbonate sedimentation, subsurface Devonian reef complex, Canning Basin, Western Australia. In: Loucks, R.G. and Sarg, J.F. (Eds), Carbonate sequence stratigraphy; recent developments and applications. *AAPG Memoir*. American Association of Petroleum Geologists, 157-179.

Stagg, H.M.J. and Colwell, J.B., 1994. The structural foundations of the Northern Carnarvon Basin. In: Purcell, P.G. and Purcell, R.R. (Eds), The Sedimentary Basins of Western Australia. Petroleum Exploration Society of Australia, 349-364.

Stein, A., 1994. Rankin Platform, Western Australia: structural development and exploration potential. In: Purcell, P.G. and Purcell, R.R. (Eds), The Sedimentary Basins of Western Australia. Petroleum Exploration Society of Australia, 509-523.

Tucker, M.E., 1985. Shallow-marine carbonate facies and facies models. In: Brenchley, P.J. and Williams, B.P.J. (Eds), Sedimentology; recent developments and applied aspects. Blackwell Sci. Publ., 147-167.

Tucker, M.E., Wilson, J.L., Crevello, P.D., Sarg, J.R. and Read, J.F., 1990a. Carbonate platforms; facies, sequences and evolution, Special Publication of the International Association of Sedimentologists. Blackwell, 328.

Tucker, M.E., Wright, V.P. and Dickson, J.A.D., 1990b. Carbonate sedimentology. Blackwell Sci. Publ., 482.

Vail, P.R. and Mitchum, R.M., Jr., 1977b. Seismic stratigraphy and global changes of sea level; Part 1, Overview. In: Payton, C.E. (Ed), Seismic stratigraphy; applications to hydrocarbon exploration. *Memoir - American Association of Petroleum Geologists*. American Association of Petroleum Geologists, 51-52.

Vail, P.R., Mitchum, R.M., Jr. and Thompson, S., III, 1977a. Seismic stratigraphy and global changes of sea level; Part 3, Relative changes of sea level from coastal onlap. In: Payton, C.E. (Ed), Seismic stratigraphy; applications to hydrocarbon exploration. *Memoir - American Association of Petroleum Geologists*. American Association of Petroleum Geologists, 63-81.

Van Wagoner, J.C., Mitchum, R.M., Campion, K.M. and Rahmanian, V.D., 1990. Siliciclastic sequence stratigraphy in well logs, cores, and outcrops; concepts for high-resolution correlation of time and facies, Methods in Exploration Series. American Association of Petroleum Geologists, 55.

Van Wagoner, J.C., Posamentier, H.W., Mitchum, R.M., Jr., Vail, P.R., Sarg, J.F., Loutit, T.S. and Hardenbol, J., 1988. An overview of the fundamentals of sequence stratigraphy and key definitions. In: Wilgus, C.K., Hastings, B.S., Ross, C.A., Posamentier, H.W., Van, W.J. and Kendall, C.G.S.C. (Eds), Sea-level changes; an integrated approach. *Special Publication - Society of Economic Paleontologists and Mineralogists*. SEPM (Society for Sedimentary Geology), 39-45.

Veenstra, E., 1985. Rift and drift in the Dampier Sub-basin, a seismic and structural interpretation, The APPEA Journal. Australian Petroleum Production & Exploration Association, 177-189.

Veevers, J.J., 1991. Mid-Cretaceous tectonic climax, Late Cretaceous recovery, and Cainozoic relaxation in the Australian region. In: Williams, M.A.J., de, D.P. and Kershaw, A.P. (Eds), The Cainozoic in Australia; a re-appraisal of the evidence. *Special Publication - Geological Society of Australia*. Geological Society of Australia, 1-14.

Veevers, J.J. and Powell, C.M., 1984. Dextral shear within the eastern Indo-Australian Plate. In: Veevers, J.J. (Ed), Phanerozoic Earth History of Australia. Clarendon Press, 102-103.

Veevers, J.J., Powell, C.M. and Roots, S.R., 1991. Review of seafloor spreading around Australia; I, Synthesis of the patterns of spreading. *Australian Journal of Earth Sciences*, **38,** 373-389.

Westphal, H. and Aigner, T., 1997. Seismic stratigraphy and subsidence analysis in the Barrow-Dampier Sub-basin, Northwest Australia. *AAPG Bulletin*, **81,** 1721-1749.

Wheeler, H.E., 1958. Time-stratigraphy. *Bulletin of the American Association of Petroleum Geologists*, **42,** 1047-1063.

Wilber, R.J., Milliman, J.D. and Halley, R.B., 1988. Holocene export and accumulation of bank-top sediment to the western margin and slope of Great Bahama Bank. In: Anonymous (Ed), Geological Society of America 1988 centennial celebration. *Abstracts with Programs - Geological Society of America*. Geological Society of America (GSA), 209-210.

Wilber, R.J., Milliman, J.D. and Halley, R.B., 1990. Accumulation of bank-top sediment on the western slope of Great Bahama Bank; rapid progradation of a carbonate megabank. *Geology (Boulder)*, **18,** 970-974.

Wilgus, C.K., Hastings, B.S., Ross, C.A., Posamentier, H.W., Van, W.J. and Kendall, C.G.S.C., 1988. Sea-level changes; an integrated approach, Special Publication - Society of Economic Paleontologists and Mineralogists. SEPM (Society for Sedimentary Geology), 407.

Wilson, J.L., 1975. Carbonate facies in geologic history. Springer-Verlag, 471.

Woodside Offshore Petroleum, 1988. A review of the petroleum geology and hydrocarbon habitat of the Barrow-Dampier Sub-basins and environs. In: Purcell, P.G. and Purcell, R.R. (Eds), The North West Shelf Australia. Petroleum Exploration Society of Australia, 115-128.

Wright, C.A., 1973. Planktonic foraminiferal biostratigraphy of the Paleocene to Eocene interval, North West Shelf, Western Australia. BOC Australia Ltd.

Wright, C.A. and Apthorpe, M., 1976. Planktonic foraminiferids from the Maastrichtian of the Northwest Shelf, Western Australia. *Journal of Foraminiferal Research*, **6**, 228-240.

Yeates, A.N., Bradshaw, M.T., Dickins, J.M., Brakel, A.T., Exon, N.F., Langford, R.P., Mulholland, S.M., Totterdell, J.M. and Yeung, M., 1987. The Westralian Superbasin; an Australian link with Tethys. *International Symposium on Shallow Tethys 2*, 199-213. Wagga Wagga.

Young, G.C. and Laurie, J.R., 1996. An Australian Phanerozoic Timescale. Oxford University Press, 279.

Young, H.C., in prep. Sequence stratigraphic evolution of the Albian to Recent section of the Barrow Sub-basin, North West Shelf of Australia. Ph.D. Thesis, University of South Australia.